EFFECTS OF DENSITY DIFFERENCES ON LATERAL MIXING IN OPEN-CHANNEL FLOWS

by

Edmund A. Prych

W. M. Keck Laboratory of Hydraulics and Water Resources
Division of Engineering and Applied Science
CALIFORNIA INSTITUTE OF TECHNOLOGY
Pasadena, California

Report No. KH-R-21

May 1970

FILE COPY

EFFECTS OF DENSITY DIFFERENCES ON LATERAL MIXING IN OPEN-CHANNEL FLOWS

by

Edmund A. Prych

Project Supervisor:

Norman H. Brooks
Professor of Civil Engineering

Funded by
Federal Water Pollution Control Administration

W. M. Keck Laboratory of Hydraulics and Water Resources
Division of Engineering and Applied Science
California Institute of Technology
Pasadena, California

Report No. KH-R-21

May 1970

ACKNOWLEDGEMENTS

This study, one of a group of investigations at the California Institute of Technology titled "Dispersion in Hydrologic and Coastal Environments", was funded by the Federal Water Pollution Control Administration through Grants No. 16000 DGY and No. 16070 DGY. During the study the writer also received financial assistance in the form of stipends and tuition payments while a U. S. Public Health Service Trainee (1967-70) and while a National Science Foundation Trainee (1966-67). The writer thanks each of these agencies for their support.

To Dr. Norman H. Brooks, adviser and fruitful source of "the right questions", the writer expresses his sincere gratitude. The writer also thanks Dr. Vito A. Vanoni for comments made during the study, and Dr. E. John List for his comments during the writing of this report.

For their assistance in constructing and modifying laboratory equipment, the writer offers a hearty thanks to Mr. Elton F. Daly, supervisor of the shop and laboratory; to Mr. Robert L. Greenway, his talented assistant; and to Mr. Carl A. Green, Jr., who also prepared most of the drawings in this text. A warm thank you is extended to Mrs. Arvilla F. Krugh, for typing this manuscript; to Mr. Carl T. Eastvedt, for doing the photographic work; and to Mrs. Patricia A. Rankin, for performing many of the secretarial duties for this project. The writer also acknowledges the efforts of the student assistants who

performed a variety of tasks during this investigation; they are: Messrs. Raul Basu, George Chan, Yoshiaki Daimon, Edward F. Thompson, W. H. Waggy, Paul T. Wegener, and Mashio Yatsuzuka.

This report was submitted in May 1970 as a Ph. D. thesis by the author to the California Institute of Technology.

ABSTRACT

This study investigates lateral mixing of tracer fluids in turbulent open-channel flows when the tracer and ambient fluids have different densities. Longitudinal dispersion in flows with longitudinal density gradients is investigated also.

Lateral mixing was studied in a laboratory flume by introducing fluid tracers at the ambient flow velocity continuously and uniformly across a fraction of the flume width and over the entire depth of the ambient flow. Fluid samples were taken to obtain concentration distributions in cross-sections at various distances, x, downstream from the tracer source. The data were used to calculate variances of the lateral distributions of the depth-averaged concentration. When there was a difference in density between the tracer and the ambient fluids, lateral mixing close to the source was enhanced by density-induced secondary flows; however, far downstream where the density gradients were small, lateral mixing rates were independent of the initial density difference. A dimensional analysis of the problem and the data show that the normalized variance is a function of only three dimensionless numbers, which represent: (1) the x-coordinate, (2) the source width, and (3) the buoyancy flux from the source.

A simplified set of equations of motion for a fluid with a horizontal density gradient was integrated to give an expression for the density-induced velocity distribution. The dispersion coefficient due

to this velocity distribution was also obtained. Using this dispersion coefficient in an analysis for predicting lateral mixing rates in the experiments of this investigation gave only qualitative agreement with the data. However, predicted longitudinal salinity distributions in an idealized laboratory estuary agree well with published data.

TABLE OF CONTENTS

Chapter		Page
1.	INTRODUCTION	1
	1.1 Purpose	1
	1.2 Method of Investigation	2
2.	BACKGROUND AND REVIEW OF PREVIOUS WORK	5
	2.1 The Conservation Equation	5
	2.2 Mass Transport in Open-Channel Flows of Homogeneous Density	6
	2.2.1 Longitudinal Dispersion	6
	2.2.2 Longitudinal Diffusion	8
	2.2.3 Lateral Diffusion	10
	2.2.3.1 Diffusion at the Free Surface	10
	2.2.3.2 Depth-Averaged Diffusion Coefficient	10
	2.2.4 Vertical Diffusion	15
	2.3 Effects of Density Differences on Mass Transfer	16
	2.3.1 Vertical Density Gradients	16
	2.3.2 Horizontal Density Gradients	17
3.	EXPERIMENTAL APPARATUS AND TECHNIQUES	20
	3.1 Description of Experiments	20
	3.2 Flume	21
	3.2.1 Description	21

TABLE OF CONTENTS (Cont'd)

Chapter		Page
	3.2.2 Water Circulation	23
	3.2.3 Rough Bottom	24
	3.3 Water Depth and Velocity Measuring Equipment	26
	3.4 Tracer Fluid System	26
	3.4.1 Fluid Handling System	26
	3.4.2 Sources	28
	3.4.2.1 Narrow Sources	28
	3.4.2.2 The Intermediate Width Sources	31
	3.4.2.3 Wide Source	33
	3.5 Fluid Sampling Apparatus	35
	3.6 Sample Analysis	38
	3.6.1 Description of the Technique	38
	3.6.2 Accuracy of the Technique	42
	3.7 Measurements of Fluid Density	43
	3.8 Experimental Procedures	45
	3.8.1 Preparation	45
	3.8.2 Positioning the Sampling Tubes	46
	3.8.3 Taking the Samples	47
	3.9 Experiments With Floating Particles	49
	3.9.1 Apparatus	49
	3.9.2 Procedures	51
4.	EXPERIMENTAL DATA	54
	4.1 Hydraulic Data	54

TABLE OF CONTENTS (Cont'd)

Chapter			Page
	4.1.1	Flow Condition Code and Flume Bottom	54
	4.1.2	Water Depth	54
	4.1.3	Slope	56
	4.1.4	Shear Velocity	58
	4.1.5	Metered Discharge and Discharge Velocity	58
	4.1.6	Velocity in Central 60 cm of Flume	58
	4.1.7	von Karman's k	59
	4.1.8	Friction Factors	62
	4.1.9	Reynolds Number and Froude Number	62
4.2	Experiments With Fluid Tracers		63
	4.2.1	Introduction	63
	4.2.2	Concentration Distributions in Cross-Sections	65
	4.2.3	Depth-Averaged Concentration Distributions	79
		4.2.3.1 Calculating the Depth-Averaged Concentrations	79
		4.2.3.2 The Lateral Distributions of $\overline{C}$	80
	4.2.4	Variances of the Lateral Concentration Distributions	95
		4.2.4.1 Calculations of the Variances	95
		4.2.4.2 Presentation of the Variances	103
	4.2.5	Photographs of Experiments	118
	4.2.6	Variation of Concentration With Depth	127

TABLE OF CONTENTS (Cont'd)

Chapter		Page
	4.3 Experiments With Floating Particles	135
	4.3.1 Calculating the Variance	135
	4.3.2 Presentation of Data	140
5.	DATA ANALYSIS	145
	5.1 Experiments Without Density Differences	145
	5.1.1 Experiments With Tracer Fluids	145
	5.1.2 Experiments With Floating Particles	147
	5.2 Experiments With Density Differences	149
	5.2.1 Introduction	149
	5.2.2 Selection of Dimensionless Numbers	149
	5.2.3 The Dimensionless Variance	152
	5.2.3.1 The Excess Variance	153
	5.2.3.2 The Fraction r	160
	5.2.3.3 Maximizing Lateral Mixing	163
	5.2.4 The Average Coefficient of Variation	166
	5.2.5 Predicting Concentration Distributions	168
6.	ANALYTIC STUDY	170
	6.1 Introduction	170
	6.2 Basic Equations	170
	6.3 Simplification of the Basic Equations	173
	6.3.1 Lateral Mixing	173
	6.3.2 Longitudinal Mixing	180

TABLE OF CONTENTS (Cont'd)

Chapter			Page
	6.4	Solution for the Velocity w and the Dispersion Coefficient D_z	181
	6.5	Application of Theory to Experiments of This Study	186
		6.5.1 Sources of Finite Width	186
		6.5.2 Two Wide Parallel Streams	191
	6.6	Application of Theory to MIT Experiments	193
		6.6.1 Description of Experiments	193
		6.6.2 Theoretical Analysis of Experiment	196
		6.6.3 Comparison of Theory With Experiment	198
7.	SUMMARY OF RESULTS		204
	7.1	Experiments	204
		7.1.1 Experiments Without Density Differences	204
		7.1.2 Experiments With Density Differences	205
	7.2	Theory	207
LIST OF SYMBOLS			209
LIST OF REFERENCES			214
APPENDIX			218

LIST OF FIGURES

Number	Description	Page
2.1	Longitudinal pressure gradients and velocity distributions in an estuary	19
3.1	The 40-meter flume	22
3.2	Photograph of expanded metal lath used for roughness on the bottom of the flume	25
3.3	Dimensioned sketch of metal lath used for roughness on the bottom of the flume	25
3.4	Schematic drawing of the tracer-fluid handling system	27
3.5	The 1-cm-wide source	29
3.6	The 20-cm-wide source	29
3.7	Photograph looking down the flume	34
3.8	The manifold for the wide source	34
3.9	A fluid sampling rake	37
3.10	The pressure box and sampling rakes on the instrument carriage	37
3.11	Sample of polyethlene particles used in study of lateral diffusion at the free surface	50
3.12	Compartmented-sieve particle collector; the compartments are 1 cm wide	50
4.1	Profiles of the energy grade line, water surface, and flume bottom for flow S2	57
4.2	Cross-sections of the flume showing isovels 25 meters downstream from the flume inlet	60

LIST OF FIGURES (Cont'd)

Number	Description	Page
4.3	Velocity profiles observed 25 meters downstream from the flume inlet	61
4.4	Lines of equal relative concentration in cross-sections downstream from a 1-cm-wide source which discharged a fluid with a density the same as the ambient fluid and with a relative concentration of 1.0.	67
4.5	Lines of equal relative concentration in cross-sections downstream from a 1-cm-wide source which discharged a fluid with a density 0.0160 gm/cm^3 greater than the ambient fluid and with a relative concentration of 1.0	68
4.6	Lines of equal relative concentration in cross-sections downstream from a 1-cm-wide source which discharged a fluid with a density 0.0158 gm/cm^3 less than the ambient fluid and with a relative concentration of 1.0	69
4.7	Cross-section of flume showing density-induced secondary circulation patterns downstream from a source of narrow or intermediate width	71
4.8	Cross-sections with lines of equal relative concentration downstream from the confluence of two wide parallel streams of the same density	76
4.9	Cross-sections with lines of equal relative concentration downstream from the confluence of two wide parallel streams of different density	77
4.10	Cross-sections of the flume showing density-induced secondary circulation pattern downstream from the confluence of two wide parallel streams of different density	78
4.11	Definition sketch for terms in Eq. 4.1b	80
4.12	Depth-averaged concentration distributions downstream from a 1-cm-wide source which discharged a fluid with a density the same as the ambient fluid and with a relative concentration of 1.0; Exp. 125	82

LIST OF FIGURES (Cont'd)

Number	Description	Page
4. 13	Depth-averaged concentration distributions downstream from a 1-cm-wide source which discharged a fluid with a density the same as the ambient fluid and with a relative concentration of 1. 0; Exp. 116	83
4. 14	Depth-averaged concentration distributions downstream from a 1-cm-wide source which discharged a fluid with a density 0. 0160 gm/cm^3 more dense than the ambient fluid and with a relative concentration of 1. 0; Exp. 113	84
4. 15	Depth-averaged concentration distributions downstream from a 1-cm-wide source which discharged a fluid with a density 0. 0158 gm/cm^3 less than the ambient fluid and with a relative concentration of 1. 0; Exp. 128	85
4. 16	Depth-averaged concentration distributions downstream from a 20-cm-wide source which discharged a fluid with a density the same as the ambient fluid and with a relative concentration of 0. 0370; Exp. 150	88
4. 17	Depth-averaged concentration distributions downstream from a 20-cm-wide source which discharged a fluid with a density 0. 00186 gm/cm^3 more dense than the ambient fluid and with a relative concentration of 0. 0385; Exp. 152	89
4. 18	Depth-averaged concentration distributions downstream from the confluence of two wide parallel streams of the same density; Exp. 177	91
4. 19	Depth-averaged concentration distributions downstream from the confluence of two wide parallel streams of different density; Exp. 181	92
4. 20	Depth-averaged concentration distributions, on arithmetic probability paper, downstream from the confluence of two wide parallel streams; Flow S1	94
4. 21	Cumulative distributions of depth-averaged concentrations from Exp. 125, $\Delta\rho/\rho_a = 0$	102
4. 22	a) Variance- and b) Coefficient of variation-distance curves from experiments with flow S1 and the 1-cm-wide source	106

LIST OF FIGURES (Cont'd)

Number	Description	Page
4.23	a) Variance- and b) Coefficient of variation-distance curves from experiments with flow S1 and the 12.5-cm-wide source	107
4.24	a) Variance- and b) Coefficient of variation-distance curves from experiments with flow S1 and the 20-cm-wide source	108
4.25	a) Variance- and b) Coefficient of variation-distance curves from experiments with flow S1 and the 10-cm-wide source	109
4.26	a) Variance- and b) Coefficient of variation-distance curves from experiments with flow S1 and the wide source	110
4.27	a) Variance- and b) Coefficient of variation-distance curves from experiments with flow S2 and the 1-cm-wide source	111
4.28	a) Variance- and b) Coefficient of variation-distance curves from experiments with flow S2 and the 20-cm-wide source	112
4.29	a) Variance- and b) Coefficient of variation-distance curves from experiments with flow S3 and the 1-cm-wide source	113
4.30	a) Variance- and b) Coefficient of variation-distance curves from experiments with flow R1 and the 1-cm-wide source	114
4.31	a) Variance- and b) Coefficient of variation-distance curves from experiments with flow R1 and the wide source	115
4.32	a) Variance- and b) Coefficient of variation-distance curves from experiments with flow R2 and the 1-cm-wide source	116
4.33	a) Variance- and b) Coefficient of variation-distance curves from experiments with flow R2 and the 20-cm-wide source	117
4.34	Photographs of experiments with flow S1 and the 1-cm-wide source	120

LIST OF FIGURES (Cont'd)

Number	Description	Page
4.35	Photographs of experiments with flow R1 and the 1-cm-wide source	121
4.36	Photographs of experiments with flow S1 and the 20-cm-wide source	123
4.37	Photographs of experiments with flow S2 and the 1-cm-wide source	124
4.38	Photographs of experiments with flow R1 and the wide source	125
4.39	Photographs of experiments with flow S1 and the wide source	126
4.40	Vertical concentration distributions downstream from a 1-cm-wide source which discharged a fluid with a density the same as the ambient fluid and with a relative concentration of 1.0; flow S2; Exp. 116	130
4.41	Vertical concentration distributions downstream from a 1-cm-wide source which discharged a fluid with a density 0.0160 gm/cm^3 greater than the ambient fluid and with a relative concentration of 1.0; flow S2; Exp. 113	131
4.42	Vertical concentration distributions downstream from a 1-cm-wide source which discharged a fluid with a density 0.0158 gm/cm^3 less than the ambient fluid and with a relative concentration of 1.0; flow S2; Exp. 128	132
4.43	Vertical concentration distributions downstream from the confluence of two wide parallel streams of the same density; flow S1; Exp. 177	133
4.44	Vertical concentration distributions downstream from the confluence of two wide parallel streams of different density; flow S1; Exp. 181	134
4.45	Cumulative distributions of particles; a) Exp. 102, b) Exp. 101	136
4.46	Variance-distance curves for a) Exp. 102; b) Exp. 101	138
4.47	Assumed secondary flow pattern in flume	139

LIST OF FIGURES (Cont'd)

Number	Description	Page
4.48	Variance-distance curves for experiments with floating particles; flow S1	141
4.49	Variance-distance curves for experiments with floating particles; (a) flow S2, and (b) flow S3	142
4.50	Variance-distance curves for experiments with floating particles; (a) flow R1, and (b) flow R2	143
5.1	Definition sketch for r and ΔV	153
5.2	The dimensionless excess variance, ΔV, as a function of the dimensionless source strength, M_b, and the dimensionless source width, B	155
5.3	The dimensionless excess variance, ΔV, as a function of the dimensionless source strength, M_d, and the dimensionless source width, B	157
5.4	The intercept, M_b^1, as a function of the dimensionless source width, B	159
5.5	The fraction of the excess variance, r, as a function of the dimensionless distance downstream, X	161
5.6	a) Variance-, and b) Maximum concentration-distance curves from some experiments with similar flow conditions and values of M_b but different source widths	164
5.7	Laterally averaged coefficient of variation, $\overline{C}_v$, as a function of the dimensionless distance downstream, X	167
6.1	Theoretical velocity profiles, $w(\eta)$ with $\overline{w} = 0$, for three different sets of boundary conditions	185
6.2	Comparison of ΔV given by Eq. 6.42 and by experiment	189
6.3	Schematic diagram of the flume used in the MIT experiments (Ref. 2)	194
6.4	Solutions to Eq. 6.61, $-\overline{C} = \frac{d\overline{C}}{d\xi} + J\left(\frac{d\overline{C}}{d\xi}\right)^3$	199

LIST OF FIGURES (Cont'd)

Number	Description	Page
6.5	Depth-averaged relative concentration $\bar{C}$ as a function of ξ, the dimensionless longitudinal coordinate; for MIT Runs 21 to 24	200
6.6	The dimensionless distance ξ_* as a function of the parameter J	202

LIST OF TABLES

Number	Description	Page
2.1	Summary of published data on longitudinal diffusion of floating particles in open-channels	9
2.2	Summary of published data on lateral diffusion of floating particles in open-channels	11
2.3	Summary of published data on lateral diffusion of solutes in open-channels	13
3.1	Specific resistance at $18^{\circ}C$ as a function of NaCl concentration	40
3.2	Data from tests to check accuracy of technique for determining relative concentrations	40
3.3	Probability that the error in σ_s^2 is exceeded as a function of the number of particles collected	53
4.1	Summary of hydraulic data	55
4.2	List of experiments with tracer fluids	64
4.3	Sample table from Ref 1	66
4.4	Variances of lateral distributions of depth-averaged concentrations in Exp. 125	102
5.1	Lateral turbulent diffusion coefficients from this study	146
6.1	Coefficients in Eq. 6.30 and 6.31 for $w(\eta)$ and D_z	184
A1	Summary of data from experiments with the 1-cm-, 12.5-cm-, and 20.0-cm-wide sources	219
A2	Summary of data from experiments with the wide source	224
A3	Summary of data from experiments with floating particles	225

CHAPTER 1

INTRODUCTION

1.1 PURPOSE

Many waste effluents which are discharged into streams have densities slightly different from those of the receiving waters. This study investigates the effects of density differences on the horizontal, cross stream mixing of such effluents. Longitudinal mixing under certain restrictive conditions is also examined.

Two typical cases in which the effluents and the receiving waters have different densities are: heated cooling water discharges from industries or steam power plants, and domestic or industrial waste discharges into brackish estuary waters. In the case of the cooling water discharges, a temperature difference of $10^{\circ}C$ causes a density difference of approximately 0.25 percent. In the second case, a waste discharging into an estuary, the density differences due to differences is concentrations of dissolved salts can be as high as 2.5 percent. In both these cases the densities of the effluents are less than that of the receiving waters.

Situations also exist where the effluents are more dense than the receiving waters. These include wastes with high concentrations

of dissolved matter that are discharged into fresh water streams, and also waste discharges with suspensions of fine particulate matter that is more dense than water. Density differences due to concentrations of dissolved or suspended matter can range up to a few percent, although a fraction of a percent may be more typical.

Although the magnitude of the density differences given above may seem small, differences of these magnitudes and smaller often have large effects on the dynamics of oceans, lakes and the atmosphere. This study investigates their importance in streams.

1.2 METHOD OF INVESTIGATION

In this study the effects of density differences on cross stream mixing were studied experimentally in a laboratory flume. In the experiments, which are described in Chapter 3, tracer fluids with densities equal to and slightly different from the density of the ambient water in the flume were introduced over some part of the width and uniformly over the whole depth. If the tracer and ambient fluids have the same density, crosswise mixing is primarily by turbulent diffusion. However, if the densities of the tracer and ambient fluids are different, crosswise mixing is enhanced by a density-induced secondary flow. The forces driving the secondary flow are due to an inbalance of hydrostatic pressure caused by lateral density gradients. The phenomenon of density-induced circulation is discussed in more detail in the literature review of Chapter 2 and in the discussion of the data in Chapter 4.

Some of the data, showing the characteristic features of the concentration distributions observed in the experiments, are given in Chapter 4. The concentrations measured at all points in all experiments are made available in Ref. 1, but they are not included in this text because the data are too numerous.

A dimensional analysis of the problem of lateral mixing in an open channel is given in Chapter 5. The results of the analysis and the experimental data yield empirical curves for parameters which characterize the tracer-plume width and the variation of concentration with depth as functions of distance downstream from the source, the initial density difference, the source width, and the hydraulic parameters of the stream. Concentration distributions can be estimated by using these curves.

A simplified theory for the effect of horizontal density gradients on horizontal mixing is given in Chapter 6. The velocity distribution caused by a horizontal density gradient was derived, and an expression for the dispersion coefficient due to the density-induced velocity was calculated. An analysis using this dispersion coefficient predicts that the characteristic width of a tracer plume in an open channel is a function of the same dimensionless parameters that were obtained from the dimensional analysis and data. However, because some of the simplifying assumptions made in the derivation of the density-induced velocity distribution are not valid for this problem, quantitative agreement between theory and experiment is not good.

The approximations in the derivation of the density-induced velocities are more nearly correct for some experiments in an idealized laboratory estuary described by Ippen, Harleman, and Lin (2). Good agreement was found between their experimental data and the theory derived herein.

CHAPTER 2

BACKGROUND AND REVIEW OF PREVIOUS WORK

2.1 THE CONSERVATION EQUATION

In most mathematical analysis of turbulent flows, the transport of solutes or other tracers is often described by an appropriate time-averaged conservation equation for the tracer. The equation usually used for aqueous solutions, which are nearly incompressible but not necessarily of uniform density, is

$$\frac{\partial c}{\partial t} + u\frac{\partial c}{\partial x} + v\frac{\partial c}{\partial y} + w\frac{\partial c}{\partial z} = \frac{\partial}{\partial x}\left(\epsilon_x \frac{\partial c}{\partial x}\right) + \frac{\partial}{\partial y}\left(\epsilon_y \frac{\partial c}{\partial z}\right) + \frac{\partial}{\partial z}\left(\epsilon_z \frac{\partial c}{\partial z}\right) \qquad (2.1)$$

(see e.g. Harleman (3)). In this expression, t is time; c is a time-averaged concentration; u, v, and w are time-averaged velocities in the rectilinear coordinate directions, x, y, and z; and ϵ_x, ϵ_y, and ϵ_z are turbulent diffusion coefficients for mass. (The velocities and concentrations in Eq. 2.1 are averages over a time that is long compared to the time scale for turbulence, but short compared to the time scale for the gross phenomena being investigated.)

If the density of the fluid is a function of c, then u, v, w, ϵ_x, ϵ_y, and ϵ_z may be functions of c also. Under these conditions, Eq. 2.1 is nonlinear in c and must be solved simultaneously with the equations of motion for the fluid. For tracers whose presence

does not affect the dynamics of the flow, Eq. 2.1 is linear in c and the equations of motion for the fluid may be solved separately. However, even under these simplified conditions, analytic solutions for Eq. 2.1 have been obtained only for very simple flow fields.

Below, a review is given of existing information on mass transport in turbulent open-channel flows of homogeneous density. It is followed by a discussion of the effects of density differences on mass transport.

2.2 MASS TRANSPORT IN OPEN-CHANNEL FLOWS OF HOMOGENEOUS DENSITY

2.2.1 Longitudinal Dispersion.- The coordinate system for an open channel flow is chosen with the origin on the channel bottom, the x-axis in the direction of flow, the y-axis normal to the bottom and positive upwards, and the z-axis horizontal and in the lateral direction. For a uniform steady flow of a fluid of uniform density in a wide channel of uniform depth, $v = w = 0$, and $\partial\epsilon_x/\partial x = \partial\epsilon_z/\partial z = 0$. For these conditions, Eq. 2.1 becomes

$$\frac{\partial c}{\partial t} + u\frac{\partial c}{\partial x} = \epsilon_x \frac{\partial^2 c}{\partial x^2} + \frac{\partial}{\partial y}\left(\epsilon_y \frac{\partial c}{\partial y}\right) + \epsilon_z \frac{\partial^2 c}{\partial z^2} \qquad (2.2)$$

One now substitutes into Eq. 2.2 the expressions:

$$u = \overline{u} + u'$$

$$c = \overline{c} + c'$$

$$\epsilon_x = \overline{\epsilon}_x + \epsilon'_x$$

and

$$\epsilon_z = \overline{\epsilon}_z + \epsilon'_z \ ,$$

where the overbarred quantities are depth-averaged variables and the primed quantities denote deviations from the averages. Averaging the resulting expression over the depth, and recognizing that $\partial u'/\partial x = 0$, yields

$$\frac{\partial \overline{c}}{\partial t} + \overline{u}\frac{\partial \overline{c}}{\partial x} + \frac{\partial}{\partial x}\left(\overline{u'c'}\right) = \overline{\epsilon}_x \frac{\partial^2 \overline{c}}{\partial x^2} + \overline{\epsilon'_x \frac{\partial^2 c'}{\partial x}} + \overline{\epsilon}_z \frac{\partial^2 \overline{c}}{\partial z^2} + \overline{\epsilon'_z \frac{\partial^2 c'}{\partial z^2}} \quad . \tag{2.3}$$

The second term on the left-hand side of Eq. 2.3 represents differential convection by the mean velocity, $\overline{u}$, and the third term represents differential convection due to the correlation between u' and c'. Elder (4) showed that for two-dimensional flows in which $\partial c/\partial z = 0$, one can write for large time

$$\overline{u'c'} = -D_x \frac{\partial \overline{c}}{\partial x} \quad , \tag{2.4}$$

where D_x is called the longitudinal dispersion coefficient. He showed that D_x is only a function of u' and ϵ_y and is given by

$$D_x = -d^2 \int_0^1 u'(\eta) \int_0^\eta \frac{1}{\epsilon_y(\eta')} \int_0^{\eta'} u'(\eta'')\, d\eta\, d\eta'\, d\eta'' \quad , \tag{2.5}$$

where η, η', and η'' are y/d. Using the Prandtl-von Karman logarithmic velocity distribution to obtain u' and the Reynolds analogy to obtain ϵ_y (see Subsection 2.2.3), Elder integrated Eq. 2.5 to give

$$D_x = \frac{0.404}{k^3}\, u_* d \quad , \tag{2.6}$$

where k is von Karman's constant; u_* is the shear velocity, and d is the water depth. When $k = 0.41$, the coefficient in Eq. 2.6 equals 5.86. His experiments confirmed this result.

2.2.2 Longitudinal Diffusion. Because transport by longitudinal dispersion, as described above, and transport in the longitudinal direction by turbulent diffusion are additive, and because $D_x >> \epsilon_x$, little experimental data on ϵ_x exist.

Data on longitudinal diffusion at the free surface are available from experiments by Sayre and Chang (5) and by Engelund (6). In these studies, small floating particles were released at a point on the free surface, and either the distribution in time for particles to travel a fixed distance or the longitudinal distribution of particles after a fixed time from release were observed. Longitudinal turbulent diffusion coefficients at the free surface, ϵ_{xs}, were calculated using

$$\epsilon_{xs} = \frac{1}{2} \frac{d\sigma_x^2}{dt} \tag{2.7a}$$

or

$$\epsilon_{xz} = \frac{u_s^3}{2} \frac{d\sigma_t^2}{dx} \quad , \tag{2.7b}$$

where σ_x^2 and σ_t^2 are the variances of the distributions of the particles in space and time, and u_s is the mean longitudinal particle velocity.

Sayre and Chang normalized ϵ_{xs} by dividing by u_*d, but Engelund chose to divide his coefficients by $u_s d$. Both normalizations were made on both sets of data and the results are given in Table 2.1. Neither normalization of the published data gives more consistent results than the other; however, using the re-evaluated coefficient for Engelund's Run B, which is obtained by recomputing ϵ_{xz} from his published basic data, the normalization by u_*d gives slightly more consistent results. Normalization by u_*d is also more appropriate because u_* characterizes turbulence better than u_s.

Table 2.1 Summary of published data on longitudinal diffusion of floating particles in open channels.

Reference	Run No.	Channel	Floating Particles	Depth d (cm)	Shear Velocity u_* (cm/sec)	Ave. Water Velocity $\bar{u}$ (cm/sec)	Particle Velocity u_s (cm/sec)	Diffusion Coefficient ϵ_{xs} (cm^2/sec)	$\frac{\epsilon_{xs}}{u_* d}$	$\frac{\epsilon_{xs}}{u_s d}$
Engelund (6)	A	Laboratory flume 230 cm wide; 2.3 cm diam. sand roughness on bottom	Plastic ball 0.9 cm diam sp. gr. = 0.288	5.45	3.60	30.0	38.3	10.0	0.510	0.0479
	B	Laboratory flume 230 cm wide; 0.1 cm diam. sand roughness on bottom	Plastic ball 0.9 cm diam. sp. gr. = 0.288	17.3	1.60	30.6	34.4	25.0 [2] (18.5)[3]	0.903 [2] (0.668)[3]	0.0420 [2] (0.0311)[3]
Sayre and Chang (5)	LO-P-1	Laboratory flume 239 cm wide; roughness blocks 1.9 cm high, 7.6 cm wide, 1.6 cm long on bottom	Polyethylene discs 0.32 cm diam. 0.16 cm thick sp. gr. = 0.96	14.8	3.81	23.5	33.5	30.7	0.544	0.0639
	LO-P-2			24.8	4.90	34.4	45.5	57.0	0.470	0.0505
	LO-P-3 [1]			37.1	6.04	47.5	65.9	23.8	1.06	0.0975

[1] Average of two experiments.
[2] Published data.
[3] Re-evaluated data.

Comparing the data in Table 2.1 with Eq. 2.6 confirms that $D_x >> \epsilon_x$.

2.2.3 Lateral Diffusion

2.2.3.1 Diffusion at the Free Surface. Data from experiments with floating particles have also been used to obtain values of ϵ_{zs}, the lateral diffusion coefficient at the free surface. Experiments of this type were first made by Orlob (7), later by other investigators, and also in this study. A summary of the experimental data from these investigations is given in Table 2.2. Values of ϵ_{zs} were calculated by either the formula

$$\epsilon_{zs} = \frac{1}{2}\frac{d\sigma_s^2}{dt} \tag{2.8a}$$

or

$$\epsilon_{zs} = \frac{u_s}{2}\frac{d\sigma_s^2}{dx} , \tag{2.8b}$$

where σ_s^2 is the variance of the lateral distribution of particles at a fixed time after release or after traveling a fixed distance. The dimensionless coefficient α_s is defined by

$$\alpha_s = \frac{\epsilon_{zs}}{u_* d} . \tag{2.9}$$

The average values of α_s from each of the studies listed in Table 2.2 range from 0.172 to 0.241. They are less than the normalized longitudinal coefficients given in Table 2.1.

2.2.3.2 Depth-Averaged Diffusion Coefficient. Because of vertical mixing, observations of lateral mixing of solutes yield only

Table 2.2 Summary of published data on lateral diffusion of floating particles in open channels.

Reference	Run No.	Channel	Floating Particles	Depth d (cm)	Shear Velocity u_* (cm/sec)	Water Velocity $\bar{u}$ (cm/sec)	Particle Velocity u_s (cm/sec)	Diffusion Coefficient ϵ_{zs} (cm^2/sec)	$\alpha_s = \frac{\epsilon_{zs}}{u_* d}$
Orlob (7)		Laboratory flume 122 cm wide, expanded metal screen roughness on bottom	Polyethylene discs 0.32 cm diam. 0.16 cm thick sp. gr. =0.975	1.62 to 12.8					0.172 [1]
Sayre and Chamberlain (8)		Laboratory flume 239 cm wide, sand dunes on bottom	Polyethylene discs 0.32 cm diam. 0.16 cm thick sp. gr. =0.96	17.4	3.51	49.8	62.5	15.0	0.241
Sayre and Chang (5)	LA-P-1	Laboratory flume 239 cm wide; roughness blocks 1.9 cm high, 7.6 cm wide, 1.6 cm long on bottom	Polyethylene discs 0.32 cm diam. 0.16 cm thick sp. gr. =0.96	14.8	3.81	23.5	33.5	13.3	0.236
	LA-P-2			24.8	4.90	34.4	45.5	23.4	0.196
	LA-P-3			37.1	6.04	47.5	65.9	59.2	0.264
									0.232
Engelund (6)	A	Laboratory flume 230 cm wide; 2.3 cm diam. sand roughness on bottom	Plastic ball 0.9 cm diam. sp. gr. =0.288	5.45	3.60	30.0	38.3	4.0	0.204
	B	Laboratory flume 230 cm wide; 0.1 cm diam. sand roughness on bottom	Plastic ball 0.9 cm diam. sp. gr. =0.288	17.3	1.60	30.6	34.4	6.5	0.234
									0.219
This study		Laboratory flume 110 cm wide; smooth bottom or expanded metal screen roughness on bottom	Polyethylene particles about 0.35 cm diam. sp. gr. =0.95	3.90 to 11.1					0.204 [2]

[1] Average of 120 experiments. The values of u_* and d were corrected for blockage as described in Subsection 4.1.3.

[2] Average of 13 experiments. Data for all experiments are given in Tables 4.1 and 5.1.

$\overline{\varepsilon}_z$, the depth-averaged value of the lateral turbulent diffusion coefficient. This coefficient is usually calculated with the formula

$$\overline{\varepsilon}_z = \frac{\overline{u}}{2}\frac{d\sigma^2}{dx} \tag{2.10a}$$

or

$$\overline{\varepsilon}_z = \frac{\overline{u}}{2}\frac{d\sigma_d^2}{dx} \quad , \tag{2.10b}$$

where σ^2 is the variance of the lateral distribution of the depth-averaged concentration, $\overline{c}$, and σ_d^2 is the variance of the lateral distribution of $\partial\overline{c}/\partial z$.

Eq. 2.10a and b are obtained from Eq. 2.3 as follows. Far downstream from a source of a neutrally buoyant tracer, experimental data show that $c' << \overline{c}$; therefore, one can delete each of the terms in Eq. 2.3 that contain c' because there are corresponding similar terms containing $\overline{c}$. One can also delete the term $\overline{\varepsilon}_x \frac{\partial \overline{c}}{\partial x}$ because it is less than the deleted term $\frac{\partial}{\partial x}(\overline{u'c'})$. Therefore, for a steady source Eq. 2.3 becomes

$$\overline{u}\frac{\partial \overline{c}}{\partial x} = \overline{\varepsilon}_z \frac{\partial^2 \overline{c}}{\partial z^2} \, . \tag{2.11}$$

Taking moments of this expression in the z-direction yields Eq. 2.10a, or taking the derivative of Eq. 2.11 with respect to z and then taking moments yields Eq. 2.10b.

Values of $\overline{\varepsilon}_z$ and the dimensionless coefficient

$$\alpha = \frac{\overline{\varepsilon}_z}{u_* d} \tag{2.12}$$

from a number of investigations are given in Table 2.3. These data can be divided into two groups, one from experiments in straight channels

Table 2.3 Summary of published data on lateral diffusion of solutes in open channels.

Reference	Run No.	Channel	Tracer	Concentrations Determined by	Depth d cm	Shear Velocity u_* (cm/sec)	Water Velocity $\bar{u}$ (cm/sec)	Diffusion Coefficient $\bar{\varepsilon}_z$ (cm²/sec)	$\alpha = \frac{\bar{\varepsilon}_z}{u_* d}$
Elder (4)		Laboratory flume 35.5 cm wide; smooth bottom.	Potassium permanganate dye	Analysis of photographs with microdensitometer	≈1.5				0.164[1]
Sayre and Chang (5)	LA-D-1	Laboratory flume 239 cm wide; roughness blocks 1.9 cm high, 7.6 cm wide 1.6 cm long on bottom.	Fluorescent dyes	Continuous sampling fluorometer	14.8	3.81	23.5	9.58	0.170
	LA-D-2				24.5	4.90	34.4	20.2	0.179
	LA-D-3				37.1	6.04	37.1	36.9	0.160
									0.167
Sullivan (9)		Laboratory flume, 76 cm wide; smooth bottom.	Gentian violet dye	Analysis of photographs with microdensitometer	10.2	0.827	15.3	0.90[2]	0.107[2]
					8.95	0.988	18.5	0.97[2]	0.110[2]
					7.33	1.21	22.9	1.18[2]	0.133[2]
									0.117
Glover [3,4] (10, p. 26)		Laboratory flumes 242 cm and 122 cm wide; rough and smooth bottoms.	Salt	Measurement of fluid conductivity in situ	14.7			33.5	0.36
					13.8			8.28	0.22
					28.8			7.16	0.14
		Columbia River near Richland, Wash.; approx 300 m wide	Radionuclides in a cooling water discharge	Radiation counting of samples	≈305		134	1860	0.72
Fischer (11)	6/21	Atrisco Feeder Canal near Bernalillo, N.M.; approx 17.5 m wide; 30-cm-high, sand dunes on bottom straight reach	Rhodamine WT dye	Analysis of samples with fluorometer	68.3	6.29	63.5	102	0.24
	6/23				66.7	6.13	66.1	102	0.25
Yatsukura, Fischer, and Sayre (12)		Missouri River near Blair, Nebraska approx. 225 m wide.	Rhodamine B dye	Analysis of samples with fluorometer	≈270	7.4	≈175	1200	0.6
Fischer (13)	2	Curved laboratory channel; 76.3 cm wide, smooth bottom.	Rhodamine WT dye	Analysis of samples with fluorometer	3.02	2.66	31.7	11.3	1.4
	3				5.28	1.70	27.0	21.4	2.4
	4				3.72	2.13	26.8	10.6	1.3
	5				2.03	1.37	19.0	1.96	0.70
	6				2.20	1.68	19.7	1.88	0.51
Okoye (14)		Laboratory flumes 110 cm wide and 85 cm wide; smooth and gravel bottoms.	Sodium chloride	Measurement of fluid conductivity in situ	1.6 to 21.1				≈0.14
This study		Laboratory flume 110 cm wide; smooth and rough bottoms.	Sodium chloride	Measurement of specific resistance of samples	3.90 to 11.1				0.135[5]

[1] Elder's published average value, $\alpha = 0.228$, was multiplied by $(1/1.18)^2$ because according to Sullivan (9), Elder used half the distance between points where the concentrations were half the peak value in place of σ in Eq. 2.10a.

[2] Sullivan's reported values have been divided by 2 because he omitted the factor $\frac{1}{2}$ in Eq. 2.10a.

[3] Tracers were not neutrally buoyant.

[4] Hydraulic radius used in place of depth for computing α.

[5] Average of 13 experiments. Data for all experiments are given in Tables 4.1 and 5.1.

(Ref. 4, 5, 9, 10, 11, 14, this study) and the other from experiments in curved channels (Ref. 10, 12, 13). Except for the data by Glover, which were from experiments in which the tracer was not neutrally buoyant, the data from straight channels yield values of α between 0.10 and 0.25. (One should observe that the often quoted value published by Elder (4) has been corrected in Table 2.3). All values from curved channels are greater than 0.5. The higher values in curved channels have been explained by Fischer (13) as due to secondary currents induced by the bends. These currents transport material in the lateral direction by a process analogous to longitudinal dispersion as described in Subsection 2.2.1. Fischer was able to calculate a lateral dispersion coefficient using Eq. 2.5 with lateral velocity deviations, w', in place of the longitudinal velocity deviations, u'.

A suitable explanation for the variation in α for straight channels does not yet exist. However, it is worth noting that the range in α found by one investigator is usually not as large as the range of the means of values given by different investigators. Therefore, much of the variation may be due to weak secondary currents characteristic of the different flumes or channels. Attempts to correlate α to the width-to-depth ratio of the flow cross-section and to other parameters is presently being investigated by Okoye (14).

In both the study by Sayre and Chang (5) and in this study, where experiments were made to obtain both α and α_s, one finds that α_s is about 50 percent larger than α. Although Sayre and Chang found that

the difference between α and α_s was small if they used $\overline{u}$ in place of u_s in Eq. 2.8, the data from this study do not confirm this result.

2.2.4 Vertical Diffusion. An estimate of the vertical diffusion coefficient for mass in a wide open-channel flow, ε_y, can be obtained from the Reynolds analogy. One first expresses τ_{xy}, the apparent shear stress on a horizontal plane, as

$$\tau_{xy} = (\lambda_y \varepsilon_y)\, \rho \frac{\partial u}{\partial y} \quad , \tag{2.13}$$

where ρ is the fluid density, and the product $\lambda_y \varepsilon_y$ is the eddy viscosity. The term λ_y is the turbulent Schmidt number and is the ratio of the diffusion coefficients for momentum to mass. Using the Prandtl-von Karman logarithmic velocity distribution,

$$u(y) - u(d) = \frac{u_*}{k} \ell n \frac{y}{d} \quad , \tag{2.14}$$

and a linear distribution of shear stress,

$$\tau_{xy} = \rho u_*^2 \left(1 - \frac{y}{d}\right) \quad , \tag{2.15}$$

Eq. 2.13 yields

$$\lambda_y \varepsilon_y = k u_* y \left(1 - \frac{y}{d}\right) . \tag{2.16}$$

This expression for $\lambda_y \varepsilon_y$ is zero at $y = 0$ and $y = d$, and is symmetric about $y = \frac{d}{2}$. The depth-averaged value is given by

$$\overline{\lambda_y \varepsilon_y} = \frac{k}{6} u_* d \quad . \tag{2.17}$$

Vanoni (15) observed the vertical distributions of suspended sediment in an open-channel flow and used the data to calculate ε_y for sediment. He found that the distribution of ε_y was similar to $\varepsilon_y \lambda_y$ given by Eq. 6.12,

and that $\lambda_y \approx 1$. Jobson and Sayre (16) introduced dye at the surface of an open-channel flow and observed the vertical distributions of dye as a function of distance downstream. They used the data to calculate ϵ_y and also found that ϵ_y and $\lambda_y \epsilon_y$ were similarly distributed and that $\lambda_y \approx 1$. Similar experiments with fine sediment gave nearly the same results.

2.3 EFFECTS OF DENSITY DIFFERENCES ON MASS TRANSFER

2.3.1 Vertical Density Gradients. Observations of vertical turbulent diffusion in the atmosphere, in natural water bodies, and in the laboratory show that stable vertical density gradients reduce vertical diffusion (Ref. 17 and 18). Observations also show that the vertical diffusion of mass or heat is reduced more than the diffusion of momentum. Taylor (19) noticed that stable density gradients in the atmosphere reduce turbulent wind velocity fluctuations in all three directions; hence, one may suspect that a stable vertical density gradient may reduce turbulent diffusion in the horizontal direction also.

Ellison and Turner (18) have given a physical explanation for the reduction in vertical diffusion by a stable density gradient. They reasoned that a parcel of fluid which is displaced from its equilibrium postition by turbulence may return to its equilibrium position before it mixes completely with the surrounding fluid. They also reason that the reduction in the diffusion of momentum is not as great as the reduction in the diffusion of heat or mass because the parcel can

exchange momentum without mixing by the action of pressure, but in order to transfer heat or mass the parcel of fluid must mix with its surroundings.

Most investigators attempt to relate the decrease in diffusion caused by a stable density gradient to Ri, the Richardson number,

$$Ri = \frac{g}{\rho}\frac{\partial \rho}{\partial y} \Big/ \left(\frac{\partial u}{\partial y}\right)^2 , \tag{2.18}$$

where g is the acceleration due to gravity, and $\partial u/\partial y$ is the vertical gradient of the primary flow which is considered to be horizontal. Munk and Anderson (17) suggest the empirical equations:

$$\epsilon_y \lambda_y = (\epsilon_y \lambda_y)_o \, (1 + Ri)^{-\frac{1}{2}} \tag{2.19}$$

and

$$\epsilon_y = (\epsilon_y)_o \, (1 + \frac{10}{3} \, Ri)^{-\frac{3}{2}}, \tag{2.20}$$

where $(\epsilon_y \lambda_y)_o$ and $(\epsilon_y)_o$ are the values of $\epsilon_y \lambda_y$ and ϵ_y under neutral conditions, Ri = 0. Okubo (20) reviews formulae suggested by other investigators.

Because the longitudinal dispersion coefficient, D_x, given by Eq. 2.5 is inversely proportional to ϵ_y, one may expect that D_x would be larger for stable density-stratified flows than for flows of uniform density.

2.3.2 Horizontal Density Gradients. Observations show that density differences in the horizontal direction can increase mass transfer by inducing density currents. Harleman, Jordaan, and Lin (21) observed the horizontal mixing of two fluids of different density in a

homogeneous turbulent field. They found that the rate of mixing of the two fluids increased with increasing density difference. Jen, Wiegel, and Mobarek (22) and Hayashi and Shuto (23) performed experiments with heated jets of water that discharged horizontally near a free surface; they found that lateral spreading of the jets increased with increasing difference in temperature between the discharged and ambient fluids.

Density-induced velocities also occur in estuaries, where longitudinal density gradients exist due to the difference in density between salt water from the ocean and fresh water from rivers. Experiments in an idealized laboratory estuary by Ippen, Harleman, and Lin (2), which are analysed and are described in more detail in Chapter 6, show that as the difference in density between the water in the ocean and incoming river increases, the apparent longitudinal diffusion coefficient increases also. Ippen (24) has explained conceptually the effect of longitudinal density gradients on the velocity distributions in estuaries, and Hansen and Rattray (25) have treated the problem analytically. If the pressure distribution over the vertical is hydrostatic, and if the estuary is well mixed vertically so that the variation in density with depth is small, the pressure is given by

$$p = (d-y)\,\rho g.$$

If the x-axis is horizontal, the longitudinal pressure gradient is then given by

$$(y-d)\,g\frac{\partial \rho}{\partial x} + S\rho g = -\frac{\partial p}{\partial x}\ , \qquad (2.21)$$

where $S = -\partial d/\partial x$ is the longitudinal water surface slope. The

vertical distribution of each of the terms in Eq. 2.21 are shown in Fig. 2.1 for a seaward sloping water surface. Because the pressure gradient due to the water surface slope is invariant with depth, and because the pressure gradient due to the density gradient is zero at the water surface and reaches a maximum at the bottom, the resultant pressure gradient near the surface and near the bottom can be in opposite directions. The result can be an upstream flow near the bottom but a downstream flow near the surface. When used in Eq. 2.5, velocity distributions of this type yield higher longitudinal diffusion coefficients than unidirectional velocity distributions with the same mean velocity. Because the upstream flow in the lower layer must return seaward in the upper layer, the flow pattern resembles a longitudinal circulation of the primary flow.

The present study investigates the effects of density-induced secondary circulation on lateral mixing in turbulent open-channel flows with lateral density gradients.

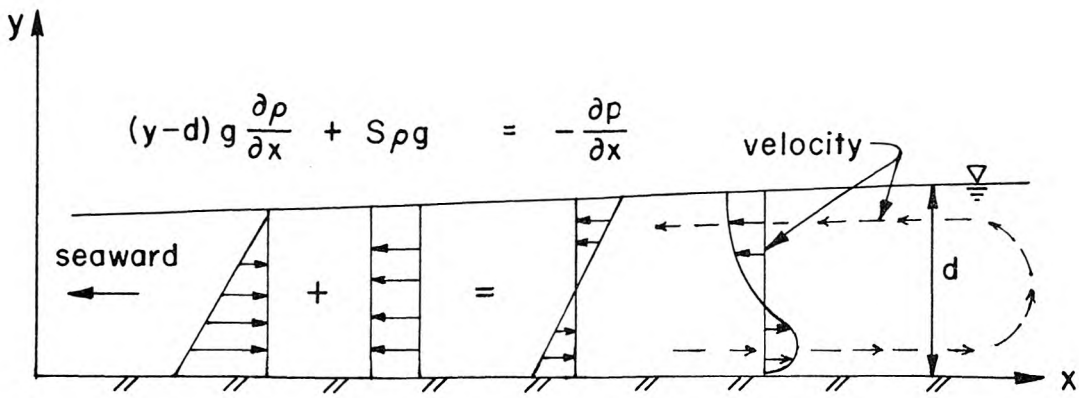

Figure 2.1 Longitudinal pressure gradients and velocity distributions in an estuary.

CHAPTER 3

EXPERIMENTAL APPARATUS AND TECHNIQUES

3.1 DESCRIPTION OF EXPERIMENTS

Experiments were made in a laboratory flume to observe the lateral mixing of fluids with densities different from that of the ambient flow. The objective of the experiments was to obtain data for developing and checking techniques for predicting horizontal mixing rates in turbulent flows with horizontal density gradients.

In the experiments, a tracer fluid was introduced continuously into the flume uniformly over the depth and across some fraction of the flume width. The tracer fluid was introduced into the flume at the same velocity as the ambient flow in the flume. In most experiments, the source was located on the flume center line, and the width of the source was small compared with the width of the flume. However, in some experiments that were made to observe the mixing of two wide parallel streams, the tracer fluid initially occupied all that part of the cross-section on one side of the flume center line.

Most experiments were made with tracer fluids whose densities were slightly greater or the same as the density of the ambient water in the flume. However, two experiments were made with tracer

fluids which were less dense than the ambient water. All tracer fluids were salt water (NaCl) solutions. The densities of the heavy tracer fluids were varied by changing the salt concentrations. Tracer fluids of neutral density were prepared by adding methyl alcohol to a salt-water solution. The light tracer fluids were made by adding additional amounts of alcohol. The tracer fluids were often colored with an organic dye to make them visible.

Distributions of tracer fluid in cross-sections downstream from a source were obtained by taking water samples from points in the cross-sections and by measuring the specific electrical resistance of each sample to determine the tracer concentration in each sample.

The lateral diffusion of small floats was observed during experiments in which the tracer fluid was neutrally buoyant and also in experiments in which no tracer fluid was introduced into the flume. The purpose of these experiments was to provide additional data to compare the turbulent diffusing characteristics of the flows in the flumes used in this study with the flows in the flumes used by other investigators.

3.2 FLUME

3.2.1 Description. The experiments were conducted in a 40-meter-long recirculating flume located in the sub-basement of the W. M. Keck Laboratory of Hydraulics and Water Resources. Fabrication details of the flume are given by Vanoni, Brooks, and Raichlen (26). The flume is shown schematically in Fig. 3.1, and

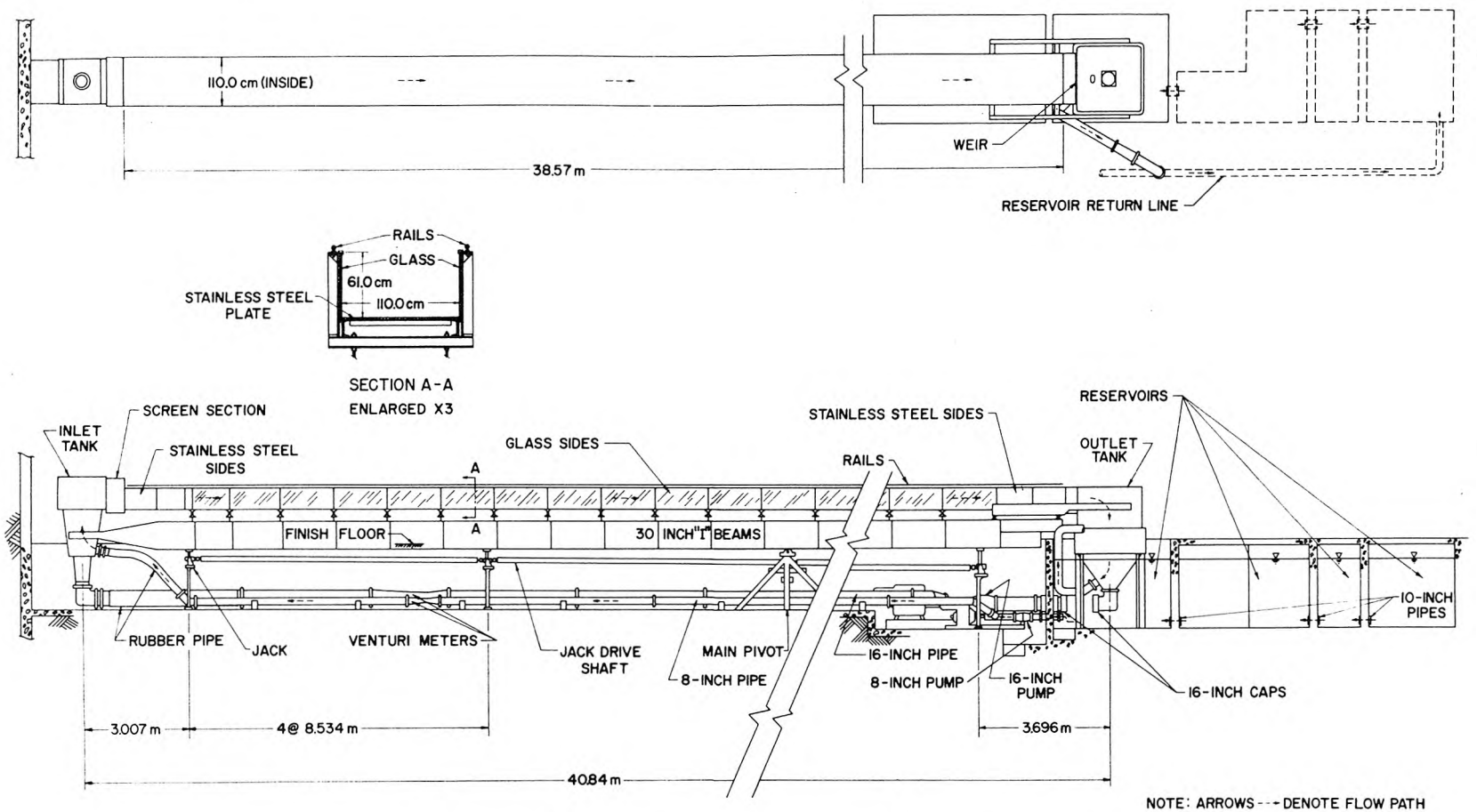

Figure 3.1 The 40-meter flume. (Drawing modified from Vanoni et al.(26)).

in the photograph in Fig. 3.7. The bottom of the flume is made of stainless steel plate and is 110 cm wide; the vertical sidewalls are 61 cm high and are glass along most of the flume's length. An instrument carriage rides on rails which are mounted on the tops of the sidewalls.

The flume is supported in pivot bearings near its mid-point and is supported elsewhere by four pairs of power-driven screw jacks (as shown in Fig. 3.1). The flume slope is obtained by reading a vertical staff attached to the flume approximately 17 meters upstream from the pivot. The staff was calibrated by observing the slope of the flume bottom with respect to a still water level.

3.2.2 Water Circulation. Water entered the upstream end of the flume through a metal screen (8 mesh/inch) from a baffled inlet tank. An adjustable weir was installed at the downstream end of the flume to control the tail-water depth. Water flowed over the weir into an outlet tank.

The design of the flume permits a number of alternatives for returning the water from the outlet tank to the inlet tank. In order to minimize changes in the tracer concentration of the ambient flow during an experiment, the return system was modified to utilize the maximum water volume. Water flowed from the outlet tank through a pipe and a laboratory floor drain into the farthest of the four reservoirs. The reservoirs are connected in series by short lengths of 10-inch pipes. The reservoirs have a combined capacity of approximately 63 cubic meters. Water was pumped

from the last reservoir, which is under the outlet tank, through a nominal 8-inch pipe, which runs under the flume, to the inlet tank. The pump was driven by a 10-horsepower motor through a continuously variable V-belt drive. Water discharge was measured with a venturi meter (Keck Lab. No. Q-6) in the 8-inch pipe. The 16-inch pipe which runs beneath the flume was not used for the return flow and was capped near the outlet tank but was allowed to fill with water from the inlet tank.

3.2.3 Rough Bottom. The bottom of the flume was made rough for some experiments by laying expanded metal sheets (Fig. 3.2) on the stainless steel bottom. The sheets, which are manufactured for use as plastering lath, are made of steel and are galvanized; their approximate dimensions are given in Fig. 3.3. Although the total thickness of the lath is 0.31 cm, the solid volume is equivalent to that of a solid sheet only 0.025 cm thick.

The lath was cut into panels 73 cm by 109 cm which were installed with the 109 cm length spanning the width of the flume. The panels were held to the stainless steel botom with mastic stripping 1/2 inches wide by 1/8 inches thick. Single strips of mastic were laid about 5 cm from each wall along the entire length of the flume, and three pieces about 8 cm long were laid longitudinally at the joints between panels. The panels were pressed into the mastic so that they lay flat on the stainless steel bottom.

The hydraulic resistance of this rough bottom is given with other hydraulic data in Chapter 4.

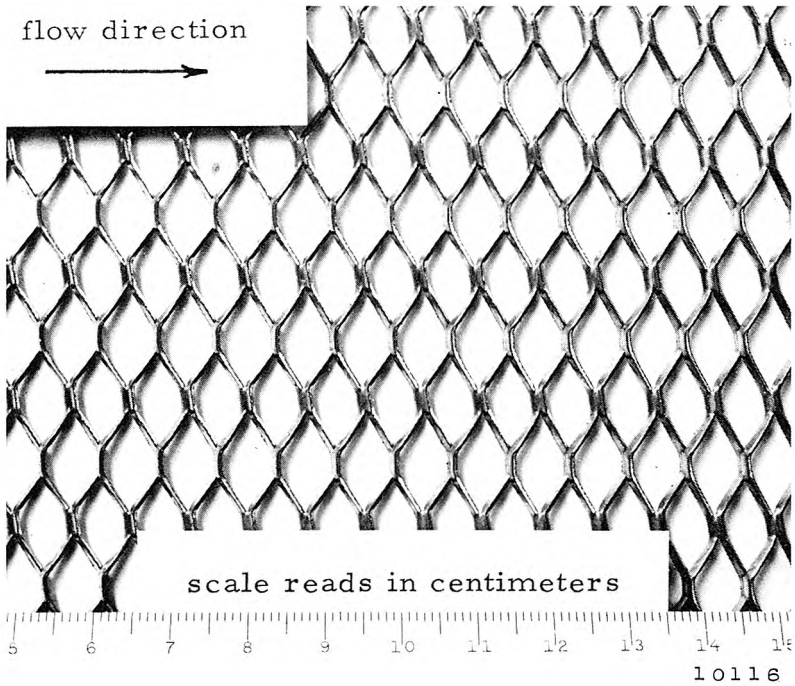

Figure 3.2 Photograph of expanded metal lath used for roughness on the bottom of the flume.

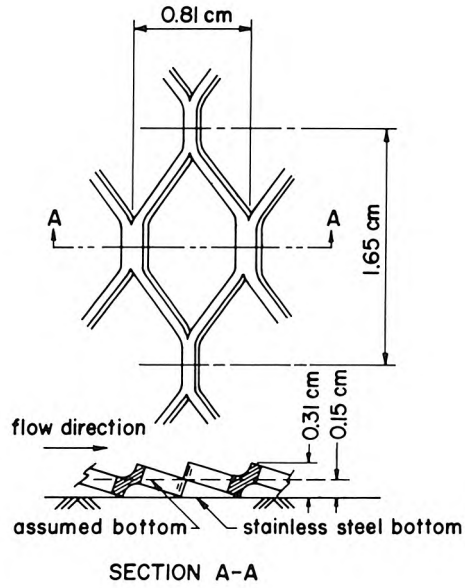

Figure 3.3 Dimensioned sketch of metal lath used for roughness on the bottom of the flume.

3.3 WATER DEPTH AND VELOCITY MEASURING EQUIPMENT

Water depths in the flume were measured with a point gage which could be read to the nearest 0.01 cm and which was mounted on the instrument carriage.

Water velocities were measured with a 1/8 inch (0.32-cm) diameter pitot-static tube. The differences in pressure between the dynamic and static ports were measured electronically with a pressure transducer and strip-chart recorder. The system was calibrated by imposing pressures on the transducer with a water manometer which could be read to within 0.001 inches (0.0025 cm). The difference between calibrations before and after an experiment was always less than two percent.

The pitot-static tube was attached to the traveler of a point gage on the instrument carriage for positioning it in the flume. To obtain the velocity at a point,the output of the pressure transducer was recorded for 30 seconds and was averaged by eye.

3.4 TRACER FLUID SYSTEM

3.4.1 Fluid Handling System. The tracer fluids were prepared in a mixing tank and were pumped into the flume through various types of sources which are described in Section 3.4.2. The mixing tank was open at the top and had a capacity of approximately 600 liters. The tank and associated plumbing are shown schematically in Fig. 3.4.

The mixing tank was filled with water from the 16-inch pipe which runs under the flume. Weighed amounts of salt and

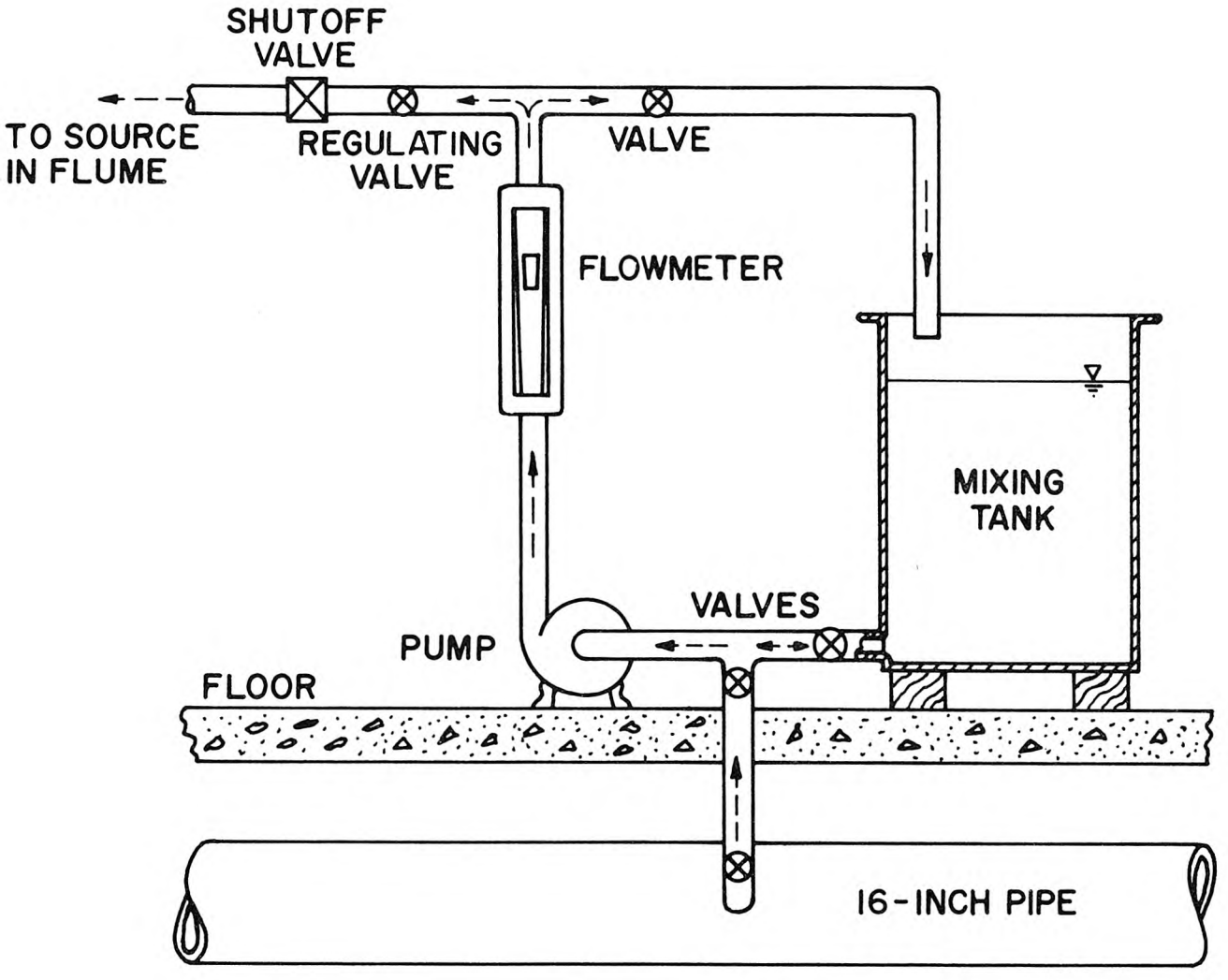

Figure 3.4 Schematic drawing of the tracer-fluid handling system.

alcohol (if any) were added to the tank and were mixed by pumping water out of the bottom of the tank and returning it at the top. For some experiments dye was also added to the solution.

During most experiments, fluid was pumped from the mixing tank to the source in the flume. However, for some experiments, water with no tracer and with the same density as the fluid in the flume was pumped directly from the 16-inch pipe to the source. The flow rate to the source was measured with a variable area flowmeter (Keck Lab. No. Q-29) and was regulated with a gate valve. A shutoff ball valve was put in series with the regulating valve for convenience.

3.4.2 Sources. The tracer sources in the flume were designed to distribute the tracer uniformly over the depth and across some selected width within the flume. They were also designed to cause minimum disturbances to the ambient flow. Three designs were used: one design was used for the narrow sources, 1 cm and 2 cm wide; a second design was used for the 12.5-cm- and 20-cm-wide intermediate width sources; and the third design was used for the wide source in which the tracer was distributed over one-half of the 110-cm-wide flume.

3.4.2.1 Narrow Sources. The narrow 1-cm-wide source, which is shown in Fig. 3.5, was made by placing a vertical manifold between two vertical guide walls. The manifold was a flattened length of thin-walled brass tubing with holes drilled in the downstream edge. The holes were spaced at approximately

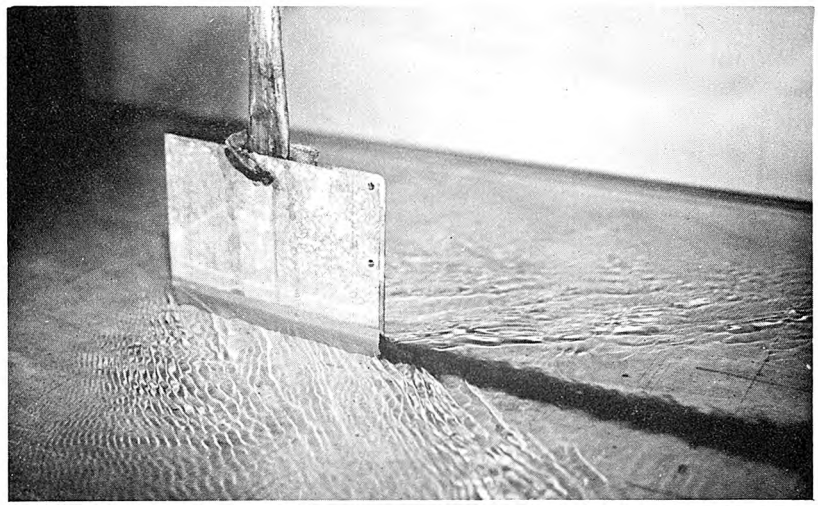

10109

Figure 3.5 The 1-cm-wide source.

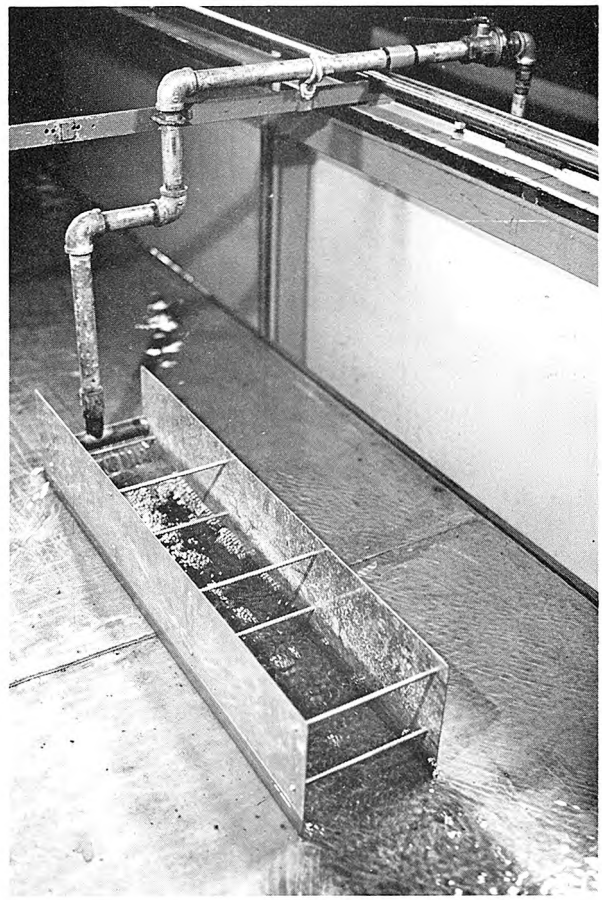

10114

Figure 3.6 The 20-cm-wide source.

0.3 cm intervals along a vertical line starting near the bottom and extending about 11 cm high. Holes above the water surface were covered with plastic tape. The holes were made with a 1/8-inch-diameter drill and every third hole was enlarged to a 3/16-inch-diameter. A piece of rolled wire screen was placed in front of the manifold to break up the jets from the manifold.

The vertical guide walls were made of 24-gage (0.028-inch) galvanized steel sheet. They were 1 cm apart and parallel at the downstream end but met to form a sharp edge at the upstream end. The total length of this source was 25 cm. The surface waves generated by this shape were less than 0.15 cm high and were not much larger than the waves made by a single piece of sheet metal placed parallel to the flow.

The discharge from the 1-cm-wide source was equal to the discharge through a 1-cm-wide vertical strip in the central part of the flume. The velocity distribution at the mouth of the source was observed to be approximately uniform over the depth. The downstream end of this source was located 15 meters downstream from the screen in the inlet box of the flume.

A 2-cm-wide source, 61 cm long, was constructed similar to the 1-cm-wide source. However, the 2-cm-wide source was used only in an experiment to observe the lateral diffusion of floating particles.

3.4.2.2 The Intermediate Width Sources. The 12.5-cm- and 20-cm-wide sources were made by placing a horizontal manifold between two parallel vertical guide walls. The guide walls were open at each end to allow the water in the flume to flow between them. A tracer fluid from the mixing tank was sprayed by the manifold onto the surface of the water flowing between the guide walls. This design did not require mixing, storing, and pumping large volumes of water as would be required if the sources were constructed in the same way as the narrow sources. The 20-cm-wide source is shown in Fig. 3.6.

The same guide walls were used for both sources. They were 91.5 cm long, 20.3 cm high, and were made from 18-gage (0.049-inch) stainless steel sheet. The walls were fastened to metal rods of the proper length which held them apart and upright. The contact between the guide walls and the rough lath bottom was sealed with mastic. Plastic tape was used to seal the contact between the guide walls and the smooth bottom.

An inverted T-shaped manifold was fabricated for each source. The vertical inlet stem was a short piece of brass pipe which was soldered to the mid-point of a horizontal cross-piece. The cross-piece was a piece of $1\frac{1}{4}$-inch thin-walled brass tubing which was capped at both ends. The length of the cross-piece was slightly less than the width of the source. Outlet ports were made in each manifold by drilling a single line of holes along the length of the

cross-piece. The holes were spaced 1.25 cm apart in the manifold for the 20-cm-wide source, and 0.65 cm apart in the manifold for the 12.5-cm-wide source. The holes were approximately 0.25 cm in diameter; the holes were made slightly larger near the center and smaller near the ends in order to make the tracer concentration distribution more nearly uniform across the source.

Flow rates through these manifolds were the same or less than the flow rates through the manifold in the narrow 1-cm-wide source. The combination of these flow rates and manifold port sizes produced jets which penetrated the water to give sufficient mixing over the depth but did not excessively disturb the flow. The manifolds were tilted slightly to give the jets a small downstream component of momentum to oppose the hydraulic resistance of the guide walls on the flow between them. The downstream ends of the guide walls for both these sources were 17.8 meters downstream from the screen in the inlet box.

Almost all experiments with the 1-cm-, 12.5-cm-, and 20-cm-wide sources were conducted with the sources on the center line of the flume. To test the applicability of the data from the experiments to problems in which an effluent is discharged along the bank of a stream, a 10-cm-wide source was placed against the left sidewall of the flume. Data from experiments with this source were analysed as if the wall were a line of symmetry for the 20-cm-wide source. The 10-cm-wide source was constructed using a manifold similar

to those used in the 12.5-cm- and 20-cm-wide sources, but using only one guide wall, which was placed 10 cm from the sidewall of the flume.

3.4.2.3 Wide Source. The widest source used in the experiments occupied half the width of the 110-cm-wide flume. This source was used to study mixing of two wide parallel streams of the same depth and flowing with the same velocity but having different concentrations or densities. This wide source, shown in Fig. 3.7, was made by partitioning the flume along part of its length with a longitudinal dividing wall and spraying a tracer into one side of the flume. Because of the symmetry of the apparatus, one can observe simultaneously in one experiment the mixing of a heavy fluid into a light one, and a light fluid into a heavy one.

The dividing wall was 7.3 meters long and 20 cm high. The upstream end was 5.3 meters downstream from the screen in the inlet box of the flume. The wall was made from three pieces of 18-gage (0.049-inch) galvanized steel sheet which were put end to end. Each sheet was stiffened by bending the top at a right angle to form a narrow flange. The wall was laterally braced every 60 cm by wedging wooden struts between the wall and the sides of the flume. Leakage under the wall was prevented by sealing the contact between the wall and the smooth bottom with tape; the contact between the wall and the rough lath bottom was sealed with mastic.

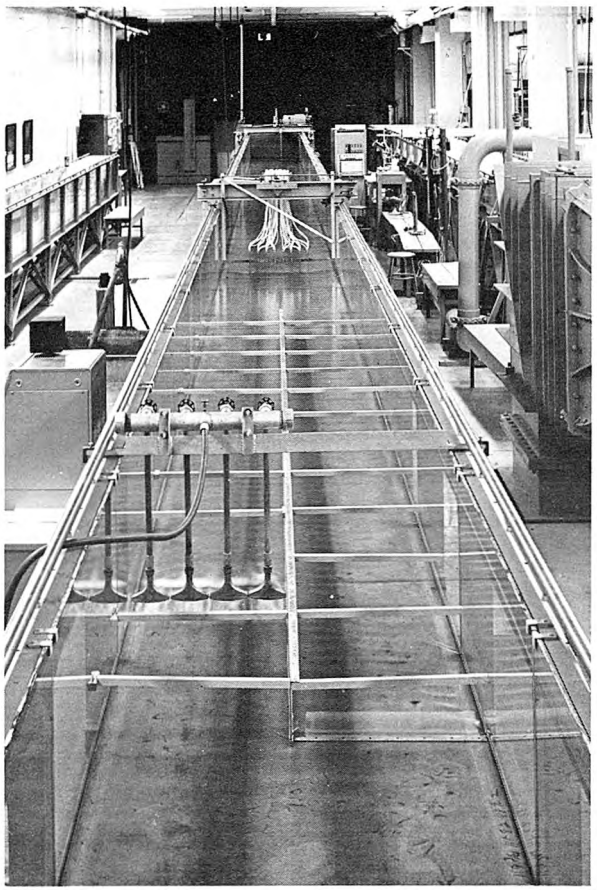

10048

Figure 3.7 Photograph looking down the flume. The splitter wall for the wide source is in the center, and the manifold is on the left.

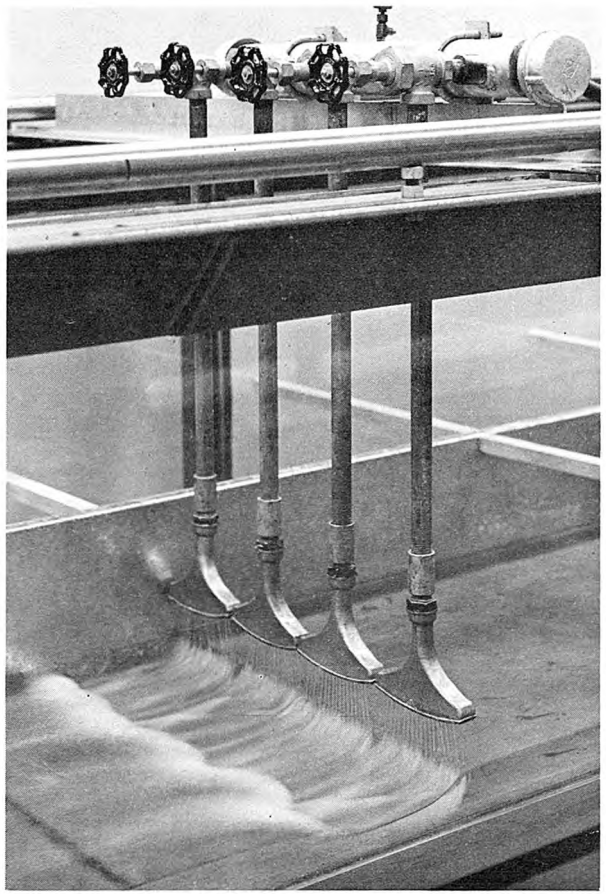

10034

Figure 3.8 The manifold for the wide source.

The tracer fluid was sprayed from a manifold into the flume on the left side (looking downstream) of the dividing wall. The manifold, which can be seen in Fig. 3.7 and in more detail in Fig. 3.8, was located approximately 1 meter downstream from the upstream edge of the wall. The tracer was sprayed into the flume through four fan-shaped, garden sprinklers. The flow rate through each sprinkler was regulated with a right angle globe valve.

The discharge from the sprinklers into the flume hindered the free flow of water down the flume on the left side of the splitter wall. Equal flow rates on both sides of the wall were obtained by slightly hindering the flow on the right side of the wall also. For this purpose a 1-inch by 3/16-inch galvanized steel bar was laid flat on the bottom across the right half of the flume at the upstream end of the dividing wall.

One can see in Fig. 3.8 that the discharge from the sprinklers caused a major disturbance to the flow. This disturbance decayed and the vertical velocity profiles became re-established before the flow reached the end of the dividing wall.

3.5 FLUID SAMPLING APPARATUS

Water samples were taken from the flume to obtain tracer distributions in cross-sections downstream from the source. For this purpose a suction type sampling system was constructed, which was capable of sampling at 40 points in a cross-section simultaneously. This system consisted of 8 rakes of 5 sampling tubes each, a pressure box to hold the rack of 40 test

tubes in which the samples were collected, a vacuum pump and a reservoir to supply suction, a compressed air source to purge the sampling lines and to stop the sampling, plus control valves and interconnecting tubing.

Each sampling rake (see Fig. 3.9 and 3.10) was made from five L-shaped brass tubes and a bracket. The tubes had a 1/8-inch outside diameter and a 0.085 inch inside diameter. The vertical positions of the tubes were adjustable in the brackets. The brackets were clamped onto a rectangular steel bar which was suspended across the flume from the instrument carriage. The lateral positions of the rakes could be changed by sliding them along the bar, and they could be rigidly clamped to the bar with a thumb screw. The lateral coordinates of the rakes were read to the nearest 0.1 cm on a scale which was cemented to the top surface of the bar and also on a scale which was laid on the bottom of the flume at the tips of the sampling tubes.

The water samples were collected in 40 test tubes contained in a pressure box which was mounted on top of the instrument carriage (see Fig. 3.10). The test tubes contained approximately 35ml samples each when filled. The pressure box was fabricated with a steel bottom and sides but with a transparent plastic top so that one could see when the test tubes were full. Nipples made from short pieces of 1/8-inch brass tubing penetrated the plastic top above each test tube. Lengths of transparent vinyl tubing connected the nipples to the sampling tubes.

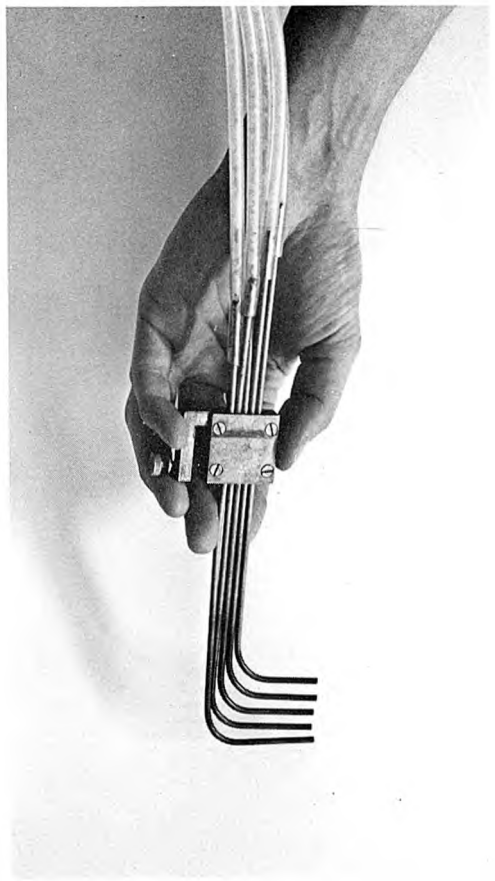

10041

Figure 3.9 A fluid sampling rake.

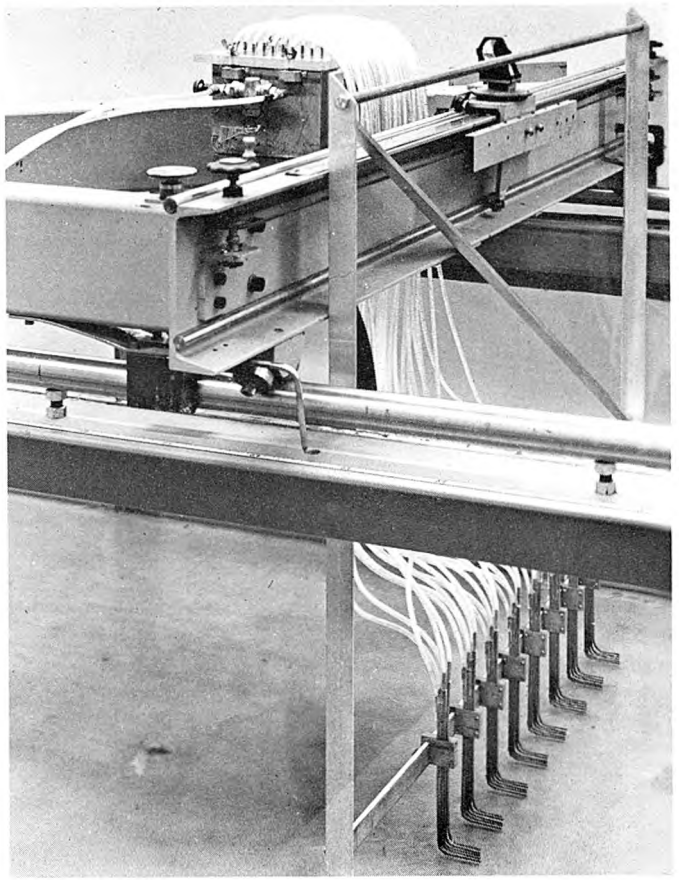

10046

Figure 3.10 The pressure box and sampling rakes on the instrument carriage.

The pressure inside the box could be made positive or negative as controlled with a three-port valve mounted on the box. Compressed air at 1.5 atmospheres was supplied through a pressure regulator from a central compressed air source in the laboratory. Suction up to one atmosphere was supplied from a 13-liter reservoir which was evacuated continuously with a vacuum pump. A needle valve was used to control the rate at which air was sucked out of the box. When the pressure in the box was negative, water flowed into the sampling tubes and discharged into the test tubes. When the pressure was positive, the water in the sampling lines was forced back into the flume. The lengths of tubing used in each of the sampling lines were identical so that the flow rate through each sampling line was the same.

3.6 SAMPLE ANALYSIS

3.6.1 Description of the Technique. The NaCl concentrations in water samples were determined by measuring the specific resistances and temperatures of the samples, and then calculating the concentrations using published data which relates the specific resistance to NaCl concentration and temperature. This concentration was used to calculate a relative concentration appropriately normalized with respect to the concentration of the tracer fluid in the mixing tank. The accuracy of this method is discussed in Subsection 3.6.2.

The specific resistance of each sample was measured with an electronic bridge (Model RC 16) and pipette cell (CEL G1) both manufactured by Industrial Instruments, Inc. Because the specific resistance of a solution is a function of temperature, the samples were put into a constant temperature bath prior to analysis. All samples from any one experiment were analyzed within 0.1°C of some arbitrary reference temperature, which was usually close to the room temperature, 21°C. The specific resistance of a sample at 18°C was calculated from the measured specific resistance and temperature by using the formula

$$R_{18^o} = R_{T^o} \Big/ \left[1-(0.020/^oC)\,(T^o-18^o)\right] , \qquad (3.1)$$

where R_{18^o} and R_{T^o} are the specific resistances at 18° and T°C, respectively. The temperature coefficient 0.020/°C is an average value for NaCl solutions between 18° and 25°C. Table 3.1, a table of NaCl concentrations and their logarithms as a function of specific resistances at 18°C and their logarithms, was prepared from data in Ref. 27, Vol. 6, p 233. The NaCl concentrations of the samples were calculated by using linear interpolation in the logarithmic columns of this table. This interpolation scheme was used because it is more accurate than linear interpolation in the arithmetic columns and is more convenient than using higher order schemes.

When using Table 3.1 it is necessary to assume that NaCl is the only material present in a water sample which affects its specific resistance. Because tap water containing other dissolved

Table 3.1 Specific resistance at 18°C as a function of NaCl concentration.

NaCl Concentration c 10^{-3} moles/liter	$\text{Log}_{10} c$	$\text{Log}_{10}(R_{18^\circ})$	Specific Resistance R_{18° ohm·cm
0.1	-1.00000	4.96706	92695.0
0.2	-0.69897	4.66715	46468.0
0.5	-0.30103	4.27184	18700.0
1.0	0.00000	3.97359	9410.0
2.0	0.30103	3.67651	4748.0
5.0	0.69897	3.28592	1931.6
10.0	1.00000	2.99260	983.1
20.0	1.30103	2.70157	503.0
50.0	1.69897	2.32098	209.4
100.0	2.00000	2.03703	108.9
200.0	2.30103	1.75679	57.12
500.0	2.69897	1.39375	24.76
1000.0	3.00000	1.12969	13.48
2000.0	3.30103	0.88829	7.732
3000.0	3.47712	0.77159	5.910
4000.0	3.60206	0.76849	5.868

Table 3.2 Data from tests to check accuracy of technique for determining relative concentrations.

Tracer Fluid A[1]		
Actual Relative Concentration C	Concentration from Table 3.1 c 10^{-3} moles/liter	Calculated Relative Concentration C
1	174	0.9096
0.1000	30.4	0.0994
0.0500	21.7*	0.0500
0.0200	16.4	0.0199
0.0100	14.7	0.0102
0.0040	13.6	0.0040
0.0010	13.0	0.0006
0	12.9**	0

[1] Tracer fluid made by adding approximately 10.3 gm NaCl and (10.3 gm)·(3.88)=40.0 gm methyl alcohol to water to make 1.000 liters of solution.

* Concentration c_{dt}

** Concentrations c_a and c_d

Tracer Fluid B[2]		
Actual Relative Concentration C	Concentration from Table 3.1 c 10^{-3} moles/liter	Calculated Relative Concentration C
1	587	0.9965
0.1000	68.0*	0.1000
0.0100	15.8	0.0099
0.0010	10.7	0.0010
0.0001	10.2	0.0001
0	10.1**	0

[2] Tracer fluid made by adding 34.2 gm Na Cl to water to make 1.000 liters of solution.

* Concentration c_{dt}

** Concentrations c_a and c_d

salts was used in all experiments, and because dye and methyl alcohol were sometimes added to the tracer fluids, the assumption is not true. However, the data given in Subsection 3.6.2 show that the errors introduced into this study by the use of Table 3.1 are small.

For the purpose of this study, only the relative concentrations of tracer in the samples were required; absolute NaCl concentrations were not needed. The scale for the relative concentration was usually chosen so that the concentration of the ambient fluid was zero and the concentration of the tracer fluid in the mixing tank was unity. The relative concentration, C, of a sample was defined by the expression

$$C = \frac{c - c_a}{c_t - c_a} , \qquad (3.2)$$

where c, c_a and c_t are the apparent NaCl concentrations of the fluid sample, the ambient fluid, and the tracer fluid in the mixing tank. In the experiments with two wide parallel streams, C was redefined so that it equalled unity for one stream and zero for the other. Both c and c_a were obtained by measuring the specific resistances of the solutions and then using Table 3.1; however, c_t was determined from the specific resistance of a diluted tracer solution for reasons given below.

Because the NaCl concentrations in the tracer fluids were relatively high, their specific resistances were low and were difficult to measure accurately with the bridge and cell that were used.

Also the concentrations of methyl alcohol in the neutrally buoyant tracer fluids had measurable effects on the specific resistances of these fluids. Therefore, tracer fluids were diluted about 20 or 50 to 1 to raise their specific resistances to acceptable levels and to minimize the effects of methyl alcohol. The specific resistances of the diluted tracer fluid and the diluting fluid were measured, and their NaCl concentrations were obtained from Table 3.1. The NaCl concentration of the tracer fluid, c_t, was calculated with the formula

$$c_t = c_{dt}D - c_d(D-1) , \qquad (3.3)$$

where c_{dt} and c_d are the NaCl concentrations of the diluted tracer fluid and the diluting fluid, and D is the dilution ratio defined as the volume of the diluted tracer fluid divided by the volume of the tracer fluid. The concentration c_t given by Eq. 3.3 was used in Eq. 3.2 to calculate the relative concentration, C.

3.6.2 Accuracy of the Technique. The accuracy of the above technique for determining C, the relative concentration, was tested for several different tracers. The tests showed that the accuracy of the technique was better than 2 percent of the peak concentration (C= 0.03) typically observed in a cross-section. The results of two of these tests are given in Table 3.2.

In each test known dilutions of a tracer were prepared. The specific resistance of each dilution was measured, and C was calculated according to the procedure given in the preceding section.

Tracer A was a typical neutrally buoyant tracer fluid made by adding salt, alcohol, and dye to water taken from the flume. Tracer B was a dense tracer fluid made by adding only salt to water. The accuracy was good over most of the range $0 < C < 0.1$ for both of these tracers. The apparent error at $C = 0.0010$ for tracer A is due to the poor resolution of the difference $c - c_a$ in Eq. 3.2. The accuracy at $C = 1$ for tracer A was poor because of the effect of alcohol on the specific resistance of the fluid. The accuracy was good over the entire range of C for tracer B because the higher salt concentrations gave better resolutions at the lower values of C and because there was no alcohol in the tracer fluid to cause errors at the high values of C.

Additional tests were made to determine more specifically the effects of alcohol and dye on the specific resistances of the solutions. The tests showed that the effects were not important at the concentrations found in samples taken during experiments.

3.7 MEASUREMENTS OF FLUID DENSITY

The difference between the density of the tracer fluid discharged from the source, ρ_1, and the density of the ambient fluid in the flume, ρ_a, was obtained from measurements of the specific gravities of the tracer fluid in the mixing tank and the ambient fluid in the flume. The densities in gm/cm^3 were assumed to equal the specific gravities. The specific gravities of fluids with densities between 0.993 gm/cm^3 and 1.038 gm/cm^3 were measured with a

hydrometer graduated in increments of 0.001 and which could be read to the nearest 0.0002. Fluids with densities outside this range were either diluted with water from the flume to make their densities fall within this range or their specific gravities were measured with a hydrometer with a wider range but which was graduated in increments of 0.005 and which could be read only to the nearest 0.001. The difference between the densities of the fluid in the mixing tank, ρ_t, and the density of the ambient fluid could always be determined with an accuracy of better than two percent of the difference.

In experiments with the narrow 1-cm-wide source, fluid from the mixing tank was discharged undiluted from the source. Therefore, in these experiments the difference $\Delta\rho = \rho_1 - \rho_a$ was equal to $\rho_t - \rho_a$.

In experiments with wider sources, the tracer fluids from the mixing tank were diluted between the guide walls of the sources; as a result, the differences, $\Delta\rho$, usually were too small to be determined accurately by measuring with a hydrometer the specific gravities of the ambient fluids and the diluted tracer fluids which were discharged from the sources. Therefore, $\Delta\rho$ was calculated from the densities of the undiluted fluid in the mixing tank, ρ_t, and the density of the ambient fluid, ρ_a; from the relative concentration, C, of the fluid discharged from the source; and by using a graph of the difference in densities between salt water and fresh water as a function of salt concentration. The graph was prepared from data

in Ref. 28 p.1909. This graph was also used to determine ρ_t from measurements of the specific gravity of diluted tracer fluids. To calculate $\Delta\rho$ for these experiments, a concentration corresponding to a density difference of $\rho_t - \rho_a$ was obtained from the graph. This concentration was multiplied by the relative concentration of the fluid discharged from the source. The quantity $\Delta\rho$ was then read from the graph as the density difference corresponding to a concentration equal to the above product. The accuracy of $\Delta\rho$ determined by this method is believed to be better than 4 percent.

3.8 EXPERIMENTAL PROCEDURES

3.8.1 Preparation. In preparation for an experiment, uniform flow was established in the flume, and the tracer fluid was prepared in the mixing tank. Uniform flow was established in the flume by adjusting the speed of the main pump to give the desired flow rate in the flume, by setting the slope of the flume to the proper grade for that discharge and the desired normal depth, and by adjusting the elevation of the weir at the downstream end of the flume until normal depth existed a few meters upstream from the weir. Because the flow was subcritical, uniform flow at normal depth existed upstream from this point. The tracer-fluid pump was used to pump water from the 16-inch pipe to the source while uniform flow was being established.

The proper slope for uniform flow at a particular discharge and depth was determined by trial and error in previous experiments.

Periodic checks showed that this slope did not vary with time, nor was it a function of the type of source, if any, in the flume. Losses caused by flow around the sampling tubes did not measurably affect the water depth.

The tracer was prepared by first filling the mixing tank with water to the level of one of several reference marks on the wall of the tank. A measured amount of salt and alcohol (if any) were added to the water, and the solution was mixed thoroughly. Sometimes dye was added also. The specific gravities of water samples taken from the flume and from the mixing tank were measured. If the tracer fluid was supposed to be neutrally buoyant, a small sample of dyed tracer fluid was put into a beaker of quiescent water taken from the flume. The motion of the dyed tracer fluid was observed to assure that the two fluids were the same density.

The temperature of the water in the flume and the tracer fluid in the mixing tank were measured in place. In the majority of the experiments the temperature of the water in the flume was within $1^{\circ}C$ of $20.5^{\circ}C$, and the temperature of the water in the mixing tank seldom differed from the temperature of the water in the flume by more than $1^{\circ}C$.

3.8.2 Positioning the Sampling Tubes. The vertical positions of the sampling tubes in the sampling rakes were set before the start of an experiment. The vertical coordinates of respective tubes in all rakes were the same and were not changed during an experiment. The sampling tubes in a rake were spaced closer

together in the region where vertical concentration gradients were the largest. In experiments with dense tracers the sampling tubes were spaced closer together near the bottom of the flume. For convenience and consistency this same spacing was used in experiments with neutrally buoyant tracers. In the two experiments with a light tracer fluid the tubes were spaced closer together near the surface.

The lateral spacing of the sampling rakes in a cross-section depended on the width of the tracer plume in each cross-section. In the experiments with the sources of narrow and intermediate width, the rakes were spaced approximately uniformly across that part of the cross-section occupied by the tracer plume. In the experiments with the wide source, the rakes were distributed across the mixed zone between the two fluid masses. The width of the tracer plume or mixed zone was estimated in advance from the widths at other cross-sections during the same experiment or from data from previous experiments. Widths estimated by visually observing a dyed tracer plume were usually too narrow.

3.8.3 Taking the Samples. When the above preparations were complete and the sampling tubes were distributed across the desired cross-section, tracer fluid was pumped from the mixing tank through the source into the flume. After about one minute, which was required for the tracer distribution in the flume to reach a steady state, the pressure box containing the test tubes for the water samples was put under positive pressure to blow out the water present in

the sample lines. Next, the box was put under vacuum and water from the flume was drawn up into the lines. Just before the water was about to be discharged into the test tubes, the box was again put under positive pressure to purge the lines. To assure that the samples to be taken would not be contaminated, the sampling lines were filled and purged at least three times before water was allowed to flow into the test tubes. The rate at which air was removed from the pressure box was regulated so that water entered the sampling tubes at a velocity equal to or less than the free stream velocity. About 20 seconds were required to fill the test tubes. When the test tubes were full, the box was put under positive pressure to stop the sampling and the tracer-fluid pump was shut off. The test tubes were then taken out of the pressure box and an empty set was put in. Next, the carriage was moved to a different cross-section, the sampling rakes were redistributed across the width, and the sampling procedure was repeated.

Every time samples were taken from the flume to determine the concentration distribution in a cross-section, a 100 ml sample was siphoned from the flume upstream from the source to define the tracer concentration of the ambient fluid. Changes in concentration of the ambient fluid during the 20 seconds required to take the samples were too small to be detected.

3.9 EXPERIMENTS WITH FLOATING PARTICLES

3.9.1 Apparatus. The additional material and equipment needed to study the lateral diffusion of floating particles were: the particles, a device for putting them into the flume, and a device for determining their lateral distributions at locations downstream.

The experiments were made with polyethylene particles which had a specific gravity of 0.95; a sample is shown in Fig. 3.11. All particles passed through a No. 5 sieve (0.396-cm-diam.) and were retained on a No. 6 sieve (0.337-cm-diam.). Individual particles were dropped manually into the flume through a funnel. The tip of the funnel was about 1 cm above the water surface. The particles were always dropped onto the center line of the flume at the downstream end of the tracer-fluid source, if one were being used. If no source was in the flume, the particles were introduced into the flume 15 meters downstream from the inlet screen.

The particles were caught at various distances downstream in a compartmented-sieve particle collector. The particle collector, shown in Fig. 3.12, was constructed similar to those used by Orlob (7), and also by Sayre and Chamberlain (8) and by Sayre and Chang (5). It was 104 cm wide, 5.5 cm high, and 1.6 cm deep. The back and bottom of the collector was made from one piece of wire mesh (8 mesh/inch) screen which was fastened to the back of a rigid aluminum bar. The screen was divided into 104 compartments, each 1 cm wide, by strips of 26-gage (0.018-inch) stainless steel sheet. Each of the compartments was numbered. The entire

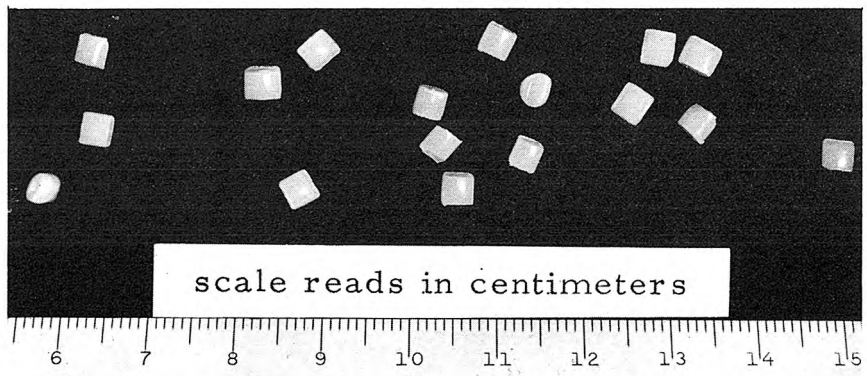

10032

Figure 3.11 Sample of polyethylene particles used in study of lateral diffusion at the free surface.

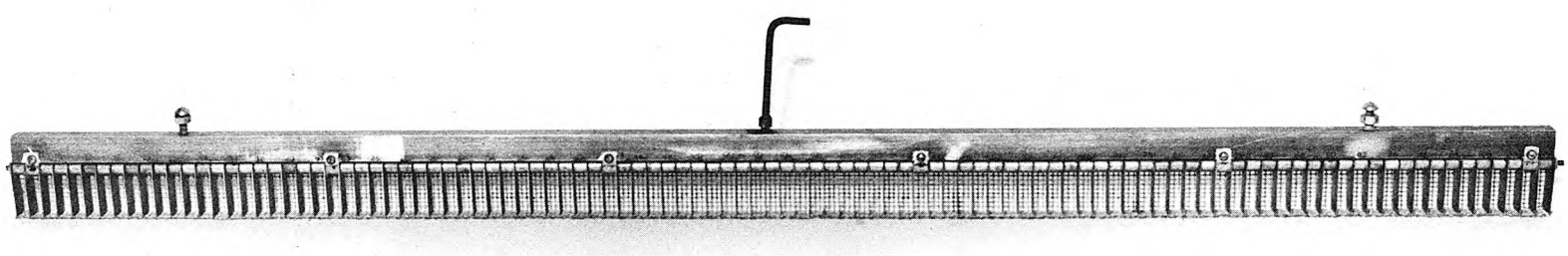

10040

Figure 3.12 Compartmented-sieve particle collector; the compartments are 1 cm wide.

assembly was suspended from the instrument carriage across the flume with the bottom 1/2 cm of the collector submerged. A particle floating downstream was stopped by the screen and remained in one compartment until purposely removed.

3.9.2 Procedures. In preparation for the experiments to observe lateral diffusion of particles at the free surface, uniform flow was established in the flume. If a tracer source were in the flume, water was pumped from the 16-inch pipe to the source. The flume slope, water discharge, and water depth were adjusted with the particle collector in the flume by following the procedures described in Section 3.8. The particle collector had a small influence on the water depth; therefore, the elevation of the weir had to be changed in order to maintain uniform flow upstream from the particle collector whenever the collector was moved.

During an experiment, particles were dropped individually into the flume at intervals of 3 to 5 seconds until 50 to 80 particles were caught in the collector at some cross-section downstream. The collector was then taken out of the flume and the number of particles in each compartment was counted and recorded. Next, the collector was emptied and put back into the flume. This process was repeated until an accumulated total of approximately 400 particles were collected at a cross-section. The collector was then moved to a different cross-section, the elevation of the weir was adjusted, and particles were collected at the new location.

The average velocity of the particles was determined during each experiment by measuring the length of time required for particles to travel a measured distance of about 20 meters. The velocities of 20 particles were calculated and averaged in each experiment.

The data from the experiments were used to calculate the variance, σ_s^2, of the lateral distribution of particles collected in each cross-section. The variance and velocity were used to calculate diffusion coefficients, which are presented in Chapter 4.

Visual observations during the experiments showed that the collector was capable of holding 50 to 80 particles without seriously disturbing the flow pattern in front of the collector and without allowing particles to move from one compartment to another. Visual observations also showed that dropping the particles at 3 to 5 second intervals spaced them far enough apart so that the motion of any one particle was statistically independent of the motion of the others.

The number of particles collected at a cross-section, 400, was a compromise between a larger number, which would yield a better estimation of σ_s^2 but would require more effort, and a smaller number, which would require less effort but would give a poorer estimate of σ_s^2. If the motion of each particle were statistically independent of the motion of all others, the error in the experimental determination of σ_s^2 can be estimated from the

statistical properties of the variances of samples taken from a normal population. The error in σ_s^2 as a function of the number of particles collected was calculated from the chi-square probability distribution (see e. g. Mendenhall (29) p. 205, and tables and approximate formulae by Abramowitz and Stegun (30) p. 941, 984-985); the results of the calculations are tabulated in Table 3. 3. The number 400 was selected subjectively after observing the data in this table.

Table 3. 3 Probability that the error in σ_s^2 is exceeded as a function of the number of particles collected.

Number of Particles	Error			
	±5%	±10%	±15%	±25%
100	0. 70	0. 47	0. 28	0. 09
200	0. 60	0. 31	0. 14	0. 02
400	0. 47	0. 16	0. 04	<0. 01
800	0. 31	0. 05	<0. 01	<0. 01

CHAPTER 4

EXPERIMENTAL DATA

Experimental data are presented in the three sections of this chapter. In the first section, the hydraulic data for the flows used in the experiments are given; in the second, data from the experiments performed to observe lateral mixing of fluids are presented; in the third, data from the experiments with floating particles are given.

4.1 HYDRAULIC DATA

Five different flows were used in the experiments. The hydraulic data for each of these flows is given in Table 4.1 and a brief explanation of the data in each column is given below.

4.1.1 Flow Condition Code and Flume Bottom. The flow condition codes in Col. 1 are introduced here for convenient use later. The letters S or R denote whether the bottom was stainless steel plate or if the bottom was rough metal lath.

4.1.2 Water Depth. The water depth given in Col. 3 is the average of 10 or more measurements made along the axis of the flume. The average depth was reproducible from one experiment to the next to within 0.02 cm; however, the depths measured at some of the individual points differed from the average by more

Table 4.1 Summary of hydraulic data.

(1)	(2)	(3)	(4)	(5)	(6)	(7)	(8)	(9)	(10)	(11)	(12)	(13)
Flow Condition Code	Bottom	Depth d (cm)	Slope S	Shear Velocity $u_* = \sqrt{gdS}$ (cm/sec)	Metered Discharge (cm^3/sec)	Discharge Velocity (cm/sec)	Difference Between Computed and Metered Discharges	Velocity in Central 60 cm of Flume $\bar{u}$ (cm/sec)	von Karman's k	Friction Factor $f = 8\left(\frac{u_*}{\bar{u}}\right)^2$	Reynolds Number $\frac{4\bar{u}d}{\nu}$	Froude Number $\frac{\bar{u}}{\sqrt{gd}}$
S1	stainless steel plate	4.05	0.000961	1.96	15,300	34.4	2.6%	35.4*	0.405	0.0246	5.78×10^4	0.562
S2	stainless steel plate	6.55	0.000803	2.27	31,600	43.8	3.6%	45.2**	0.359	0.0202	1.19×10^5	0.564
S3	stainless steel plate	11.1	0.000432	2.17	54,500	44.6	1.8%	46.0	0.389	0.0178	2.06×10^5	0.441
R1	rough lath	3.90 (4.05)	0.00391	3.86 (3.94)	15,300	35.7 (34.4)	1.4%	37.3 (35.9)	0.355 (0.311)	0.0854 (0.0963)	5.87×10^4	0.601 (0.569)
R2	rough lath	6.40 (6.55)	0.00284	4.23 (4.28)	31,600	44.8 (43.8)	4.8%	45.9 (44.8)	0.370 (0.373)	0.0680 (0.0731)	1.18×10^5	0.580 (0.560)

* Average of four experiments

** Average of two experiments

Numbers in parentheses are data from experiments with rough lath bottom uncorrected for blockage.

than 0. 10 cm partly because of difficulties in estimating the mean position of a wavy water surface but mostly because of slight warps in the stainless steel plate bottom.

The depth measured in the laboratory was the distance between the water surface and the stainless steel bottom; however, for those flows with the rough lath bottom this distance was corrected by subtracting 0. 15 cm in order to adjust the cross-sectional area for blockage caused by the lath in the lower 0. 31 cm of the cross-section (see Fig. 3. 3). Better agreement between data from experiments with the smooth bottom and data from experiments with the rough bottom was obtained when the corrected depth was used in the analysis in Chapter 5. Similar corrections have been made by other investigators who studied flow over very rough surfaces. (See, for example, Einstein and El Samni (31), and Taylor (32).) The corrected depths are given in Col. 3 and are used in the computations of the other hydraulic parameters. For comparison, hydraulic parameters calculated using the uncorrected depths are given in parentheses.

4. 1. 3 Slope. The slope given in Col. 4 is the slope of the energy grade line, which is also equal to the slope of the water surface and bottom of the flume. A profile for flow S2 is shown in Fig. 4. 1. The elevation of the bottom given in Fig. 4. 1 was determined by measuring the distance between the bottom and a still water level. The accuracy of the slope is governed mostly

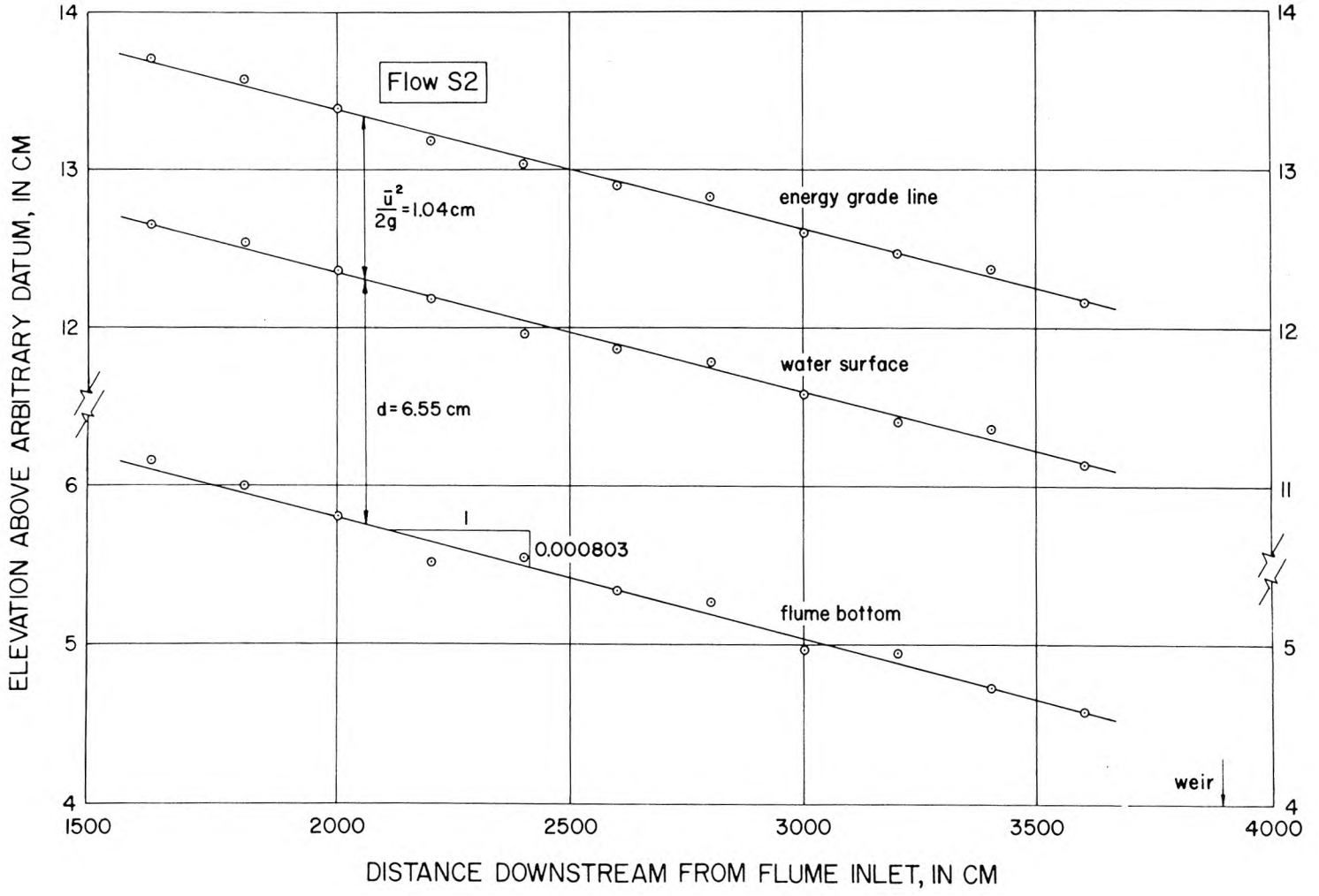

Figure 4.1 Profiles of the energy grade line, water surface, and flume bottom for flow S2.

by the accuracy of the measurement of the change in water surface elevation in a distance of 20 meters. The probable error is about ±0.04 cm/2000 cm = ±0.000020.

4.1.4 Shear Velocity. The bottom shear velocity, u_*, given in Col. 5 was calculated from the expression

$$u_* = \sqrt{gdS} \ , \tag{4.1}$$

which is valid for infinitely wide channels but gives values slightly too large when used for channels of finite width because of the shear on the side walls.

4.1.5 Metered Discharge and Discharge Velocity. The discharge in Col. 6 is the sum of the discharge entering the upstream end of the flume, which was measured with the venturi meter, and the discharge pumped from the mixing tank, which was measured with the variable area flowmeter. The flow pumped to each of the sources, except the widest, was about 1 percent of the total; the flow to the widest source was about 3 percent of the total. The error in the sum is governed by the error in the venturi meter calibration, which is probably less than 1 percent.

The discharge velocity given in Col. 7 was obtained by dividing the discharge in Col. 6 by the cross-sectional area which is the product of the depth, given in Col. 3, and the flume width, 110 cm.

4.1.6 Velocity in Central 60 cm of Flume. The mean velocity in the central 60 cm of the flume cross-section, where most of the mixing in the experiments occurred, was calculated from velocities measured with the pitot-static tube and from the metered discharge.

Cross-sections of the flume showing isovels for each of the flows are presented in Fig. 4.2, and some vertical velocity profiles for flows S1 and R1 are shown in Fig. 4.3.

Velocity profiles were measured along vertical lines spaced 4 to 10 cm apart in the central part of the flume and closer together near the side walls. The velocities measured at 0.2, 0.4, and 0.8 depths from the stainless steel bottom were averaged to estimate the average velocity for each profile. These average velocities were multiplied by the depth and integrated across the central 60 cm of the flume to give a discharge through that part of the cross-section. The discharge through the total cross-section was calculated in the same way. Because the calculated total discharge was always a few percent greater than the metered discharge (by the amount shown in Col. 8), and because the metered discharge is probably more accurate, the discharge through the central 60 cm of the flume was corrected by subtracting the percentage shown in Col. 8. This corrected discharge through the central 60 cm of the flume was used to compute the mean velocity, $\bar{u}$, listed in Col. 9.

4.1.7 von Karman's k. Values of von Karman's k were calculated using Eq. 4.2 with the slopes of the velocity profiles drawn on semi-logarithmic coordinates, and the shear velocity in Col. 5;

$$k = 2.3\, u_* / \text{(change in u per } \log_{10} y \text{ cycle)}. \qquad (4.2)$$

The values given in Col. 10 are averaged over the central 60 cm of the flume cross-section. Velocity profiles with local values of k for flows S1 and R1 are shown in Fig. 4.3.

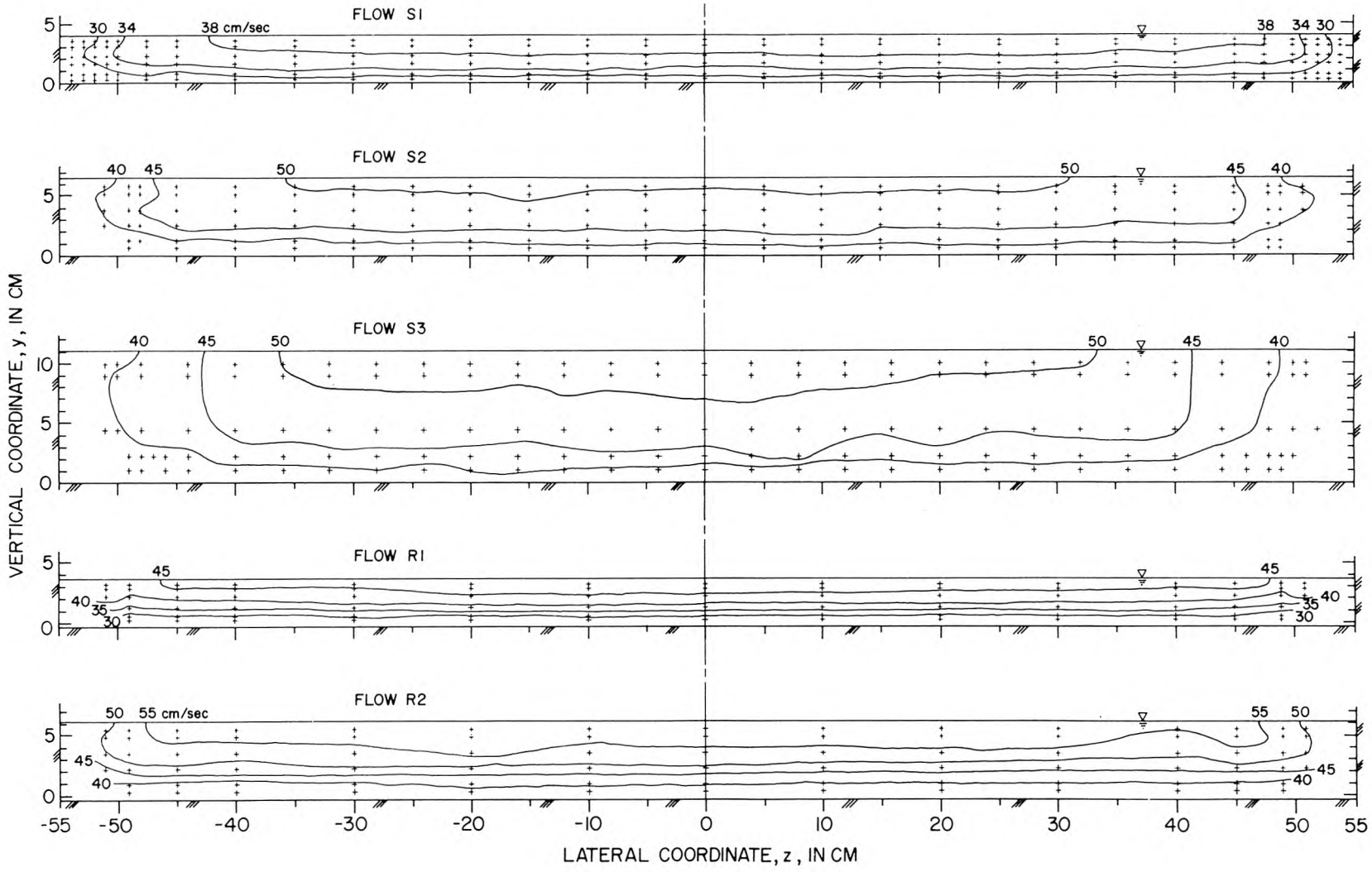

Figure 4.2 Cross-sections of the flume showing isovels 25 meters downstream from the flume inlet. Crosses designate points where the velocity was observed. For flows R1 and R2, y is measured from a plane 0.15 cm above the stainless steel bottom.

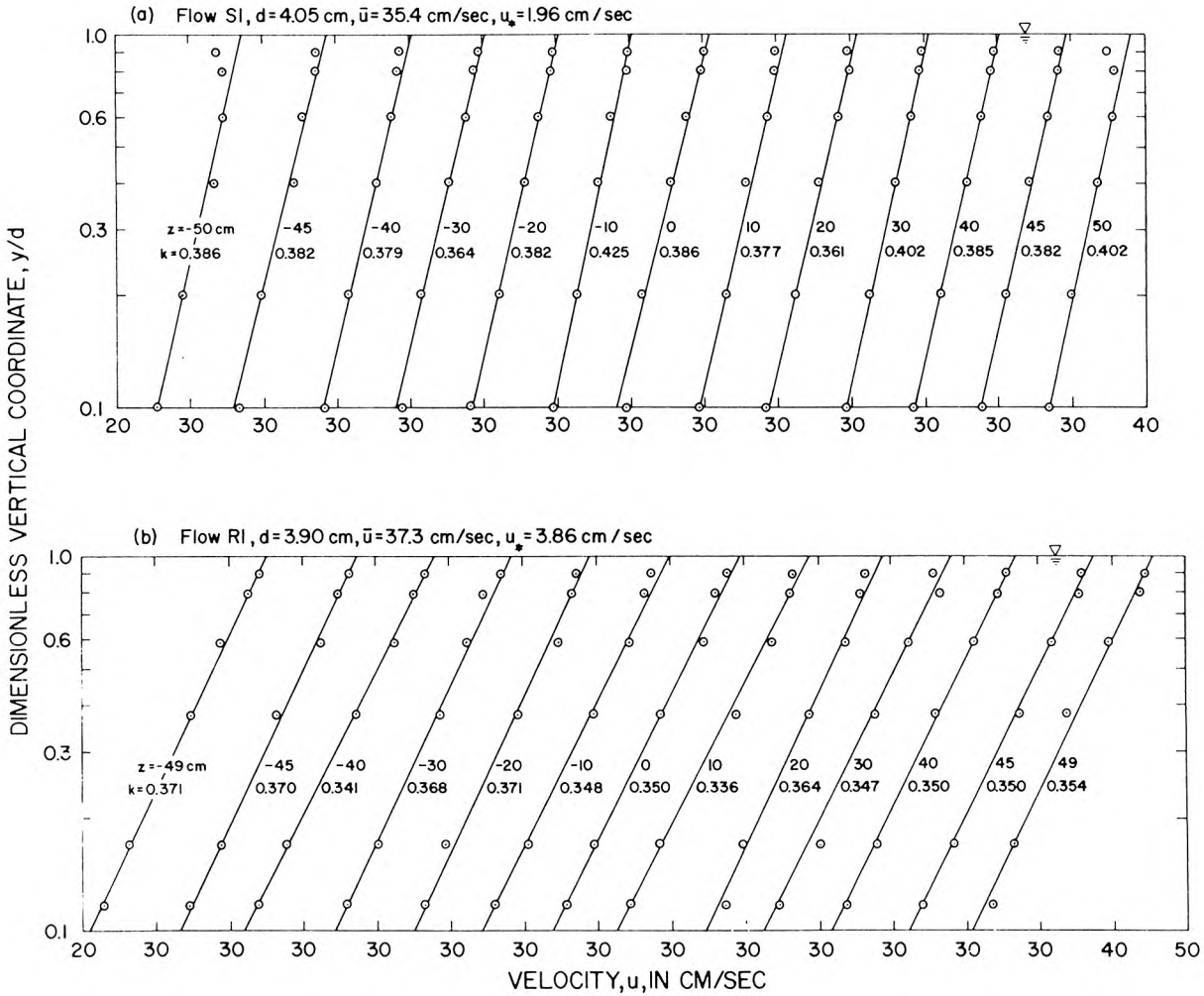

Figure 4.3 Velocity profiles observed 25 meters downstream from the flume inlet. (a) Flow S1, (b) Flow R1. The lateral coordinate z is measured from the flume center line, and k is von Karman's constant. For flow R1, y is measured from a plane 0.15 cm above the stainless steel bottom.

4.1.8 Friction Factors. The friction factors given in Col. 11 were calculated with the formula

$$f = 8\left(\frac{u_*}{\overline{u}}\right)^2 , \qquad (4.3)$$

where u_* and $\overline{u}$ were obtained from Col. 5 and 9, respectively. Data from experiments with flow over the plain stainless steel plate bottom showed that this boundary is in transition between hydraulically smooth and rough. The equivalent sand grain roughness for the steel plate boundary is about 0.013 cm. Data from experiments with the rough lath bottom showed that this boundary is hydraulically rough. The equivalent sand grain roughness for the lath is about 1.1 cm but is a function of the water depth.

4.1.9 Reynolds Number and Froude Number. The Reynolds numbers in Col. 11 and Froude numbers in Col. 12 were calculated using the depths in Col. 3 and the velocities in Col. 9. A viscosity of 0.991×10^{-2} cm^2/sec, which is the viscosity of water at 20.5° C, was used in the calculations of the Reynolds numbers.

4.2 EXPERIMENTS WITH FLUID TRACERS

4.2.1 Introduction. In this section, data are presented from experiments performed to observe lateral mixing of tracer fluids of different densities. Although most analyses and interpretations of the data are given in Chapter 5, this section includes the methods used to reduce the basic data to obtain some of the dependent integral parameters which are used in the subsequent analyses.

Because of the large volume of the data, the concentrations observed at all the points in all the experiments are not included in this text. Instead,these data have been made available in Ref. 1 (Technical Memorandum 70-3 of the W. M. Keck Laboratory of Hydraulics and Water Resources, California Institute of Technology, Pasadena, California 91109). A sample of the data from one of the experiments, as given in the Memorandum, is given in this section. Also, samples of reduced data from various experiments, including most of the different cases studied, are presented graphically in this section. These data include detailed concentration distributions in cross-sections, lateral distributions of the depth-averaged concentrations, and vertical concentration profiles. The variances of the lateral distributions of the depth-averaged concentrations, and averaged coefficients of variation for the theoretical concentration distributions are presented for all experiments in this section because they form the basis for the analyses in Chapter 5.

A list of all experiments made with tracer fluids with some of the parameters is given in Table 4.2.

Table 4.2 List of experiments with tracer fluids.

Experiment Number	Flow Condition Code	Source Width b (cm)	Density Difference[1] $\Delta\rho/\rho_a$	Pages With Data Presented Graphically	Pages With Photographs
113	S2	1.0	0.0160	68,84,111,131	124
114	S2	1.0	0.0160	111	
115	S2	1.0	0	111	
116	S2	1.0	0	67,83,111,130	124
117	S2	1.0	0.0307	111	
118	S2	1.0	0.0304	111	124
120	S1	1.0	0	106	120
121	S1	1.0	0.0158	106	120
122	S1	1.0	0.0318	106,164	
125	S3	1.0	0	82,102,113	
127	S3	1.0	0.0159	113	
128	S2	1.0	-0.0158	69,85,111,132	124
129	S3	1.0	0.0078	113	
130	S1	1.0	0.0453	106	120
136	S1	20.0	0	108	
137	S1	20.0	0.00088	108	
139	S1	20.0	0	108	123
140	S1	20.0	0.00158	108,164	
141	S1	20.0	0.00238	108	
142	S1	20.0	0.00487	108	123
143	S1	20.0	0.00270	108	123
144	S1	20.0	0.00373	108	
147	S1	1.0	-0.0164	106	120
150	S2	20.0	0	88,112	
151	S2	20.0	0.00079	112	
152	S2	20.0	0.00186	89,112	
153	S2	20.0	0	112	
154	S2	20.0	0.00121	112	
156	S1	12.5	0		
157	S1	12.5	0		
158[a]	S1	12.5	0.00132		
159[a]	S1	12.5	0.00283		
160[a]	S1	12.5	0.00431		
161[a]	S1	12.5	0.00636		
162	S1	12.5	0	107	
163	S1	12.5	0.00138	107	
164	S1	12.5	0.00275	107,164	
165	S1	12.5	0.00414	107	
166	S1	12.5	0	107	
167	S1	12.5	0.00543	107	
170	S1	2X10	0	109	
171	S1	2X10	0.00145	109	
172	S1	2X10	0.00414	109	
175	S1	WIDE	0	110	
177	S1	WIDE	0	76,91,94,110,133	126
178	S1	WIDE	0.00057	110	
179	S1	WIDE	0.00114	110	
180	S1	WIDE	0.00173	110	
181	S1	WIDE	0.00232	77,92,94,110,134	
183	S1	WIDE	0.00286	110	126
192	R2	1.0	0	116	
193	R2	1.0	0	116	
194	R2	1.0	0.0545	116	
195	R2	1.0	0.0360	116	
196	R1	1.0	0	114	121
197	R1	1.0	0.0388	114	121
198	R1	1.0	0.0756	114	121
199	R2	20.0	0	117	
200	R2	20.0	0.00263	117	
201	R2	20.0	0.00406	117	
202	R2	20.0	0.00571	117	
203	R1	WIDE	0	115	
204	R1	WIDE	0	115	125
205	R1	WIDE	0.00432	115	
206	R1	WIDE	0.00861	115	
207	R1	WIDE	0.0114	115	125

[1] $\Delta\rho/\rho_a > 0$ denotes tracer fluids more dense than ambient fluid.
$\Delta\rho/\rho_a < 0$ denotes tracer fluids less dense than ambient fluid.

[a] Data from these experiments not used in analyses.

4.2.2 Concentration Distributions in Cross-Sections. The relative concentration, C, of tracer fluid in each of the samples collected during an experiment was determined by the procedure given in Chapter 3. All calculations were done on a digital computer. The computer output giving the relative concentration at each of the 40 sampling points in each cross-section for a typical experiment, Exp. 113, is shown in Table 4.3. Ref. 1 is made up of similar tables for all experiments. The longitudinal coordinate x is measured from the downstream end of the source, y is the distance above the stainless steel bottom of the flume, and z is measured laterally, usually from the center line of the source. The rows labeled AVE., and C.V. are depth-averaged concentrations, and coefficients of variation for the vertical concentration distributions, respectively. The precise definition used in the calculation of both these quantities is given later.

The concentration distributions in cross-sections downstream from the 1-cm-wide source are shown for three experiments in Fig. 4.4, 4.5, and 4.6. The hydraulic conditions for all three experiments were the same; only the differences in density between the tracer and ambient fluids were different. In Exp. 116, shown in Fig. 4.4, the densities of the ambient and tracer fluids were equal. The variation in tracer concentration over the depth was small in cross-sections 500 cm or more downstream from the source, but the tracer had spread over a slightly greater width in the upper part of the flow than in the lower part. The

Table 4.3 Sample table from Ref. 1. AVE is depth-averaged concentration; C. V. is coefficient of variation for vertical concentration distribution.

EXPERIMENT NO. 113

RELATIVE CONCENTRATIONS AT X= 200 CENTIMETERS

Z (CM) / Y (CM)	-14.0	-9.0	-4.0	0.0	2.0	6.0	11.0	17.0
6.0	0.0007	0.0048	0.0121	0.0137	0.0130	0.0091	0.0017	0.0001
4.0	0.0020	0.0183	0.0335	0.0257	0.0263	0.0322	0.0082	0.0002
2.5	0.0054	0.0487	0.0645	0.0432	0.0454	0.0625	0.0196	0.0002
1.5	0.0074	0.0816	0.0934	0.0625	0.0653	0.0890	0.0311	0.0004
0.5	0.0089	0.1183	0.1261	0.0974	0.0995	0.1164	0.0419	0.0003
AVE.	0.0043	0.0462	0.0580	0.0430	0.0442	0.0544	0.0176	0.0002
C.V.	0.7130	0.8659	0.6818	0.6556	0.6604	0.6866	0.8085	0.3928

RELATIVE CONCENTRATIONS AT X= 500 CENTIMETERS

Z (CM) / Y (CM)	-24.0	-16.0	-8.0	0.0	4.0	12.0	20.0	28.0
6.0	0.0005	0.0082	0.0205	0.0214	0.0221	0.0159	0.0022	0.0
4.0	0.0007	0.0134	0.0302	0.0314	0.0311	0.0217	0.0026	0.0001
2.5	0.0010	0.0151	0.0394	0.0410	0.0403	0.0281	0.0034	0.0
1.5	0.0010	0.0173	0.0444	0.0457	0.0457	0.0325	0.0035	0.0
0.5	0.0011	0.0182	0.0476	0.0479	0.0482	0.0349	0.0040	0.0
AVE.	0.0008	0.0139	0.0346	0.0357	0.0357	0.0253	0.0030	0.0000
C.V.	0.2921	0.2533	0.2841	0.2742	0.2690	0.2732	0.2188	1.6485

RELATIVE CONCENTRATIONS AT X= 1000 CENTIMETERS

Z (CM) / Y (CM)	-25.0	-16.0	-8.0	0.0	4.0	12.0	20.0	32.0
6.0	0.0035	0.0144	0.0247	0.0296	0.0279	0.0181	0.0076	0.0008
4.0	0.0039	0.0165	0.0274	0.0314	0.0299	0.0205	0.0084	0.0014
2.5	0.0042	0.0183	0.0292	0.0331	0.0310	0.0226	0.0099	0.0008
1.5	0.0042	0.0180	0.0298	0.0333	0.0319	0.0234	0.0099	0.0011
0.5	0.0043	0.0180	0.0308	0.0329	0.0317	0.0241	0.0101	0.0008
AVE.	0.0040	0.0168	0.0280	0.0318	0.0303	0.0214	0.0090	0.0010
C.V.	0.0738	0.0895	0.0763	0.0444	0.0491	0.1013	0.1123	0.2553

RELATIVE CONCENTRATIONS AT X= 1500 CENTIMETERS

Z (CM) / Y (CM)	-36.0	-24.0	-12.0	0.0	6.0	18.0	30.0	42.0
6.0	0.0006	0.0059	0.0188	0.0279	0.0258	0.0122	0.0022	0.0001
4.0	0.0006	0.0067	0.0200	0.0279	0.0259	0.0123	0.0025	0.0001
2.5	0.0006	0.0066	0.0204	0.0283	0.0262	0.0131	0.0026	0.0
1.5	0.0009	0.0069	0.0205	0.0281	0.0266	0.0131	0.0024	0.0
0.5	0.0008	0.0069	0.0204	0.0283	0.0266	0.0135	0.0025	0.0
AVE.	0.0007	0.0066	0.0199	0.0281	0.0261	0.0128	0.0024	0.0000
C.V.	0.1751	0.0551	0.0327	0.0056	0.0126	0.0406	0.0601	1.1005

RELATIVE CONCENTRATIONS AT X= 2000 CENTIMETERS

Z (CM) / Y (CM)	-36.0	-24.0	-12.0	0.0	6.0	18.0	30.0	42.0
6.0	0.0016	0.0079	0.0193	0.0255	0.0244	0.0139	0.0042	0.0004
4.0	0.0016	0.0081	0.0203	0.0251	0.0246	0.0139	0.0044	0.0007
2.5	0.0016	0.0085	0.0205	0.0255	0.0246	0.0139	0.0042	0.0006
1.5	0.0016	0.0089	0.0208	0.0255	0.0248	0.0139	0.0042	0.0003
0.5	0.0016	0.0089	0.0206	0.0251	0.0248	0.0139	0.0039	0.0004
AVE.	0.0016	0.0084	0.0202	0.0253	0.0246	0.0139	0.0042	0.0005
C.V.	0.0000	0.0452	0.0254	0.0073	0.0054	0.0000	0.0403	0.3088

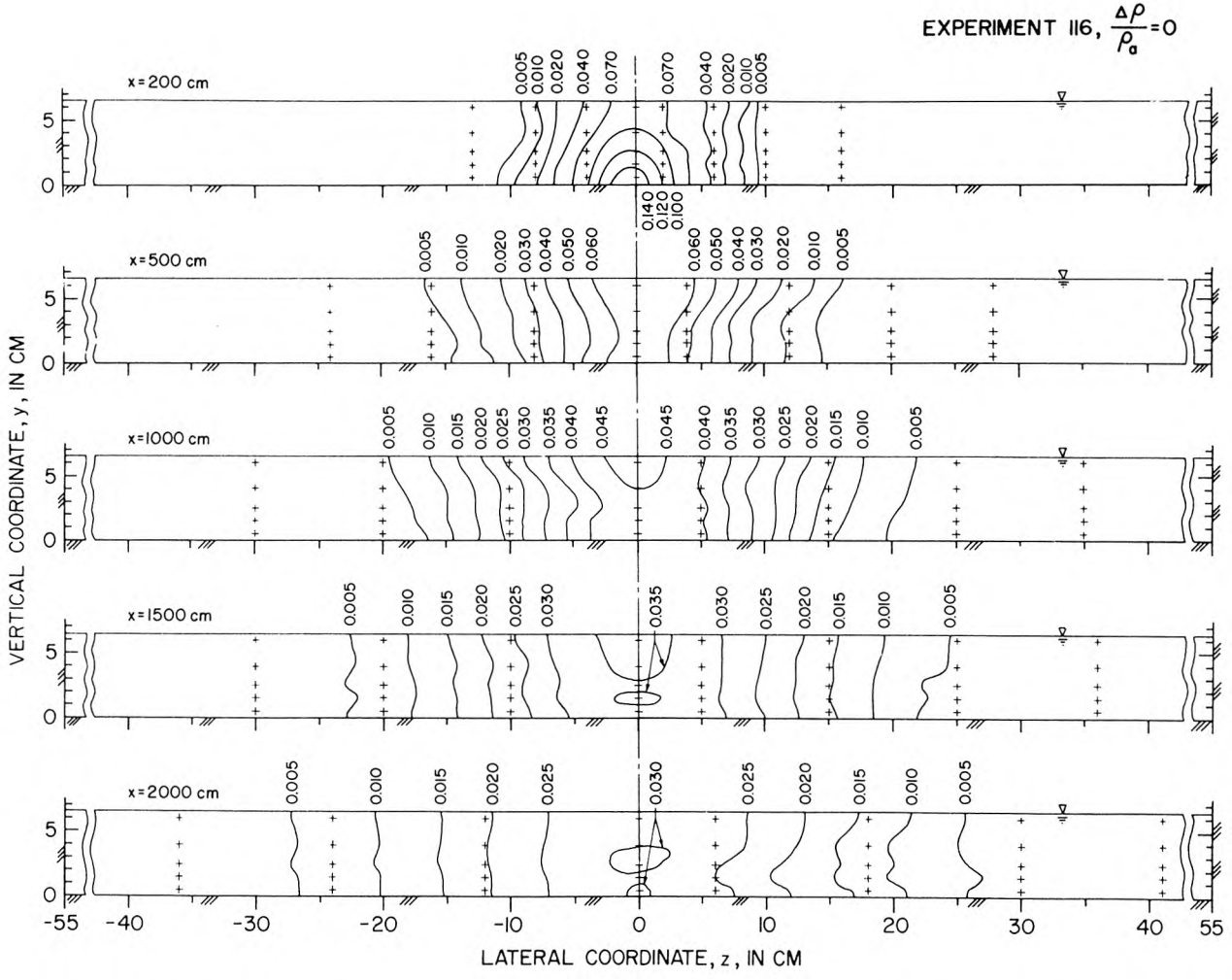

Figure 4.4 Lines of equal relative concentration in cross-sections downstream from a 1-cm-wide source which discharged a fluid with a density the same as the ambient fluid and with a relative concentration of 1.0. The flow condition was S2. The crosses designate sampling points.

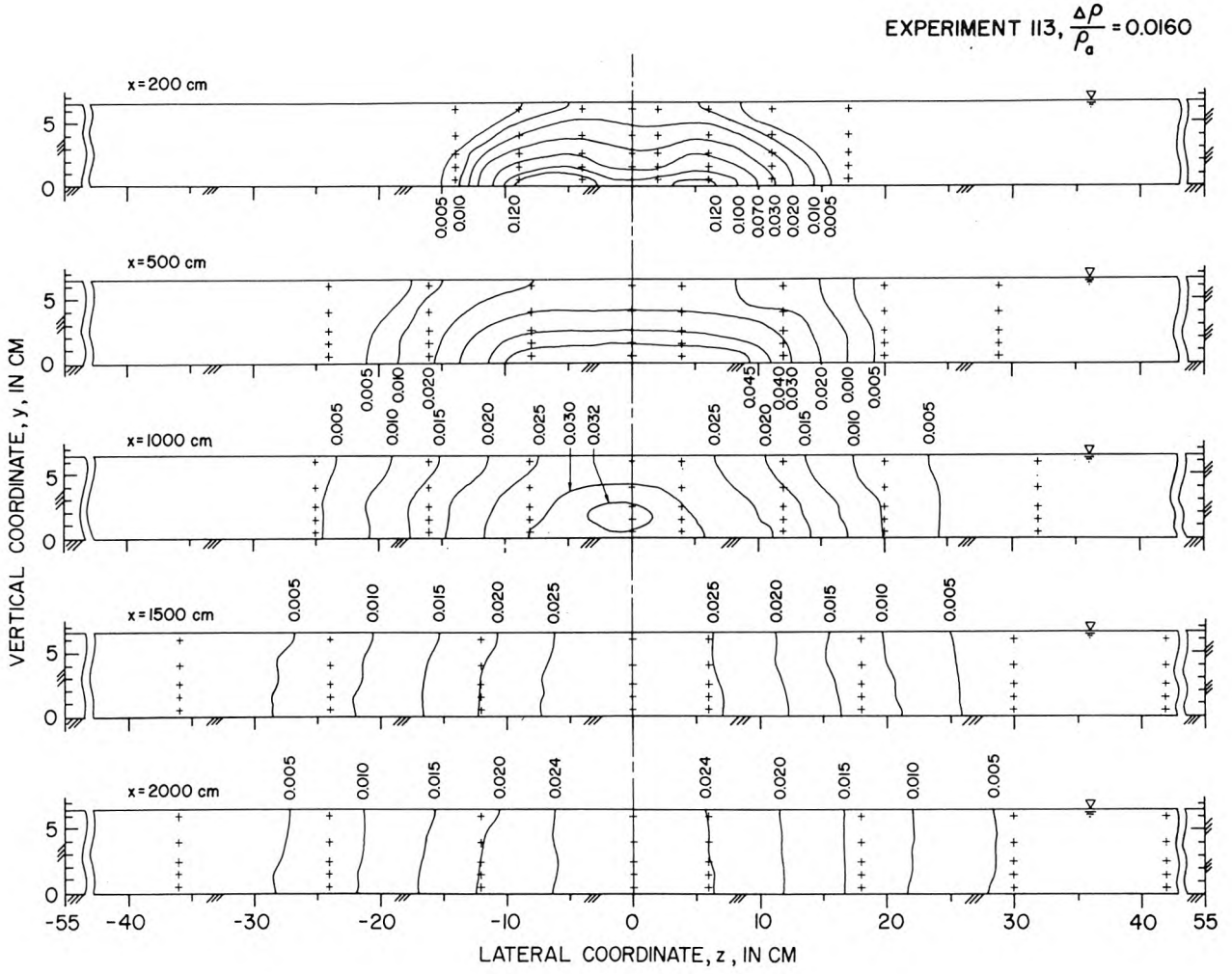

Figure 4.5 Lines of equal relative concentration in cross-sections downstream from a 1-cm-wide source which discharged a fluid with a density 0.0160 gm/cm^3 greater than the ambient fluid and with a relative concentration of 1.0. The flow condition was S2. The crosses designate sampling points.

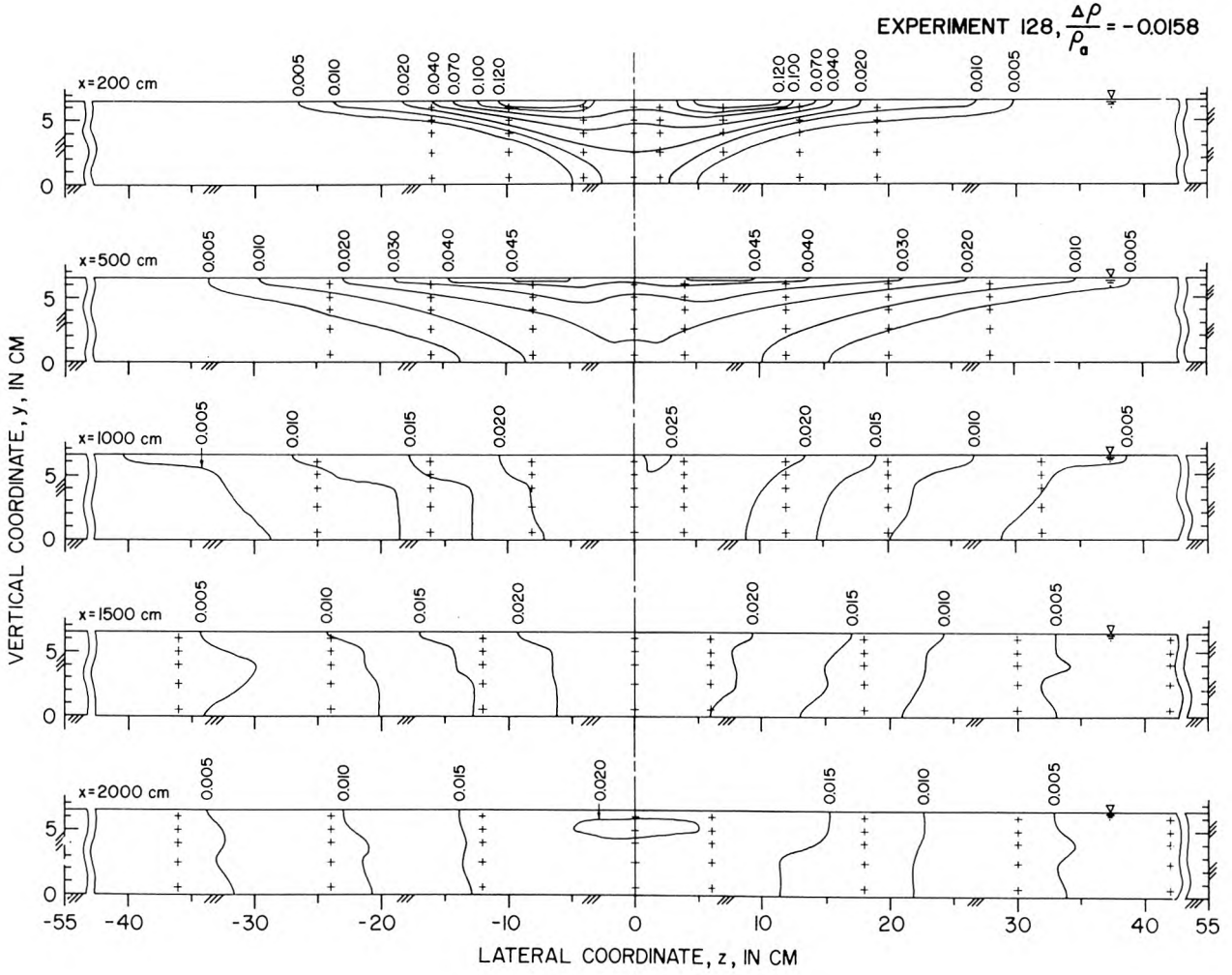

Figure 4.6 Lines of equal relative concentration in cross-sections downstream from a 1-cm-wide source which discharged a fluid with a density 0.0158 gm/cm^3 less than the ambient fluid and with a relative concentration of 1.0. The flow condition was S2. The crosses designate sampling points.

greater width in the upper part was probably due to the lateral turbulent diffusion coefficient at the surface being higher than the depth-averaged value as was mentioned in Subsection 2.2.3. The higher concentrations near the bottom of the flume at x = 200 cm were probably due to the velocity from the source being higher than the velocity of the ambient fluid near the bottom of the flume.

In Exp. 113, the tracer fluid discharged from the source was more dense than the ambient fluid by the relative amount $\Delta\rho/\rho_a = 0.0160$. The concentration isopleths for this experiment, shown in Fig. 4.5, look different from those of Exp. 116 in which the tracer and ambient fluids had the same density. In Exp. 113, the concentrations near the flume bottom were significantly higher than near the surface as far downstream as x = 1000 cm. Also, the lateral concentration distributions near the bottom were bimodal at x = 200 cm. Comparing Fig. 4.4 and 4.5 also shows that peak concentrations are decreased and lateral mixing is enhanced when the tracer fluid is more dense than the ambient fluid.

The differences in the concentration distributions observed in the two experiments are caused by density-induced secondary currents in Exp. 113 which were driven by an imbalance of hydrostatic pressures caused by the lateral density gradients. The phenomenon is analogous to longitudinal circulation in estuaries as described in Subsection 2.3.2. Although the secondary current velocities were not measured in the experiments, the circulation

patterns were probably similar to those sketched in Fig. 4.7. The outward velocities near the bottom convected fluid with high tracer concentration away from the center, and the inward velocities near the surface convected fluid with low concentration toward the center. The result was a net outward transport of tracer in the direction of the negative concentration gradient. The kinematics of the transport process is similar to that for longitudinal dispersion in shear flows as discussed in Subsection 2.2.1. The bimodal distribution in Exp. 113 was caused by the two outward flowing lower layers which persisted, due to inertia, for a sufficient length of time to begin to separate the tracer plume into two parts.

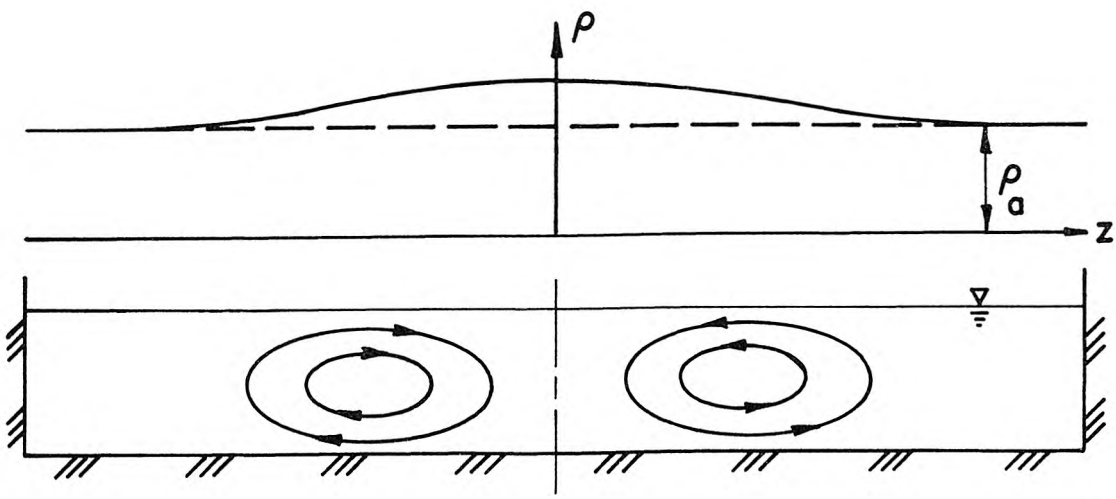

Figure 4.7. Cross-section of flume showing density-induced secondary circulation patterns downstream from a source of narrow or intermediate width.

Superimposed on the convective transport was transport by turbulent diffusion, which mixed the tracer laterally and vertically. Turbulence also acted to decrease the intensity of the density-

induced circulation by mixing fluid from the top and bottom layers of the flow which were moving in opposite lateral directions. Sufficiently far downstream where the tracer plume became very wide and the lateral density gradients, which drove the secondary currents, became small, lateral mixing was mostly by turbulent diffusion, and the concentration became uniform with depth. It will later be shown that downstream from $x \approx 1000$ cm the rate of spreading was the same for both experiments; however, the tracer plume remained wider and the peak concentrations remained lower in Exp. 113 than in Exp. 116.

The concentration distributions observed in Exp. 128 are shown in Fig. 4.6. In this experiment, the tracer fluid was less dense than the ambient fluid by the relative amount $\Delta\rho/\rho_a = -0.0158$. The density-induced secondary flow in this experiment was probably similar to that shown in Fig. 4.7 except that the direction of rotation in each of the cells was reversed. Although the differences in density between the tracer and ambient fluids in Exp. 113 and 128 were nearly the same magnitude but of opposite sign, the geometrical forms of the concentration isopleths from one experiment are not the same as those from the other turned upside down. The vertical concentration gradients at $x = 1000$ cm and less were steeper in Exp. 128 than in Exp. 113; also, the width of the plume at the surface in Exp. 128 was wider than the width near the bottom in Exp. 113.

Two reasons are offered for the differences between the concentration distributions in Exp. 113 and 128. The first is the differences that vertical density gradients had on vertical mixing in the two experiments. In Subsection 2.2.4 it was pointed out that the variation of the vertical diffusion coefficient in a wide open channel is symmetric about a line at mid-depth. However, for reasons that are given below, vertical density gradients probably suppressed vertical mixing more in Exp. 128 than in Exp. 113. Because vertical mixing decreases the intensity of the density-induced circulation, the magnitudes of the secondary current velocities were probably larger in Exp. 128 than in Exp. 113.

In Section 2.3, it was mentioned that a vertical density gradient suppresses turbulent mixing by an amount that increases with the Richardson number

$$Ri = \frac{g}{\rho} \frac{\partial \rho}{\partial y} \Big/ \left(\frac{\partial u}{\partial y}\right)^2 \quad . \tag{2.18}$$

For the same density gradient near the surface in Exp. 128 as near the bottom in Exp. 113, Ri would be higher in Exp. 128 than in Exp. 113 because the gradient of the longitudinal velocity is least near the surface. Therefore, vertical mixing in the important region near the surface in Exp. 128 would be suppressed more than near the bottom in Exp. 113.

The amount of suppression of vertical mixing by vertical density gradients will be estimated by using

$$\lambda_y \epsilon_y = (\lambda_y \epsilon_y)_o \, (1+10Ri)^{-\frac{1}{2}} \qquad (2.19)$$

with Richardson numbers calculated from the experimental data. For Exp. 128 at the point x = 200 cm, z = 6 cm, and y/d = 0.75, which is in the center of the upper half of the flow, Ri = 0.41. (In the computation of Ri, the logarithmic velocity distribution and the data in Table 4.1 were used to calculate the velocity gradient, $\partial u/\partial y = u_*/ky$; the density gradient was obtained from Fig. 4.42, where the same concentrations used to prepare Fig. 4.6 were plotted as a function of y.) For Exp. 113, a similar computation for the point x = 200 cm, z = 7 cm, and y/d = 0.25, which is in the center of the lower half of the flow, yields Ri = 0.034. The difference in the Richardson numbers from the two experiments is due mostly to a factor of three difference in the velocity gradients. Using these data in Eq. 2.19 gives $\lambda_y \epsilon_y = 0.44 \, (\lambda_y \epsilon_y)_o$ for Exp. 128 and $\lambda_y \epsilon_y = 0.86 \, (\lambda_y \epsilon_y)_o$ for Exp. 113. Thus, vertical mixing is suppressed much more in Exp. 128 than in Exp. 113; consequently, stronger density-induced secondary currents and faster lateral mixing should be expected in Exp. 128.

A second, but probably less important, cause of the differences between the concentration distributions in Exp. 128 and 113 was the existence of a resistance to flow by the flume bottom but absence of such a resistance by the free surface. If the outward density-

induced velocities tend to be higher than the inward velocities, as is strongly suggested by the shapes of the concentration isopleths from Exp. 128 but less so from Exp. 113, then the bottom would have hindered the secondary flows more in Exp. 113 than in Exp. 128. Limited data from experiments in quiescent fluids by Sharp (33, 34) suggest that the front of a density underflow propagates along a horizontal bottom about 10 percent slower than the front of a density overflow propagates along a free surface. However, differences of this magnitude are insufficient to cause the large differences between the data from Exp. 113 and 128.

Attempts to attribute the differences between the concentration distributions in the two experiments to other phenomena were not successful. The difference between the molecular diffusion coefficients for methyl alcohol, which was used to make the tracer fluid in Exp. 128 less dense, and for NaCl, which was used to make the tracer fluid in Exp. 113 more dense, is less than a few per cent (see e. g. Ref. 27, Vol. 5, pp. 67, 69). This difference is undoubtedly too small to have had a measurable influence on the experiments. Nor is it reasonable that vertical variations in the lateral diffusion coefficients were large enough to have caused the differences in the observed concentration distributions.

The concentration distributions in cross-sections downstream from the wide source, which was used in experiments to observe mixing of two wide parallel streams, are shown for two experiments in Figs. 4. 8 and 4. 9. The hydraulic conditions in both experiments

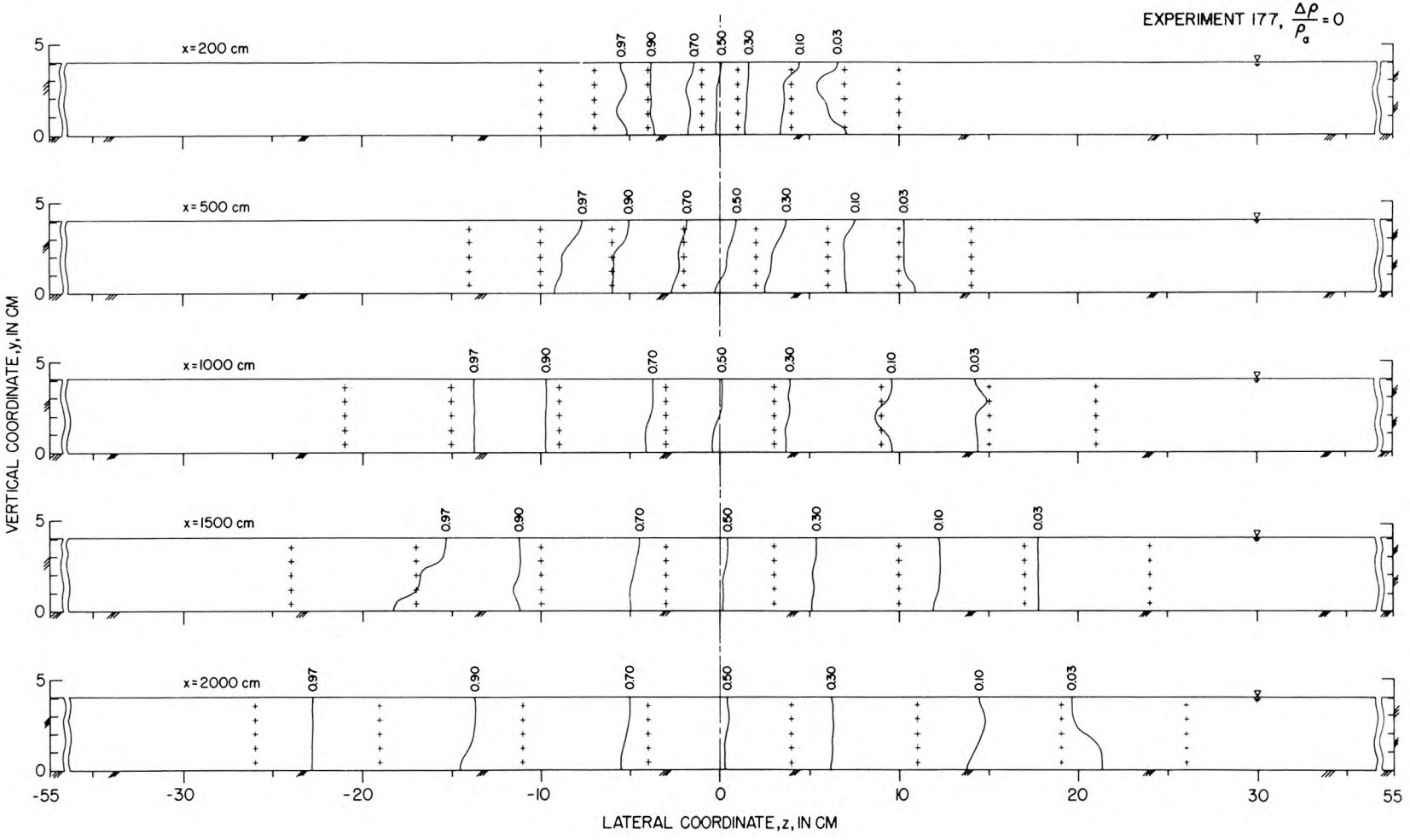

Figure 4.8 Cross-sections with lines of equal relative concentration downstream from the confluence of two wide parallel streams of the same density. The flow condition was S1. The crosses designate sampling points.

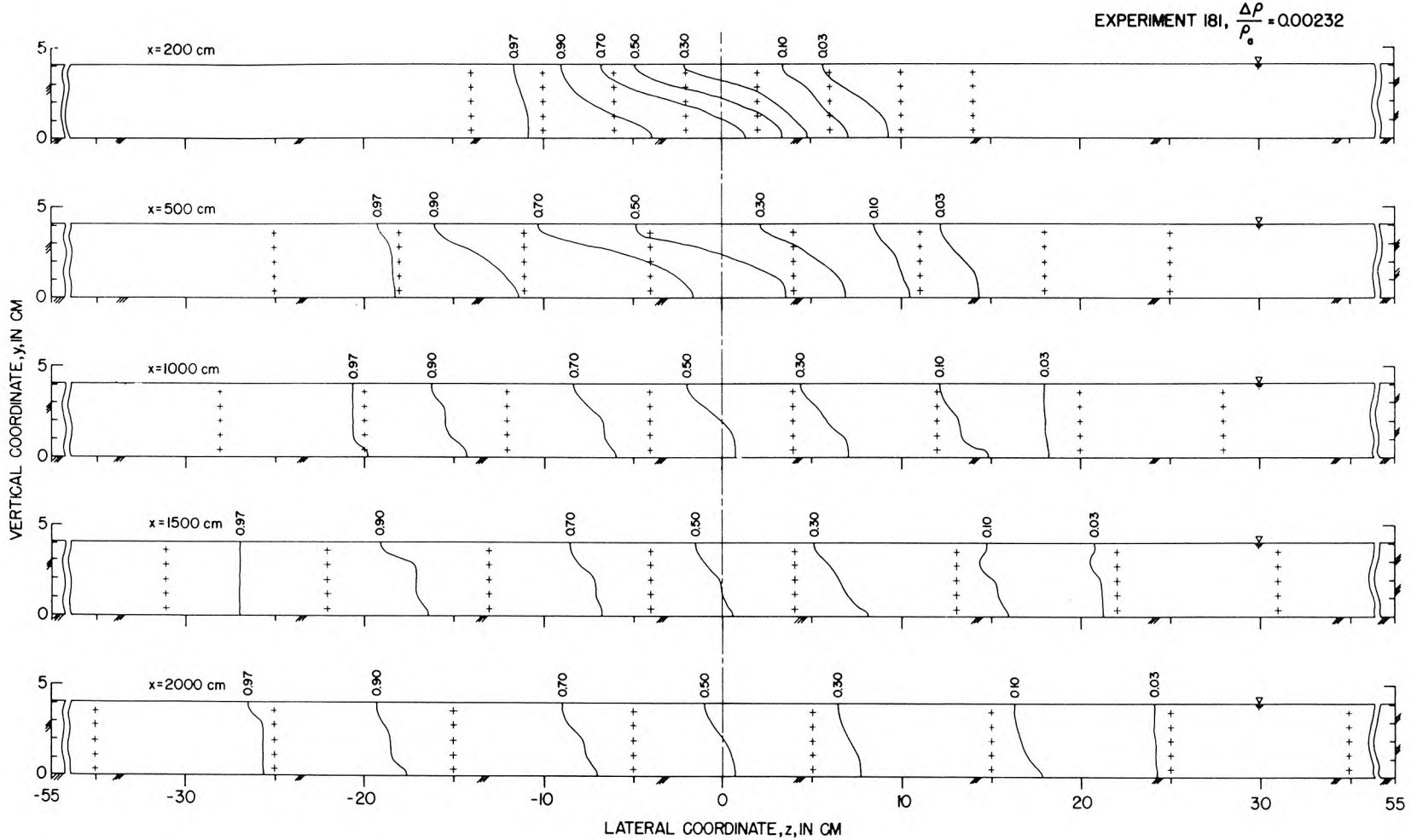

Figure 4.9 Cross-sections with lines of equal relative concentration downstream from the confluence of two wide parallel streams of different density. The fluid on the left was 0.00232 gm/cm^3 more dense than the fluid on the right. The flow condition was S1. The crosses designate sampling points.

were the same. In Exp. 177, shown in Fig. 4.8, the density of the fluid in both streams was the same; mixing was mostly by turbulent diffusion and the variation in tracer concentration over the depth was small almost everywhere. In Exp. 181, shown in Fig. 4.9, the density of the fluid in the stream on the left (with the relative concentration equal to unity) was 0.00232 gm/cm^3 more dense than the fluid in the stream on the right (with relative concentration equal to zero). Therefore, lateral mixing was by both turbulent diffusion and density-induced circulation. Because the density of the fluid in a cross-section decreased monotonically from left to right, the circulation pattern was probably single-celled as shown in Fig. 4.10. Fluid with a high tracer concentration near the bottom was convected to the right, and fluid with a lower

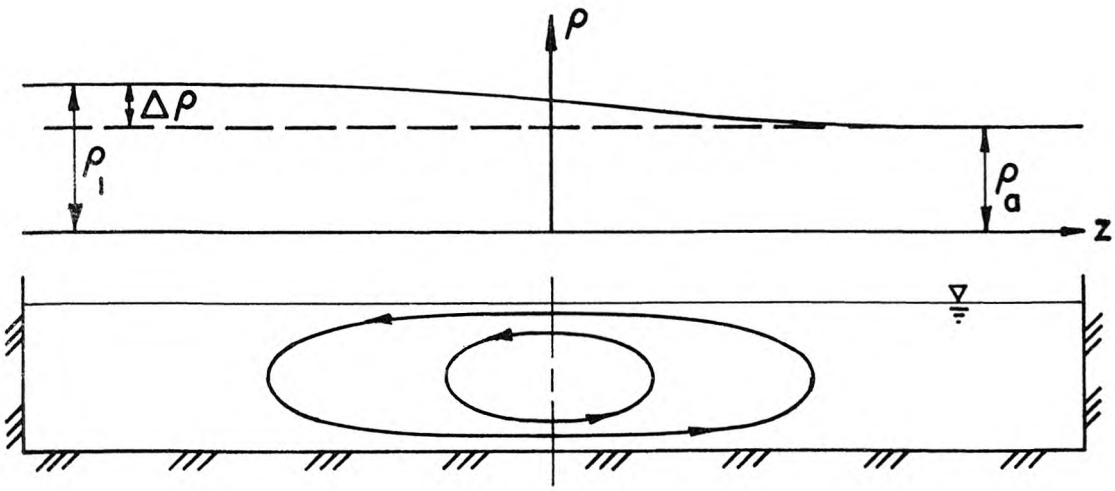

Figure 4.10 Cross-sections of the flume showing density-induced secondary circulation pattern downstream from the confluence of two wide parallel streams of different density.

concentration near the surface was convected to the left. The concentration near the surface was measurably less than near the bottom even at x = 2000 cm. Hence, one may suspect that in Exp. 181 density-induced circulation may have still been contributing to lateral mixing even at the farthest downstream cross-section where data were taken.

4.2.3 Depth-Averaged Concentration Distributions

4.2.3.1 Calculating the Depth-Averaged Concentrations. To measure the effects of density differences on lateral mixing, it was advantageous to average the concentrations over the depth at each lateral position across the width of the flume. The depth-averaged relative concentration, $\overline{C}$, was calculated numerically using Eq. 4.1b:

$$\overline{C}(x, z) = \frac{1}{d} \int_0^d C(x, y, z)\, dy \tag{4.1a}$$

$$\approx \frac{1}{d}\left[C(x, y_1, z)\frac{(y_2+y_1)}{2} + \sum_{i=2}^{4} C(x, y_j, z)\frac{\left(y_{i+1} - y_{i-1}\right)}{2} \right.$$

$$\left. + C(x, y_5, z)\left(d - \frac{(y_5+y_4)}{2}\right)\right] \tag{4.1b}$$

For all calculations, y was measured from the stainless steel bottom of the flume. The terms y_1, y_2, etc are the y-coordinates of the sampling points, where the concentrations are known. These terms and their use in Eq. 4.1b are further clarified in the definition sketch,

Fig. 4.11. The averages, $\overline{C}$, were listed as part of the computer output in the rows labeled AVE. in Table 4.3.

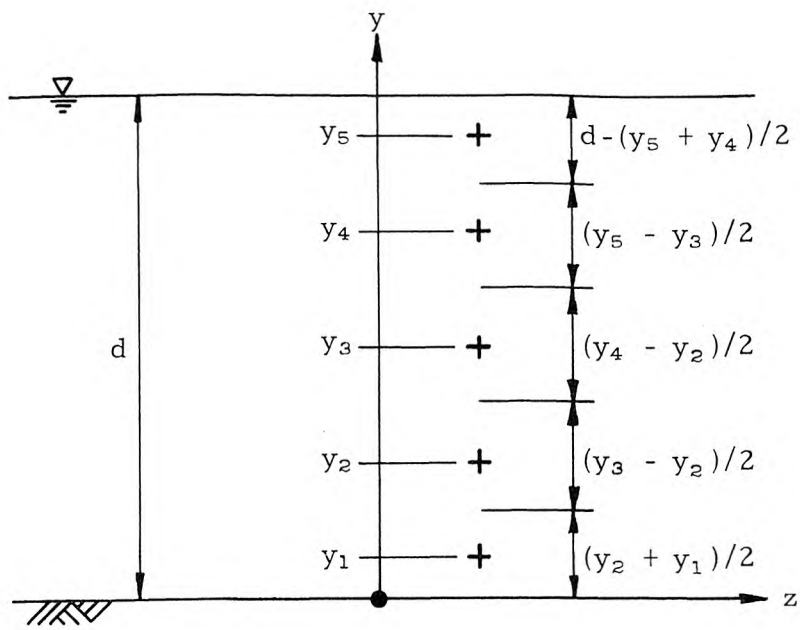

Figure 4.11 Definition sketch for terms in Eq. 4.1b. The crosses mark sampling points.

4.2.3.2 The Lateral Distributions of $\overline{C}$. The distributions of the depth-averaged relative concentration from eight of the experiments are shown in Fig. 4.12 through 4.19. The experimental data were plotted as circles and the solid curves were fitted to the data by eye. The crosses in Fig. 4.12 through 4.17 are the experimental data reflected across the center line. The crosses were used as a guide for drawing the curves, but the curves were not necessarily drawn through them.

Lateral distributions of $\overline{C}$ observed downstream from the narrow 1-cm-wide source in Exp. 125, 116, 113, and 128 are shown in Fig. 4.12 to 4.15. In Exp. 125 and 116 the densities of the tracer and ambient fluids were equal; therefore, mixing was only by turbulent diffusion. For these experiments one should expect $\overline{C}$ to be given by solutions to Eq. 4.2:

$$\overline{u}\,\frac{\partial \overline{C}}{\partial x} = \overline{\epsilon}_z \frac{\partial^2 \overline{C}}{\partial z^2} \,. \tag{4.2}$$

If one assumes that the narrow source is approximated by a vertical line source, the boundary condition at the source is given by

$$\overline{C}(0, z) = A\,\delta(z) \,,$$

where $\delta(z)$ is the Dirac delta function, and A is the source strength given by

$$A = \int_{-\infty}^{\infty} \overline{C}(x, z)dz \,.$$

The solution to Eq. 4.2 satisfying the boundary condition at x=0 and

$$\frac{\partial \overline{C}}{\partial z} = 0 \qquad \text{at } z = 0 \tag{4.3a}$$

$$\overline{C} = 0 \qquad \text{at } z \to \infty \tag{4.3b}$$

is the Gaussian distribution:

$$\overline{C}(x, z) = \frac{A}{\sqrt{4\pi\overline{\epsilon}_z x/\overline{u}}} \exp\left[\frac{-z^2}{4\overline{\epsilon}_z x/\overline{u}}\right] \,. \tag{4.4}$$

Of course, this solution is valid only where the sidewalls of the flume do not affect the mixing.

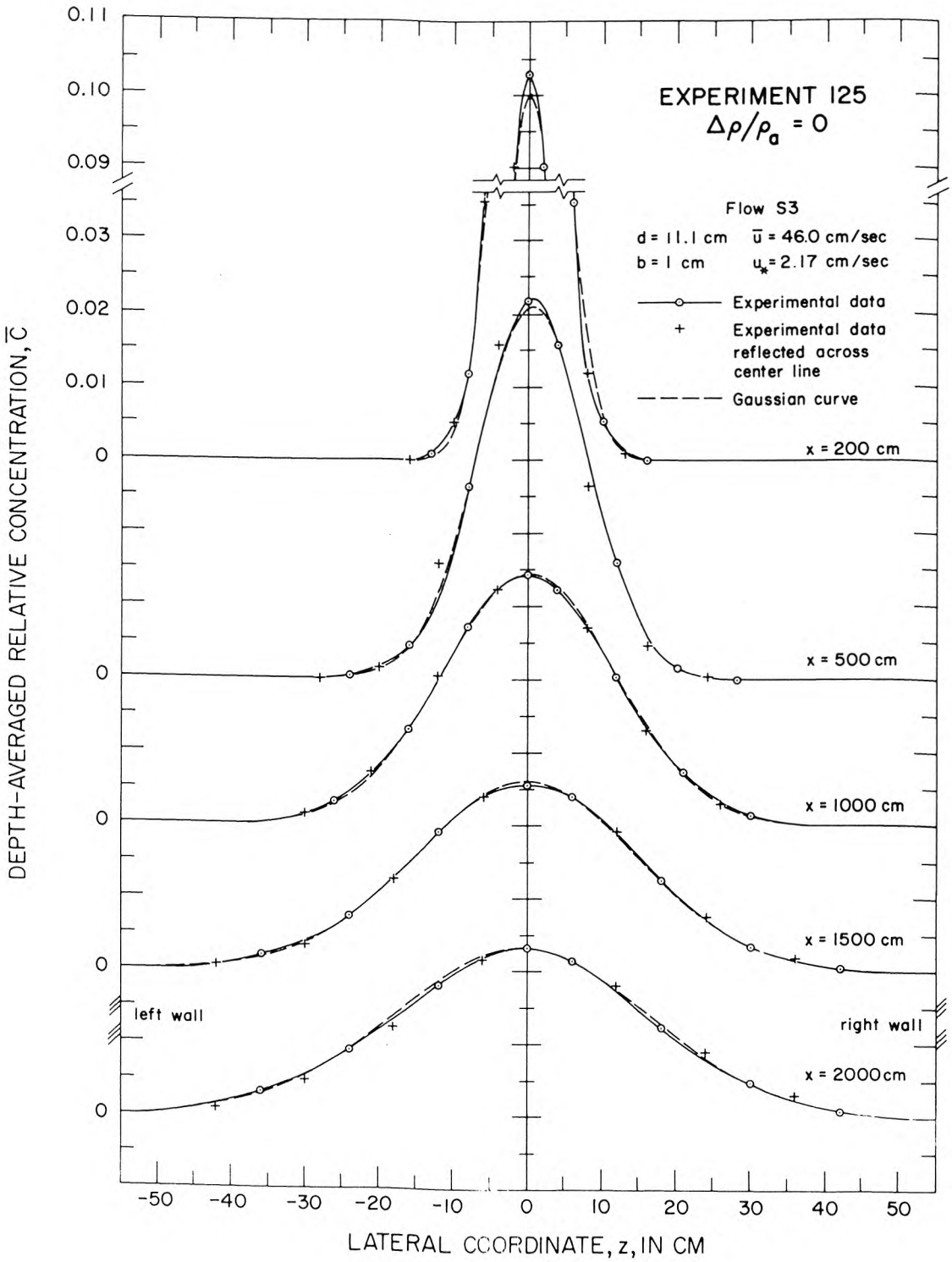

Figure 4.12 Depth-averaged concentration distributions downstream from a 1-cm-wide source which discharged a fluid with a density the same as the ambient fluid and with a relative concentration of 1.0; Exp. 125.

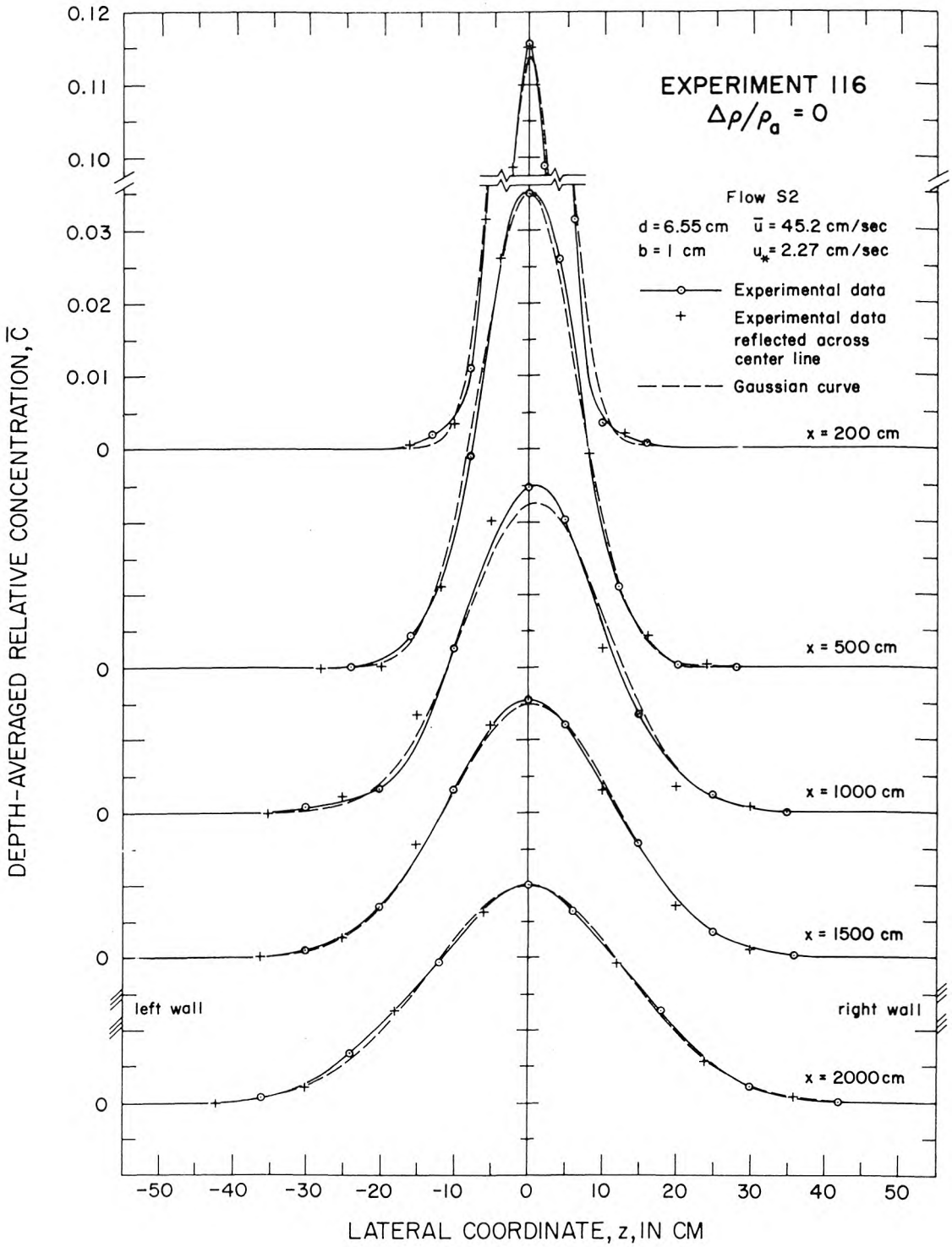

Figure 4.13 Depth-averaged concentration distributions downstream from a 1-cm-wide source which discharged a fluid with a density the same as the ambient fluid and with a relative concentration of 1.0; Exp. 116.

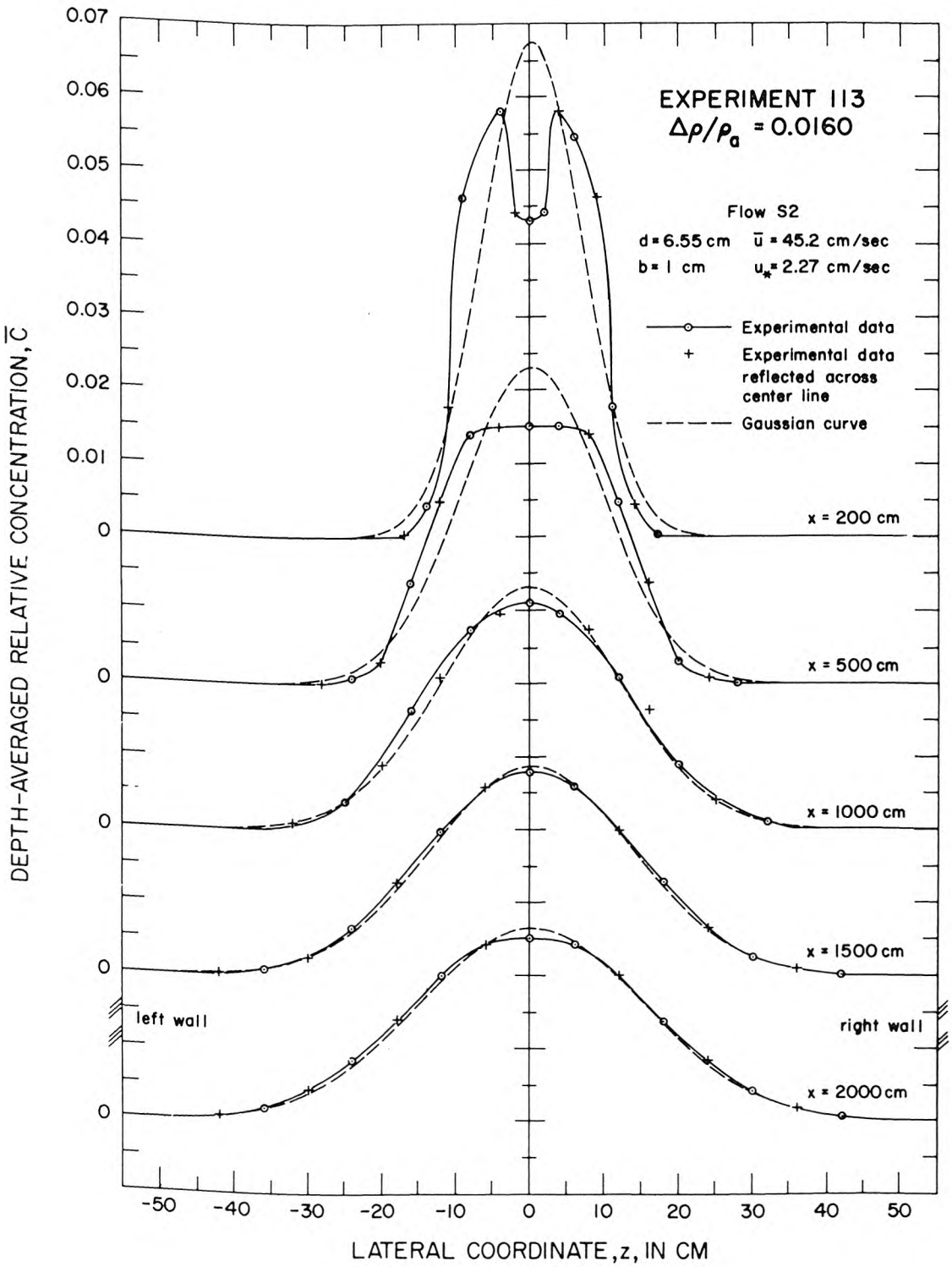

Figure 4.14 Depth-averaged concentration distributions downstream from a 1-cm-wide source which discharged a fluid with a density 0.0160 gm/cm^3 more dense than the ambient fluid and with a relative concentration of 1.0; Exp. 113.

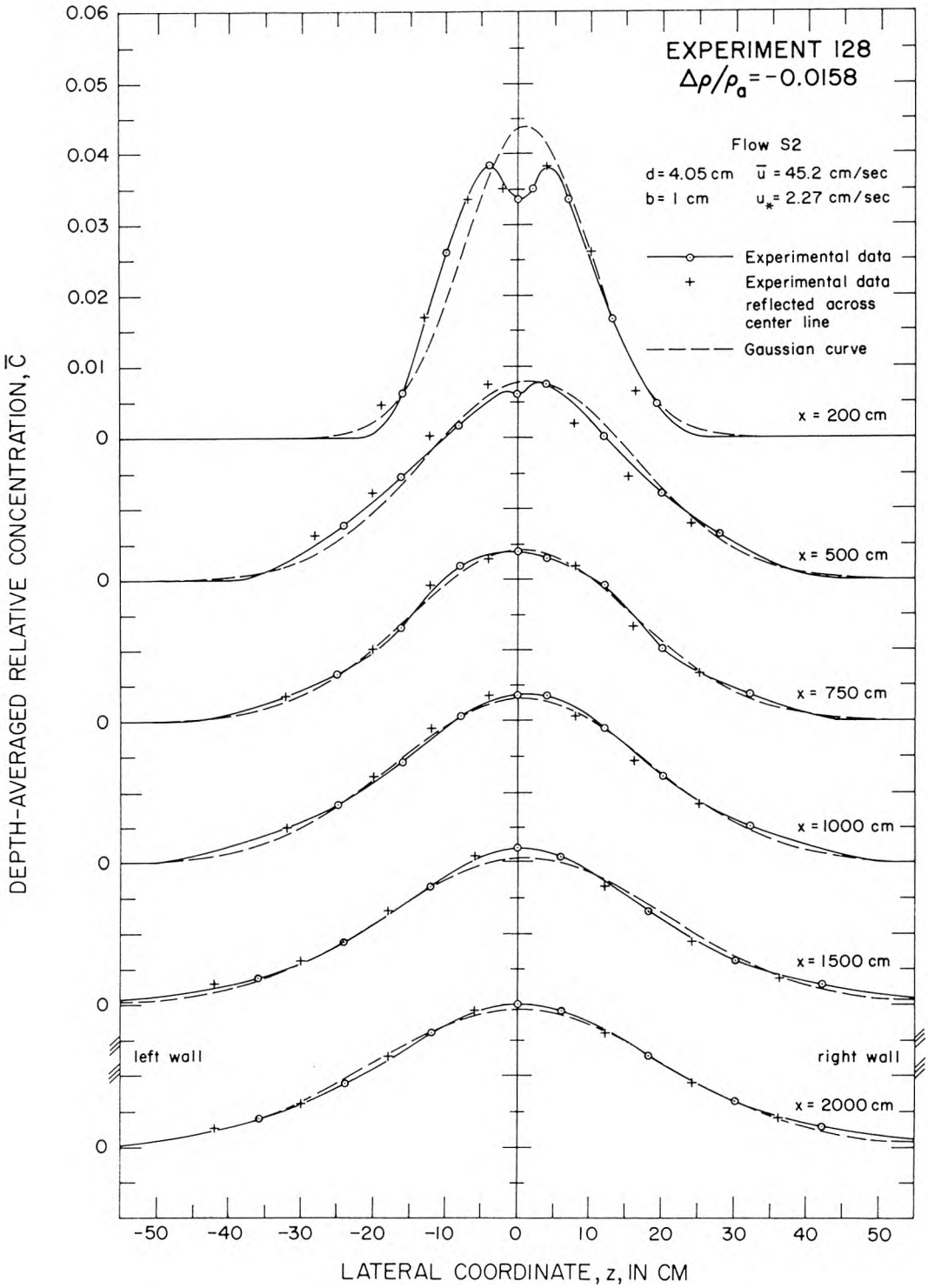

Figure 4.15 Depth-averaged concentration distributions downstream from a 1-cm-wide source which discharged a fluid with a density 0.0158 gm/cm^3 less than the ambient fluid and with a relative concentration of 1.0; Exp. 128.

The shape of the theoretical distribution was compared with the experimental data by drawing Gaussian distributions as dashed curves in Fig. 4.12 through 4.17. These Gaussian curves have the same variances, areas, and centroids as the solid curves and they fit the data from Exp. 125 and 113 well. The technique used to compute each of these observed parameters is discussed later. It will also be shown that the variances of the experimental curves grow like x as the solution, Eq. 4.4, implies.

Lateral distributions of $\overline{C}$ from Exp. 113, in which $\Delta\rho/\rho_a = 0.0160$, and from Exp. 128, in which $\Delta\rho/\rho_a = -0.0158$, are shown in Fig. 4.14 and 4.15. In these experiments, lateral mixing close to the source was by both turbulent diffusion and density-induced circulation. There, the lateral distributions of $\overline{C}$ were not Gaussian. At x = 200 cm, the distributions were bimodal, which was typical of distributions close to the source in experiments in which there was a difference in density between the tracer and ambient fluids. However, farther downstream, where the effects of the density gradients were unimportant and mixing was mostly by turbulent diffusion, the distributions became Gaussian, which is the expected assymptotic behavior. One can see in Fig. 4.13, 4.14, and 4.15 that the effect of either a positive or a negative density difference was to spread the tracer over a wider area and to dilute the tracer more than in the experiment without a density difference. It is also evident that a negative density difference has more effect than a positive density difference of the same magnitude.

Lateral distributions of $\overline{C}$ from Exp. 150 and 152 with the 20-cm-wide source are shown in Fig. 4.16 and 4.17, respectively. In Exp. 150, the fluid discharged from the source and the ambient fluid had the same density; whereas in Exp. 152, the density of the fluid discharged from the source was more dense than the ambient fluid by the relative amount $\Delta\rho/\rho_a = 0.00186$. In Exp. 150, the distribution was nearly uniform across the source at x = 0; at x = 200 cm the distribution was still uniform over a small central part of the curve, but at x = 500 cm and farther downstream the distributions became more nearly Gaussian. The distribution across the source in Exp. 152 varied more than in Exp. 150. Although the depth-averaged concentrations observed at x = 0 in front of the 20-cm- and 12.5-cm-wide sources occasionally varied from the mean by up to 10 per cent, the variations should not have had large effects on the distributions observed downstream. In Exp. 152 the distribution was bimodal at x = 500 cm, became rounded at x = 1500 cm, but was nearly Gaussian at x = 2000 cm. By comparing Fig. 4.16 and 4.17 one can again see that the tracer was spread over a wider area and peak depth-averaged concentrations were lower when there was a difference in density between the tracer and ambient fluids.

Lateral distributions of the depth-averaged concentration from two of the experiments performed to study the mixing of two wide parallel streams are shown in Fig. 4.18 and 4.19.

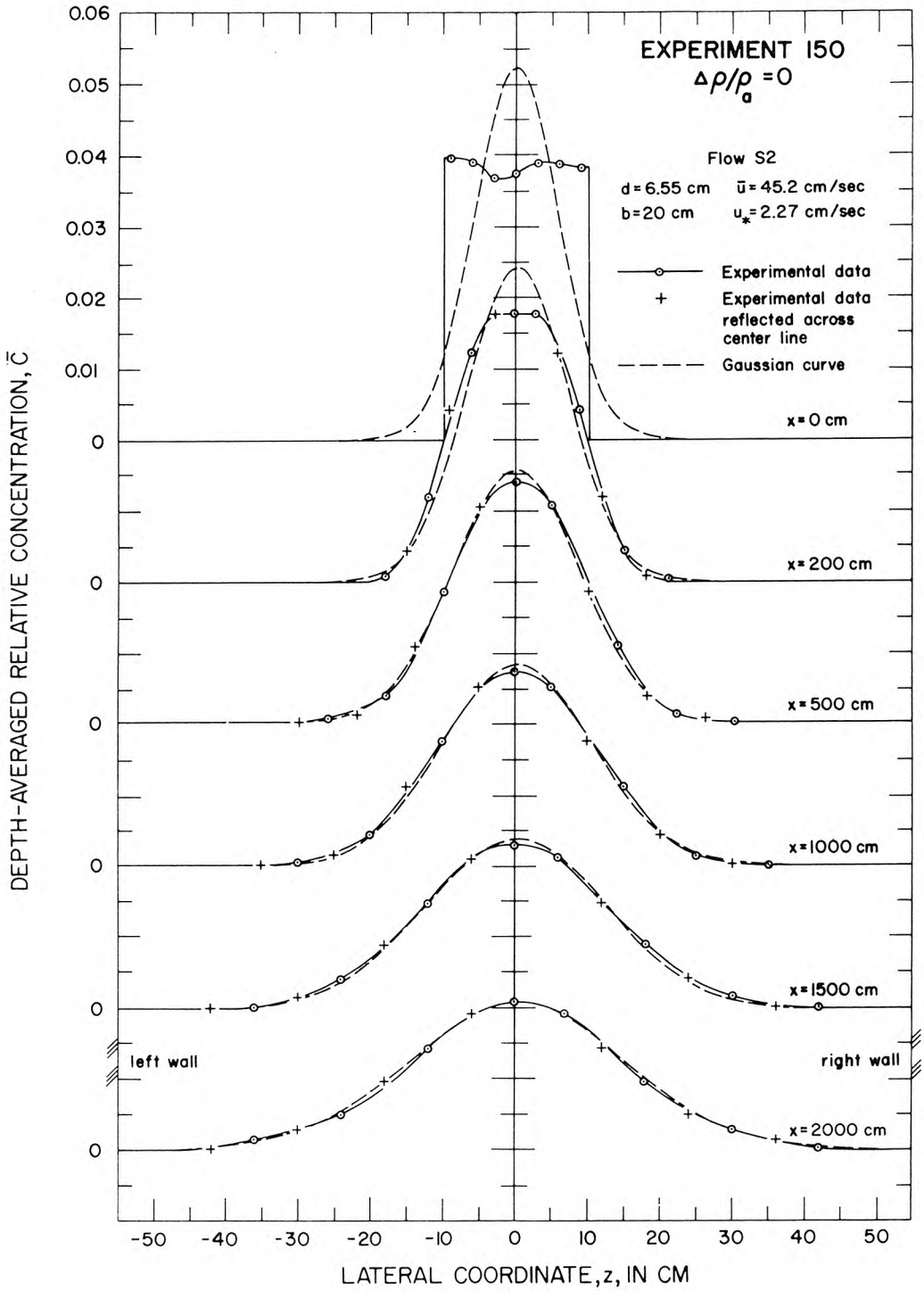

Figure 4.16 Depth-averaged concentration distributions downstream from a 20-cm-wide source which discharged a fluid with a density the same as the ambient fluid and with a relative concentration of 0.0370; Exp. 150.

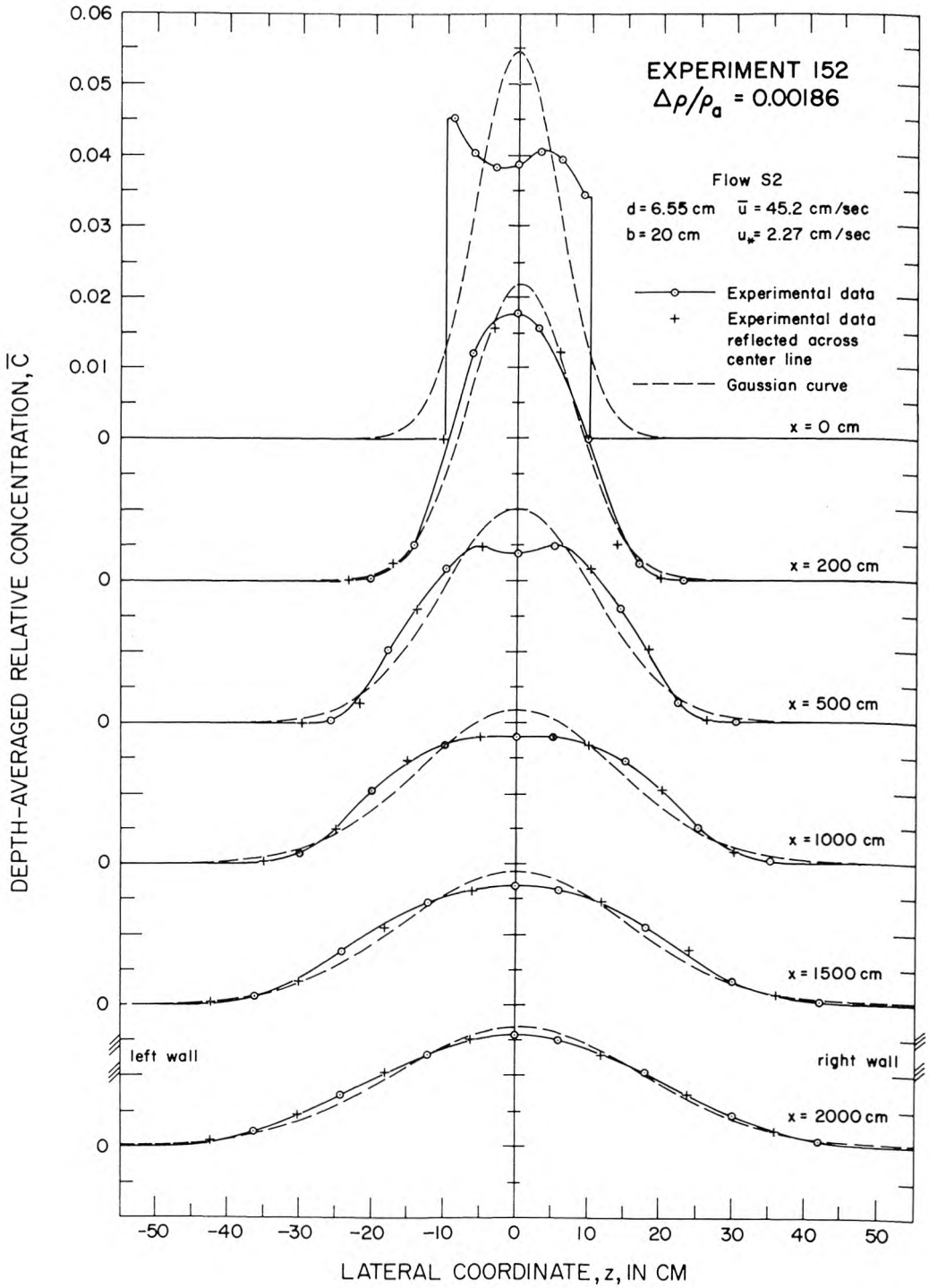

Figure 4.17 Depth-averaged concentration distributions downstream from a 20-cm-wide source which discharged a fluid with a density 0.00186 gm/cm^3 more dense than the ambient fluid and with a relative concentration of 0.0385; Exp. 152.

At x = 0 the distributions across the left half of the channel in these and other experiments were nearly uniform and usually deviated from the mean, $\overline{C} = 1$, by less than 4 per cent. The manner in which the distributions deviated from the mean was not consistent from one experiment to the next, nor with time during one experiment. Because the water samples taken to obtain the distributions at x = 0 were not taken at the same time that samples were taken to obtain distributions in cross-sections downstream, and because samples were taken only in the central mixed zone in the downstream cross-sections, it was necessary to assume concentration distributions to the left of the measured points. Uniform distributions were assumed and are shown as dashed lines in Fig. 4.18 and 4.19. At x = 0 the areas under the assumed distribution, $\overline{C} = 1$, and the measured distribution were made equal by choosing the appropriate normalizing factor in the definition of C.

In Exp. 177, mixing was only by turbulent diffusion because the densities of the fluids on both sides of the flume were the same. Hence, one should be able to predict the concentrations, as was done for Exp. 125 and 116, by solving Eq. 4.2 but with the boundary conditions

$$\overline{C}(0, z) = 0 \quad \text{for } z > 0 , \tag{4.5a}$$

$$\overline{C}(0, z) = 1 \quad \text{for } z < 0 , \tag{4.5b}$$

and

$$\overline{C}(x, z) \to 0 \quad \text{for } z \to \infty , \tag{4.5c}$$

$$\overline{C}(x, z) \to 1 \quad \text{for } z \to -\infty \quad . \tag{4.5d}$$

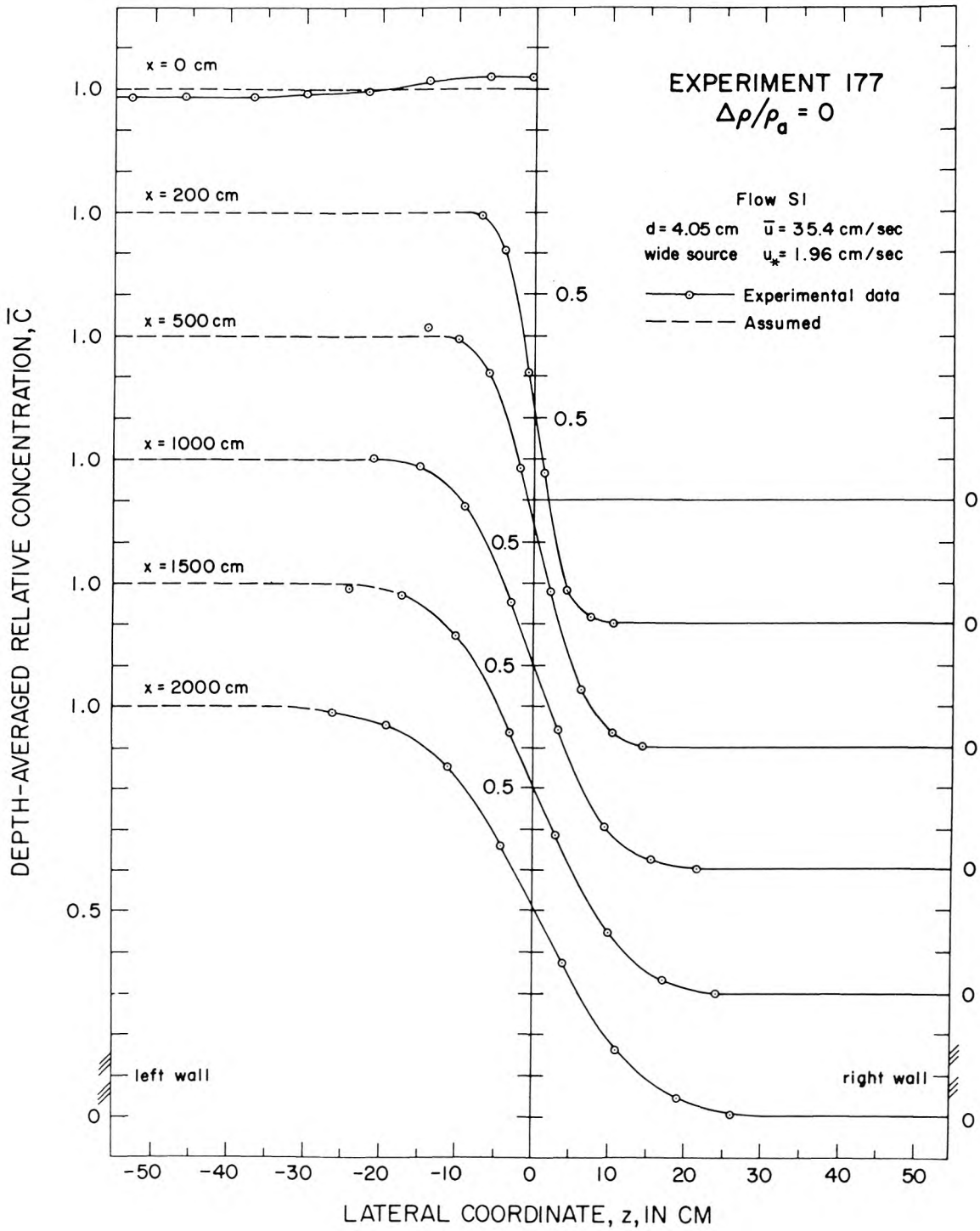

Figure 4.18 Depth-averaged concentration distributions downstream from the confluence of two wide parallel streams of the same density; Exp. 177.

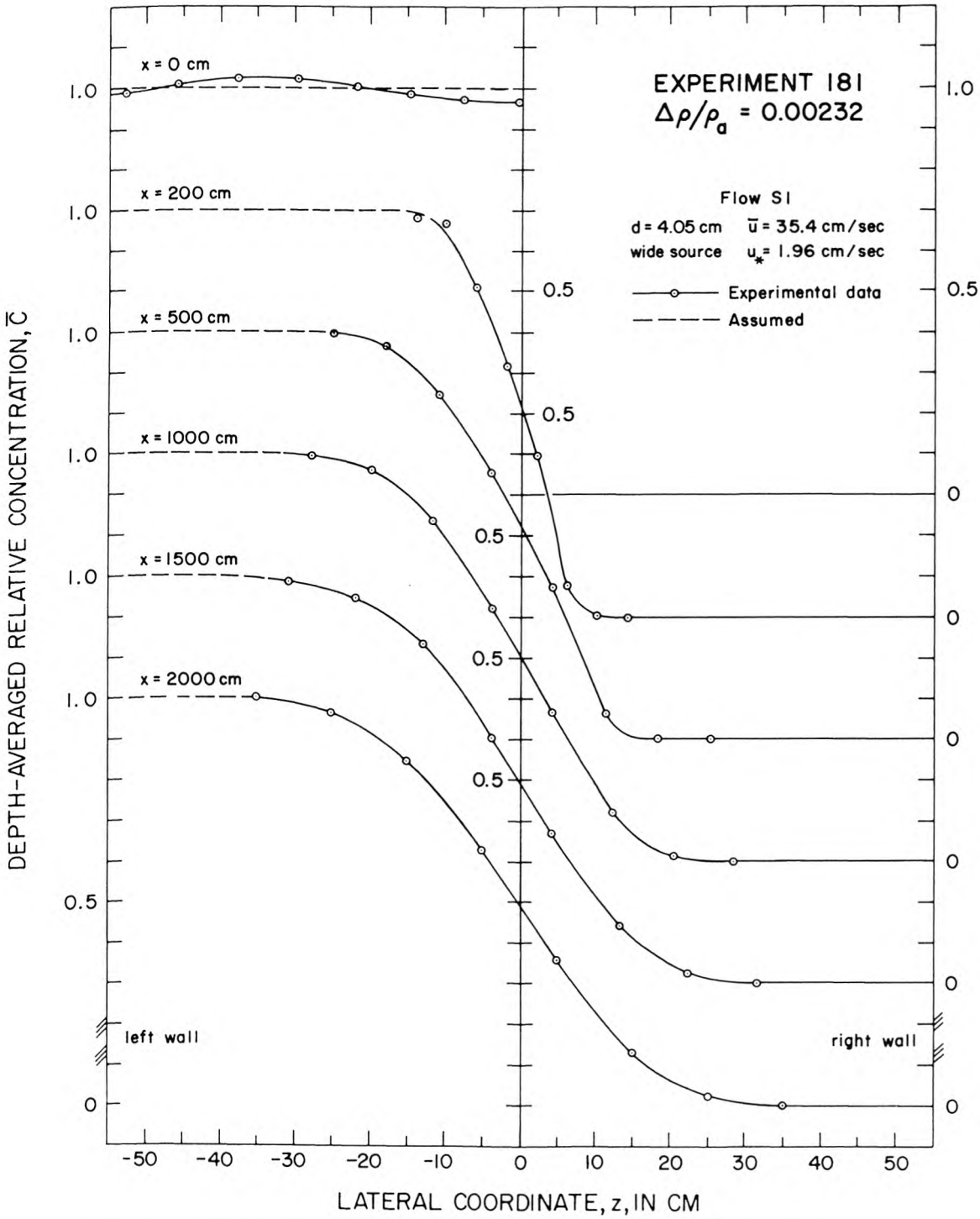

Figure 4.19 Depth-averaged concentration distributions downstream from the confluence of two wide parallel streams of different density; Exp. 181. Fluid with C=1 is 0.00232 gm/cm^3 more dense than fluid with C=0.

The solution to Eq. 4.2 with these boundary conditions is

$$\overline{C}(x, z) = \tfrac{1}{2}\left[1 - \operatorname{erf} \frac{z}{\sqrt{4\bar{\epsilon}_z x/\bar{u}}} \right], \tag{4.6}$$

where the error function, erf, is defined as

$$\operatorname{erf} \zeta = \frac{2}{\sqrt{\pi}} \int_0^{\zeta} e^{-\zeta_1^2} \, d\zeta_1 .$$

When using the boundary conditions, Eq. 4.5, one assumes that the flume is infinitely wide; therefore, just as Eq. 4.4, Eq. 4.6 is only valid where the walls of the flume do not influence the mixing.

Eq. 4.6 is a symmetrical S-shaped curve similar to the experimental curves drawn in Fig. 4.18; however, when plotted on arithmetic probability paper Eq. 4.6 is a straight line. The degree to which the shape of Eq. 4.6 fits the experimental data was checked by plotting the data on probability paper. Because the results presented in Fig. 4.20a show that the data do lie along straight lines, one may conclude that Eq. 4.6 adequately approximates the shape of the experimental concentration distributions. Later it will be shown that the variance of the lateral distribution of $\partial\overline{C}/\partial z$, which characterizes the width of the mixed zone, grew like x, as Eq. 4.6 implies.

The lateral distributions of the depth-averaged concentrations from Exp. 181, in which the fluid on the left was 0.00232 gm/cm^3 more dense than the fluid on the right, are shown in Fig. 4.19. Close to the source, where the effect of the density difference was strongest, the distributions were not symmetric as they were in

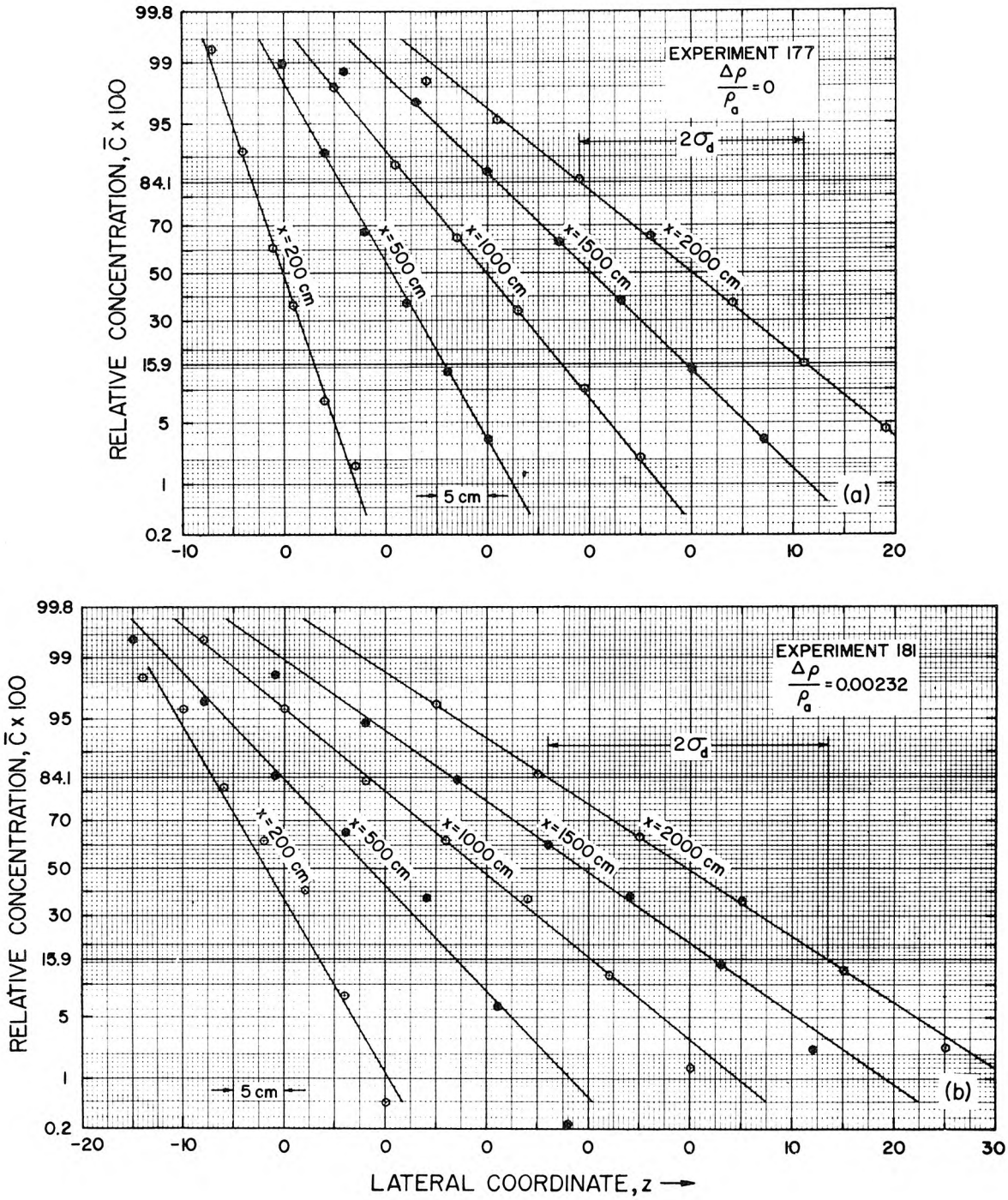

Figure 4.20 Depth-averaged concentration distributions, on arithmetic probability paper, downstream from the confluence of two wide parallel streams; Flow S1. a) Exp. 177, (b) Exp. 181.

Exp. 177. At x = 200 cm and 500 cm the curves are concave downward across most of the mixed zone. The asymmetry of the distributions was probably due to differences between the lateral components of the density-induced circulation near the bottom and close to the surface. The reason for the difference was probably caused by a difference in the Richardson numbers between the bottom and top as was mentioned in the first part of this subsection when discussing the differences between the density-induced circulations in the experiments with heavy and light tracer fluids.

The data from Exp. 181 were also plotted on probability paper and are shown in Fig. 4.20b. At x = 200 cm and 500 cm the data deviate considerably from a straight line. However, at x = 1000 cm and farther downstream the data do lie along straight lines indicating that Eq. 4.6 fits the shapes of these distributions well. One can also see that the width of the mixed zone was wider in in Exp. 181 than in Exp. 177.

4.2.4 Variances of the Lateral Concentration Distributions

4.2.4.1 Calculations of the Variances. In Chapter 2 it was mentioned that the depth-averaged lateral diffusion coefficient, $\overline{\epsilon}_z$, can be calculated with data from experiments with sources of finite width by using the expression

$$\overline{\epsilon}_z = \frac{\overline{u}}{2} \frac{d\sigma^2}{dx}, \qquad (2.10a)$$

where σ^2 is the variance of the lateral distribution of the depth-

averaged concentration. In experiments with the wide source, used to study the mixing of two wide parallel streams, σ_d^2, the variance of the lateral distribution of $\partial\overline{C}/\partial z$, is used in Eq. 2.10a in place of σ^2. The appropriate variance was calculated at each cross-section in all experiments. The data from experiments without density differences were used to calculate $\overline{\epsilon}_z$, and the variances from all experiments were used to characterize the widths of the tracer plumes or mixed zones.

The variances were calculated numerically by taking the second moments of the distributions, defined by the experimental curves, about their centroids and dividing by the areas under the distributions. The variance σ^2 was calculated using Eq. 4.7b:

$$\sigma^2(x) = \frac{\int_{-\infty}^{\infty} (z-\bar{z})^2 \, \overline{C}(x, z)\, dz}{\int_{-\infty}^{\infty} \overline{C}(x, z)\, dz} \qquad (4.7a)$$

$$\approx \frac{\sum_{i=0}^{n} (z_1 + i\Delta z - \bar{z})^2 \, \overline{C}(x, z_1 + i\Delta z)\, \Delta z}{\sum_{i=0}^{n} \overline{C}(x, z_1 + i\Delta z)\, \Delta z} \,, \qquad (4.7b)$$

and σ_d^2 was calculated using Eq. 4.8b:

$$\sigma_d^2(x) = \frac{\int_{-\infty}^{\infty} (z-\bar{z}_d)^2 \frac{\partial \bar{C}(x,z)}{\partial z}\, dz}{\int_{-\infty}^{\infty} \frac{\partial \bar{C}(x,z)}{\partial z}\, dz}\ , \tag{4.8a}$$

$$\approx \frac{\sum_{i=0}^{n} [z_1+(i+\frac{1}{2})\Delta z-\bar{z}_d]^2[\bar{C}(x, z_1+(i+1)\Delta z) - \bar{C}(x, z_1+ i\Delta z)]}{\bar{C}(x, z+(n+1)\Delta z) - \bar{C}(x, z_1)}\ . \tag{4.8b}$$

The range $z_1 < z < z_1+(n+1)\Delta z$ was chosen sufficiently wide to include all nonzero terms in the summations. The terms $\bar{z}$ and $\bar{z}_d$ are the z-coordinates of the centroids of the distributions of $\bar{C}$ and of $\frac{\partial \bar{C}}{\partial z}$, respectively. These coordinates were calculated by taking the first moments of the distributions about z = 0, and dividing by the areas;

$$\bar{z} = \frac{\int_{-\infty}^{\infty} z\bar{C}(x, z)\, dz}{\int_{-\infty}^{\infty} \bar{C}(x, z)\, dz}\ , \tag{4.9a}$$

$$\approx \frac{\sum_{i=0}^{n} (z_1+i\Delta z)\, \bar{C}(x, z_1+i\Delta z)\, \Delta z}{\sum_{i=0}^{n} \bar{C}(x, z_1+i\Delta z)\, \Delta z}\ , \tag{4.9b}$$

and

$$\bar{z}_d = \frac{\int_{-\infty}^{\infty} (z) \frac{\partial \bar{C}(x, z)}{\partial z} dz}{\int_{-\infty}^{\infty} \frac{\partial \bar{C}(x, z)}{\partial z} dz} \qquad (4.10a)$$

$$\approx \frac{\sum_{i=0}^{n} [z_1 + (i+\tfrac{1}{2}) \Delta z] [\bar{C}(x, z_1 + (i+1) \Delta z) - \bar{C}(x, z_1 + i\Delta z)]}{[\bar{C}(x, z_1 + (n+1) \Delta z) - \bar{C}(x, z_1)]} \qquad (4.10b)$$

The variances, the coordinates of the centroids, and the areas under the distributions are listed for all experiments in Tables A1 and A2 of the appendix. The variances are also presented graphically later in this chapter.

To use the above equations, values of $\bar{C}$ were obtained from the experimental curves at intervals, Δz, usually equal to 1 cm. The accuracy of the numerical integrations was checked by using Eq. 4.7b and 4.9b with an interval Δz equal to 0.2σ to compute the variance and area of a normalized Gaussian distribution which had a variance and an area equal to unity. The computations gave a variance of 0.998 and an area of 1.000.

It is possible to use the data from experiments with the wide source to obtain variances downstream from a 110-cm-wide source. One may assume that the left wall of the flume was the center line of a 110-cm-wide source which discharged fluid with a density equal to or greater than the ambient fluid. In this case the fluid to the left of the dividing wall represents half of the source and the fluid to the right of the wall represents the ambient fluid. One can also

assume that the fluid to the right of the dividing wall represents half of a 110-cm-wide source which discharged fluid with a density equal to or less than the ambient fluid. In this case, the ambient fluid is represented by the fluid to the left of the dividing wall. For either case, the variance of a lateral concentration distribution, σ^2, can be calculated by taking the second moment about the appropriate sidewall of the flume. However, when taking moments about the right wall, one must redefine the relative concentration so that $\overline{C} = 1$ to the right of the dividing wall and $\overline{C} = 0$ to the left.

A difficulty with this method of calculating σ^2 is that the calculations are very sensitive to errors in the observed concentration distributions. For this reason, only values of σ_d^2 are presented in this text. However, it is possible to show that

$$\sigma^2(x) = \sigma_d^2(x) + \sigma^2(0) \tag{4.11}$$

if the distribution of $(\overline{C}-\frac{1}{2})$ is an odd function of z. Thus, far downstream in experiments with density differences, and everywhere in experiments without density differences, one can use Eq. 4.11 and the data to compute the variances, $\sigma^2(x)$, downstream from a 110-cm-wide source.

In all experiments, except numbers 128 and 132, neither the plume nor the mixed zone reached the sidewalls of the flume. Thus, one may expect that the sidewalls did not have much effect on the measured concentration distributions nor on the computed values of

σ^2 or σ_d^2. The effects of the sidewalls on the data were investigated for some experiments by plotting the cumulative distributions of the depth-averaged concentrations on arithmetic probability paper. Because the lateral distributions of $\overline{C}$ were nearly Gaussian in experiments using the 1-cm-wide source and neutrally buoyant tracer fluids, the cumulative distributions from these experiments should approximate straight lines when plotted on arithmetic probability paper. When the cumulative distribution of a Gaussian curve is plotted on arithmetic probability paper, the variance can be obtained by measuring the distance between the points $z_{84.1}$ (where $P(x, z) = 84.1$ percent) and $z_{15.9}$ (where $P(x, z) = 15.9$ percent) and by using the expression

$$\sigma^2(x) = \left(\frac{z_{84.1} - z_{15.9}}{2}\right)^2 \quad . \tag{4.12}$$

Also, the centroid is at z_{50}, where $P(x, z) = 50$ percent.

The cumulative distribution, $P(x, z)$, expressed as a percent of the area under the depth-averaged concentration distribution, was calculated by using Eq. 4.13b;

$$P(x, z) = \frac{\int_{-\infty}^{z} \overline{C}(x, z')dz'}{\int_{-\infty}^{\infty} \overline{C}(x, z')dz'} \cdot 100 \tag{4.13a}$$

$$P(x, z_1 + (j+\tfrac{1}{2})\,\Delta z) \approx \frac{\sum_{i=0}^{j} \overline{C}(x, z_1 + i\Delta z)\,\Delta z}{\sum_{i=0}^{n} \overline{C}(x, z_1 + i\Delta z)\,\Delta z} \cdot 100 \quad . \qquad (4.13b)$$

The cumulative distributions from Exp. 125, in which the source was 1 cm wide and the tracer fluid was neutrally buoyant, are presented in Fig. 4.21. The points were obtained by using Eq. 4.13b with values of $\overline{C}$ obtained from the solid curves drawn through the original data in Fig. 4.12; the open circles in Fig. 4.21 mark the locations of data points in Fig. 4.12. The points in Fig. 4.21 lie along well defined straight lines in the range P(x, z) = 1 percent to 99 percent. The deviations from the straight lines outside this range are consistently in the direction which would be caused by the sidewalls hindering lateral diffusion at the edges of the distributions. However, because the deviations do not increase with increasing plume widths, the deviations are more likely due to either consistent errors in drawing the tails of the curves in Fig. 4.12, or the concentration distributions not being Gaussian at the edges.

Values of σ^2 were calculated for Exp. 125 by drawing straight lines through the linear parts of the distributions in Fig. 4.21 and by using Eq. 4.12. These variances are given in Table 4.4 and are compared with the variances that were calculated by using the method of moments, Eq. 4.7b. The differences between the variances that were calculated by the two

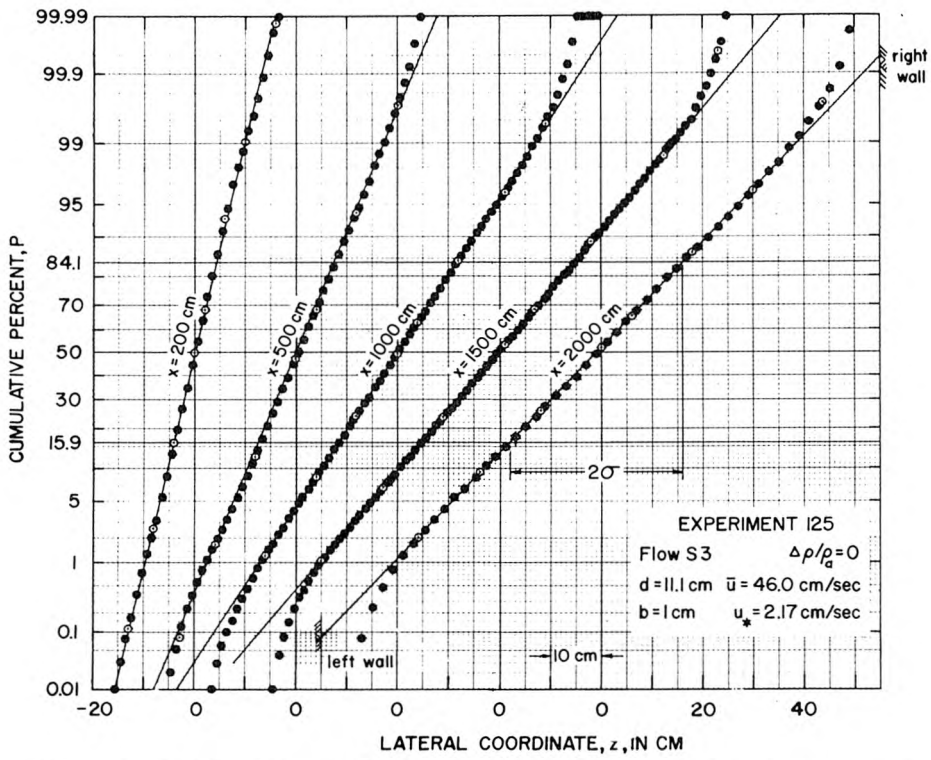

Figure 4.21 Cumulative distributions of depth-averaged concentrations from Exp. 125, $\Delta\rho/\rho_a = 0$.

Table 4.4 Variances of lateral distributions of depth-averaged concentrations in Exp. 125.

Distance downstream from source x (cm)	Variance $\sigma^2(x)$ (cm^2)	
	from second moment	from cumulative distribution
200	17	19
500	55	56
1000	136	136
1500	223	227
2000	290	291

methods are small. Because anomalies in the tails of the distributions do not affect the values of σ^2 calculated with Eq. 4.12, and because values of σ^2 given by Eq. 4.12 and 4.7b are nearly the same, one can conclude that the sidewalls had little effect on the values of σ^2 that were calculated for Exp. 125 by the method of moments. Also, because the plume was wider in Exp. 125 than in most other experiments, one can conclude that the sidewalls had little effect on the lateral mixing of tracer fluids in most of the experiments in this investigation.

In Exp. 128 and 132 in which the plumes did reach the sidewalls, the variances were calculated with Eq. 4.12; however, Eq. 4.7b was used to calculate σ^2 for all other experiments.

The right hand side of Eq. 4.12 can also be used to calculate σ_d^2 for concentration distributions defined by Eq. 4.6. The values of σ_d^2 calculated for Exp. 177 by using Eq. 4.12 also agree well with those obtained by using Eq. 4.8b; however, the latter equation was used to calculate all data presented in this text.

4.2.4.2 Presentation of the Variances. The variances σ^2 and σ_d^2, which were calculated by the methods described above, are presented in Fig. 4.22a to 4.33a as functions of x, the distance downstream from the source. The same data are presented in Table A1 and A2 of the appendix. (In parts b of these figures, $\overline{C}_v$, averaged coefficients of variation of the vertical concentration profiles are given. The quantity $\overline{C}_v$ is defined and these data are

discussed in Subsection 4.2.5 of this chapter.) All data that appear on one figure are from experiments with the same hydraulic conditions and source, but with tracer fluids of different densities. The solid curves in the figures were fitted to the data by eye.

In at least one of the experiments presented on each figure, $\Delta\rho/\rho_a = 0$. Except for very close to the source, $\sigma^2(x)$ is linear for these experiments which indicates that the depth-averaged coefficients, $\bar{\epsilon}_z$, were not functions of x. The slopes of these curves and values of $\bar{\epsilon}_z$ are given in Chapter 5. For the present, it is worth noting that the differences between the slopes of the variance-distance curves are small for experiments with the same flow conditions and with $\Delta\rho/\rho_a = 0$ but with different sources. This is true even for Exp. 170 (shown in Fig. 4.25a) in which the 10-cm-wide source was placed against the left wall of the flume and for which the data were analysed as if the wall were the center line of a 20-cm-wide source. All other data are from experiments in which the plume or mixed zones were on the flume center line.

In experiments in which there was a difference in density between the tracer and ambient fluids, the variances close to the source increased more rapidly than in experiments in which there were no density differences. Far downstream, the variances increased at the same rate as in experiments in which $\Delta\rho/\rho_a = 0$. The large initial increases in the variances were due to secondary flows which were induced by the large initial lateral density gradients.

Far downstream, where the widths of the plumes or the mixed zones became large and the lateral density gradients became small, the magnitudes of the secondary current velocities decreased, and mixing by density-induced circulation became insignificant compared to mixing by turbulent diffusion. There, the variance-distance curves were drawn so that they were linear and parallel to those obtained in the experiments with $\Delta\rho/\rho_a = 0$.

The effect of an initial density difference on a variance-distance curve far downstream from the source thus appears as a vertical displacement of the curve. The difference in variances between experiments with $\Delta\rho/\rho_a = 0$ and $\Delta\rho/\rho_a \neq 0$ measured at some value of x where the variance-distance curves are parallel will be called the excess variance denoted by $\Delta\sigma^2$. By examining the data in the figures, one can see that the excess variance increases with the initial density difference. By comparing the data in Fig. 4.22 from Exp. 147 with the data from Exp. 121, and the data in Fig. 4.27 from Exp. 128 with the data from Exp. 113 and 114, one can see that an initial negative density difference causes a larger excess variance than a positive density difference of the same magnitude. A quantitative analysis of $\Delta\sigma^2$ obtained from the data is given in Chapter 5.

In Table A1, data are presented from two sets of experiments with flow S1 and with the 12.5-cm-wide source, Exp. 156 to 161 and Exp. 162 to 167. Only the data from the second set are presented graphically in this subsection and are used in Chapter 5 in the

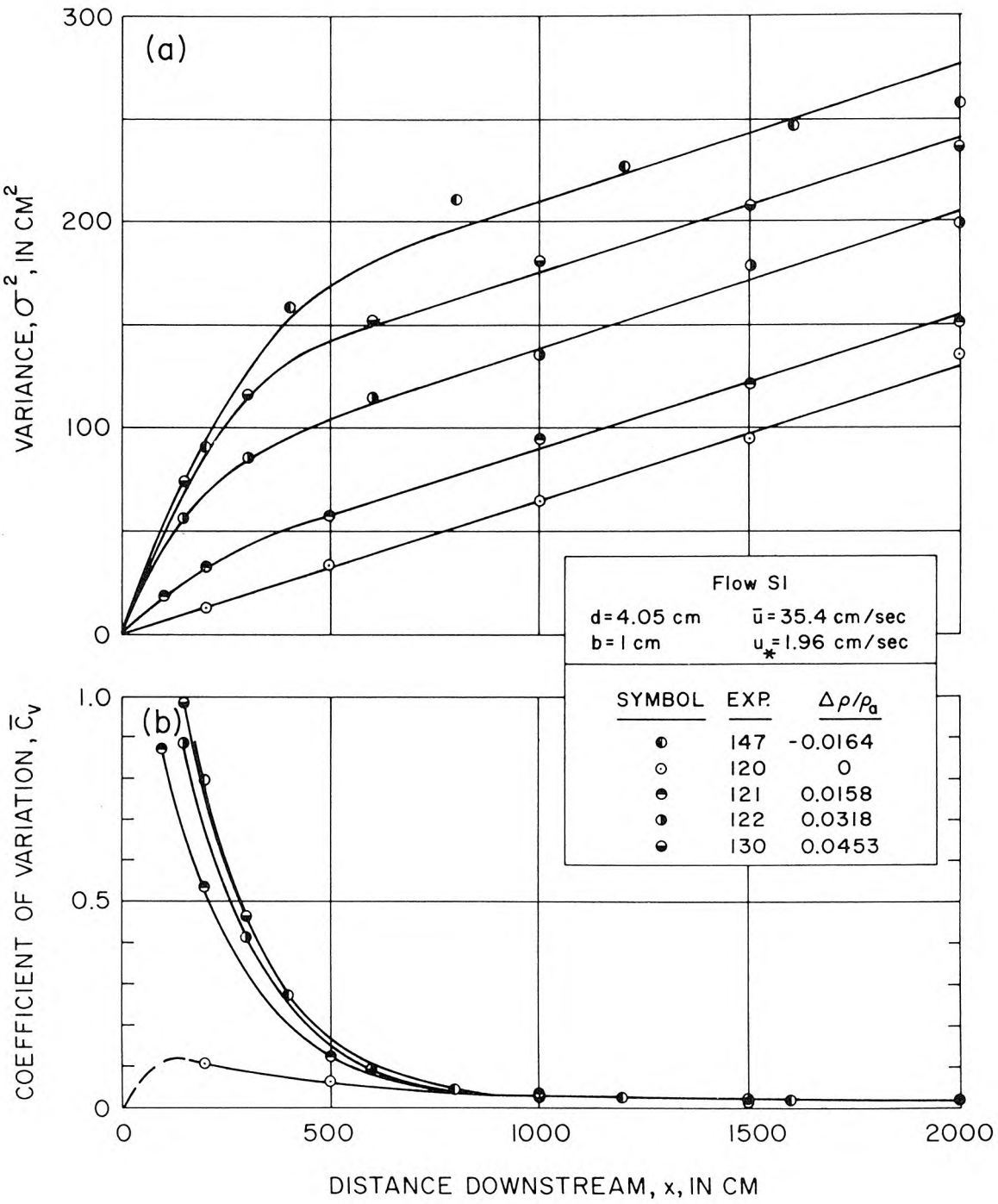

Figure 4.22 a) Variance- and b) Coefficient of variation-distance curves from experiments with flow S1 and the 1-cm-wide source.

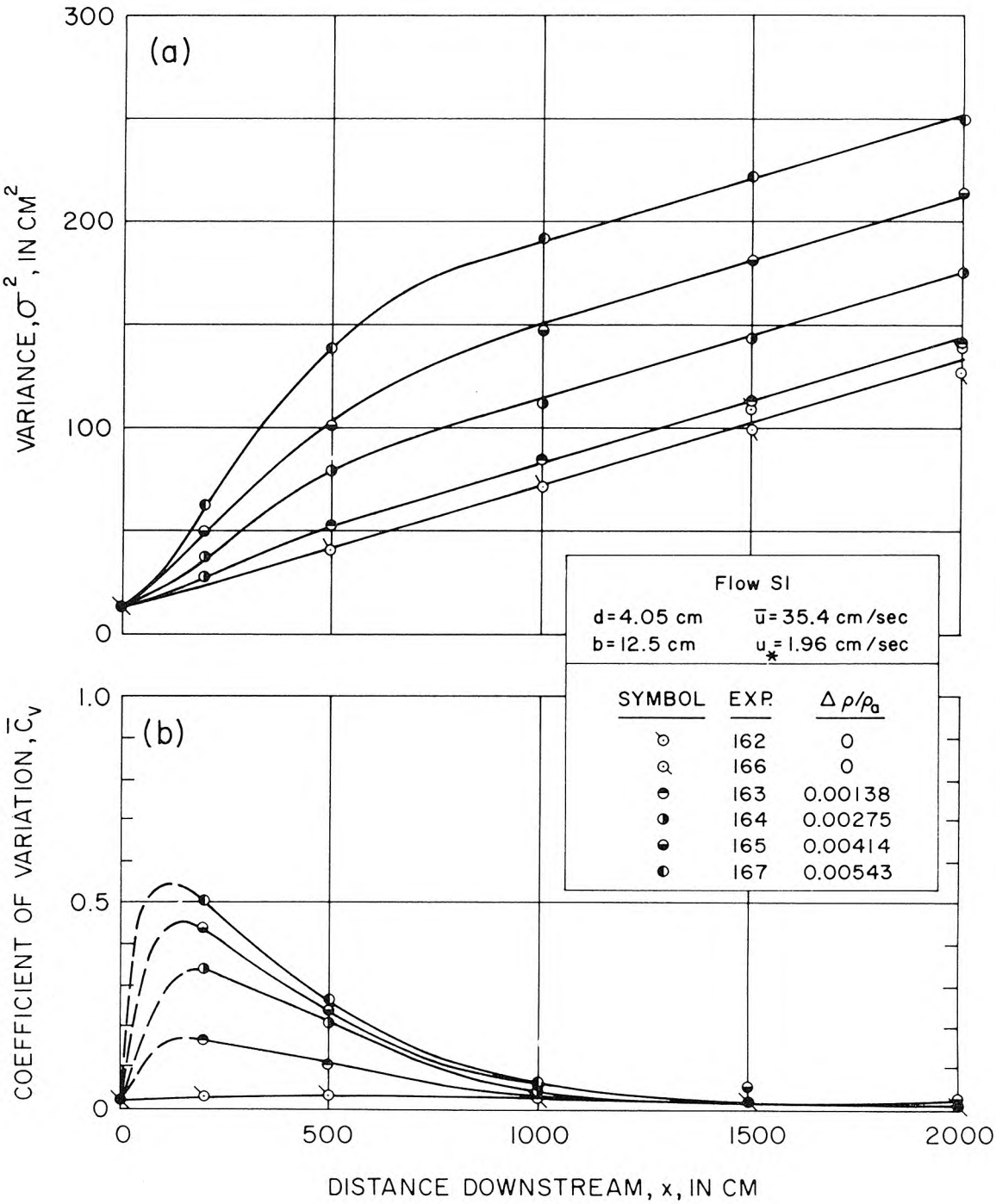

Figure 4.23 a) Variance- and b) Coefficient of variation-distance curves from experiments with flow S1 and the 12.5-cm-wide source.

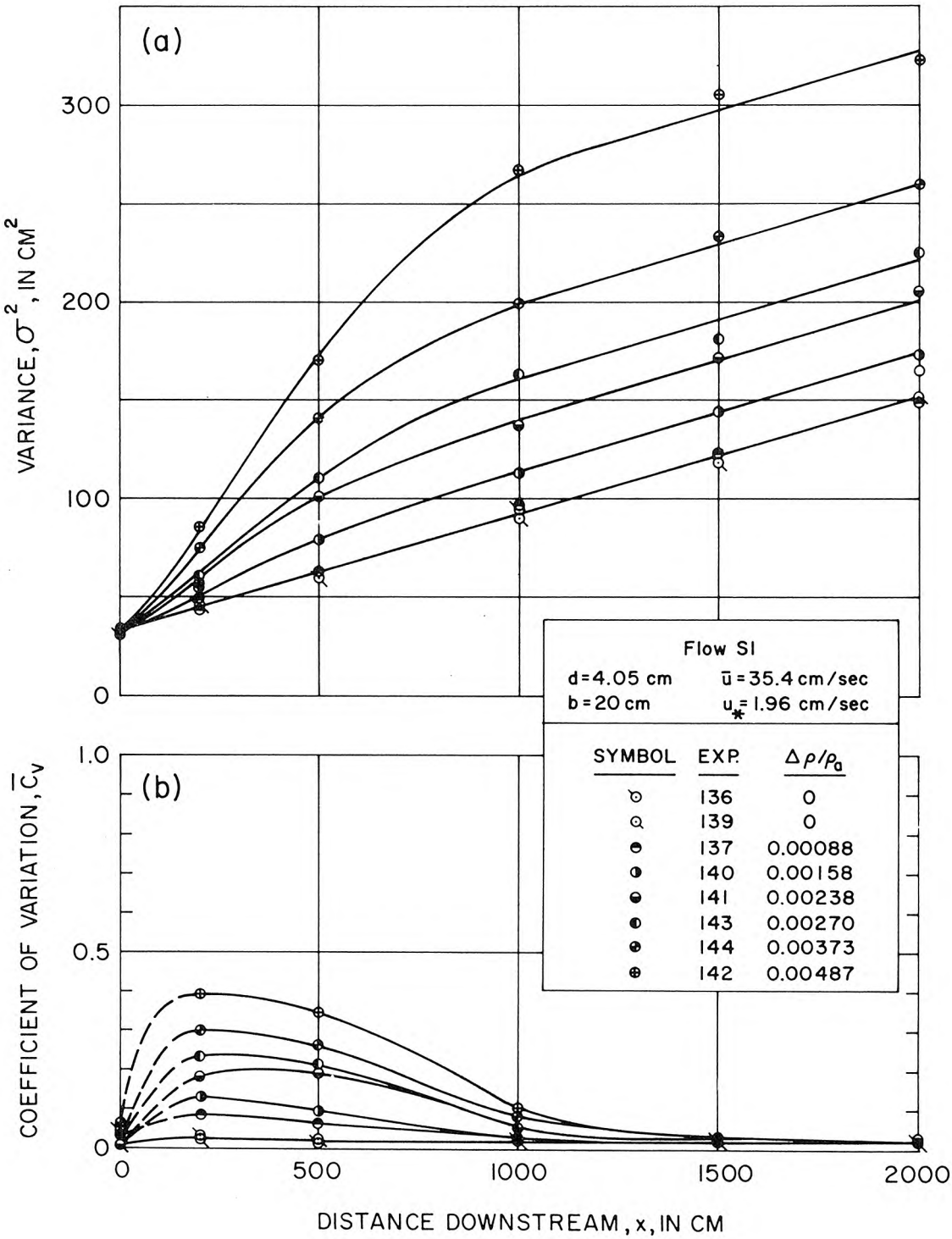

Figure 4.24 a) Variance- and b) Coefficient of variation-distance curves from experiments with flow S1 and the 20-cm-wide source.

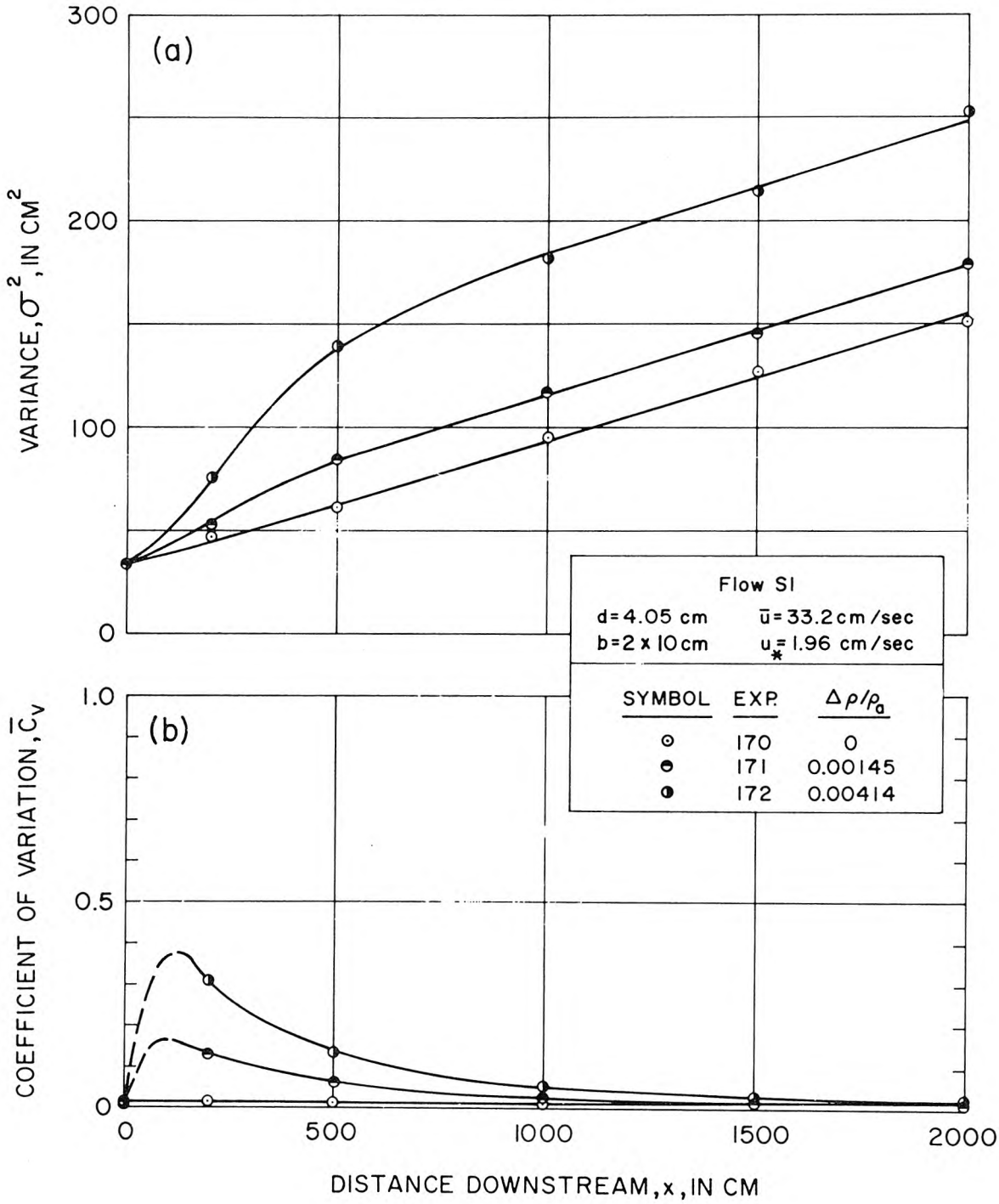

Figure 4.25 a) Variance- and b) Coefficient of variation-distance curves from experiments with flow S1 and the 10-cm-wide source. Source placed against left sidewall of flume and data analysed as if wall were center line of 20-cm-wide source.

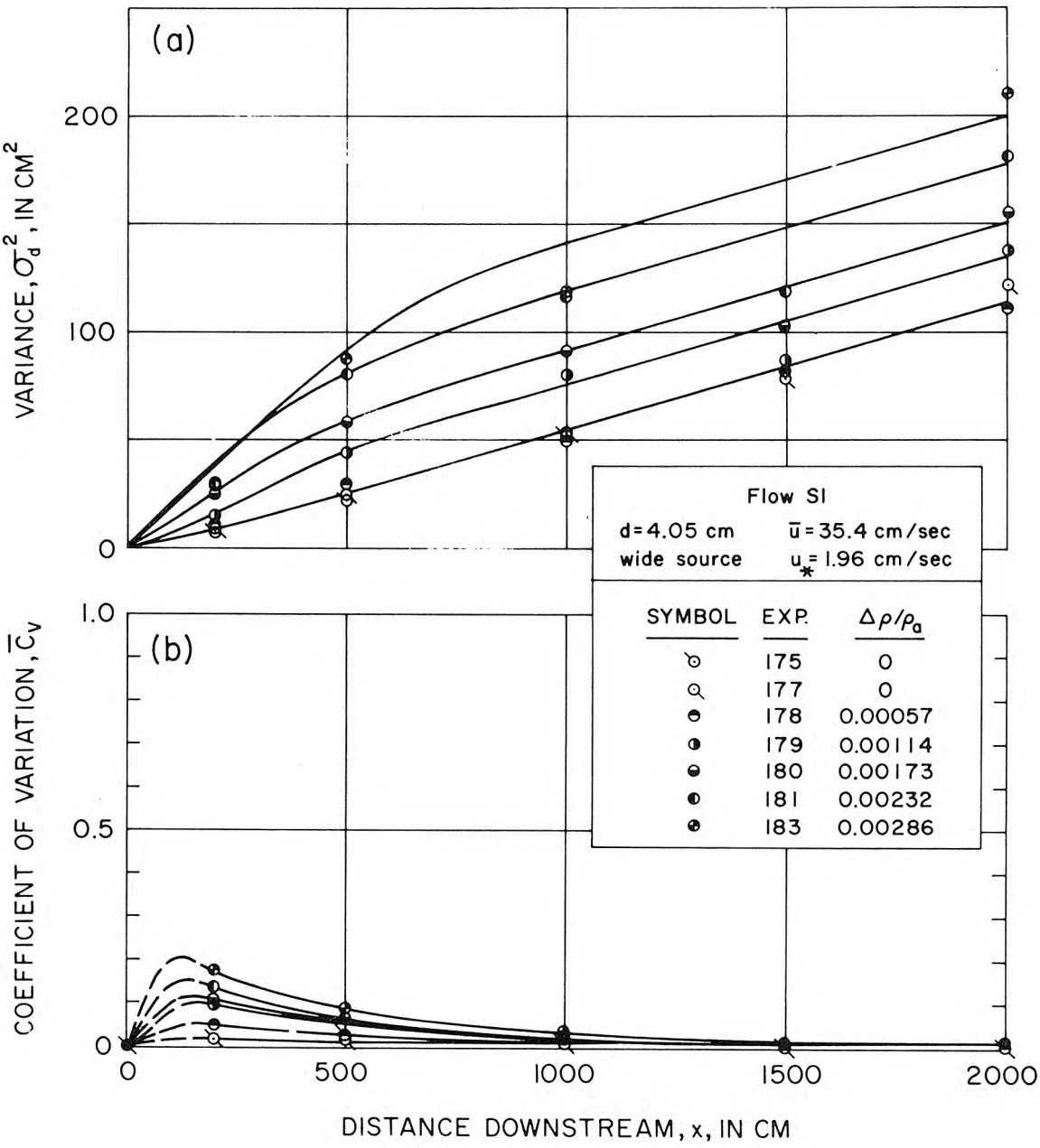

Figure 4.26 a) Variance- and b) Coefficient of variation-distance curves from experiments with flow S1 and the wide source.

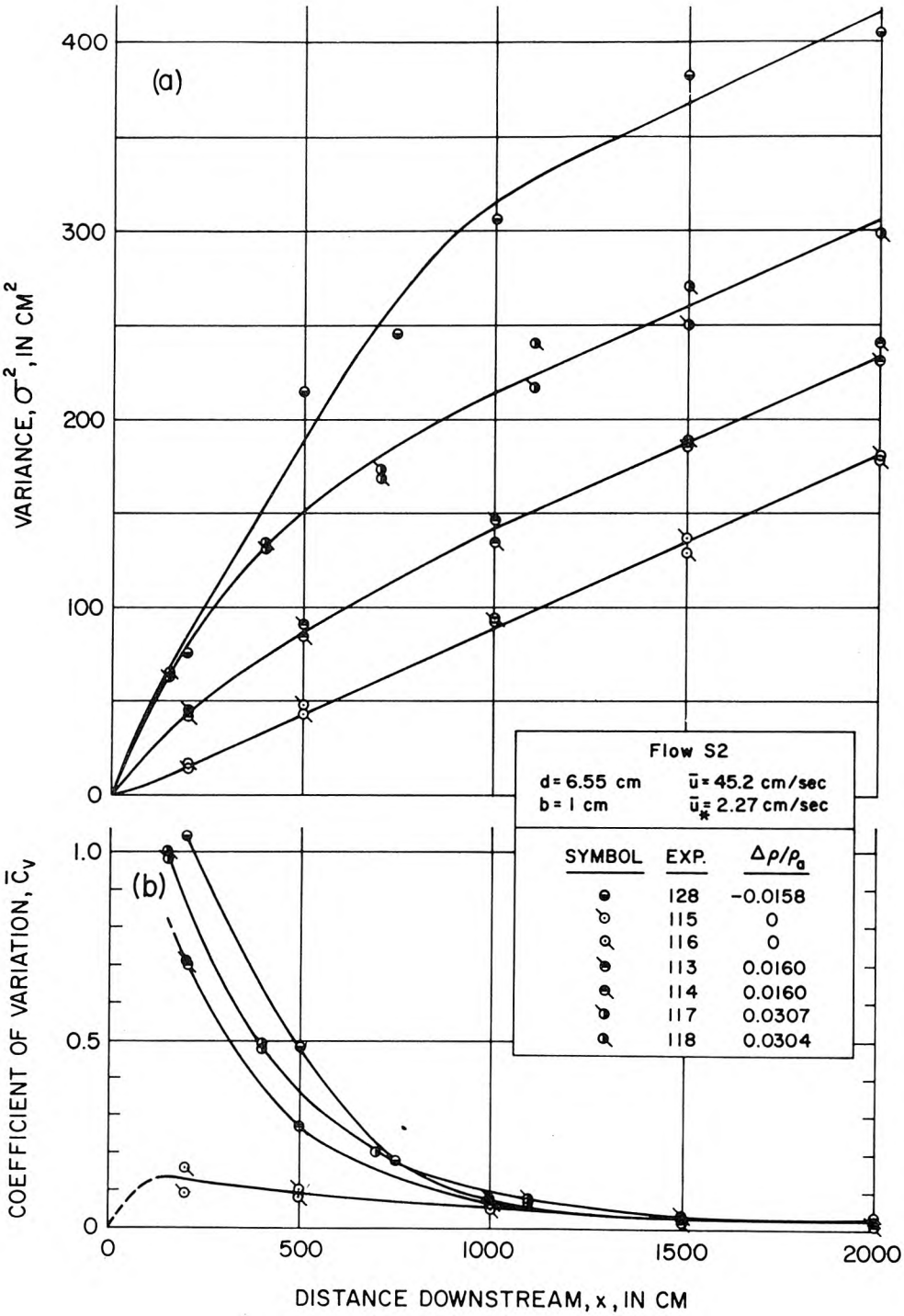

Figure 4.27 a) Variance- and b) Coefficient of variation-distance curves from experiments with flow S2 and the 1-cm-wide source.

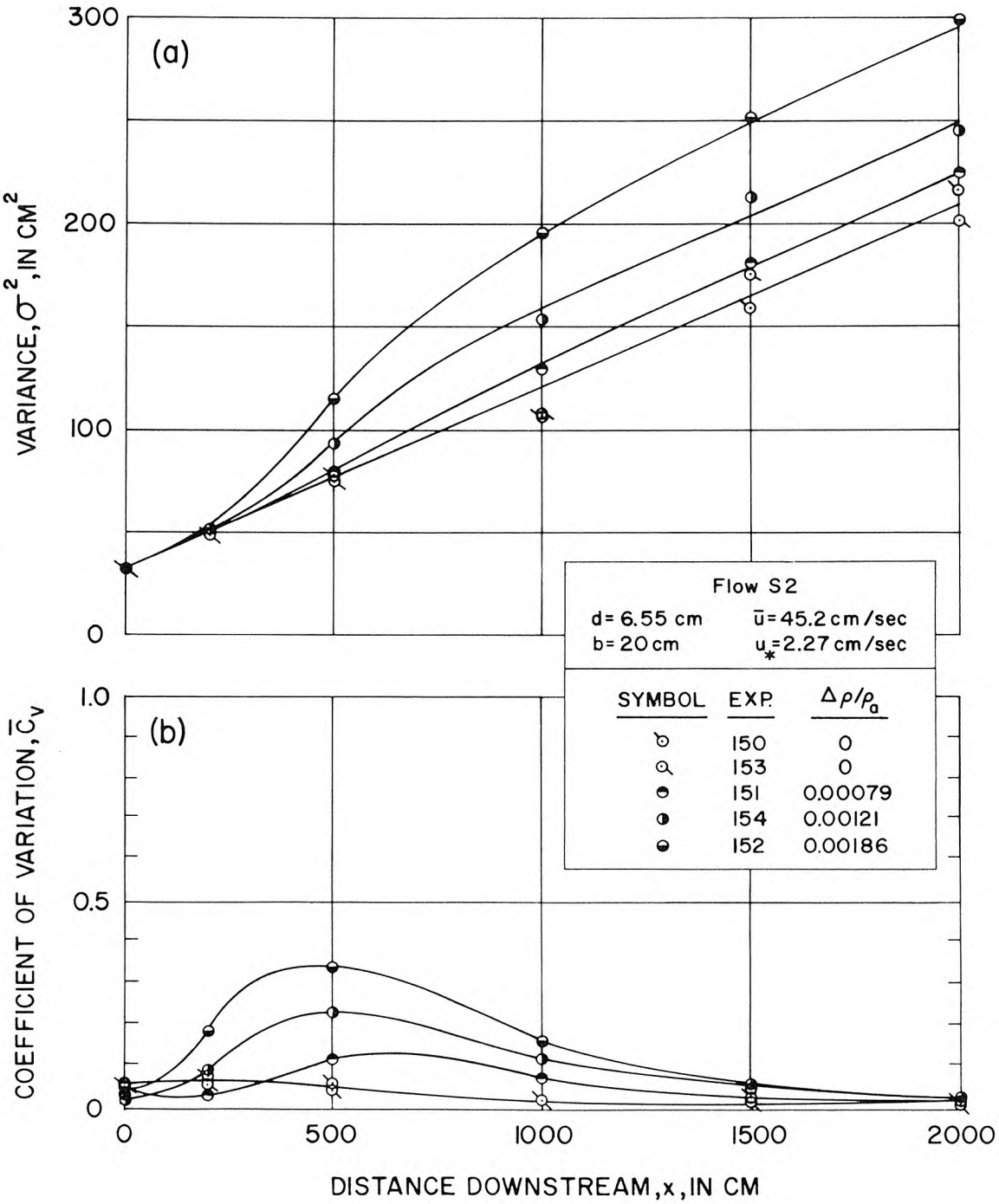

Figure 4.28 a) Variance- and b) Coefficient of variation-distance curves from experiments with flow S2 and the 20-cm-wide source.

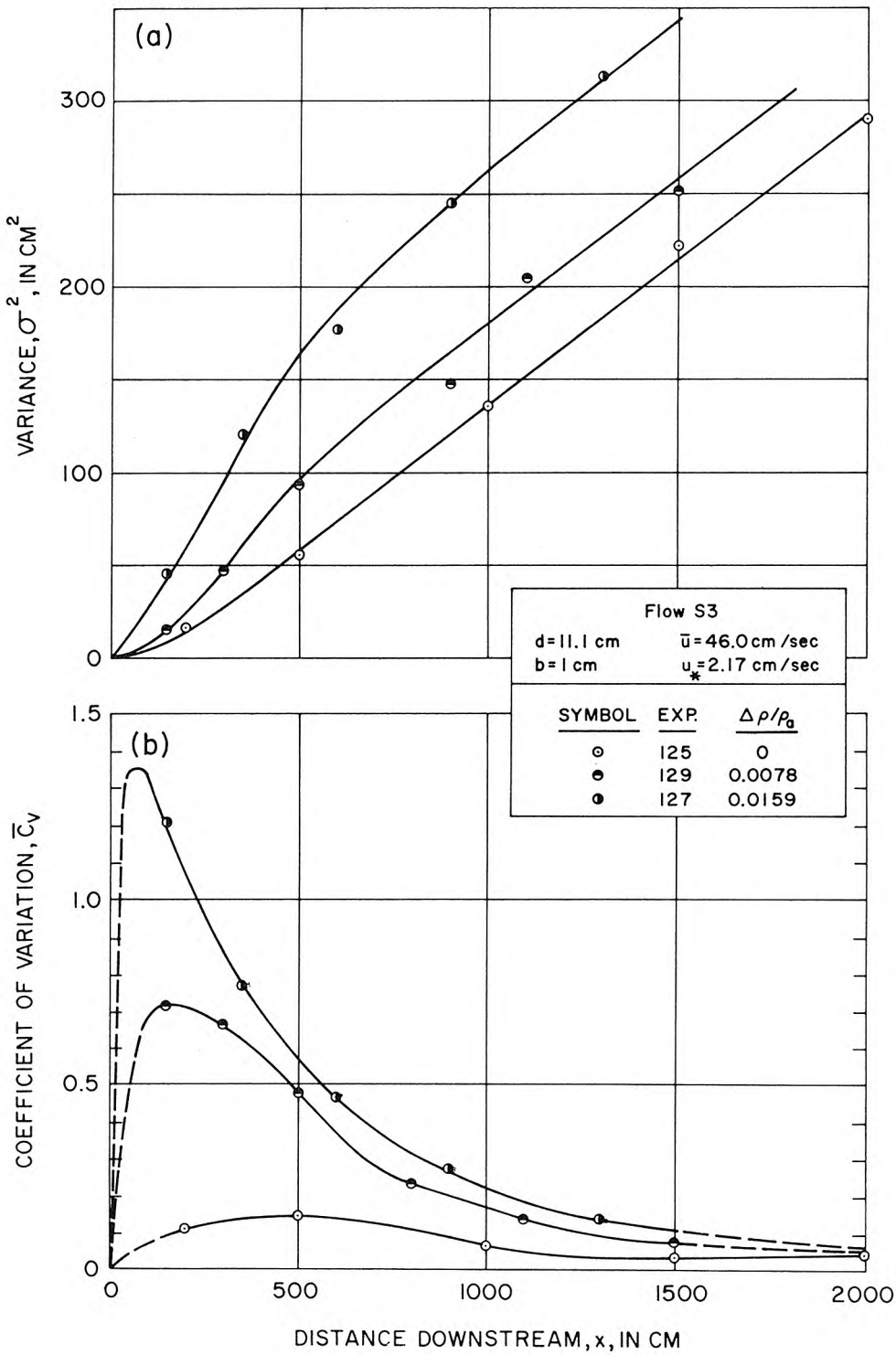

Figure 4.29 a) Variance- and b) Coefficient of variation-distance curves from experiments with flow S3 and the 1-cm-wide source.

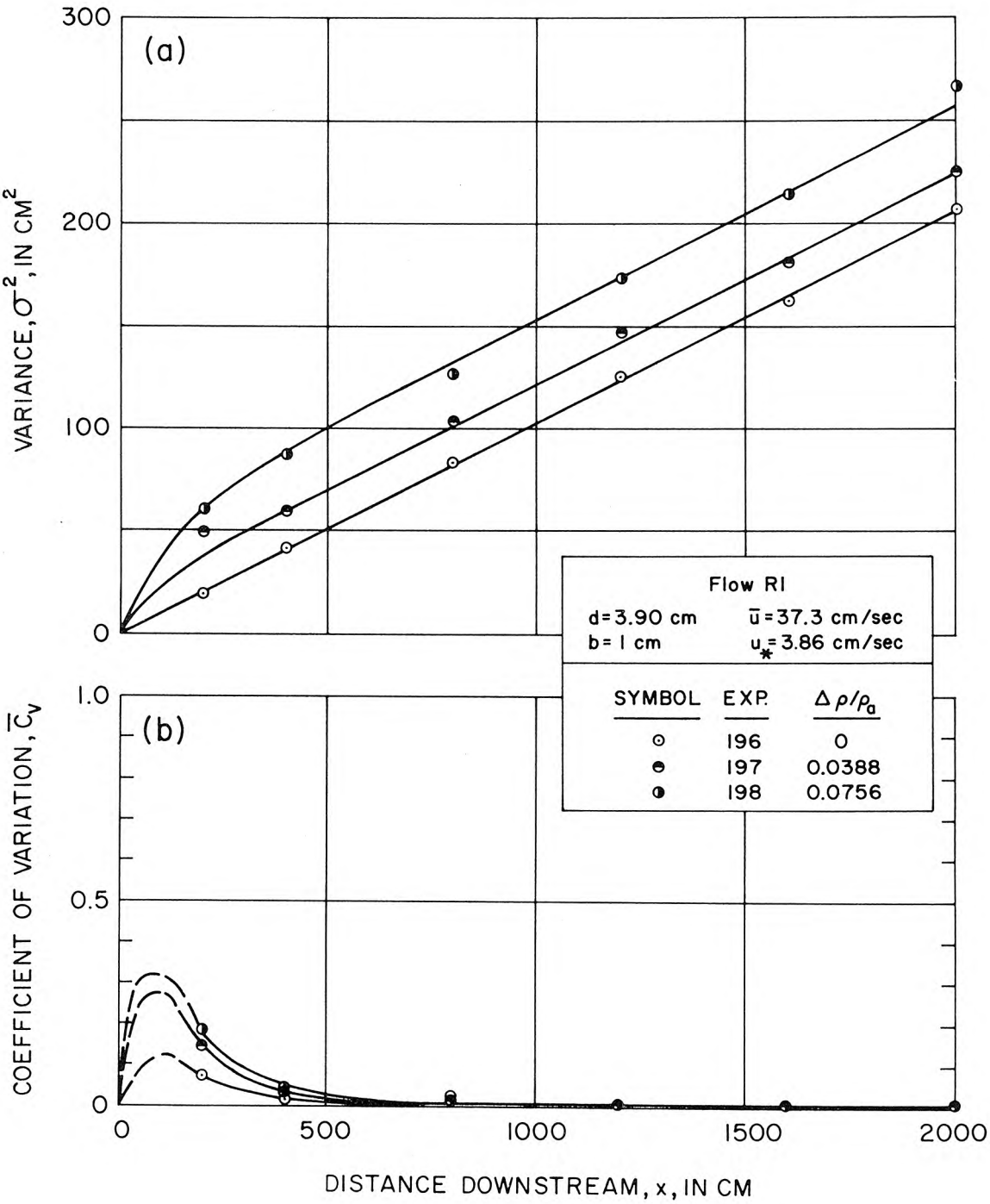

Figure 4.30 a) Variance- and b) Coefficient of variation-distance curves from experiments with flow R1 and the 1-cm-wide source.

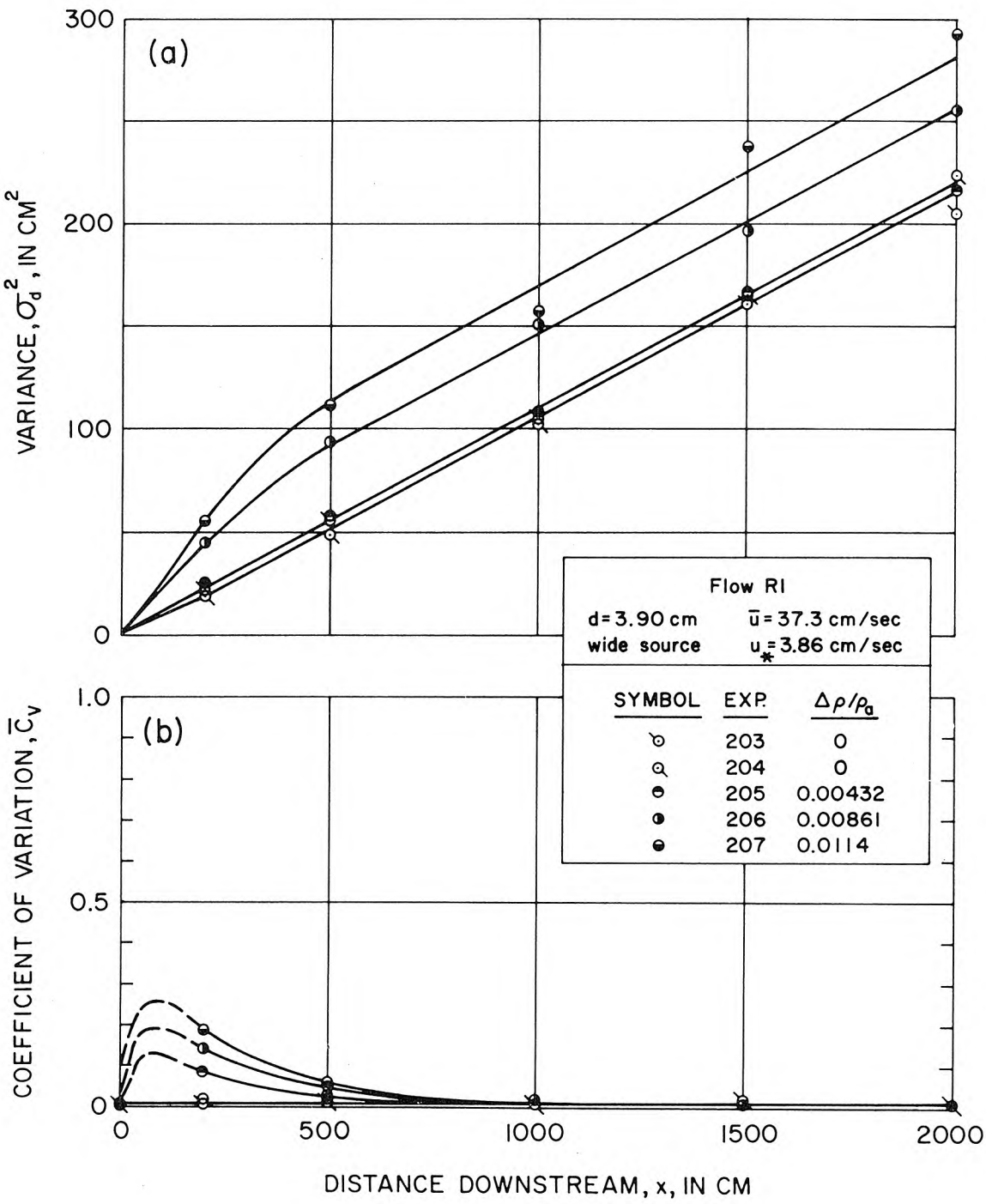

Figure 4.31 a) Variance- and b) Coefficient of variation-distance curves from experiments with flow R1 and the wide source.

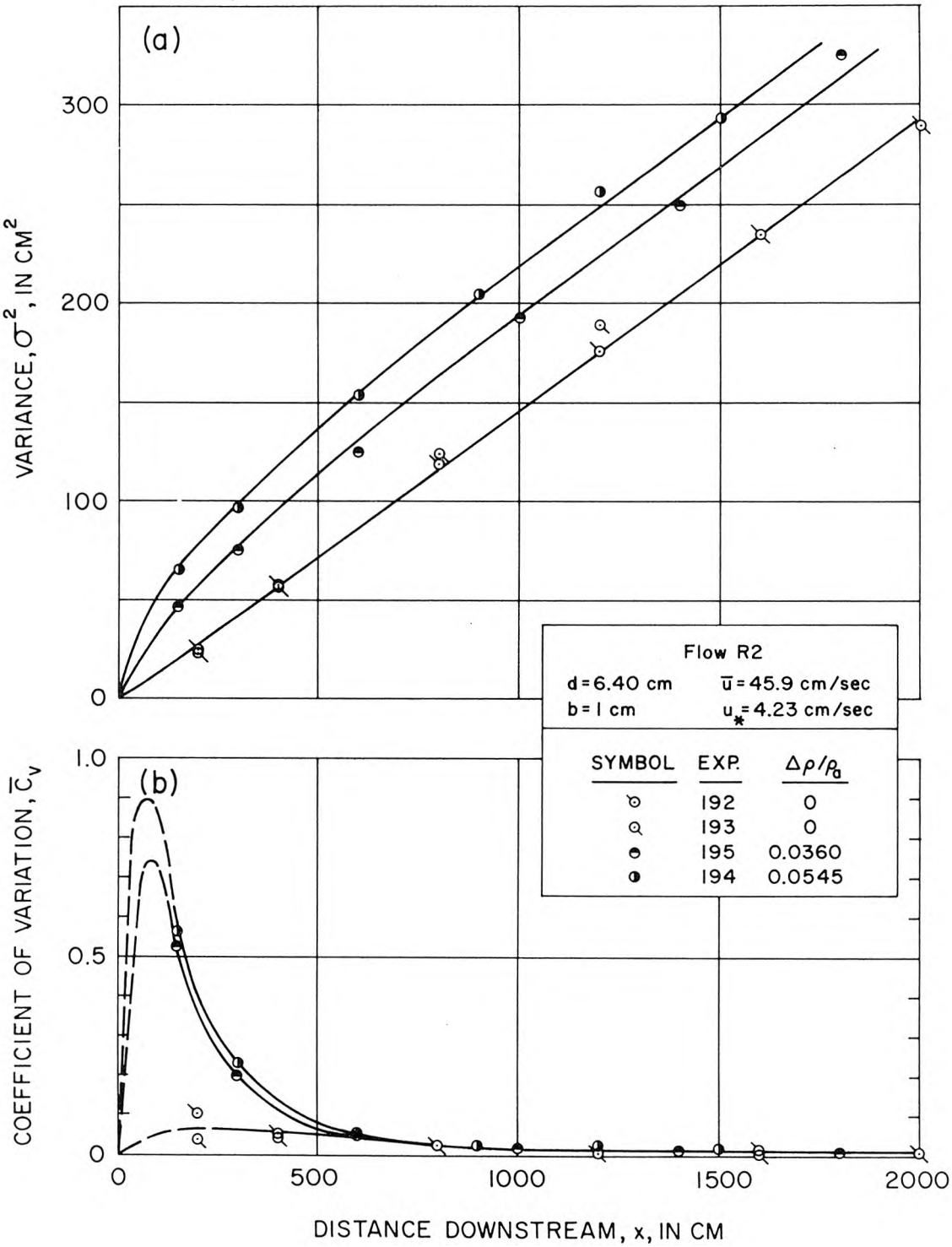

Figure 4.32 a) Variance- and b) Coefficient of variation-distance curves from experiments with flow R2 and the 1-cm-wide source.

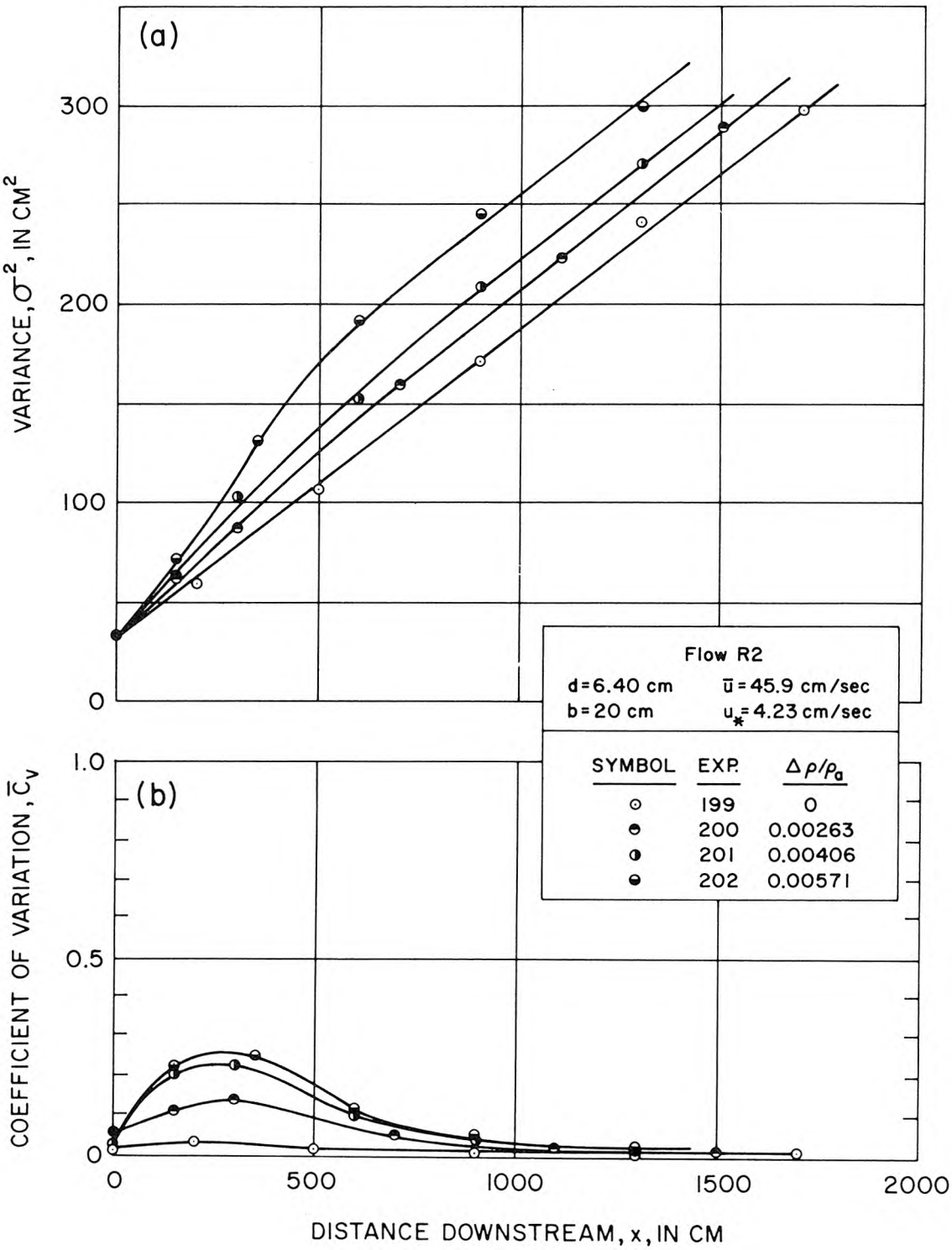

Figure 4.33 a) Variance- and b) Coefficient of variation-distance curves from experiments with flow R2 and the 20-cm-wide source.

analyses of experiments with density differences. The data from the first set were omitted because the flow immediately downstream from the source was excessively agitated by a hydraulic jump which was created between the guide walls by the jets from the manifold. Although the values of $\overline{\epsilon}_z$ were not affected, eliminating the hydraulic jump in the second set of experiments yielded larger values of $\Delta\sigma^2$ for an equal density difference because the excessive vertical mixing at small x was reduced.

4.2.5 Photographs of Experiments. Some photographs taken of experiments in which the tracer fluid was dyed are shown in Fig. 4.34 to 4.39. The camera was located about 250 cm above the flume bottom and about 500 cm upstream from each source. The eight white tags on the right-hand side of the flume mark longitudinal stations x = 0 to 700 cm at 100 cm intervals. The scale in the lateral direction is obtained by recalling that the flume is 110 cm wide. Although the photographs were not taken on the same day that quantitative data were obtained, the hydraulic conditions and the density differences for the experiment indicated below each photograph were duplicated at the time each photograph was taken. All photographs which appear in the same figure are of experiments with the same source and flow condition but different initial density differences.

Photographs of experiments with flow condition S1 and a 1-cm-wide source are shown in Fig. 4.34. As found from the quantitative data, the width of the plume increased as the initial density difference increased. Also, one can see that a negative density difference (Exp. 147) enhanced lateral spreading more than a positive density difference of the same magnitude (Exp. 121). One can also see in the photographs that the boundary between the dyed plume and clear ambient fluid was more irregular when $\Delta\rho/\rho_a$ was negative than when it was positive. The photograph of Exp. 130 has a light area in the center of the plume which is indicative of a low concentration, and therefore, a bimodal lateral concentration distribution.

Photographs of experiments with the 1-cm-wide source and flow condition R1 are presented in Fig. 4.35. By comparing the photographs of Exp. 120 in Fig. 4.34 with Exp. 196 in Fig. 4.34, one can see that the effect of a rough bottom is to increase the lateral mixing in the experiments in which $\Delta\rho/\rho_a = 0$. However, by comparing the photographs of Exp. 130 and 198, it appears that from x = 100 cm to at least x = 600 cm, the plume was narrower in Exp. 198, in which $\Delta\rho/\rho_a = 0.0765$, than in Exp. 130, in which $\Delta\rho/\rho_a = 0.0453$. The quantitative data in Figs. 4.30 and 4.22 confirm this observation. The reason for this apparent anomaly is that the more intense vertical mixing caused by the rough bottom limited the magnitude and duration of the secondary flow velocities more than the less intense vertical mixing in the experiment with the smooth bottom.

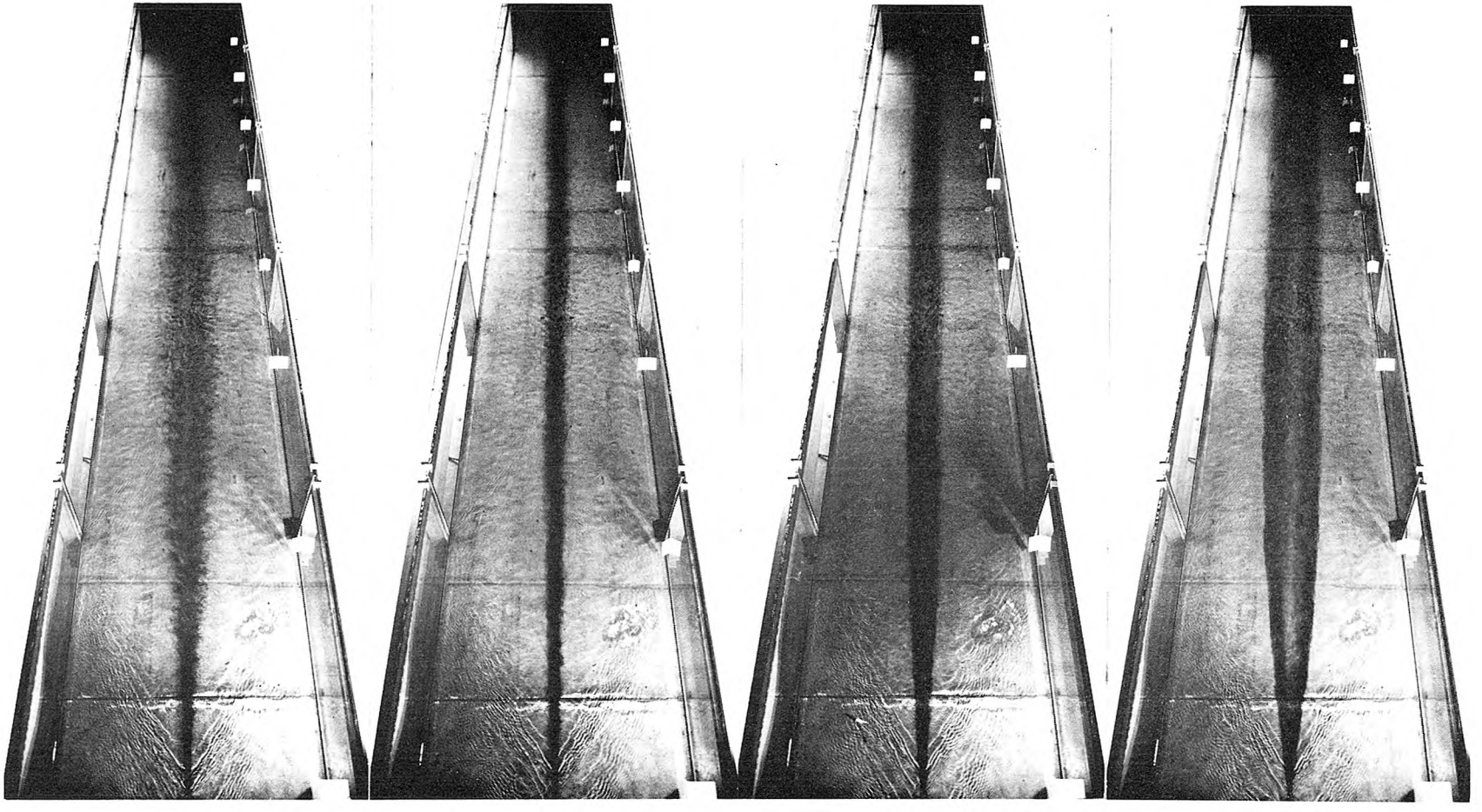

10092	10088	10089	10091
Exp. 147	120	121	130
$\Delta\rho/\rho_a$ = -0.0164	0	0.0158	0.0453

Figure 4.34 Photographs of experiments with flow S1 and the 1-cm-wide source. $d = 4.05$ cm, $\bar{u} = 35.4$ cm/sec, $u_* = 1.96$ cm/sec.

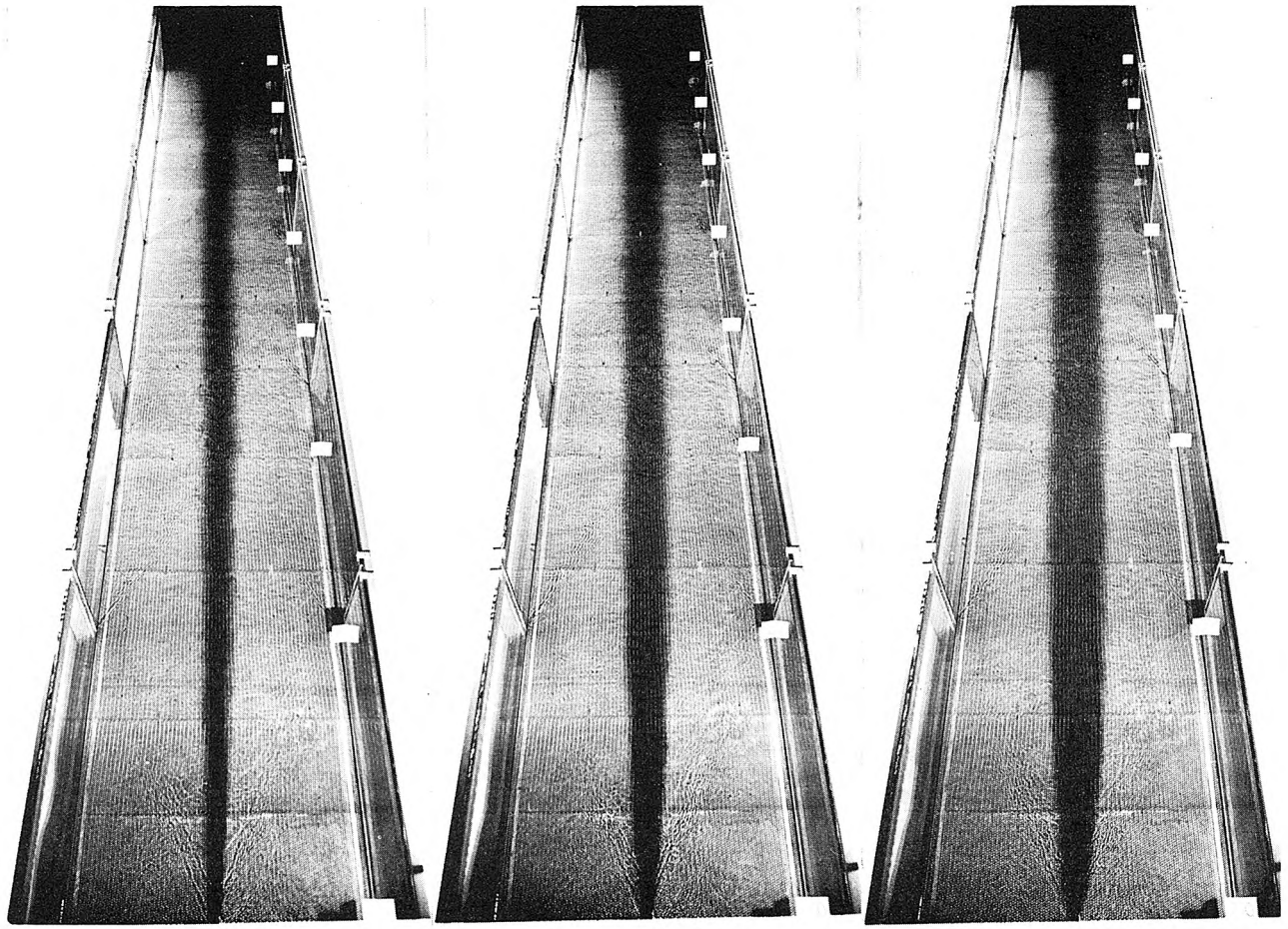

Exp. 196 10074 197 10075 198 10076

$\Delta\rho/\rho_a$ = 0 0.0388 0.0756

Figure 4.35 Photographs of experiments with flow R1 and the 1-cm-wide source. d = 3.90 cm, $\bar{u}$ = 37.3 cm/sec, u_* = 3.86 cm/sec.

In Fig. 4.36, photographs of the plumes downstream from the 20-cm-wide source in experiments with flow condition S1 are shown. Here the effects of a density difference can also be seen but not as dramatically as in the photographs of experiments with the 1-cm-wide source.

The photographs in Fig. 4.37 of experiments with the 1-cm-wide source and flow condition S2 also show the enhanced lateral mixing due to an initial density difference. The difference between the effects due to a positive and negative density differences also are evident in the photographs of Exp. 113 and 128. A light area in the center of the plume in Exp. 117 indicating a bimodal distribution is faintly discernible.

Photographs taken of the mixing of two wide parallel streams are shown in Fig. 4.38 and 4.39. Visual observations of these experiments as well as these photographs give the impression that little mixing occurred between the dyed and clear fluids. This impression is due, in part, to the inability of the eye and camera to see a smooth gradation in color from the dyed fluid on the left, with relative concentration equal to unity, to the clear fluid on the right, with relative concentration equal to zero. This inability to see a smooth gradation in color is also apparent in the photographs of the experiments with the 1-cm- and 20-cm-wide sources. It has been shown previously that the lateral concentration distributions in the experiments with a 1-cm-wide source and $\Delta\rho/\rho_a = 0$ are nearly Gaussian; but the plumes in photographs of these

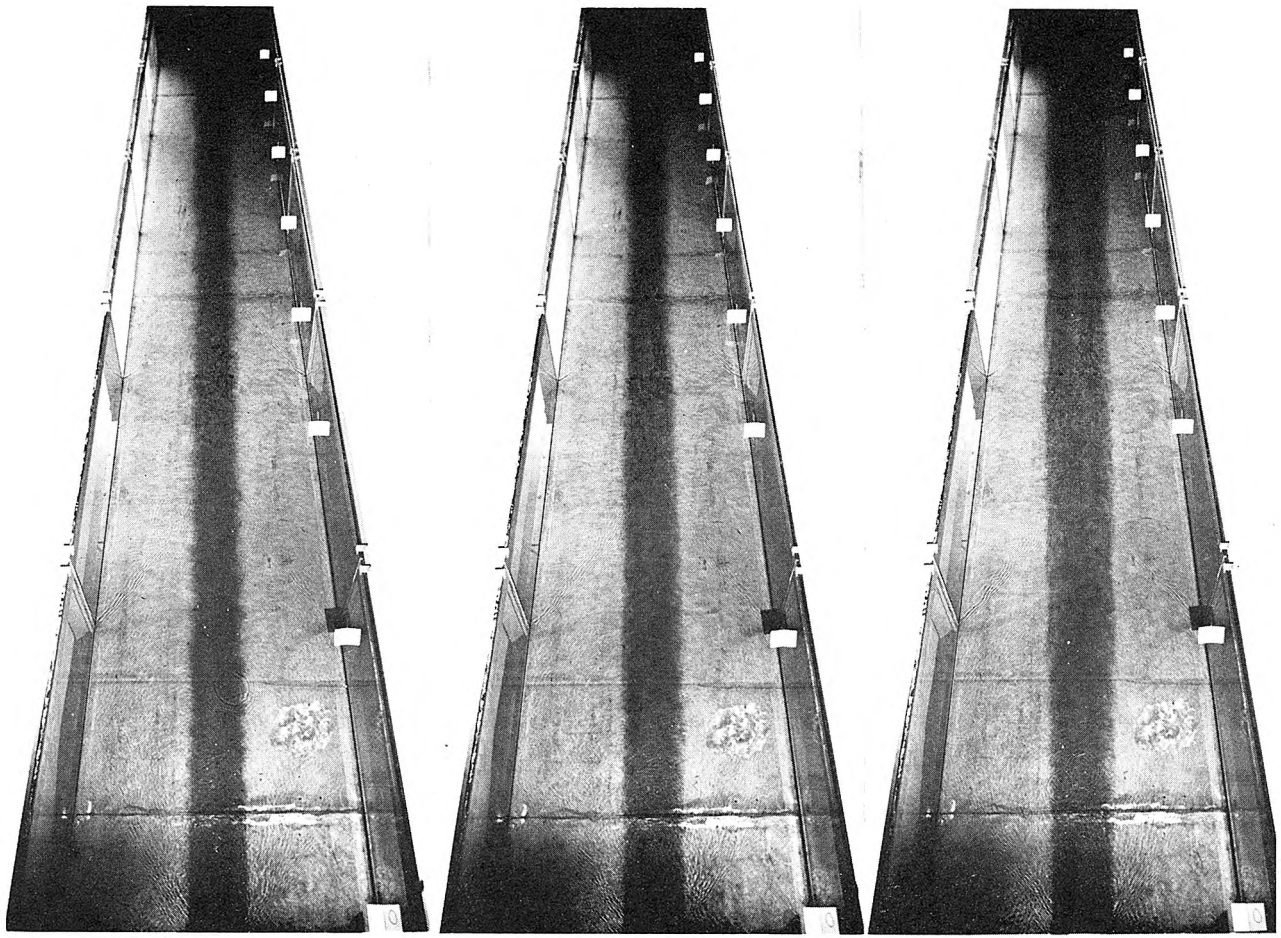

	10098	10099	10100
Exp.	139	143	142
$\Delta\rho/\rho_a$ =	0	0.00270	0.00487

Figure 4.36 Photographs of experiments with flow S1 and the 20-cm-wide source. d = 4.05 cm, $\bar{u}$ = 35.4 cm/sec, u_* = 1.96 cm/sec.

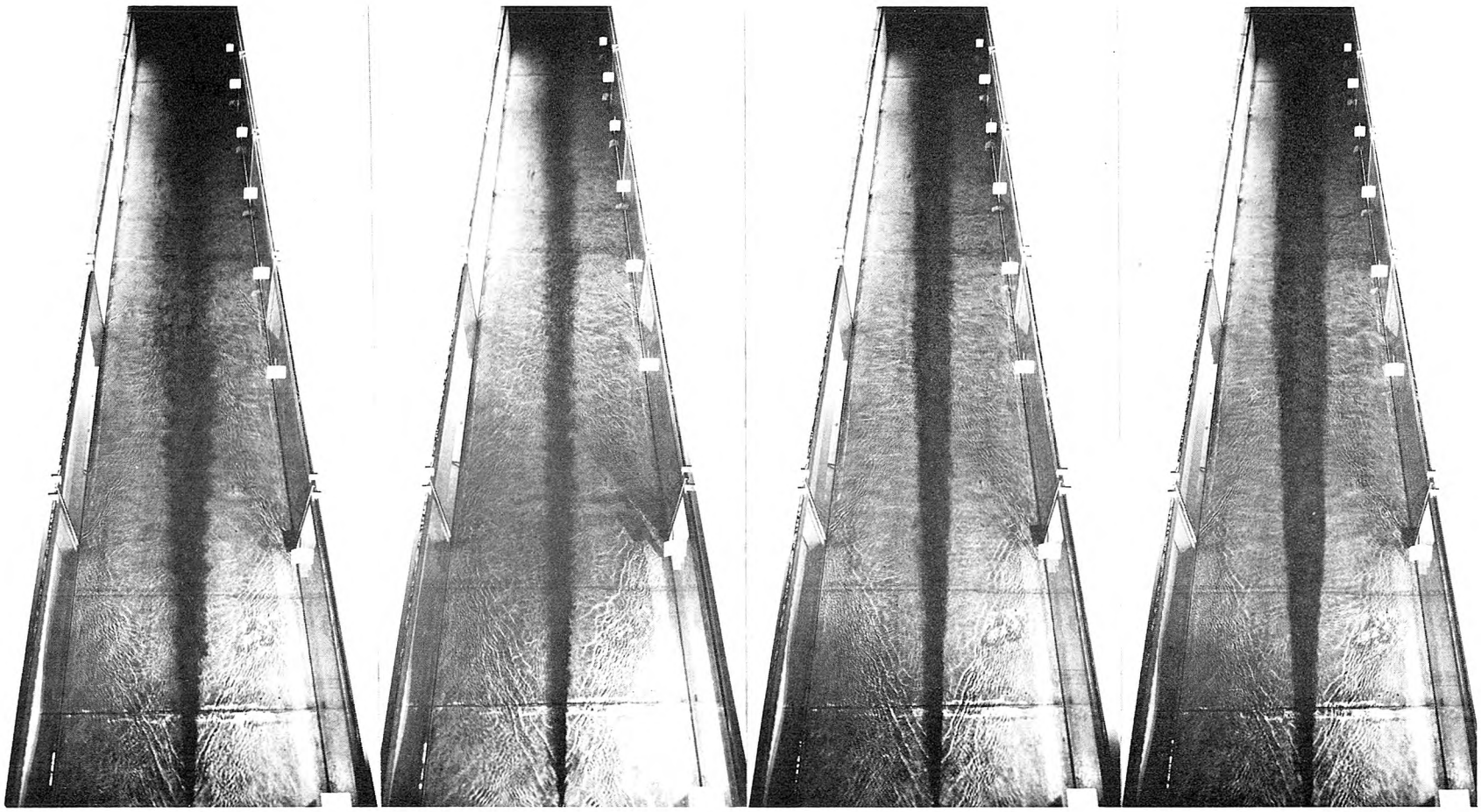

10094	10095	10096	10097
Exp. 128	116	113	118
$\Delta\rho/\rho_a$ = -0.0158	0	0.0160	0.0304

Figure 4.37 Photographs of experiments with flow S2 and the 1-cm-wide source. d = 6.55 cm, $\bar{u}$ = 45.2 cm/sec, u_* = 2.27 cm/sec.

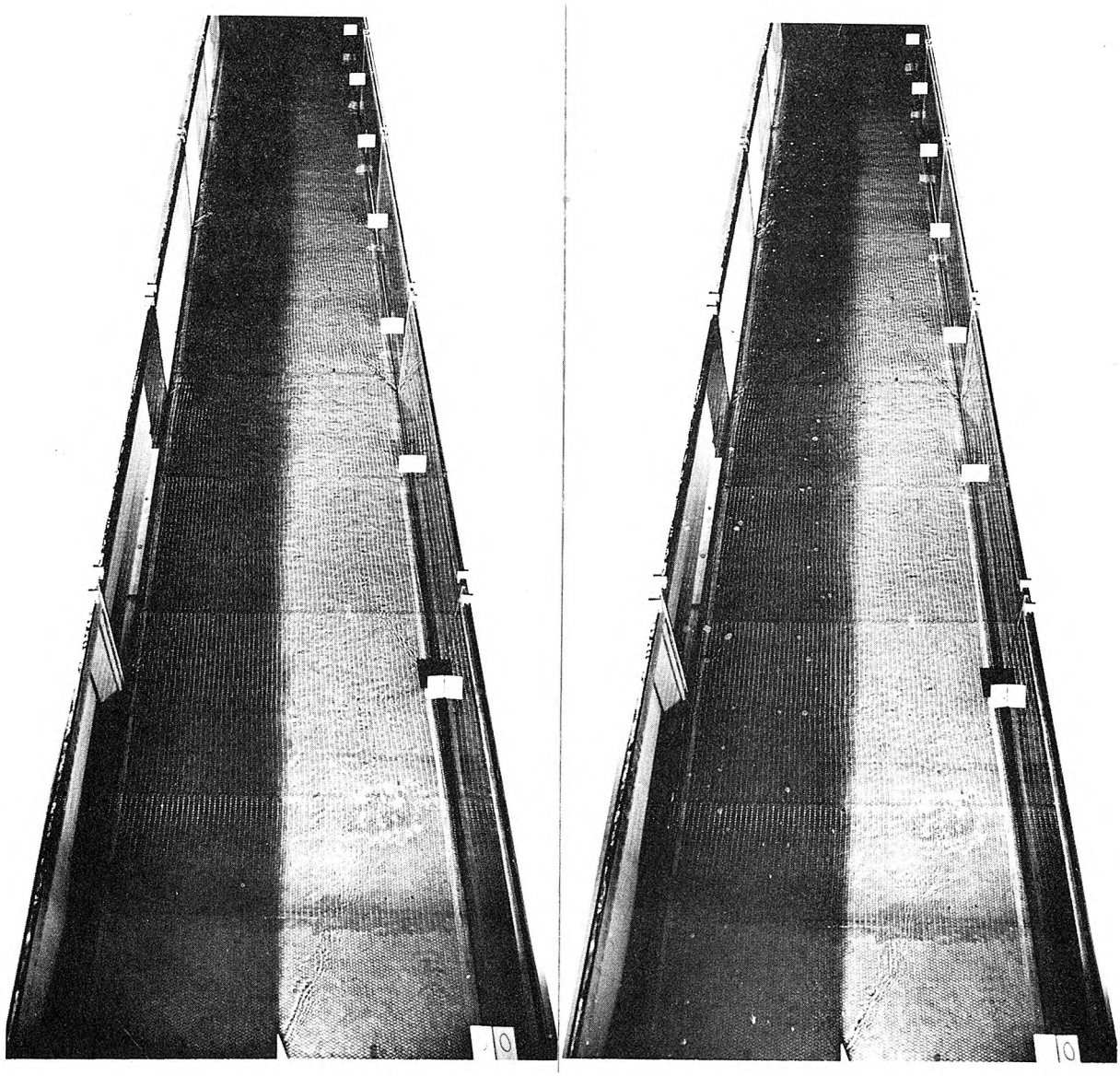

10073 10071

Exp. 204 Exp. 207

$\Delta\rho/\rho_a = 0$ $\Delta\rho/\rho_a = 0.0114$

Figure 4.38 Photographs of experiments with flow R1 and the wide source.
$d = 3.90$ cm, $\bar{u} = 37.3$ cm/sec, $u_* = 3.86$ cm/sec.

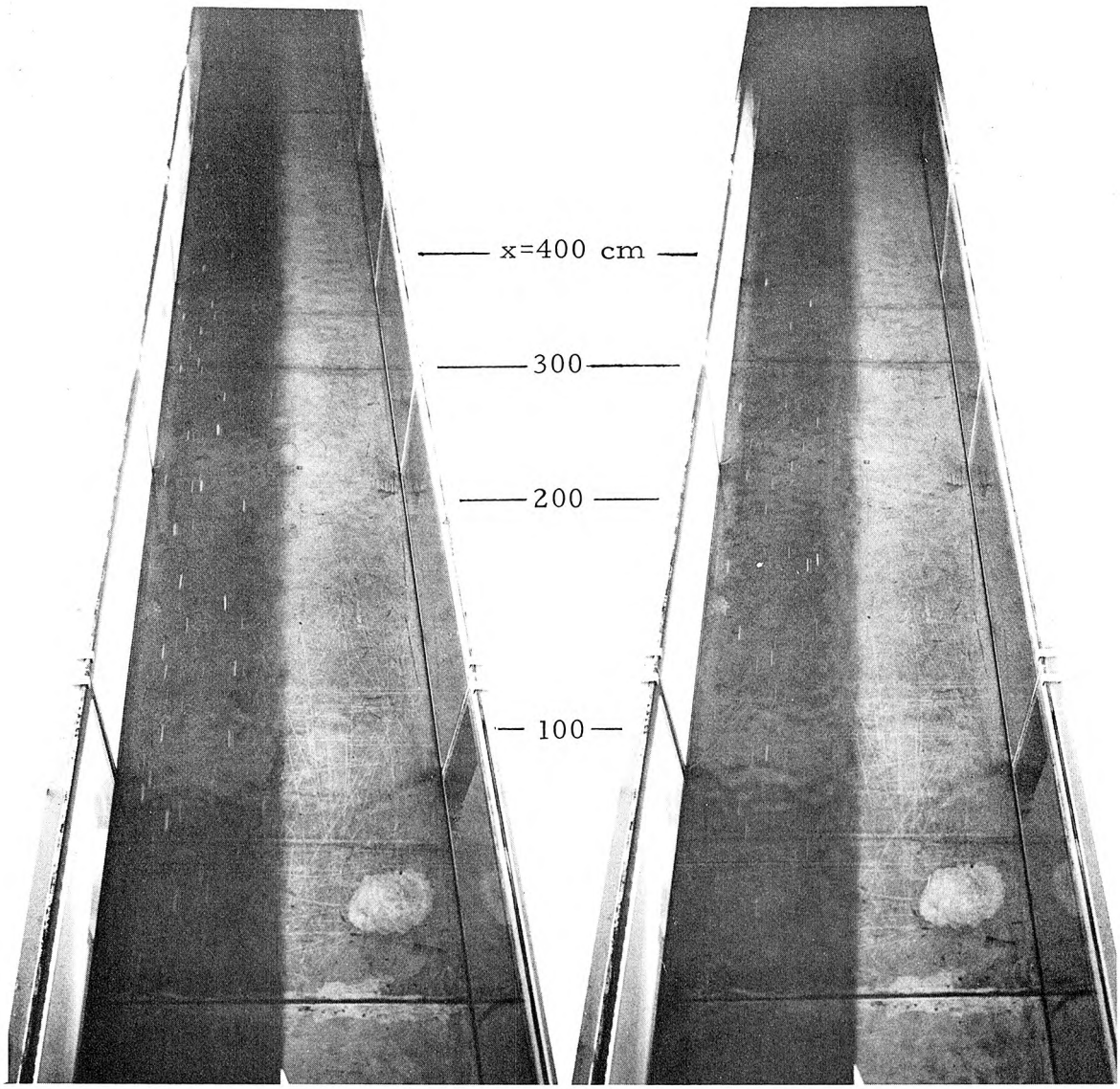

Exp. 177 $\Delta\rho/\rho_a = 0$

Exp. 183 $\Delta\rho/\rho_a = 0.00286$

Figure 4.39 Photographs of experiments with flow S1 and the wide source.
$d = 4.05$ cm, $\bar{u} = 35.4$ cm/sec, $u_* = 1.96$ cm/sec

experiments appear to be of uniform darkness or concentration across most of their width rather than grading from dark at the center to light at the edges. Similarly, the diluted mixed zones between the two parallel streams appear in Fig. 4.38 and 4.39 as dark as the undiluted fluids on the far left. The apparent boundaries between the two fluids are actually near the right edges of the mixed zones. Two dark spots, which are 20 cm apart and equidistant from the flume center line, can be seen in Fig. 4.39 on the bottom of the flume at about x = 250 cm. By noting the positions of the apparent boundaries relative to the two spots one can see that the apparent boundaries are to the right of the center line, and that the apparent boundary in Exp. 183, in which $\Delta\rho/\rho_a \neq 0$, is farther to the right than in Exp. 177, in which $\Delta\rho/\rho_a = 0$. One may also note that in the vicinity of the two spots, the apparent boundary in Exp. 177 is approximately in the same position as the right side of the plume in Exp. 120, which is shown in Fig. 4.34.

4.2.6 Variation of Concentration with Depth. The relative concentrations, C, observed in Exp. 116, 113, 128, 177 and 181 were plotted as a function of the vertical coordinate, y, and are presented in Fig. 4.40 to 4.44. Given with each vertical profile is a value of C_v, which is the coefficient of variation for the vertical concentration distribution calculated by Eq. 4.14b:

$$C_v(x,z) = \frac{\frac{1}{d}\left\{\int_0^d \left[C(x,y,z) - \overline{C}(x,z)\right]^2 dy\right\}^{\frac{1}{2}}}{\overline{C}(x,z)} \qquad (4.14a)$$

$$C_v(x,z) \approx \frac{1}{d}\left\{\left[C(x,y_1,z) - \bar{C}(x,z)\right]^2 \frac{(y_2+y_1)}{2}\right.$$

$$+\sum_{i=2}^{4}\left[C(x,y_i,z) - \bar{C}(x,z)\right]^2 \frac{(y_{i+1} - y_{i-1})}{2} \qquad (4.14b)$$

$$\left.+\left[C(x,y_5,z) - \bar{C}(x,z)\right]^2\left(d - \frac{(y_5+y_4)}{2}\right)\right\}^{\frac{1}{2}} \frac{1}{\bar{C}(x,z)} .$$

The terms y_i were defined previously in Fig. 4.11.

By comparing the data in Fig. 4.41 and 4.42 from experiments with a narrow source, one can see that in Exp. 128, in which the tracer fluid was less dense than the ambient fluid, the vertical concentration gradients were steeper than in Exp. 113, in which the tracer fluid was more dense than in the ambient fluid. Also, the data in Fig. 4.44 from an experiment with the wide source show that on the left side of the flume, where a lighter fluid was intruding into a heavier fluid, vertical concentration gradients were steeper than on the right side, where a heavier fluid was intruding into a lighter fluid.

An average coefficient of variation, $\bar{C}_v$, was defined for a cross-section as the concentration-weighted average of C_v taken in the lateral direction. This average was calculated numerically for each cross-section by using Eq. 4.15b:

$$\bar{C}_v(x) = \frac{\int_{-\infty}^{\infty} \bar{C}(x,z)\, C_v(x,z)\, dz}{\int_{-\infty}^{\infty} \bar{C}(x,z)\, dz} \qquad (4.15a)$$

$$\bar{C}_v(x) \approx \frac{\sum_{j=1}^{8} \bar{C}(x, z_j) \cdot C_v(x, z_j)}{\sum_{j=1}^{8} \bar{C}(x, z_j)} \cdot \qquad (4.15b)$$

The coordinates z_j define the eight locations in each cross-section where C_v and $\bar{C}$ were computed from the experimental data. Because the spacing of z_j was nearly uniform, the calculations were simplified by deleting the differential element Δz from the summation in Eq. 4.15b. Values of $\bar{C}_v$ for all the experiments are presented in Fig. 4.22b to 4.33b and are also listed in Tables A1 and A2 of the appendix.

One sees in Fig. 4.22b to 4.33b that $\bar{C}_v$ reached a peak close to the source and then decreased in the downstream direction. In most experiments data were not taken close enough to the source to define the rising or peaked parts of the longitudinal distributions of $\bar{C}_v$. One can see that as $\Delta\rho/\rho_a$ increased so did the values of $\bar{C}_v$. Also, the data in Fig. 4.22b and 4.27b show that $\bar{C}_v$ is a little larger when the tracer fluid is less dense than the ambient fluid than when it is more dense by an equal amount.

An analysis of the data in Chapter 5 relates $\bar{C}_v$ to the independent dimensionless variables of the problem.

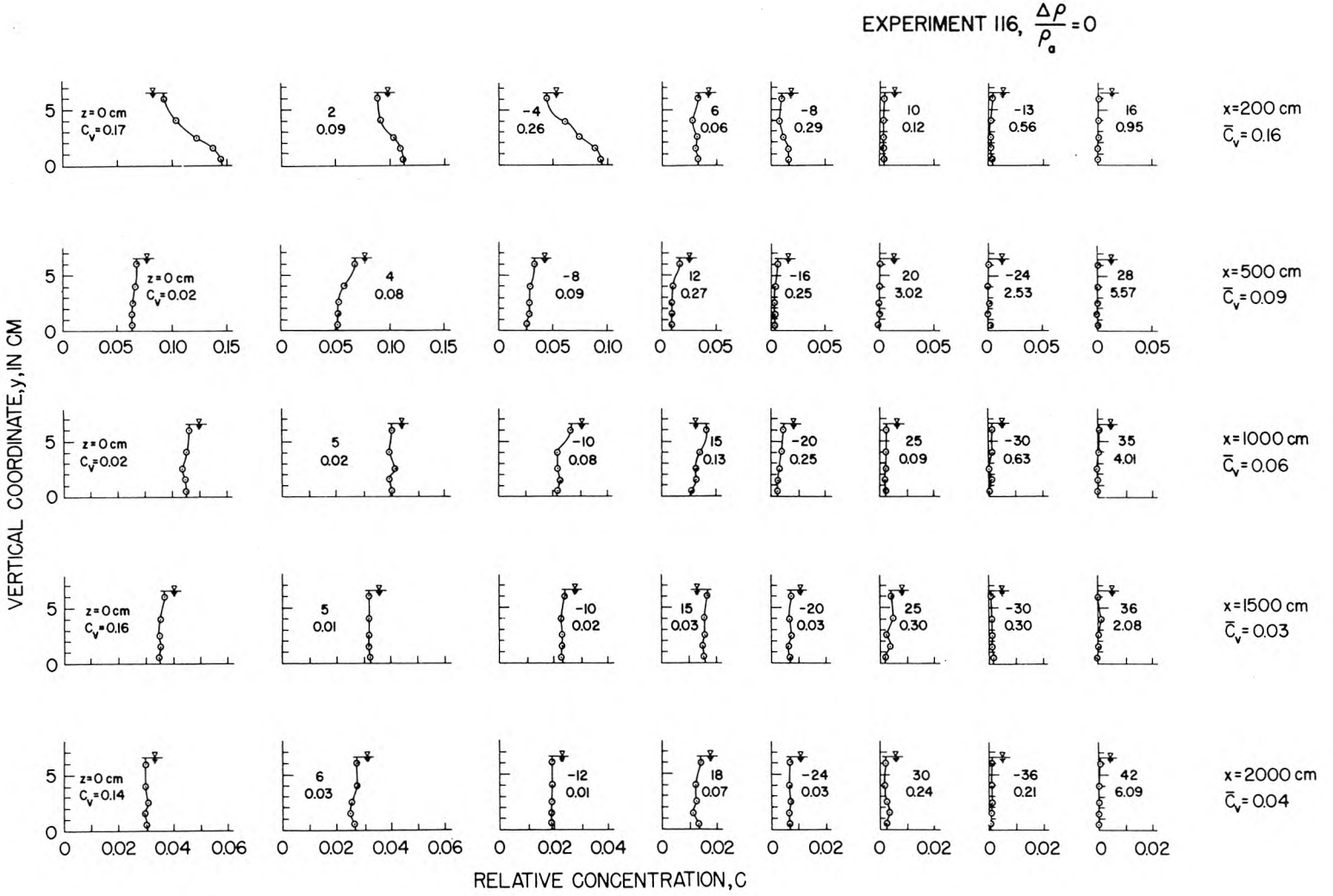

Figure 4.40 Vertical concentration distributions downstream from a 1-cm-wide source which discharged a fluid with a density the same as the ambient fluid and with a relative concentration of 1.0; flow S2; Exp. 116.

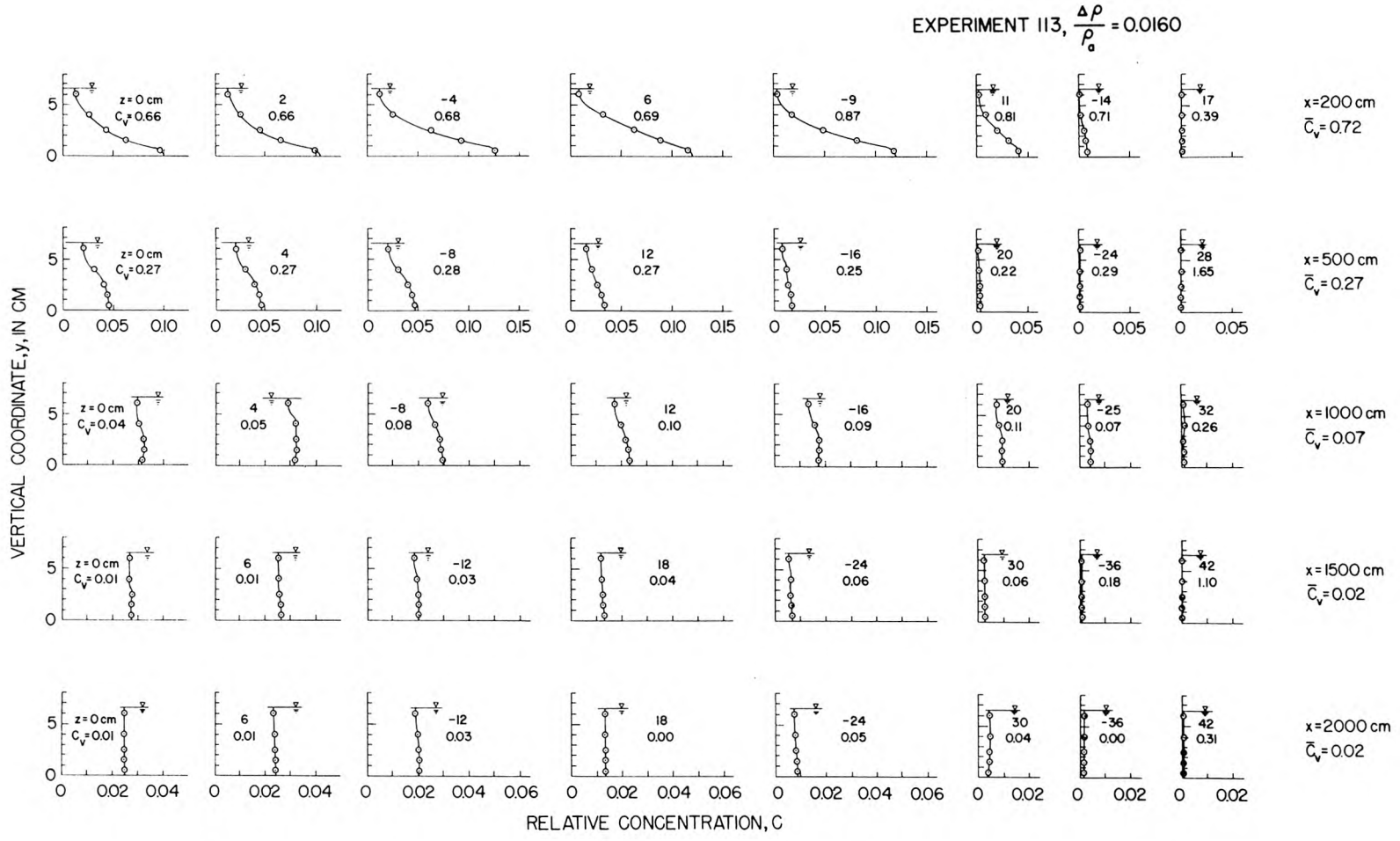

Figure 4.41 Vertical concentration distributions downstream from a 1-cm-wide source which discharged a fluid with a density 0.0160 gm/cm^3 greater than the ambient fluid and with a relative concentration of 1.0; flow S2; Exp. 113.

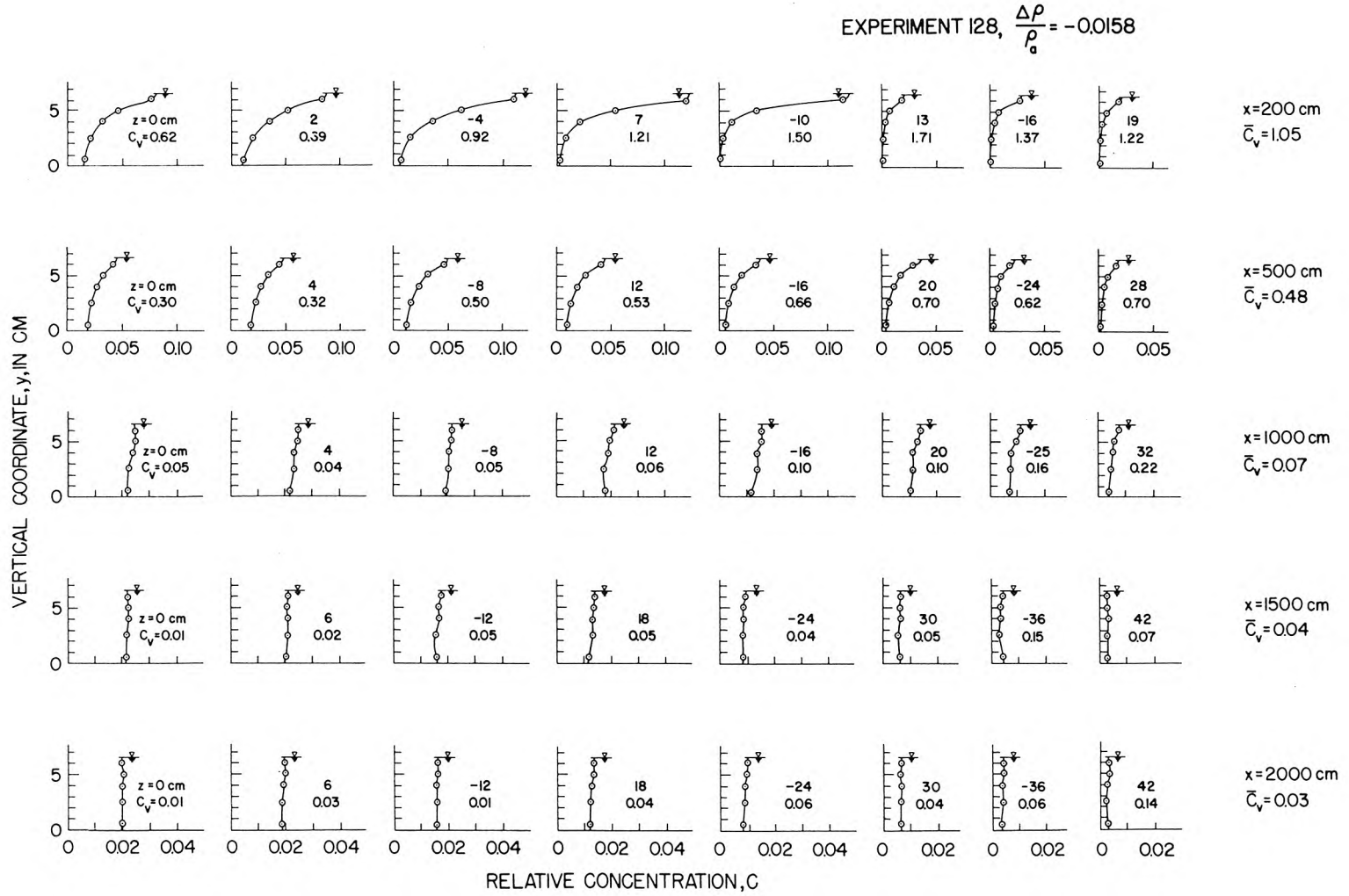

Figure 4.42 Vertical concentration distributions downstream from a 1-cm-wide source which discharged a fluid with a density 0.0158 gm/cm^3 less than the ambient fluid and with a relative concentration of 1.0; flow S2; Exp. 128.

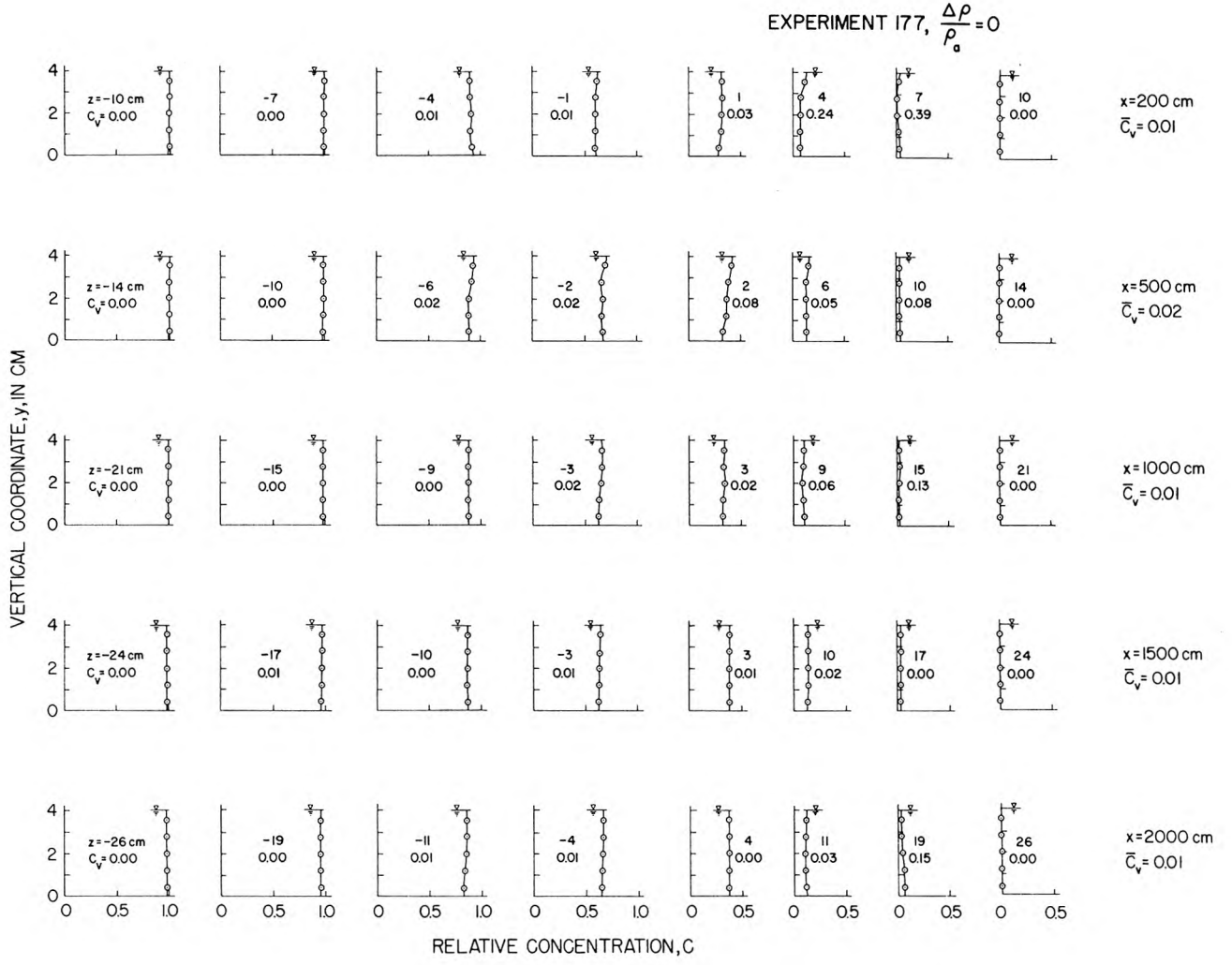

Figure 4.43 Vertical concentration distributions downstream from the confluence of two wide parallel streams of the same density; flow S1; Exp. 177.

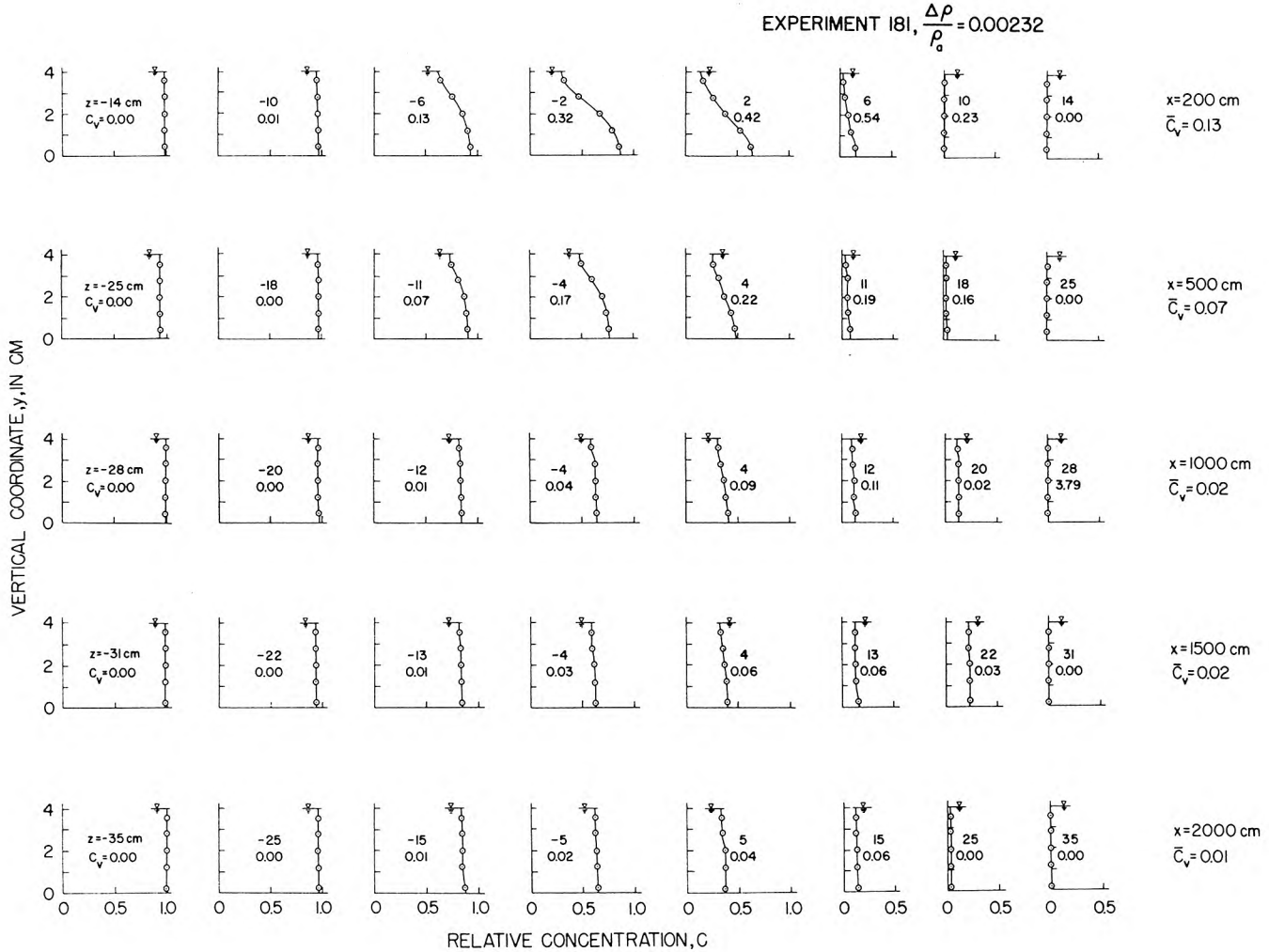

Figure 4.44 Vertical concentration distributions downstream from the confluence of two wide parallel streams of different density. The fluid on the left with C=1 was 0.00232 gm/cm^3 more dense than the fluid on the right with C=0; flow S1; Exp. 181.

4.3 EXPERIMENTS WITH FLOATING PARTICLES

4.3.1 Calculating the Variance. In the preceding section, where data from experiments with tracer fluids were presented, two methods were discussed which could be used to calculate the variance of a Gaussian distribution. They are: (1) the method of moments, and (2) the graphical method in which the cumulative distributions are plotted on arithmetic probability paper. Because of anomolies in the tails of the particle distributions, which are discussed below, the graphical method was preferred over the method of moments for computing variances of the distributions of floating particles, even though the method of moments was used in the analysis of data from experiments with tracer fluids.

The cumulative distribution P(x, z), expressed in percent, was calculated from the data by using the expression

$$P(x, z) = P(x, j-52) \approx \frac{\sum_{i=1}^{j} n_i(x)}{1 + \sum_{i=1}^{104} n_i(x)} \cdot 100 \quad , \tag{4.16}$$

where $n_i(x)$ is the number of particles caught in the i^{th} compartment of the collector. One may recall that in the collector there were 104 compartments each 1 cm wide.

The cumulative distributions observed in Exp. 102 and 101 are shown in Fig. 4.45a and b. These distributions were linear over most of the range of z; therefore, the distributions of the

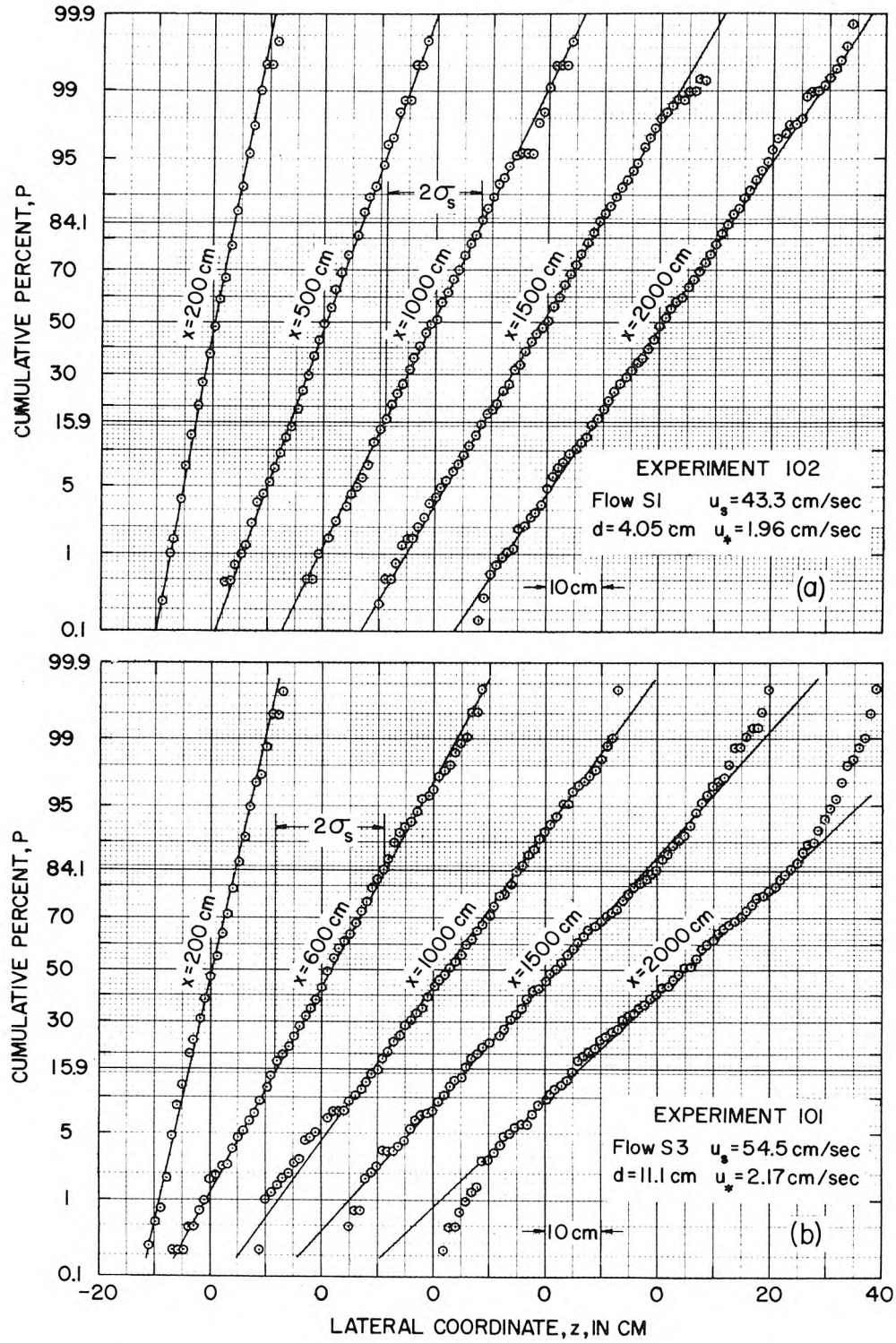

Figure 4.45 Cumulative distributions of particles; a) Exp. 102, b) Exp. 101.

particles were nearly Gaussian, as expected. The variance, σ_s^2, for each distribution was calculated by measuring $(z_{84.1} - z_{15.9})$ for each of the straight lines drawn through the points and then using Eq. 4.12. For comparison, σ_s^2 was also calculated by using the method of moments, Eq. 4.17;

$$\sigma_s^2(x) = \frac{\sum_{i=1}^{104} n_i(x)\,(i-52.5-\bar{z})^2}{\left[\sum_{i=1}^{104} n_i(x)\right]-1}, \qquad (4.17)$$

where

$$\bar{z} = \frac{\sum_{i=1}^{104} n_i(x)\,(i-52.5)}{\sum_{i=1}^{104} n_i(x)}. \qquad (4.18)$$

Fig. 4.46a and b show that the variances calculated by both methods agree well if σ_s^2 is less than about 200 cm^2. However, for the larger values of σ_s^2 the method of moments gave significantly smaller values than were given by the graphical method. The differences are due to the cumulative distributions deviating from straight lines at the larger values of $|z|$ as if something were hindering lateral diffusion near the sidewalls of the flume. Although similar deviations were also observed in the cumulative distributions

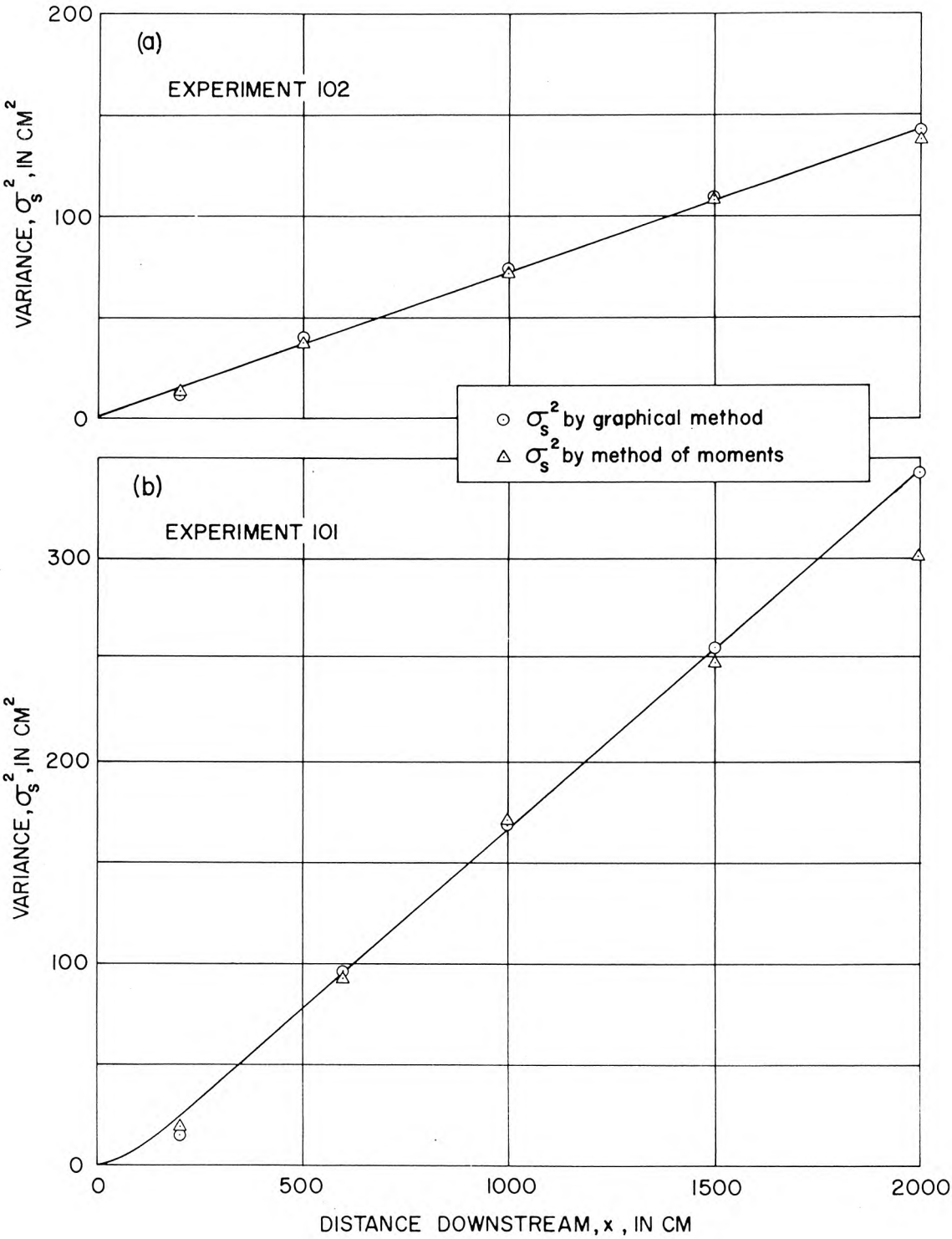

Figure 4.46 Variance-distance curves for a) Exp. 102, b) Exp. 101.

of tracer-fluid concentrations, as was shown for Exp. 125, the deviations for distributions with equal values of the variance were smaller in experiments with tracer fluids than with floating particles.

The larger deviations in experiments with floating particles are believed to have been caused by secondary currents in the corners of the flume. Secondary flows in a corner are typically away from the corner along solid boundaries, and into the corner in the interior (see e.g. Prandtl (35) p. 148-149). Such a structure is also suggested by the isovels in Fig. 4.2; therefore, secondary flow patterns as shown in Fig. 4.47 may have existed in the flume.

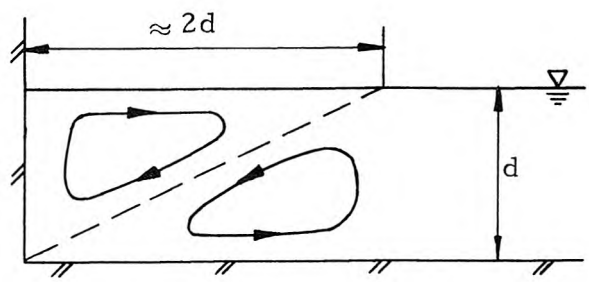

Figure 4.47 Assumed secondary flow pattern in flume.

Near the sidewalls, the secondary current would have convected floating particles inwards towards the center of the flume in opposition to the outward diffusion, and could have caused the observed

anomalies in the lateral distributions of the floating particles. However, because the depth-averaged lateral component of the secondary flow was zero, the secondary flow would not have hindered the lateral diffusion of tracer fluids distributed over the depth, and therefore, would not have caused large anomalies in the lateral distributions of depth-averaged concentrations.

4.3.2 Presentation of Data. In Fig. 4.48 to 4.51, variances of the particle distributions are presented as functions of x, the distance downstream from the point where the particles were dropped into the flume. The variances are also presented in Table A3 of the appendix together with $\bar{z}$, the coordinates of the centroids of the distributions which were also obtained graphically, and u_s, the mean longitudinal velocities of the particles.

One experiment with floating particles was made at each of the five flow conditions with no fluid-tracer source in the flume. Other experiments were also made with some of the tracer sources in the flume but always with a neutrally buoyant fluid being pumped through the sources. The data presented in the figures are grouped so that data from experiments performed with the same flow condition all appear in the same figure.

For $x > 100$ cm, the data show that $\sigma_s^2(x)$ is linear, which indicates that ϵ_{zs} is not a function of x. The slopes of the σ_s^2-x curves and values of ϵ_{zs} are given in the next chapter. Except for Exp. 145, which is shown in Fig. 4.48, the variation

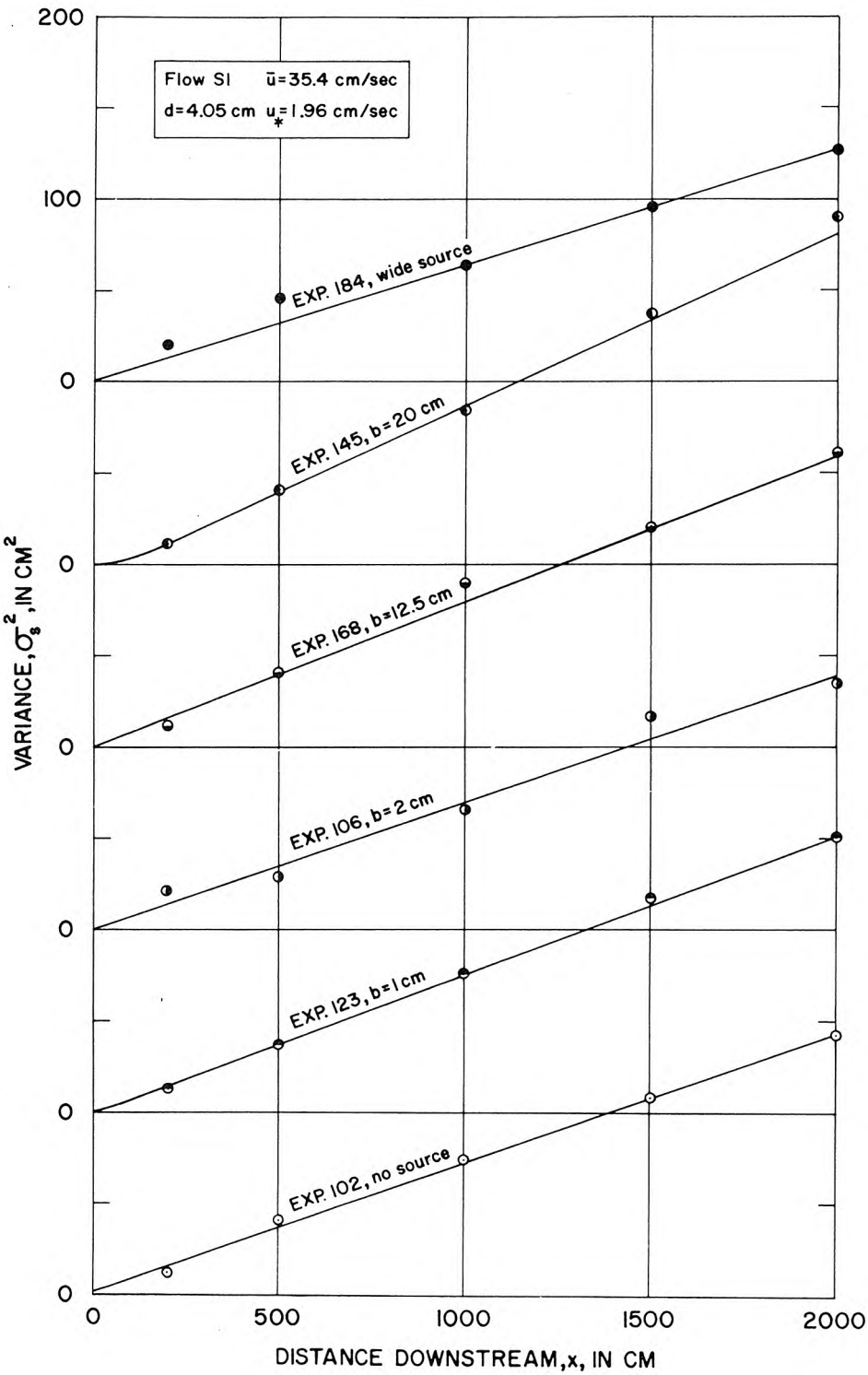

Figure 4.48 Variance-distance curves for experiments with floating particles; flow S1.

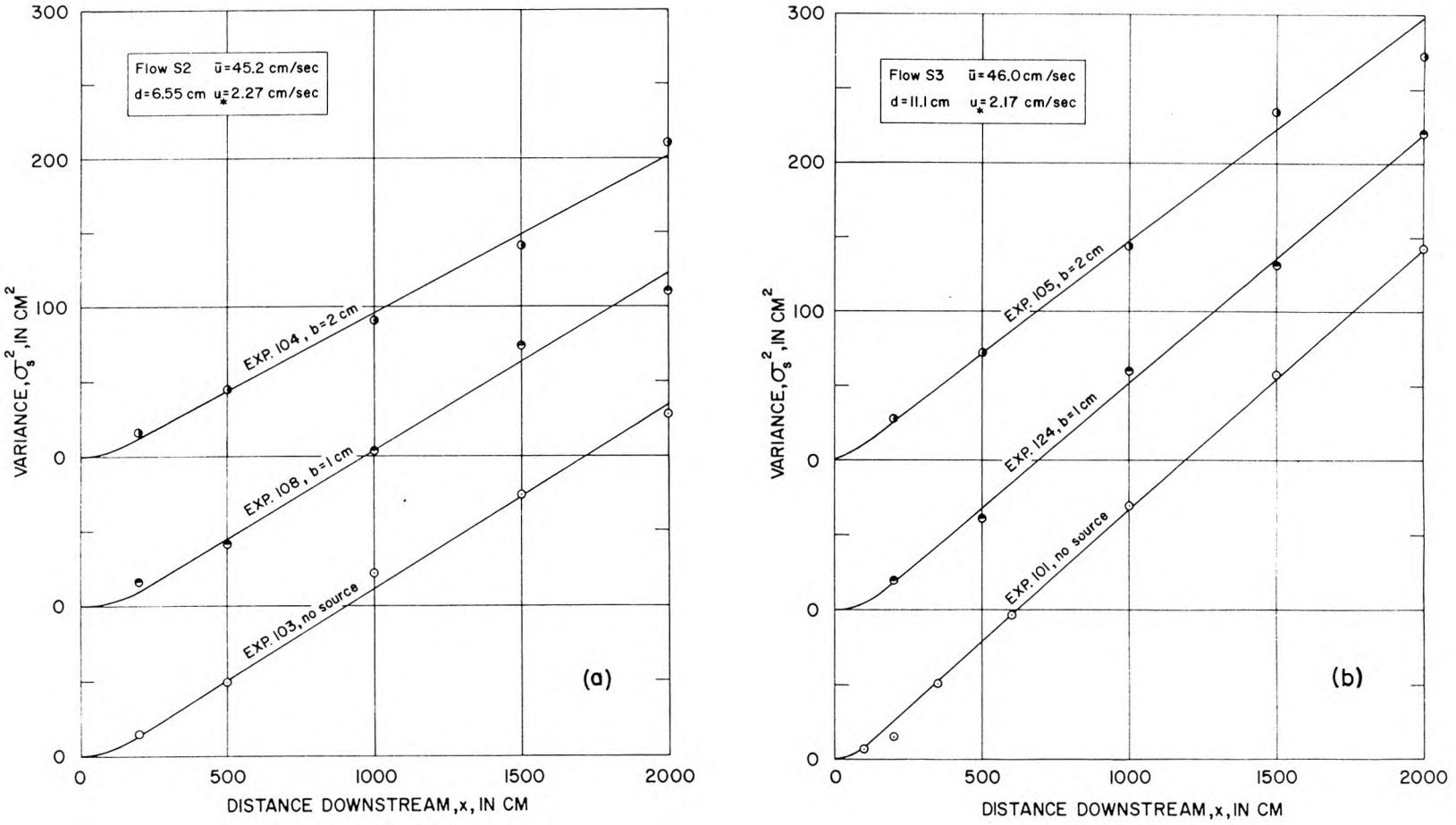

Figure 4.49 Variance-distance curves for experiments with floating particles; (a) flow S2, (b) flow S3.

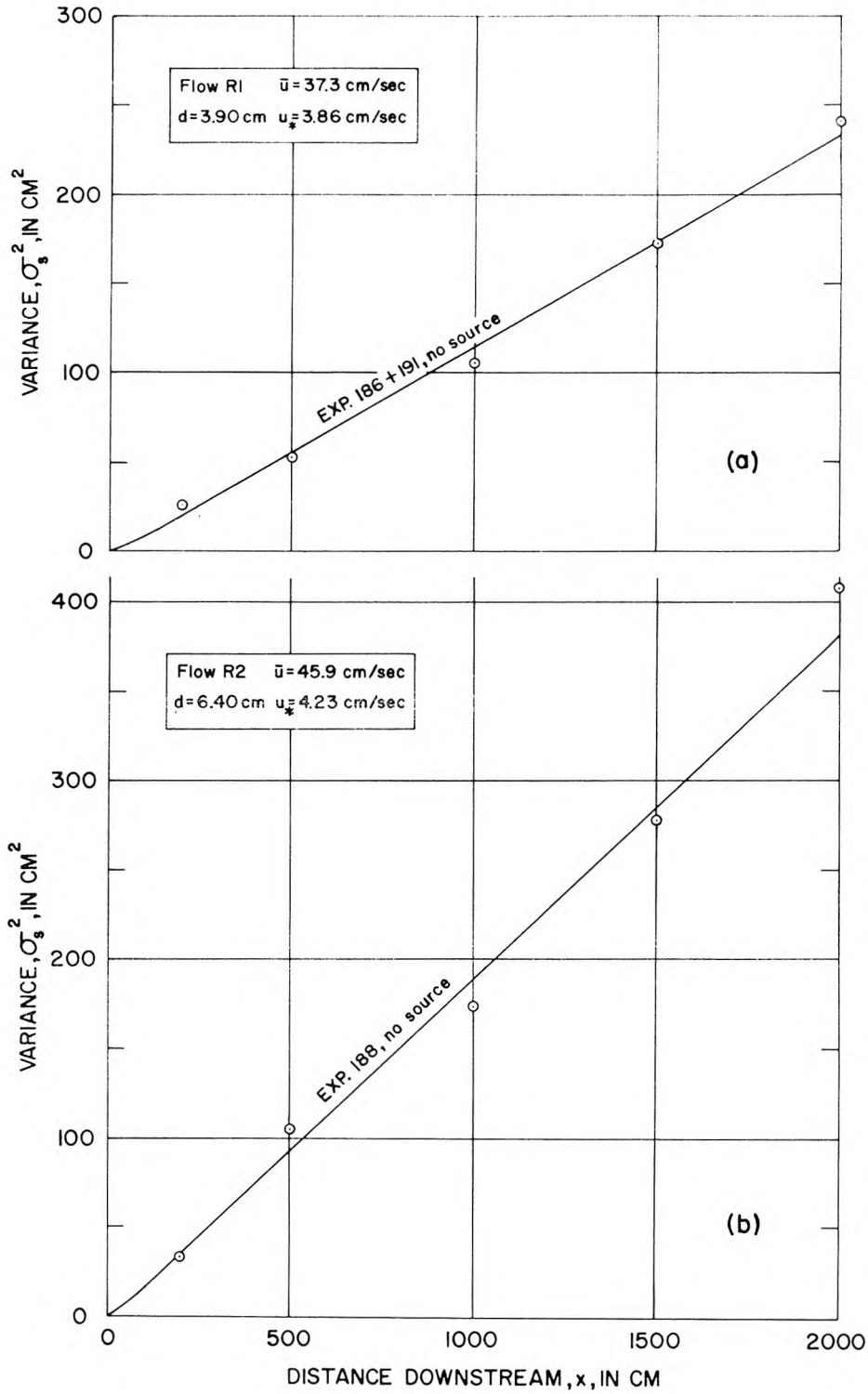

Figure 4.50 Variance-distance curves for experiments with floating particles; (a) flow R1, and (b) flow R2.

in slopes of the curves among experiments with the same flow condition was not large. No suitable explanation can be offered for the difference in the data from Exp. 145. It is difficult to believe that the 20-cm-wide source caused a disturbance to the flow which affected the lateral mixing as far downstream as 2000 cm, especially when the data from Exp. 136 and 139, shown in Fig. 4.24, show that the σ^2-x curve for a neutrally buoyant tracer fluid discharged from the same source in experiments with the same flow condition do not differ greatly from the curves obtained in experiments with other sources.

The lateral coordinates of the centroids of the particle distributions, which are listed in Table A3, were usually less than 2 cm from the center line. Thus one may conclude that the secondary currents which existed in the flume were either weak or symmetrical about the center line of the flume. The particle velocities tended to be one to two percent higher in the experiments with no fluid tracer source in the flume; hence, the sources probably decreased the velocities slightly in the central part of the flume. However, the particle velocities tended to be a few percent higher than the water velocity at the surface obtained by extrapolating the observed water velocity distributions.

CHAPTER 5

DATA ANALYSIS

5.1 EXPERIMENTS WITHOUT DENSITY DIFFERENCES

5.1.1 Experiments with Tracer Fluids. The data from experiments with neutrally buoyant tracer fluids were used in the equations

$$\overline{\epsilon}_z = \frac{\overline{u}}{2}\frac{d\sigma^2}{dx} \qquad (2.10a)$$

and

$$\overline{\epsilon}_z = \frac{\overline{u}}{2}\frac{d\sigma_d^2}{dx} \qquad (2.10b)$$

to calculate $\overline{\epsilon}_z$, the depth-averaged lateral turbulent diffusion coefficients. The gradients, $d\sigma^2/dx$ or $d\sigma_d^2/dx$ were obtained from the slopes of the variance-distance curves in Fig. 4.22 to 4.33. The velocity, $\overline{u}$, for each experiment except number 170 was assumed to equal the mean velocity in the central 60 cm of the flume and was obtained from Table 4.1. For Exp. 170, which was conducted with the 10-cm-wide source placed against the left wall of the flume, $\overline{u}$ was assumed equal to the mean velocity through a 30-cm-wide section adjacent to the left wall. The diffusion coefficients and the data used to compute them are given in Table 5.1. The dimensionless diffusion coefficients, $\alpha = \overline{\epsilon}_z/u_* d$, were calculated and are also presented in this table. The quantities u_* and d were obtained from Table 4.1.

Table 5.1 Lateral turbulent diffusion coefficients from this study.

Flow Condition Code	Source Width b (cm)	Neutrally Buoyant Tracer Fluids					Floating Particles				
		Experiment Number	Water Velocity $\bar{u}$ (cm/sec)	$\frac{d\sigma^2}{dx}$ or $\frac{d\sigma_d^2}{dx}$ (cm)	Diffusion Coefficient $\bar{\epsilon}_z$ (cm²/sec)	Dimensionless Diff. Coef. $\alpha = \frac{\bar{\epsilon}_z}{u_* d}$	Experiment Number	Particle Velocity u_s (cm/sec)	$\frac{d\sigma_s^2}{dx}$ (cm)	Diffusion Coefficient ϵ_{zs} (cm²/sec)	Dimensionless Diff. Coef. $\alpha_s = \frac{\epsilon_{zs}}{u_* d}$
S1	None						102	43.3	0.0704	1.52	0.192
	1.0	120	35.4	0.0650	1.15	0.145	123	42.4	0.0769	1.63	0.205
	2.0						168	42.5	0.0794	1.69	0.212
	12.5	162 + 166	35.4	0.0600	1.06	0.134					
	12.5	156 + 157	35.4	0.0582	1.03	0.130					
	2x10.0*	170	33.2	0.0620	1.04	0.130					
	20.0	136 + 139	35.4	0.0600	1.06	0.134	145	42.6	0.0939	2.00	0.252
	Wide	175 + 177	35.4	0.0588	1.04	0.131	184	42.0	0.0632	1.33	0.167
		Ave.		0.0607	1.06	0.134	Ave.		0.0768	1.63	0.205
S2	None						103	54.3	0.122	3.32	0.223
	1.0	115 + 116	45.2	0.0915	2.07	0.139	108	53.2	0.118	3.14	0.212
	2.0						104	53.7	0.111	2.97	0.200
	20.0	150 + 153	45.2	0.0890	2.01	0.135					
		Ave.		0.0903	2.04	0.137	Ave.		0.117	3.14	0.212
S3	None						101	54.5	0.176	4.78	0.199
	1.0	125	46.0	0.155	3.56	0.148	124	53.7	0.167	4.49	0.186
	2.0						105	53.5	0.176	4.70	0.196
		Ave.		0.155	3.56	0.148	Ave.		0.173	4.66	0.194
Average of S1, S2 and S3						0.136					0.204
R1	None						186 + 191	49.5	0.119	2.94	0.195
	1.0	196	37.3	0.104	1.93	0.128					
	Wide	203 + 204	37.3	0.110	2.03	0.136					
		Ave.		0.107	1.98	0.132	Ave.		0.119	2.94	0.195
R2	None						188	59.5	0.193	5.73	0.212
	1.0	192 + 193	45.9	0.150	3.44	0.127					
	20.0	199	45.9	0.157	3.60	0.133					
		Ave.		0.154	3.52	0.130	Ave.		0.193	5.73	0.212
Average of R1 and R2						0.131					0.204
Average of all experiments						0.135					0.204

*Source against left wall of flume

The average value of α for all experiments in this study, 0.136, is in the range of values from other studies in straight laboratory flumes (see Table 2.3). This average is less than the averages from data by Elder ($\alpha = 0.164$) and by Sayre and Chang ($\alpha = 0.167$), but greater than the average from Sullivan's data ($\alpha = 0.117$). The average also lies within the range of unpublished data by Okoye, who conducted some of his experiments in the same flume as was used in this study. As expected, the values of α in this study are less than the values observed in either curved laboratory channels or natural streams where secondary currents can increase lateral mixing to yield values of α of the order one.

In this study, the range in α among experiments with the same hydraulic conditions, but with different sources, is equal to or less than 11 percent. The range of the means for each of the flows, 0.130 to 0.148, is 13 percent. The average value of α from experiments with the rough lath bottom was only five percent less than the average from experiments with the plain stainless steel bottom. Considering that the friction factor, f, for the two bottoms differed by almost a factor of three, it appears that α is independent of f.

5.1.2 Experiments with Floating Particles. Lateral turbulent diffusion coefficients at the free surface, ϵ_{zs}, were calculated by substituting data obtained from experiments with floating particles into

$$\epsilon_{zs} = \frac{u_s}{2} \frac{d\sigma_s^2}{dx} \quad . \tag{2.8b}$$

The gradients $d\sigma_s^2/dx$ were obtained from the slopes of the curves in Fig. 4.48 to 4.50. These gradients, the particle velocities u_s, the diffusion coefficients ϵ_{zs}, and the dimensionless coefficients $\alpha_s = \epsilon_{zs}/u_* d$ are listed on the right half of Table 5.1.

The average value of α_s for all experiments, 0.204, is 10 to 15 percent less than the averages for three other investigations listed in Table 2 but is 15 percent greater than the average from Orlob's (7) data. The variation of α_s among experiments with the same hydraulic conditions but with different sources in the flume was greater than the variation of α. For flows S1, S2, and S3, the ranges of α_s were 41 percent, 10 percent and 6 percent, respectively. However, the range of the means for each of the flows flows, 0.194 to 0.215, is only 10 percent. The average value of α_s from experiments with the rough bottom is the same as from experiments with the smooth bottom.

Of all the previous investigators, only Sayre and Chang (5) studied lateral mixing of both tracer fluids and floating particles. Their studies and this present investigation show that α_s is larger than α. The averages of the Sayre and Chang data give $\alpha_s/\alpha = 1.39$; the average data from the present investigation yields $\alpha_s/\alpha = 1.50$. Sayre and Chang found that the gradients $d\sigma^2/dx$ and $d\sigma_s^2/dx$ from experiments with the same hydraulic conditions were almost equal and that the differences between α and α_s, or $\overline{\epsilon}_z$ and ϵ_{zs} were due mostly to the differences between the velocities, $\overline{u}$ and u_s, used in Eq. 2.8b and 2.10b. However, by comparing the data in Table 5.1 one can see that in the present study $d\sigma^2/dx$ or $d\sigma_d^2/dx$ was always less than $d\sigma_s^2/dx$.

5.2 EXPERIMENTS WITH DENSITY DIFFERENCES

5.2.1 Introduction. A dimensional analysis of the experimental parameters is presented in this section. The experimental data plus the results of this analysis yield a set of empirical curves for predicting σ^2, the variance of the lateral distribution of the depth-averaged concentration, and $\overline{C}_v$, the laterally-averaged coefficient of variation for the vertical concentration distributions, as functions of the distance downstream from the source, the density difference at the source, the width of the source, and the hydraulic parameters of the flow.

5.2.2 Selection of Dimensionless Numbers. The two dependent variables σ^2 and $\overline{C}_v$ are assumed to be given by the functions

$$\sigma^2 = \phi_1 \ (x, d, b, \rho_a, \Delta\rho, \overline{u}, u_*, g, \nu, D_m) \qquad (5.1)$$

and

$$\overline{C}_v = \Psi_1 \ (x, d, b, \rho_a, \Delta\rho, \overline{u}, u_*, g, \nu, D_m) \qquad (5.2)$$

where:

x = distance downstream from the source,

d = depth of the two-dimensional flow,

b = width of source,

ρ_a = density of ambient fluid,

$\Delta\rho$ = density difference at the source,

$\overline{u}$ = depth-averaged longitudinal velocity,

u_* = shear velocity,

g = acceleration due to gravity,

ν = kinematic viscosity,

D_m = molecular diffusion coefficient.

Independent variables not included in the 10 arguments of ϕ_1 and Ψ_1 are considered to be of secondary importance. By the theorems of dimensional analysis, Eq. 5.1 and 5.2 can be replaced by Eq. 5.3 and 5.4, which contain 7 dimensionless independent variables;

$$\frac{\sigma^2}{d^2} = \phi_2 \left(\frac{xu_*}{d\bar{u}}, \frac{b}{d}, \frac{\Delta\rho g b}{\rho_a u^2}, \frac{u_*}{\bar{u}}, \frac{\bar{u}^2}{gd}, \frac{\bar{u}d}{\nu}, \frac{\bar{u}d}{D_m} \right) \tag{5.3}$$

and

$$\bar{C}_v = \Psi_2 \left(\frac{xu_*}{d\bar{u}}, \frac{b}{d}, \frac{\Delta\rho g b}{\rho_a u^2}, \frac{u_*}{\bar{u}}, \frac{\bar{u}^2}{gd}, \frac{\bar{u}d}{\nu}, \frac{\bar{u}d}{D_m} \right) . \tag{5.4}$$

These functions are simplified by assuming that both $\frac{\sigma^2}{d^2}$ and $\bar{C}_v$ are only weakly dependent on the following four parameters; $\frac{u_*}{\bar{u}}$, which is proportional to the square root of the friction factor; $\frac{\bar{u}^2}{gd}$, the Froude number for the flow; and $\frac{\bar{u}d}{\nu}$ and $\frac{\bar{u}d}{D_m}$, which are Reynolds and molecular Peclet numbers for the flow. By deleting these four parameters from Eq. 5.3 and 5.4, and by substituting αu_* for u_* in the remaining parameters (reasons for the substitutions are given below), one obtains

$$V = V(X, B, M_b) \tag{5.5}$$

and

$$\bar{C}_v = \bar{C}_v (X, B, M_b) , \tag{5.6}$$

where

$$V = \frac{\sigma^2}{d^2} \quad , \tag{5.7a}$$

$$X = \frac{x}{\bar{u}} \frac{\alpha u_*}{d} \quad , \tag{5.7b}$$

$$B = \frac{b}{d} \quad , \tag{5.7c}$$

and

$$M_b = \frac{\Delta\rho}{\rho_a} gb/(\alpha u_*)^2 \quad . \tag{5.7d}$$

The parameter V is the dimensionless variance, and B is the dimensionless source width. The quantity X can be interpreted as either a dimensionless longitudinal distance, or as a dimensionless time equal to the ratio of $x/\bar{u}$, the time required for fluid to travel from the source to some point x downstream, to $d/\alpha u_*$, a characteristic vertical mixing time for the flow. The parameter M_b is called a dimensionless source strength because the numerator in Eq. 5.7d can be written $\frac{\Delta\rho gb(d\bar{u})}{\rho_a (d\bar{u})}$, which is the magnitude of the buoyancy flux from the source per mass flux through a unit width of the flow.

If one chooses, one may also define a different source strength, M_d, given by

$$M_d = \frac{M_b}{B} = \frac{\Delta\rho}{\rho_a} gd/(\alpha u_*)^2 \tag{5.8}$$

in which the water depth rather than the source width is used as a characteristic length. Thus, in place of Eq. 5.5 one may write

$$V = V(X, B, M_d) \cdot \tag{5.9}$$

In the data analysis of the following subsection, using M_b gave the simplest relationships between data from experiments with $B << 1$, but using M_d yielded simpler relationships from experiments with $B >> 1$.

The original reason for substituting αu_* for u_* was to decrease the scatter of the data in Fig. 5.2, which is presented in the following subsection. However, the substitution can be partly justified beforehand by considering the results from the experiments without density differences. Integrating Eq. 2.10a yields

$$\sigma^2(x) = \sigma^2(0) + 2\frac{x}{\bar{u}}\bar{\epsilon}_z \quad . \tag{5.10}$$

Recognizing that $\sigma^2(0) = b^2/12$, using $\epsilon_z = \alpha u_* d$, and dividing by d^2 gives

$$V(X, B, 0) = \frac{B^2}{12} + 2X \quad . \tag{5.11}$$

Because α varied slightly among experiments with different combinations of flows and sources, the function V of Eq. 5.5 could not truly represent the right hand side of Eq. 5.11 if α were deleted from the definition of X. Rather than include α as a fourth argument of V, a logical alternative is to use the product αu_* in place of u_* in the dimensional analysis.

5.2.3 The Dimensionless Variance. Below, the experimental data are used to find the relationship between the dimensionless variance, V, and the three dimensionless parameters X, B, and M_b (or M_d). For $M_b = 0$ it was shown that

$$V(X, B, 0) = \frac{B^2}{12} + 2X \, . \tag{5.11}$$

For $M_b \neq 0$, the data in Chapter 4 show that the variance-distance curves at large x are parallel to the curves for $M_b = 0$ but are displaced from them by an amount, $\Delta\sigma^2$, which has been called the excess variance. Thus, one can write

$$V(X, B, M_b) = \frac{B^2}{12} + 2X + r\Delta V \quad , \tag{5.12}$$

where $\Delta V = \Delta\sigma^2/d^2$ is the dimensionless excess variance, and r is a fraction less than one. Both r and ΔV are also defined in Fig. 5.1. Because ΔV is evaluated at some large value of X, ΔV should be a function of only B and M_b (or M_d); however r is a function of X also.

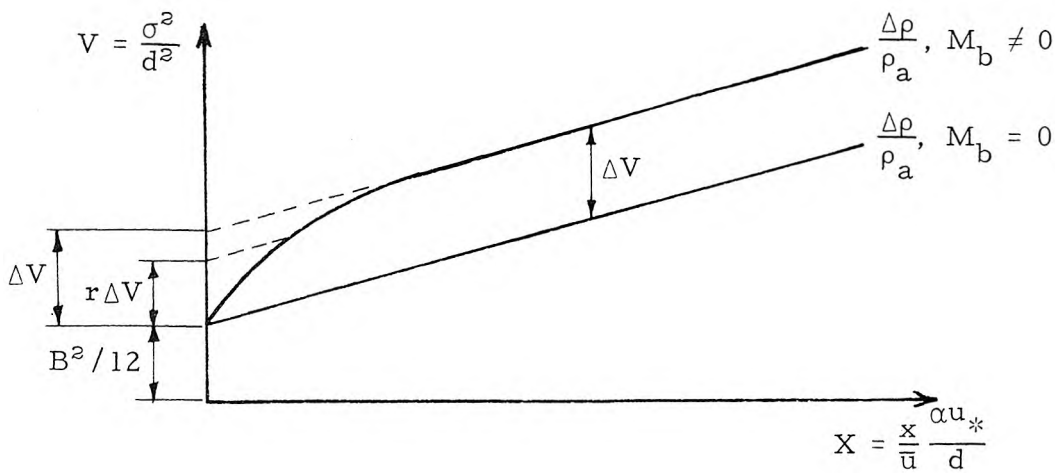

Figure 5.1 Definition sketch for r and ΔV.

5.2.3.1 The Excess Variance. Values of the excess variance, $\Delta\sigma^2$, were measured from the experimental curves in Fig. 4.22 to 4.33 and were used to calculate values of the dimensionless parameter ΔV. The computed values of ΔV were plotted

as functions of the source strengths, M_b and M_d, in Fig. 5.2 and 5.3, respectively. In the calculation of M_b and B for the experiments with the 10-cm-wide source, which was placed against the left sidewall of the flume, b was set equal to 2 x 10 cm = 20 cm; for the experiments with the wide source, which occupied one half the width of the flume, b was set equal to 2 x 55 cm = 110 cm. The value of α used in computing the dimensionless parameters for each experiment was the value calculated in an experiment with the same source and flow condition but with $\Delta\rho/\rho_a = 0$.

In Fig. 5.2, where ΔV is plotted against M_b, the data from experiments with a heavy tracer fluid ($\Delta\rho/\rho_a > 0$) define a family of curves with constant values of B. In all experiments with the 1-cm-wide source, B was small ($0.090 \leq B \leq 0.258$). On a log-log plot, the data from these experiments define a straight line which has a slope of 3/2 and is given by the equation $\Delta V = 6.0 \times 10^{-4} M_b^{3/2}$. The data from the two experiments with a light tracer fluid ($\Delta\rho/\rho_a < 0$) lie well above this line. A line with a 3/2 slope fitted to this data yields values of ΔV five times those for $\Delta\rho/\rho_a > 0$.

In the experiments with flow S1 and the 12.5-cm-wide source, and in the experiments with the deeper flows S2 and R2 with the 20-cm-wide source, the parameter B was between 3.06 and 3.12. The data from these experiments define a curve which lies below or to the right of the line defined by the data from experiments with the 1-cm-wide source. For M_b greater than about 400 or for ΔV greater than about 2 the two curves are nearly parallel; however, for lower values of M_b, the curve for $3.06 \leq B \leq 3.12$ becomes steeper.

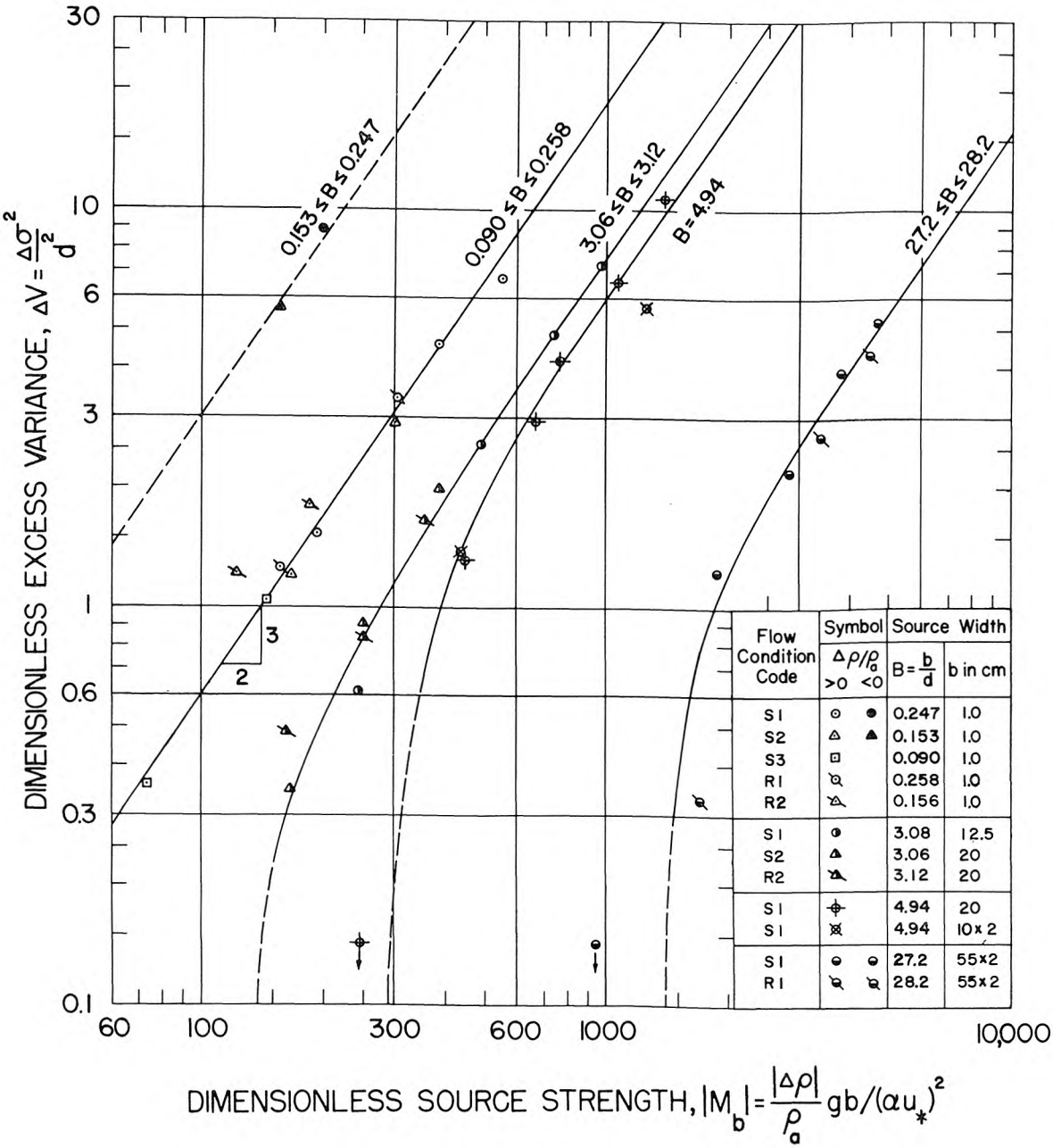

Figure 5.2 The dimensionless excess variance, ΔV, as a function of the dimensionless source strength, M_b, and the dimensionless source width, B.

Data from experiments with flow S1 and the 20-cm-wide source define the curve for B = 4.94. This curve lies to the right of the curve defined by data from experiments with $3.06 \leq B \leq 3.12$, but both curves have the same general shape. One of the two data points from experiments with flow S1 and the 10-cm-wide source, which was placed against the left sidewall of the flume, lies close to the curve for B = 4.94; the other point lies about 35 percent below the curve.

The curve for $27.2 \leq B \leq 28.2$ is defined by data from experiments with the wide source. Values of $\Delta\sigma^2$ from these experiments were obtained from Fig. 4.26 and 4.31 where σ_d^2, variances of the distributions of the concentration gradient, are given as a function of x. By using Eq. 4.11

$$\sigma^2(x) = \sigma^2(0) + \sigma_d^2(x), \tag{4.11}$$

which is valid for large x, one can deduce that $\Delta\sigma^2 = \Delta\sigma_d^2$. Eq. 4.11 is valid for calculating values of σ^2 corresponding either to the case where the fluid to the left of the dividing wall represented half of a 110-cm-wide source which discharged fluid more dense than the ambient fluid, or to the case where the fluid to the right of the dividing wall represented half of a source which discharged fluid less dense than the ambient fluid. Therefore, these values of $\Delta\sigma^2$ apply to both positive and negative values of $\Delta\rho/\rho_a$.

In Fig. 5.3, where ΔV is plotted against M_d, the data from experiments in which $\Delta\rho/\rho_a > 0$ also define a family of curves for which B is constant along each curve. Unlike in Fig. 5.2, the data from all experiments with the 1-cm-wide source do not define only

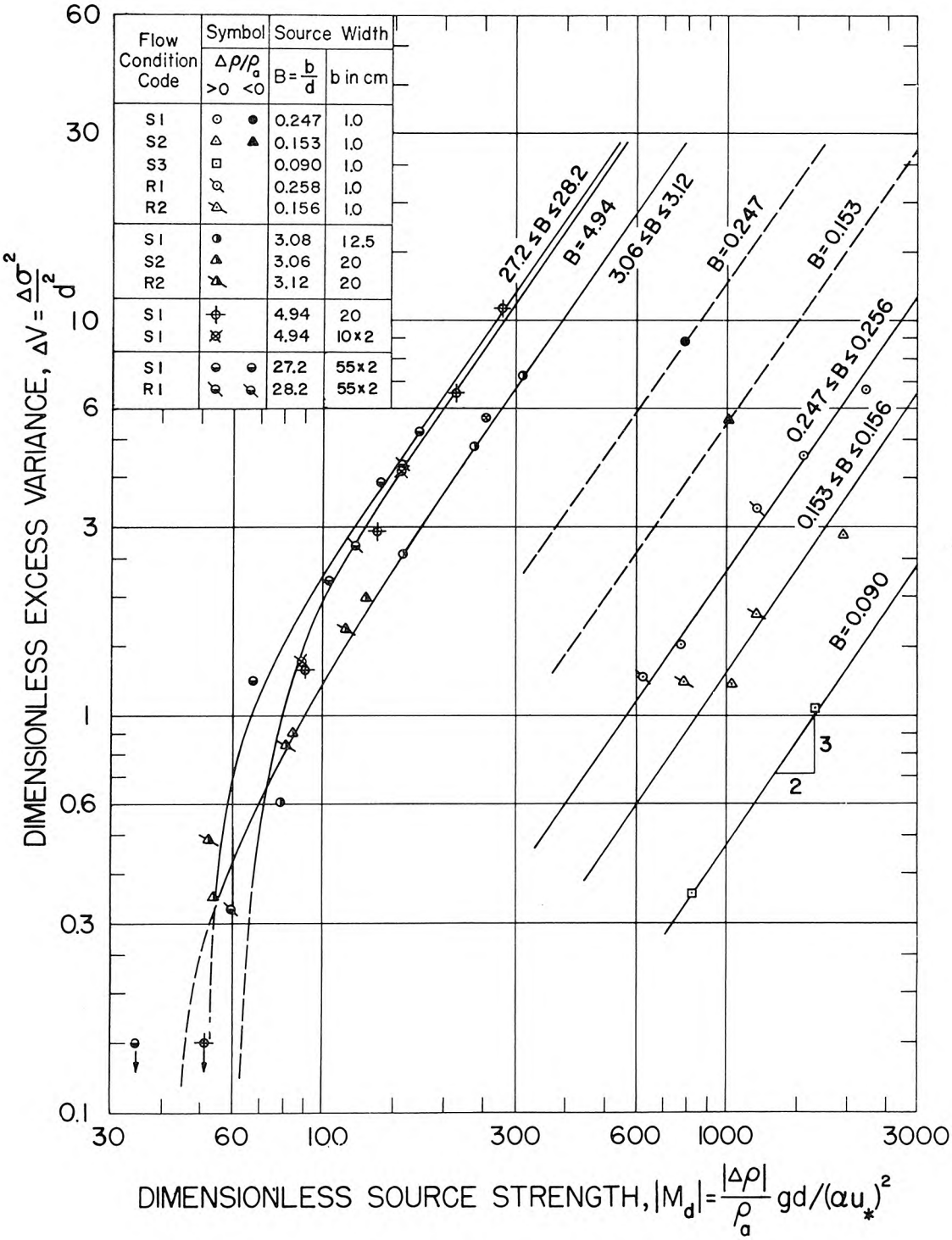

Figure 5.3 The dimensionless excess variance, ΔV, as a function of the dimensionless source strength, M_d, and the dimensionless source width, B.

one curve; for small values of B the parameter ΔV is strongly dependent on B as well as M_d. However, the curves for B = 4.94 and $27.2 \leq B \leq 28.2$ are very close together indicating that the dependence of ΔV on B becomes very weak for large B.

The ΔV-M_b or ΔV-M_d curves at values of B other than those shown in Fig. 5.2 and 5.3 can be estimated from information contained in these figures. Straight lines with slopes of 3/2 representing asymptotes at large values of ΔV were drawn for the curves in Fig. 5.2 and were extended to intersect the line $\Delta V = 1$ as is shown in the insert of Fig. 5.4. The value of M_b at the intersection is denoted by M_b^1, and the equation of the asymptote is

$$\Delta V = \left(\frac{M_b}{M_b^1}\right)^{3/2} \tag{5.13}$$

The parameter M_b^1 was plotted as a function of B in Fig. 5.4, and a smooth solid curve was drawn through the data from experiments with $\Delta\rho/\rho_a > 0$. At low values of B, the curve was drawn horizontal because, as seen in Fig. 5.2, the location of the ΔV-M_b curve is independent of B in this range. At the larger values of B, the curve was drawn with a 1 to 1 slope because, as seen in Fig. 5.3, the location of the ΔV-M_d curve is only a weak function of B in this range and because $M_b \doteq BM_d$. Sufficient data do not exist to determine the actual slope of the M_b-B curve at these larger values of B.

The dashed curve in Fig. 5.4 was drawn through the limited data from experiments with $\Delta\rho/\rho_a < 0$ and was drawn with the same

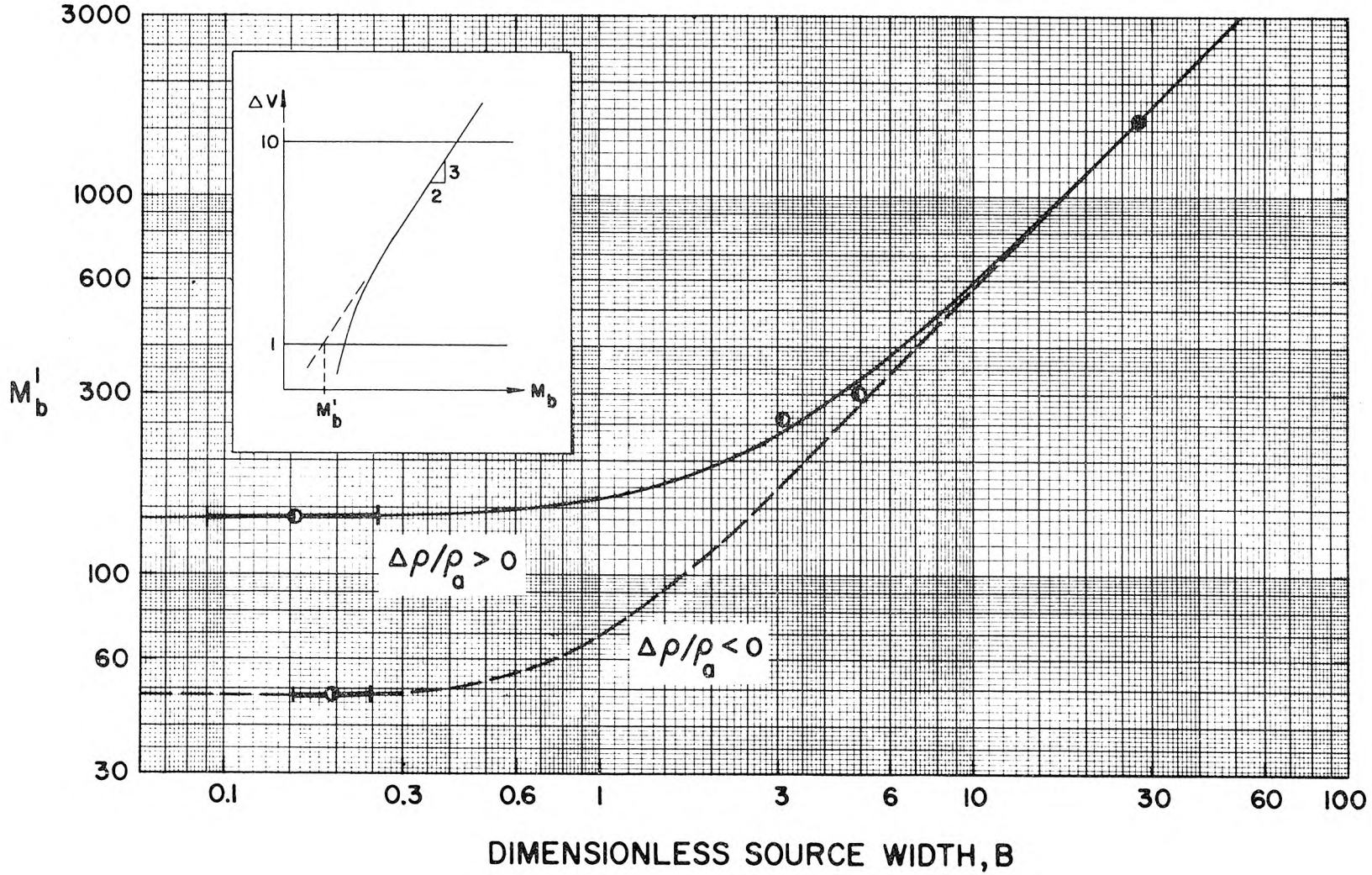

Figure 5.4 The intercept, M_b^1, as a function of the dimensionless source width, B.

general shape as the curve for $\Delta\rho/\rho_a > 0$. At small values of B, the curve for $\Delta\rho/\rho_a < 0$ lies below the curve for $\Delta\rho/\rho_a > 0$; however, for large B, the two curves coincide.

To construct a ΔV-M_b curve for any value of B, one selects the value of M_b^1 from Fig. 5.4 and draws the asymptote for large ΔV. For $B << 1$ the asymptote is the desired ΔV-M_b curve; for larger values of B the asymptote is a good approximation of the desired curve for ΔV greater than about 2 or 3. Because the lower nonlinear parts of the curves in Fig. 5.2 were not well defined for the values of B investigated, no technique is given here to determine accurately the lower parts of curves for other values of B. The nonlinear parts of the curves may be approximated by drawing them similar in shape to the curves in Fig. 5.2.

5.2.3.2 The Fraction r. The fraction of the excess variance, denoted by r and defined in Fig. 5.1, was computed from the data in Fig. 4.22 to 4.33 and was plotted as a function of X in Fig. 5.5. These values of r are also listed in Tables A1 and A2 of the appendix. The value of r for each data point was computed by taking the difference between values of σ^2 from experiments with and without density differences and dividing by $\Delta\sigma^2$. For calculating the differences, the actual experimental values of variances from experiments with density differences were used, but variances for experiments without density differences were obtained from the curves fitted to the data.

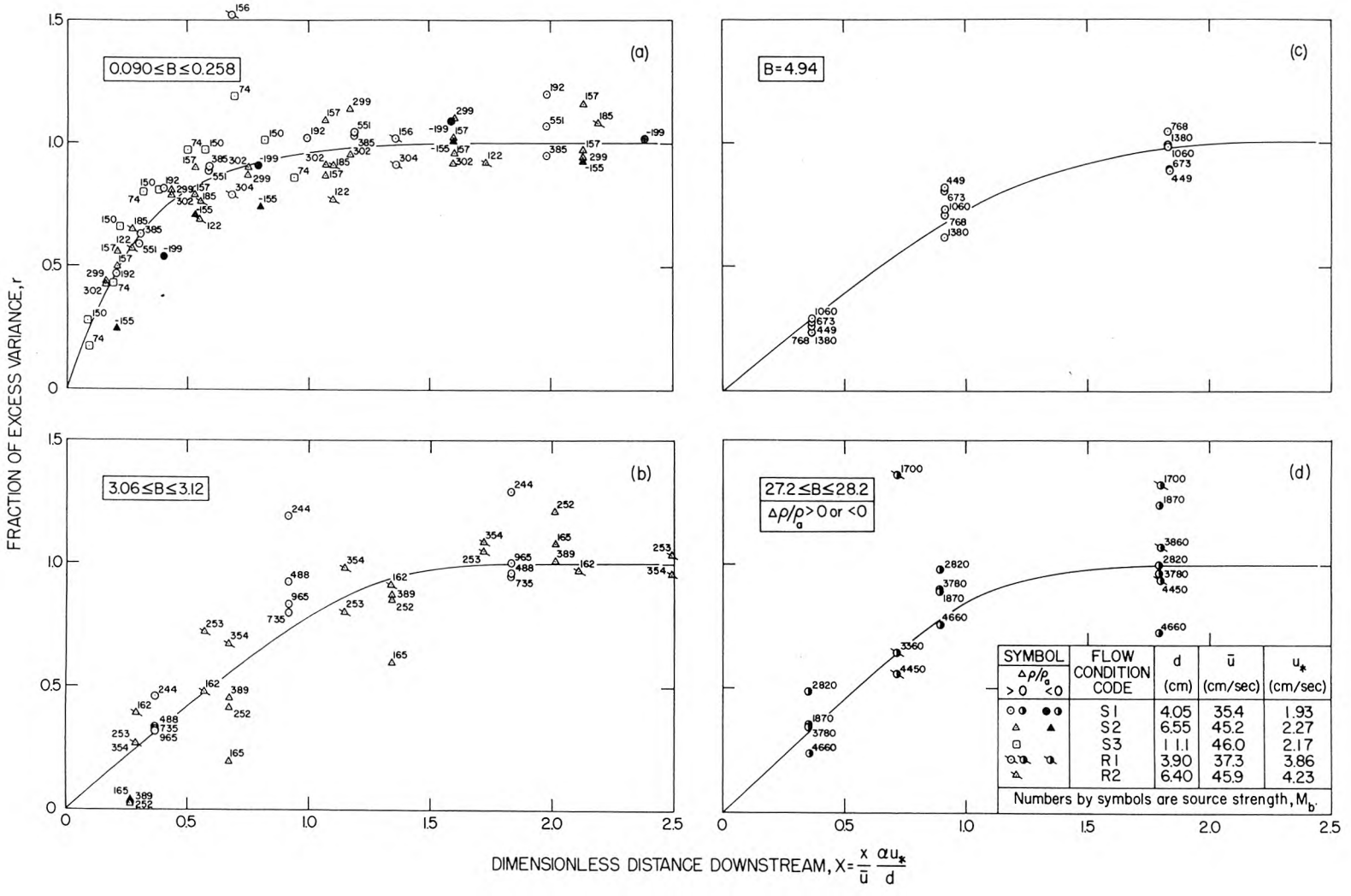

Figure 5.5 The fraction of the excess variance, r, as a function of the dimensionless distance downstream, X.

The values of r for $27.2 \leq B \leq 28.2$ were computed with data from the experiments with the wide source. Because accurate values of σ^2 for these experiments were not available, r was computed on the basis of σ_d^2 instead of σ^2, even though Eq. 4.11 was not always valid for small X. Thus the values of r at small X probably lie between the correct values for positive and negative $\Delta\rho/\rho_a$; however, it is assumed that they are representative for both.

In Fig. 5.5, data from experiments with similar values of the dimensionless source width, B, were plotted on the same set of coordinates, and values of the source strength, M_b, were written beside each point. Smooth curves were fitted to the data by eye. For $\Delta\rho/\rho_a > 0$ the data for each range of B show that r is independent M_b. Therefore, for a given source and set of hydraulic conditions, the distance downstream required to achieve any fraction of the excess variance, $\Delta\sigma^2$, is independent of the magnitude of $\Delta\sigma^2$. The limited data in Fig. 5.5a from experiments with $\Delta\rho/\rho_a < 0$ suggest that slightly larger values of X are required when $\Delta\rho/\rho_a < 0$ than when $\Delta\rho/\rho_a > 0$. The curve for experiments with $B << 1$ in Fig. 5.5a yields smaller values of X for the same values of r than the curves in Fig. 5.5b, c and d for experiments with larger values of B. There is little difference between the curves in Fig. 5.5b, c, and d.

Because the data from experiments with smooth and rough bottoms with nearly the same values of B define single curves in Fig. 5.2, 5.3, and 5.5, one can conclude that the friction factor, $f=8(u_*/\overline{u})^2$, has been included properly in the dimensional analysis, even

though f does not appear explicitly in Eq. 5.5 as an argument of V. However, when $u_*/\bar{u}$ was deleted from the definition of X, or when $\bar{u}$ was used in place of u_* or αu_* in the definitions of M_d and M_b, the data from experiments with rough and smooth bottoms did not define single curves in Fig. 5.2, 5.3, and 5.5, and f had to be included as a fourth argument of V.

5.2.3.3 Maximizing Lateral Mixing. If one wishes to mix a solute or other density-difference-causing agent across the width of a stream rapidly it is worthwhile looking at data from experiments with similar hydraulic conditions and source strengths, M_b, but different source widths. By using the definition $M_b = \frac{\Delta\rho}{\rho_a} gb / (\alpha u_*)^2$ and assuming that the relationship between density and concentration is linear, one can see that in experiments with the same hydraulic conditions and value of M_b, the salt flux from each source is the same, regardless of the source width. Obviously, the concentration of the effluent from a narrow source would be higher than the concentration of the effluent from a wide source.

In Fig. 5.6a, variance-distance curves are presented from three experiments with the same hydraulic conditions and similar values of M_b but with different source widths. In Fig. 5.6b, the maximum relative concentration observed in each cross-section is presented as a function of x. In Exp. 122, the variance at x=0 and the source strength, M_b, were less than in either Exp. 164 or 140,

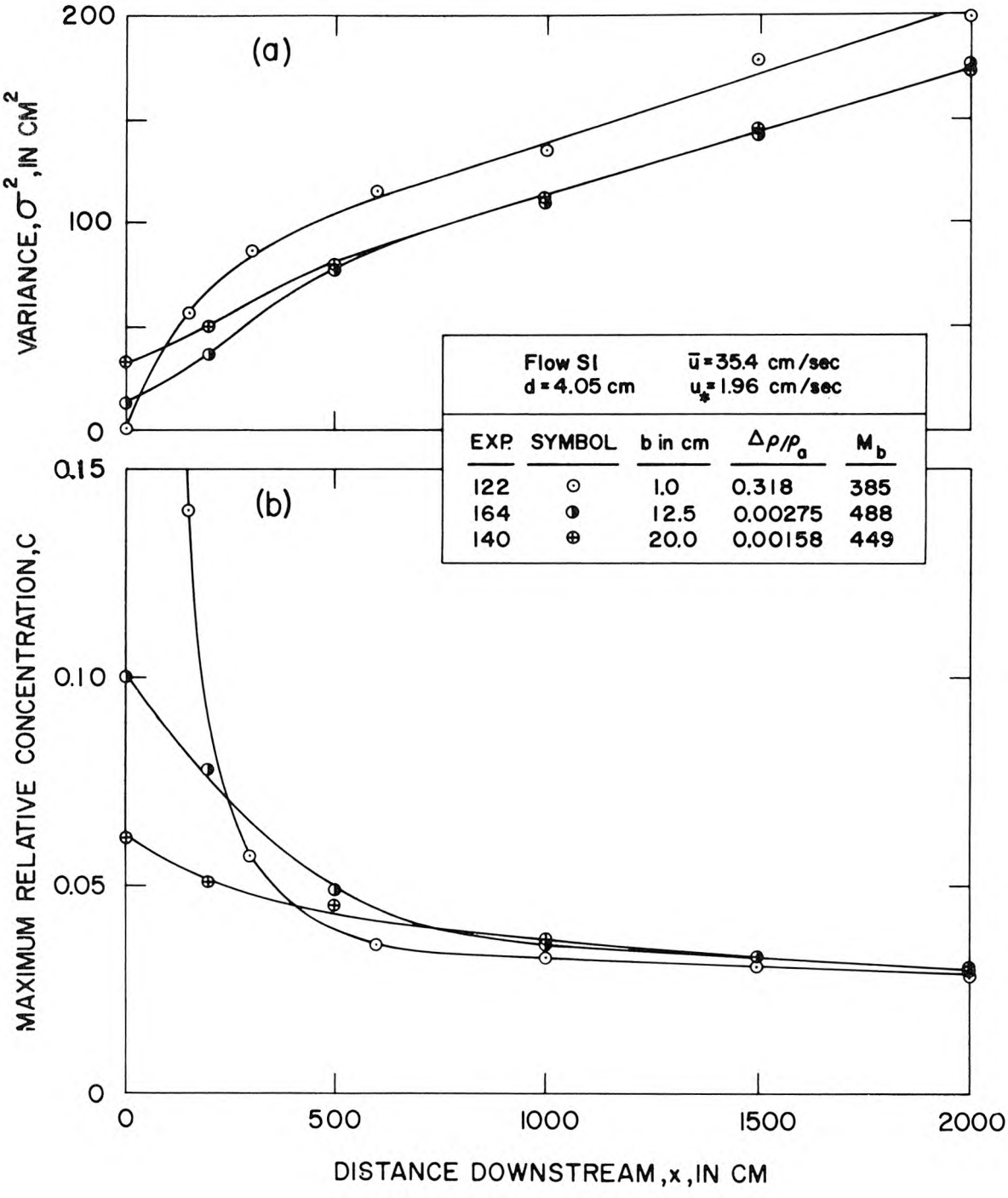

Figure 5.6 a) Variance-, and b) Maximum concentration-distance curves from some experiments with similar flow conditions and values of M_b but different source widths.

and the maximum relative concentration at x = 0 was higher than in either of the other two experiments. However, downstream from about x = 100 cm the variance in Exp. 122 was greater than in either Exp. 164 or 140, and downstream from about x = 400 cm the maximum observed relative concentration was less. In Exp. 164, the initital variance was less than in Exp. 140 and the maximum concentration at x = 0 was greater; however, downstream from about x = 500 cm the variances in both experiments were nearly the same, and downstream from about x = 1500 cm the maximum relative concentrations were nearly the same.

When comparing data from other experiments with similar hydraulic conditions and source strengths but different source widths one also finds that far downstream, variances are sometimes greater and peak relative concentrations are sometimes less in the experiments with the narrower sources. Examples are the pairs: Exp. 113 and 151 with flow S2, Exp. 117 and 152 with flow S2, and Exp. 130 and 165 with flow S1. In each of these pairs, M_b for the first experiment was equal to or less than in the second, and the source width was less in the first; however, far downstream the variance in the first experiment was greater than in the second.

These results show that if one wishes to dilute a density-difference-causing agent in a stream by crosswise mixing, it is not always advantageous to dilute the substance initially by introducing it into the stream across a wide width. In some cases

it may be advantageous to introduce the agent in concentrated form across some small width of the stream; however, under such conditions, high concentrations would exist close to the source.

5.2.4 The Average Coefficient of Variation. The concentration-weighted, laterally-averaged coefficient of variation for the vertical concentration distributions, $\overline{C}_v$, which was defined by Eq. 4.15, was plotted in Fig. 5.7 as a function of the dimensionless distance X. Data from experiments with similar values of the dimensionless source width, B, are on common sets of coordinates, and a value of the source strength, M_b or M_d, is beside each point. The source strength M_b, which includes the source width in its definition, is used with all data except those from experiments with the wide source. With these data, which were plotted in Fig. 5.7d, the source strength M_d is used. The parameter M_b was not used in Fig. 5.7d, nor was this figure labeled $27.2 \leq B \leq 28.2$ as was Fig. 5.5d because the values of $\overline{C}_v$ from these experiments were obtained by averaging only data from across the mixed zone between the two fluids and not across all that part of the flume occupied by the plume from the hypothetical 110-cm-wide source.

Smoothed curves defining the locus of points of constant source strength were drawn through the data in Fig. 5.7. These data show that $\overline{C}_v$ attains a maximum at $X < 0.2$ for $B << 1$, and at $X \approx 0.4$ for larger B. For X and B constant the data show that $\overline{C}_v$ increases with M_b, and that $\overline{C}_v$ decreases with increasing B for X and M_b

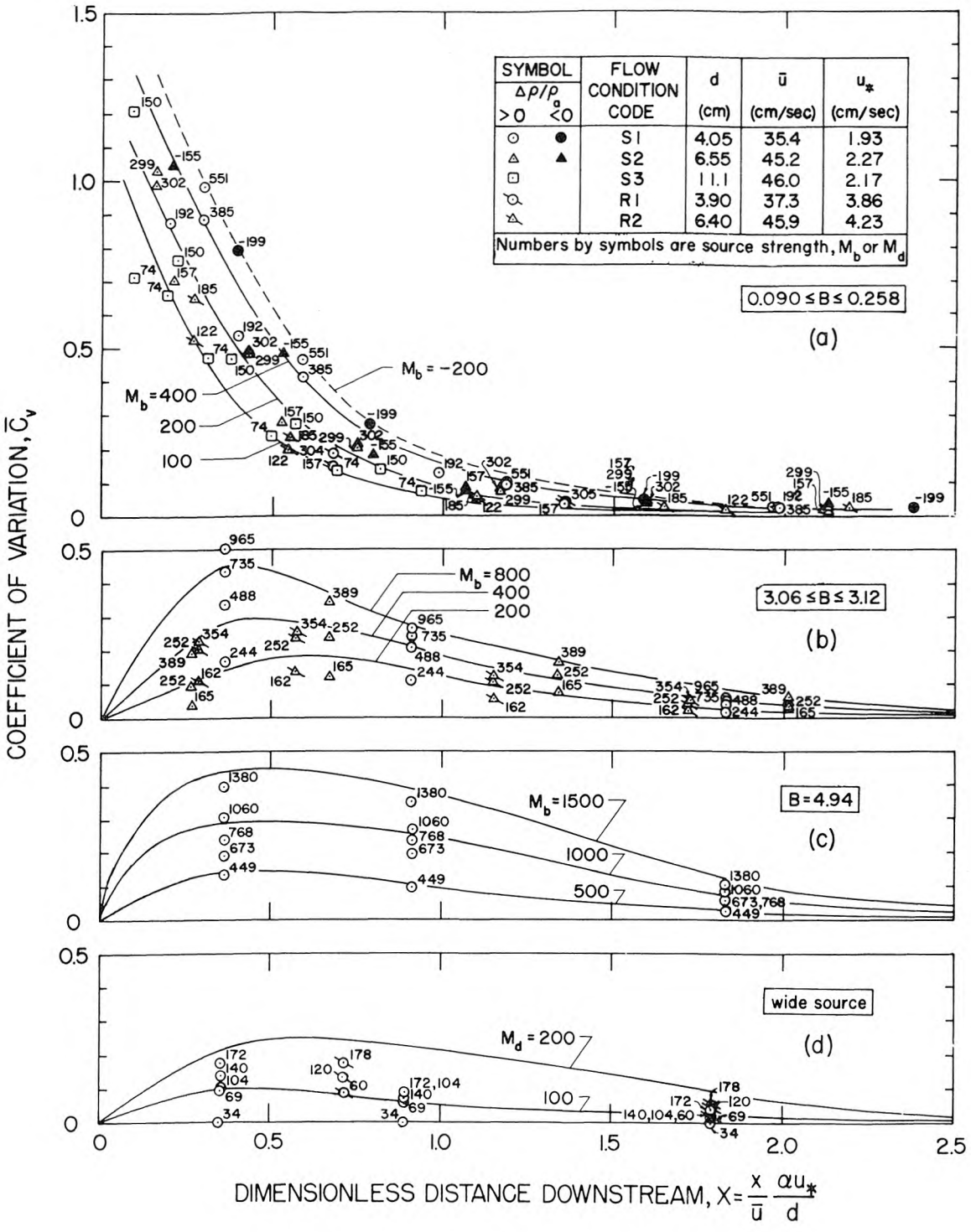

Figure 5.7 Laterally averaged coefficient of variation, $\bar{C}_v$, as a function of the dimensionless distance downstream, X.

constant. The data in Fig. 5.7a also show that $\overline{C}_v$ is larger when $\Delta\rho/\rho_a < 0$ than when $\Delta\rho/\rho_a > 0$ if M_b is the same magnitude. The data from experiments with the wide source indicate that $\overline{C}_v$ increases with M_d.

5.2.5 Predicting Concentration Distributions. The results of the analyses in this chapter can be used to estimate concentration distributions downstream from a source discharging fluid with a density different from the ambient fluid but with a velocity equal to the ambient fluid velocity. As a first step in estimating concentration distributions for a particular problem, the dimensionless variance-distance curve, V(X), is constructed from: 1) V(X) for a neutrally buoyant tracer, which is given by Eq. 5.11; 2) the excess variance, ΔV, obtained from a ΔV-M_b curve, which can be constructed using Fig. 5.4; and 3) the fraction of the excess variance, r(X), which is obtained from Fig. 5.5. The function V(X) and the corresponding $\sigma^2(x)$ are obtained from Eq. 5.12.

To calculate the dimensionless source strength, M_b, and the dimensionless source width, B, which are required to construct V(X) and to relate V(X) to $\sigma^2(x)$, one must know d, b, $\frac{\Delta\rho}{\rho_a}g$, $\overline{u}$, and αu_*. Each of the variables appearing in this list, except perhaps the dimensionless lateral diffusion coefficient, $\alpha = \overline{\epsilon}_z/u_*d$, would normally be available as basic information in a particular problem. If possible, α should be computed from observations of $\overline{\epsilon}_z$ rather than be estimated. (If α is greater than about 0.2, one should

suspect that significant secondary currents exist in the ambient flow, and therefore, the accuracy of predictions made using the experimental results of this study is uncertain.)

Next, the depth-averaged concentration distributions are assumed to be given by the solution to the diffusion equation, Eq. 4.2, with the appropriate initial condition, but, with the x-coordinate transformed so that the variances of the lateral distributions given by the solution equal those obtained from Eq. 5.12. Thus, in the solution to Eq. 4.2, one substitutes

$$\frac{\bar{u}}{2\bar{\epsilon}_z}[\sigma^2(x) - \sigma^2(0)] \qquad (5.14)$$

for x, where $\sigma^2(x)$ is obtained from Eq. 5.12.
This method of calculating $\bar{C}(x, z)$ is a good approximation for X greater than about two.

An integral measure of the variation of concentration with depth is given by the laterally-averaged coefficient of variation for the vertical concentration distributions, $\bar{C}_v$, which is obtained from Fig. 5.7. The variation in concentration corresponding to particular values of $\bar{C}_v$ can be seen in Fig. 4.40 to 4.44.

CHAPTER 6

ANALYTIC STUDY

6.1 INTRODUCTION

In the first part of this chapter, an analysis similar to that used by Hansen and Rattray (25) is used to derive expressions for the horizontal velocities induced by horizontal density gradients in a turbulent fluid. Dispersion coefficients due to the induced velocities are obtained using an expression given by Elder (4). In the last part of this chapter, the dispersion coefficients are used in an analysis of the experiments from this investigation and also in an analysis of some published data by Ippen, Harlemann and Lin (2).

6.2 BASIC EQUATIONS

The equations which form the basis for the analysis of this chapter are given below together with the assumptions embodied in these equations. The equations given are: The equation of state for the fluid, the continuity equation for the fluid, momentun equations for the three coordinate directions, and the conservation of mass equation for a dissolved substance. (If density differences

are due to differences in temperature rather than differences in the concentration of a dissolved substance, the conservation of energy or heat equation can be substituted for the last equation.)

The equation of state for an aqueous solution of low concentration can be approximated by the linear relation

$$(\rho-\rho_a) = \beta(c-c_a) \qquad (6.1)$$

in which ρ is the density of a solution with concentration c, and ρ_a is the density of a reference or ambient solution with concentration c_a. Both the concentration and density have units of mass per unit volume; the parameter β is dimensionless and is assumed to be a constant. Data from Ref. 27, p. 1909 for weak (one percent) NaCl solutions yield $\beta = 0.71$.

The continuity equation is assumed to be

$$\frac{\partial u}{\partial x} + \frac{\partial v}{\partial y} + \frac{\partial w}{\partial z} = 0 \quad , \qquad (6.2)$$

where u, v, and w are time-averaged velocities in the x-, y-, and z-directions. Eq. 6.2 is not exact because it does not include the rate of dilatation of the fluid with changing concentration, which occurs if $\beta \neq 1$. For laminar flow in a porous medium, List (36) showed that the error in the continuity equation, Eq. 6.2, is of order $(\rho-\rho_a)/\rho_a$; by using the same arguments as used by List, one can obtain the same result for a turbulent shear flow.

The equation for the conservation of mass of a solute is written as

$$\frac{\partial c}{\partial t}+\frac{\partial (uc)}{\partial x}+\frac{\partial (vc)}{\partial y}+\frac{\partial (wc)}{\partial z}=\frac{\partial}{\partial x}\left(\epsilon_x\frac{\partial c}{\partial x}\right)+\frac{\partial}{\partial y}\left(\epsilon_y\frac{\partial c}{\partial y}\right)+\frac{\partial}{\partial z}\left(\epsilon_z\frac{\partial c}{\partial z}\right), \quad (6.3)$$

where c is a time-averaged concentration. In writing Eq. 6.3 it is assumed that mass transport by turbulent diffusion in each of the three coordinate directions can be represented by the product of a turbulent diffusion coefficient and the mean concentration gradient in that direction. (Eq. 2.1 is obtained from Eq. 6.3 by using Eq. 6.2).

The momentum equations are written as

$$\rho_a\left(\frac{\partial u}{\partial t}+u\frac{\partial u}{\partial x}+v\frac{\partial u}{\partial y}+w\frac{\partial u}{\partial z}\right)=-\frac{\partial p}{\partial x}-\rho g\,\ell_x+\frac{\partial}{\partial x}\tau_{xx}+\frac{\partial}{\partial y}\tau_{xy}+\frac{\partial}{\partial z}\tau_{xz} \quad (6.4a)$$

$$\rho_a\left(\frac{\partial v}{\partial t}+u\frac{\partial v}{\partial x}+v\frac{\partial v}{\partial y}+w\frac{\partial v}{\partial z}\right)=-\frac{\partial p}{\partial y}-\rho g\,\ell_y+\frac{\partial}{\partial x}\tau_{xy}+\frac{\partial}{\partial y}\tau_{yy}+\frac{\partial}{\partial z}\tau_{yz} \quad (6.4b)$$

$$\rho_a\left(\frac{\partial w}{\partial t}+u\frac{\partial w}{\partial x}+v\frac{\partial w}{\partial y}+w\frac{\partial w}{\partial z}\right)=-\frac{\partial p}{\partial z}-\rho g\,\ell_z+\frac{\partial}{\partial x}\tau_{xz}+\frac{\partial}{\partial y}\tau_{yz}+\frac{\partial}{\partial z}\tau_{zz}\,. \quad (6.4c)$$

The quantities ℓ_x, ℓ_y, and ℓ_z are the cosines of the angles between the vertical and the x-, y-, and z- directions; the terms τ_{xx}, τ_{xy}, etc are the turbulent Reynolds stresses, and p is pressure. In the derivation of Eq. 6.4, Eq. 6.2 is used. Also, the Boussinesq approximation is made in which changes in fluid density are assumed not to affect the inertia of a fluid element; therefore, on the left hand sides of Eq. 6.4, the density is set equal to a constant, ρ_a. However, the effect of changes in density are considered in computing the submerged weight of a fluid element; therefore, on the right hand sides of the equations, the density is retained as a variable.

6.3 SIMPLIFICATION OF THE BASIC EQUATIONS

Two physical systems are now considered for which the equations presented in the previous section may be simplified sufficiently so that a solution can be obtained which predicts the effect of a horizontal density gradient on horizontal mixing.

6.3.1 Lateral Mixing. Consider first lateral mixing far downstream from a source which is discharging fluid into a wide, uniform, turbulent, open-channel flow. As in the experiments described in the previous chapters, let the fluid that is discharged from the source have a density different from the ambient fluid, but let the discharge velocity from the source be the same as the velocity of the ambient flow. Choose the same coordinate system as was used in the experiments. The origin is located on the channel bottom at the center line of the source. The x-axis is parallel to the channel bottom and in the direction of the ambient flow; the z-coordinate is horizontal and perpendicular to x; the y-coordiante is normal to x and z and is positive upwards. In the case of horizontal mixing between two wide parallel streams, the origin is located on the channel bottom at the confluence of the two streams.

Let the distances over which density-induced velocities change be characterized in the y-direction by d, the depth of flow; in the z-direction by σ or σ_d, the standard deviation of the lateral distribution of the concentration or lateral concentration gradient; and in the x-direction by x, the distance downstream from the

source. At large values of x one expects

$$x >> (\sigma \text{ or } \sigma_d) >> d. \tag{6.5}$$

It is assumed that the density-induced velocities are much smaller than the mean longitudinal velocity. Also, it is assumed that u changes sufficiently slowly in the x-direction so that the first term in Eq. 6.2, the continuity equation, is of the same or of smaller magnitude than either of the other two terms. An order of magnitude analysis then yields

$$v = O(w\frac{d}{\sigma}), \tag{6.6}$$

where O( ) denotes order of magnitude.

Next, it is assumed that the Reynolds stresses in Eq. 6.4 can be represented by the terms on the right hand side of the matrix equation

$$\begin{bmatrix} \tau_{xx} & \tau_{xy} & \tau_{xz} \\ \tau_{xy} & \tau_{yy} & \tau_{yz} \\ \tau_{xz} & \tau_{yz} & \tau_{zz} \end{bmatrix} = \rho_a \begin{bmatrix} \lambda_x \epsilon_x \frac{\partial u}{\partial x} & \lambda_y \epsilon_y \frac{\partial u}{\partial y} & \lambda_z \epsilon_z \frac{\partial u}{\partial z} \\ \lambda_x \epsilon_x \frac{\partial v}{\partial x} & \lambda_y \epsilon_y \frac{\partial v}{\partial y} & \lambda_z \epsilon_z \frac{\partial v}{\partial z} \\ \lambda_x \epsilon_x \frac{\partial w}{\partial x} & \lambda_y \epsilon_y \frac{\partial w}{\partial y} & \lambda_z \epsilon_z \frac{\partial w}{\partial z} \end{bmatrix}. \tag{6.7}$$

The terms ϵ_x, ϵ_y, and ϵ_z are turbulent diffusion coefficients for mass, and λ_x, λ_y, and λ_z are turbulent Schmidt numbers, which are the ratios of the diffusion coefficients for momentum to the diffusion coefficients for mass so that the products $\lambda_x \epsilon_x$, etc. are momentum diffusion coefficients or eddy viscosities. The ambient density, ρ_a, is used in place of the actual density to be consistent with the Boussinesq approximation which was used in the derivation of Eq. 6.4.

By using Eqs. 6.5, 6.6 and 6.7, one can compare the relative importance of the various terms in Eq. 6.4. Comparing the last three terms on the right-hand side and all terms on the left-hand side of Eq. 6.4b with corresponding terms in Eq. 6.4c, one finds that the terms in Eq. 6.4b are of order d/σ times those in Eq. 6.4c. Because $d/\sigma << 1$, these terms can be omitted from Eq. 6.4b; for $\ell_y \approx 1$ one obtains

$$0 = -\frac{\partial p}{\partial y} - \rho g. \tag{6.8}$$

Thus, the equation of motion in the y-direction is reduced to a hydrostatic relationship.

When Eq. 6.7 is substituted into Eq. 6.4, the right-hand side of Eq. 6.4c becomes

$$-\frac{\partial p}{\partial z} - \rho g \ell_z + \rho_a \frac{\partial}{\partial x}\left(\lambda_x \epsilon_x \frac{\partial w}{\partial x}\right) + \rho_a \frac{\partial}{\partial y}\left(\lambda_y \epsilon_y \frac{\partial w}{\partial y}\right) + \rho_a \frac{\partial}{\partial z}\left(\lambda_z \epsilon_z \frac{\partial w}{\partial z}\right). \tag{6.9}$$

Results given in Chapter 2 from previous investigations in homogeneous fluids show that ϵ_x, ϵ_y, and ϵ_z are no more than an order of magnitude apart. One can assume that the same is true for $\lambda_x \epsilon_x$, $\lambda_y \epsilon_y$, and $\lambda_z \epsilon_z$ when the Richardson number is small. With this assumption and the inequality 6.5, one can show that the third and last terms in expression 6.9 are smaller than the fourth term and therefore can be deleted. Because $\ell_z = 0$, the second term is also deleted. Eq. 6.4c is further simplified by deleting the entire left-hand side, which is valid if each of the terms on the left is much smaller than $\rho_a \frac{\partial}{\partial y}\left(\lambda_y \epsilon_y \frac{\partial w}{\partial y}\right)$. It is assumed that the

first term on the left-hand side of Eq. 6.4c is of the same or smaller order of magnitude than the second term; by using Eq. 6.6 it is possible to show that the last two terms are of the same order. Thus, to delete the left-hand side of Eq. 6.4c it is only necessary that

$$\rho_a u \frac{\partial w}{\partial x} << \rho_a \frac{\partial}{\partial y}\left(\lambda_y \epsilon_y \frac{\partial w}{\partial y}\right) \tag{6.10}$$

and

$$\rho_a w \frac{\partial w}{\partial z} << \rho_a \frac{\partial}{\partial y}\left(\lambda_y \epsilon_y \frac{\partial w}{\partial y}\right) . \tag{6.11}$$

These inequalities are generally true if

$$\frac{uw}{x} << \frac{\lambda_y \epsilon_y w}{d^2} \tag{6.12}$$

and

$$\frac{w^2}{\sigma} << \frac{\lambda_y \epsilon_y w}{d^2} \tag{6.13}$$

respectively, which in turn are true if

$$\left(\frac{ud}{\lambda_y \epsilon_y}\right)\left(\frac{d}{x}\right) << 1 \tag{6.14}$$

and

$$\left(\frac{wd}{\lambda_y \epsilon_y}\right)\left(\frac{d}{\sigma}\right) << 1 . \tag{6.15}$$

Because the left-hand side of inequalities 6.14 and 6.15 go to zero as x and σ become very large, inequalities 6.10 and 6.11 are true for x sufficiently large. With the above substitution and deletions, Eq. 6.4c, the equation of motion in the z-direction, becomes

$$0 = -\frac{\partial p}{\partial z} + \rho_a \frac{\partial}{\partial y}\left(\lambda_y \epsilon_y \frac{\partial w}{\partial y}\right) . \qquad (6.16)$$

Physically Eq. 6.16 states that the lateral pressure gradient, $\frac{\partial p}{\partial z}$, is balanced totally by shearing of the lateral velocity, w, and all accelerations are negligible.

Eq. 6.2, the continuity equation, can be integrated from y=0 to d to yield for d=constant

$$\frac{\partial \overline{u}}{\partial x} + \frac{\partial \overline{w}}{\partial z} = 0 \ , \qquad (6.17)$$

where $\overline{u}$ and $\overline{w}$ are depth-averaged values of u and w. For uniform flow $\frac{\partial \overline{u}}{\partial x} = 0$, therefore $\frac{\partial \overline{w}}{\partial z} = 0$ or

$$\overline{w} = \frac{1}{d}\int_0^d w\, dy = \text{constant} . \qquad (6.18)$$

For the problem being considered, $\overline{w} = 0$.

Eq. 6.3, the expression for the conservation of mass for a solute, is also integrated over the depth; for the depth equal to a constant,

$$\frac{\partial \overline{c}}{\partial t} + \overline{u}\frac{\partial \overline{c}}{\partial x} + \overline{w}\frac{\partial \overline{c}}{\partial z} + \frac{\partial}{\partial x}\left(\overline{u'c'}\right) + \frac{\partial}{\partial z}\left(\overline{w'c'}\right) + \overline{c}\left(\frac{\partial \overline{u}}{\partial x} + \frac{\partial \overline{w}}{\partial z}\right) =$$

$$\frac{\partial}{\partial x}\left(\overline{\epsilon}_x \frac{\partial \overline{c}}{\partial x}\right) + \frac{\partial}{\partial x}\left(\overline{\epsilon'_x \frac{\partial c'}{\partial x}}\right) + \frac{\partial}{\partial z}\left(\overline{\epsilon}_z \frac{\partial \overline{c}}{\partial z}\right) + \frac{\partial}{\partial z}\left(\overline{\epsilon'_z \frac{\partial c'}{\partial z}}\right) , \qquad (6.19)$$

where an over-bar denotes an average over the depth, and a primed quantity is the difference between the value of a variable at a point and the depth-averaged value of that variable. (One should remember that all the terms are considered to be time-averaged.)

The quantity $\overline{u'c'}$ represents transport due to longitudinal dispersion as described in Chapter 2, and the term $\overline{w'c'}$ represents mass transport by a similar process in the lateral direction. Therefore, it is assumed that these two terms can be represented by

$$\overline{u'c'} = -D_x \frac{\partial \bar{c}}{\partial x} \tag{6.20}$$

and

$$\overline{w'c'} = -D_z \frac{\partial \bar{c}}{\partial z} \ , \tag{6.21}$$

where D_x and D_z are dispersion coefficients for the x- and z-directions. Because the concept of longitudinal dispersion is justified only for long dispersion times and for uniform, unidirectional flow, the use of Eq. 6.20 and 6.21 may be questionable. However, if inequalities 6.14 and 6.15 are true, then dispersion times are long and the time scale for changes in the velocity of a particle travelling along a streamline is small compared to the vertical mixing time. For these conditions, Eq. 6.20 and 6.21 are valid approximations.

It is also assumed that variations in concentrations are sufficiently small over the depth, $c' << c$, so that on the right-hand side of Eq. 6.19, the second term is small compared to the first term, and the last term is small compared to the third term. Deleting these small terms and using Eqs. 6.17, 6.20, and 6.21 in Eq. 6.19 yields

$$\frac{\partial \bar{c}}{\partial t} + \bar{u}\frac{\partial \bar{c}}{\partial x} + \bar{w}\frac{\partial \bar{c}}{\partial z} = \frac{\partial}{\partial x}\left[\left(D_x + \bar{\epsilon}_x\right)\frac{\partial \bar{c}}{\partial x}\right] + \frac{\partial}{\partial z}\left[\left(D_z + \bar{\epsilon}_z\right)\frac{\partial \bar{c}}{\partial z}\right] \qquad (6.22)$$

As shown in Chapter 2, the first term on the right-hand side of Eq. 6.22, which represents differential transport by dispersion and turbulent diffusion in the longitudinal direction, is small compared to the second term on the left-hand side, which represents differential longitudinal transport by convection. Deleting this small term on the right and considering only steady state problems so that the term $\frac{\partial \bar{c}}{\partial t}$ can be omitted, Eq. 6.22 becomes

$$\bar{u}\frac{\partial \bar{c}}{\partial x} + \bar{w}\frac{\partial \bar{c}}{\partial z} = \frac{\partial}{\partial z}\left[\left(D_z + \bar{\epsilon}_z\right)\frac{\partial \bar{c}}{\partial z}\right]. \qquad (6.23)$$

Although $\bar{w} = 0$ in the problem presently being considered, the term $\bar{w}\frac{\partial \bar{c}}{\partial z}$ is retained here for convenience in the next subsection where a slightly different problem is investigated.

In summary, the basic equations presented in Section 6.2 have been simplified as follows. The equations of motion in the y- and z-directions have become

$$0 = -\frac{\partial p}{\partial y} - \rho g \qquad (6.8)$$

and

$$0 = -\frac{\partial p}{\partial z} + \rho_a \frac{\partial}{\partial y}\left(\lambda_y \epsilon_y \frac{\partial w}{\partial y}\right). \qquad (6.16)$$

The equation of motion in the x-direction has been omitted because the velocity u does not appear in any of the other equations and it is sufficient to assume that u is not affected by the density differences and that it is known. The continuity equation has been reduced to

$$\overline{w} = \frac{1}{d} \int_0^d w \, dy = \text{constant.} \tag{6.18}$$

The conservation equation for the solute is

$$\overline{u} \frac{\partial \overline{c}}{\partial x} + \overline{w} \frac{\partial \overline{c}}{\partial z} = \frac{\partial}{\partial z} \left[\left(D_z + \overline{\varepsilon}_z \right) \frac{\partial \overline{c}}{\partial z} \right], \tag{6.23}$$

where D_z is a dispersion coefficient which is a function of w. The equation of state is unchanged,

$$(\rho - \rho_a) = \beta (c - c_a) . \tag{6.1}$$

6.3.2 Longitudinal Mixing. A second but very similar problem for which the basic equations of Section 6.2 can be simplified is longitudinal mixing in a turbulent open channel-flow in which there is a longitudinal density gradient. For certain conditions, the basic equations can also be simplified for this problem to yield the same simplified set of equations as was obtained in the previous subsection for lateral mixing.

Consider now turbulent flow in a wide open channel in which the variation of all variables in the lateral direction is sufficiently small so that one can consider the flow to be two dimensional. Let the discharge be steady and uniform, and assume a steady state longitudinal density gradient. This physical system may be interpreted as representing an idealized estuary connected to a tideless ocean.

Because of the similarity of this problem with that of lateral mixing considered previously, it is advantageous to change the

coordinate system so that the density gradient is in the z-direction. Therefore, let the z-axis be in the longitudinal direction which is assumed to be horizontal; let x be horizontal and in the lateral direction, and let the y-axis be vertical and positive upwards.

If one makes the reasonable assumption that the longitudinal scale of the problem is much larger than the depth, and considers only systems in which the discharge velocity, which is in the z-direction, is no larger than the density induced velocities, all the assumptions made in the previous subsection for simplifying the basic equations can be made here and the same simplified equations can be obtained. The only difference is that in Eq. 6.23, $\bar{u} = 0$ but $\bar{w} \neq 0$.

6.4 SOLUTION FOR THE VELOCITY w AND THE DISPERSION COEFFICIENT D_z

The velocity w is obtained by integrating Eq. 6.8 and 6.16. Integrating Eq. 6.8 with the assumption that the density variation with depth is sufficently small so that one can replace ρ by the depth-averaged density $\bar{\rho}$ yields

$$p = \bar{\rho} g (d-y) . \tag{6.24}$$

Taking the derivative of Eq. 6.24 with respect to z gives

$$\frac{\partial p}{\partial z} = \frac{\partial \bar{\rho}}{\partial z} g(d-y) - \bar{\rho} g S' , \tag{6.25}$$

where $S' = -\frac{\partial d}{\partial z}$, the slope of the water surface in the z-direction.

Although such a slope is inconsistent with the previous assumptions of a uniform depth and zero slope of the bottom in the z-direction, a small slope is necessary to maintain continuity of flow in the z-direction.

By replacing $\bar{\rho}$ by ρ_a in the last term of Eq. 6.25, substituting the resulting expression into Eq. 6.16, integrating once with respect to y, and using the second of the two boundary conditions:

$$w = 0 \text{ at } y = 0 \tag{6.26a}$$

$$\lambda_y \epsilon_y \frac{\partial w}{\partial y} = 0 \text{ at } y = d \,, \tag{6.26b}$$

one obtains

$$0 = \frac{\partial \bar{\rho}}{\partial z} g\left(\frac{d^2}{2} - yd + \frac{y^2}{2}\right) + \rho_a gS' (y-d) + \rho_a \lambda_y \epsilon_y \frac{\partial w}{\partial y} \quad . \tag{6.27}$$

Assuming that $\lambda_y \epsilon_y = \overline{\lambda_y \epsilon_y}$, a constant equal to the depth-averaged value, integrating Eq. 6.27 from 0 to y, and eliminating S' by using the relation

$$\bar{w} = \frac{1}{d} \int_0^d w dy \,, \tag{6.18}$$

gives

$$w(\eta) = \frac{g}{\rho_a} \frac{\partial \bar{\rho}}{\partial z} \frac{d^3}{\overline{\lambda_y \epsilon_y}} \left[-\frac{\eta^3}{6} + \frac{5}{16}\eta^2 - \frac{\eta}{8}\right] + \bar{w}\left[-\frac{3}{2}\eta^2 + 3\eta\right] \,, \tag{6.28}$$

where $\eta = y/d$. (Eq. 6.28 can be obtained from a stream function derived by Hansen and Rattray (Ref. 25, their Eq. 17) if one sets the shear stress at the surface equal to zero.)

By using Elder's (4) expression,

$$D_x = -d^2 \int_0^1 u'(\eta) \int_0^\eta \frac{1}{\epsilon_y(\eta')} \int_0^{\eta'} u'(\eta'')d\eta''d\eta'd\eta \,, \qquad (2.5)$$

one can now calculate the dispersion coefficient, D_z, by substituting w' for u', and D_z for D_x. Using $\epsilon_y(\eta) = \bar{\epsilon}_y$, the depth-averaged value, one obtains

$$D_z = \frac{d^2}{\bar{\epsilon}_y}\left[1.31 \times 10^{-5} \left(\frac{d^3}{\lambda_y \epsilon_y} \frac{g}{\rho_a} \frac{\partial \bar{\rho}}{\partial z} \right)^2 + 9.43 \times 10^{-4} \left(\frac{d^3}{\lambda_y \epsilon_y} \frac{g}{\rho_a} \frac{\partial \bar{\rho}}{\partial z} \right) \bar{w} + 1.90 \times 10^{-2} \bar{w}^2 \right], \qquad (6.29)$$

where the numerical coefficients are approximations of some cumbersome fractions. By using Eq. 6.1, the equation of state, one can replace $\frac{\partial \bar{\rho}}{\partial z}$ by $\beta \frac{\partial \bar{c}}{\partial z}$ in Eq. 6.29 and substitute the resulting expression into Eq. 6.23 which then becomes a non-linear diffusion equation for $\bar{c}$.

Before proceeding to investigate solutions to Eq. 6.23, some of the properties of Eq. 6.28 and 6.29 and other expressions for $w(\eta)$ and D_z are examined. Expressions similar to Eq. 6.28 and 6.29 are obtained if different boundary conditions are used when integrating Eq. 6.16 and 6.27. Generalized solutions for $w(\eta)$ and D_z are given by Eq. 6.30 and 6.31, and in Table 6.1, numerical values are given for the coefficients corresponding to the solutions with the following boundary conditions: $w = 0$ at $y = 0$ and $\frac{\partial w}{\partial y} = 0$ at $y = d$; $w = 0$ at $y = 0$ and $y = d$; and $\frac{\partial w}{\partial y} = 0$ at $y = 0$ and $y = d$.

Table 6.1 Coefficients in Eq. 6.30 and 6.31 for $w(\eta)$ and D_z.

Boundary Conditions		Coefficients for $w(\eta)$							Coefficients for D_z		
y = 0	y = d	a_1	a_2	a_3	a_4	a_5	a_6	a_7	b_1	b_2	b_3
w = 0	$\frac{\partial w}{\partial y} = 0$	$-\frac{1}{6}$	$\frac{5}{16}$	$-\frac{1}{8}$	0	$-\frac{3}{2}$	3	0	1.31×10^{-5}	9.43×10^{-4}	1.90×10^{-2}
w = 0	w = 0	$-\frac{1}{6}$	$\frac{1}{4}$	$-\frac{1}{12}$	0	- 6	6	0	2.76×10^{-6}	0	4.76×10^{-3}
$\frac{\partial w}{\partial y} = 0$	$\frac{\partial w}{\partial y} = 0$	$-\frac{1}{6}$	$\frac{1}{4}$	0	$-\frac{1}{24}$	0	0	1	8.54×10^{-4}	0	0

$$w(\eta) = \frac{d^3}{\lambda_y \epsilon_y} \frac{g}{\rho_a} \frac{\partial \bar{\rho}}{\partial z} \left(a_1 \eta^3 + a_2 \eta^2 + a_3 \eta + a_4 \right) + \bar{w} \left(a_5 \eta^2 + a_6 \eta + a_7 \right) \qquad (6.30)$$

$$D_z = \frac{d^2}{\epsilon_y} \left[b_1 \left(\frac{d^3}{\lambda_y \epsilon_y} \frac{g}{\rho_a} \frac{\partial \bar{\rho}}{\partial z} \right)^2 + b_2 \left(\frac{d^3}{\lambda_y \epsilon_y} \frac{g}{\rho_a} \frac{\partial \bar{\rho}}{\partial z} \right) \bar{w} + b_3 \bar{w}^2 \right] \qquad (6.31)$$

The three solutions for $w(\eta)$ with $\bar{w} = 0$ are given in dimensionless form in Fig. 6.1.

One can show that if ϵ_y and $\lambda_y \epsilon_y$ are considered to be functions of y, $w(\eta)$ is still given by a function of the form

$$w(\eta) = \frac{d^3}{\lambda_y \epsilon_y} \frac{g}{\rho_a} \frac{\partial \bar{\rho}}{\partial z} f_1(\eta) + \bar{w} f_2(\eta) \ , \qquad (6.32)$$

and D_z is still given by Eq. 6.31. Thus for any vertical distributions of the vertical diffusion coefficients and for a wide variety of boundary conditions, the density-induced velocity is directly proportional to the lateral density gradient and to the the depth cubed, but inversely proportional to the depth-averaged eddy viscosity. Also, for $\bar{w} = 0$ the dispersion coefficient due to the density-induced velocity is directly proportional to the quantity

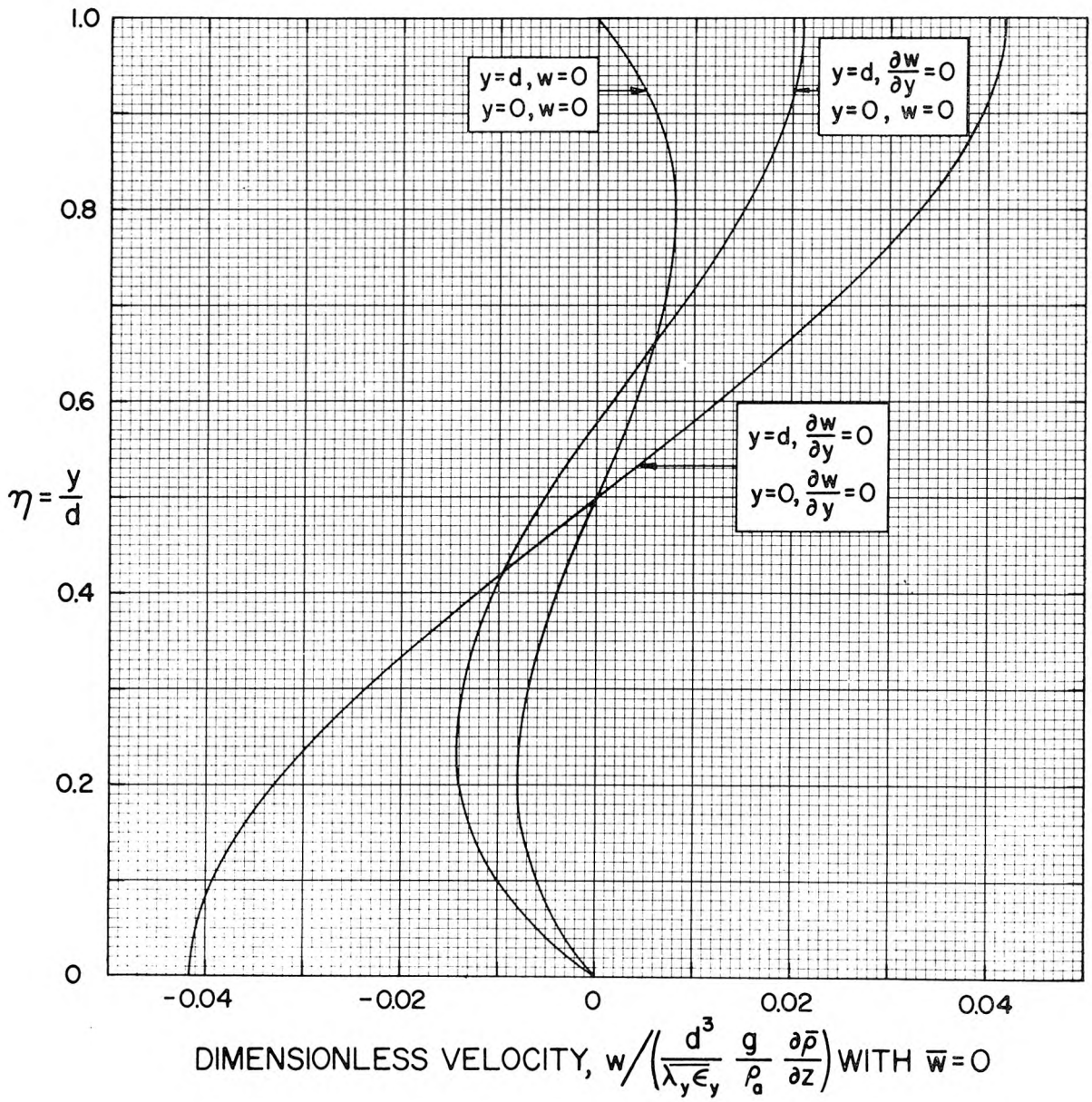

Figure 6.1 Theoretical velocity profiles, $w(\eta)$ with $\bar{w} = 0$, for three different sets of boundary conditions.

$$\frac{d^2}{\bar{\epsilon}_y}\left(\frac{d^3}{\lambda_y \epsilon_y}\frac{g}{\rho_a}\frac{\partial \bar{\rho}}{\partial z}\right)^2 \quad .$$

6.5 APPLICATION OF THEORY TO EXPERIMENTS OF THIS STUDY

6.5.1 Sources of Finite Width. Eq. 6.23 and 6.30 are now used to derive an expression for the variance of the lateral distribution of the depth-averaged concentration downstream from a source discharging fluid into a uniform open-channel flow at a velocity equal to the ambient fluid velocity but with a density different from the ambient fluid.

For this problem $\bar{w} = 0$ so that equations 6.23 and 6.30 become

$$\bar{u}\frac{\partial \bar{c}}{\partial x} = \frac{\partial}{\partial z}\left[(D_z + \bar{\epsilon}_z)\frac{\partial \bar{c}}{\partial z}\right] , \tag{6.33}$$

and

$$D_z = b_1 \frac{d^2}{\bar{\epsilon}_y}\left(\frac{g}{\rho_a}\frac{\partial \bar{\rho}}{\partial z}\frac{d^3}{\lambda_y \epsilon_y}\right)^2 . \tag{6.34}$$

Because $\frac{\partial \bar{\rho}}{\partial z}$ is a function of x and z, D_z is also; however, the analysis is simplified by eliminating the variations with z by replacing $\frac{\partial \bar{\rho}}{\partial z}$ with $\left(\frac{\partial \bar{\rho}}{\partial z}\right)_{ave}$, a representative value at each cross-section. From Eq. 6.1, the equation of state, from Eq. 3.2 which defines the relative concentration C, and from the definition of the variance, σ^2, one can deduce that

$$\left(\frac{\partial \bar{\rho}}{\partial z}\right)_{ave} \sim \frac{(\bar{\rho} - \rho_a)_{max}}{\sigma} \sim \frac{\Delta \rho b}{\sigma^2} \quad ,$$

where b is the source width, and $\Delta\rho$ is the density difference at the source. Therefore, the expression

$$\frac{\partial \bar{\rho}}{\partial z} = A_1 \frac{\Delta\rho b}{\sigma^2} , \tag{6.35}$$

where A_1 is a constant of proportionality, is used in Eq. 6.34.

For $(D_z + \bar{\epsilon}_z)$ not a function of z, taking moments of Eq. 6.33 yields

$$D_z + \bar{\epsilon}_z = \frac{\bar{u}}{2} \frac{d\sigma^2}{dx} . \tag{6.36}$$

Substituting Eq. 6.35 into 6.34 and 6.34 into 6.36, assuming that $\overline{\lambda_y \epsilon_y}$, the depth-averaged eddy viscosity, is given by

$$\overline{\lambda_y \epsilon_y} = \frac{k}{6} u_* d , \tag{2.17}$$

assuming that

$$\bar{\lambda}_y \bar{\epsilon}_y = \overline{\lambda_y \epsilon_y} , \tag{6.37}$$

and recalling that

$$\bar{\epsilon}_z = \alpha u_* d ,$$

Eq. 6.36 becomes

$$\alpha u_* d + b_1 \frac{6\bar{\lambda}_y d}{k u_*} \left(g \frac{\Delta\rho}{\rho_a} \frac{A_1 b}{\sigma^2} \frac{6 d^2}{k u_*} \right)^2 = \frac{\bar{u}}{2} \frac{d\sigma^2}{dx} . \tag{6.38}$$

Dividing by $\alpha u_* d$ yields

$$1 + \frac{A_b^2 M_b^2}{V^2} = \frac{1}{2} \frac{dV}{d\bar{X}} , \tag{6.39}$$

where A_b^2 is a group of dimensionless numbers,

$$A_b^2 = b_1 \bar{\lambda}_y A_1^2 \left(\frac{6\alpha}{k}\right)^3 , \qquad (6.40)$$

and V, X, B, and M_b are the dimensionless variance, distance downstream from the source, source width, and source strength, which were defined in Eq. 5.7a, b, c, and d. Integrating Eq. 6.39 and using the initial condition $V = B^2/12$ at $X = 0$ yields

$$V(X, B, M_b) = \frac{B^2}{12} + 2X + A_b M_b \left[\tan^{-1}\left(\frac{V}{A_b M_b}\right) - \tan^{-1}\left(\frac{B^2/12}{A_b M_b}\right)\right] . \qquad (6.41)$$

For $M_b = 0$ Eq. 6.41 reduces to the expression for turbulent mixing only, Eq. 5.11,

$$V(X, B, 0) = \frac{B^2}{12} + 2X . \qquad (5.11)$$

The dimensionless excess variance, ΔV, is obtained by subtracting Eq. 5.11 from Eq. 6.41 and evaluating $\Delta V = V(X, B, M_b) - V(X, B, 0)$ for $X \to \infty$ to give

$$\Delta V = A_b M_b \left[\frac{\pi}{2} - \tan^{-1}\left(\frac{B^2/12}{A_b M_b}\right)\right] . \qquad (6.42)$$

Eq. 6.42 is compared with the experimental data in Fig. 6.2, where curves computed using Eq. 6.42 are superimposed on the ΔV-M_b graph presented before as Fig. 5.2. In the computations, the quantity $A_b = 2.25 \times 10^{-3}$ was used. This value was obtained by choosing $b_1 = 1.31 \times 10^{-5}$ from Table 6.1, which corresponds to the solution with the boundary conditions $w = 0$ at $y = 0$, and $\partial w/\partial y = 0$ at $y = d$; by choosing $k = 0.38$ and $\alpha = 0.135$, which are the averages from all experiments; by letting $\bar{\lambda} = 1$; and by using $A_1 = 0.20$,

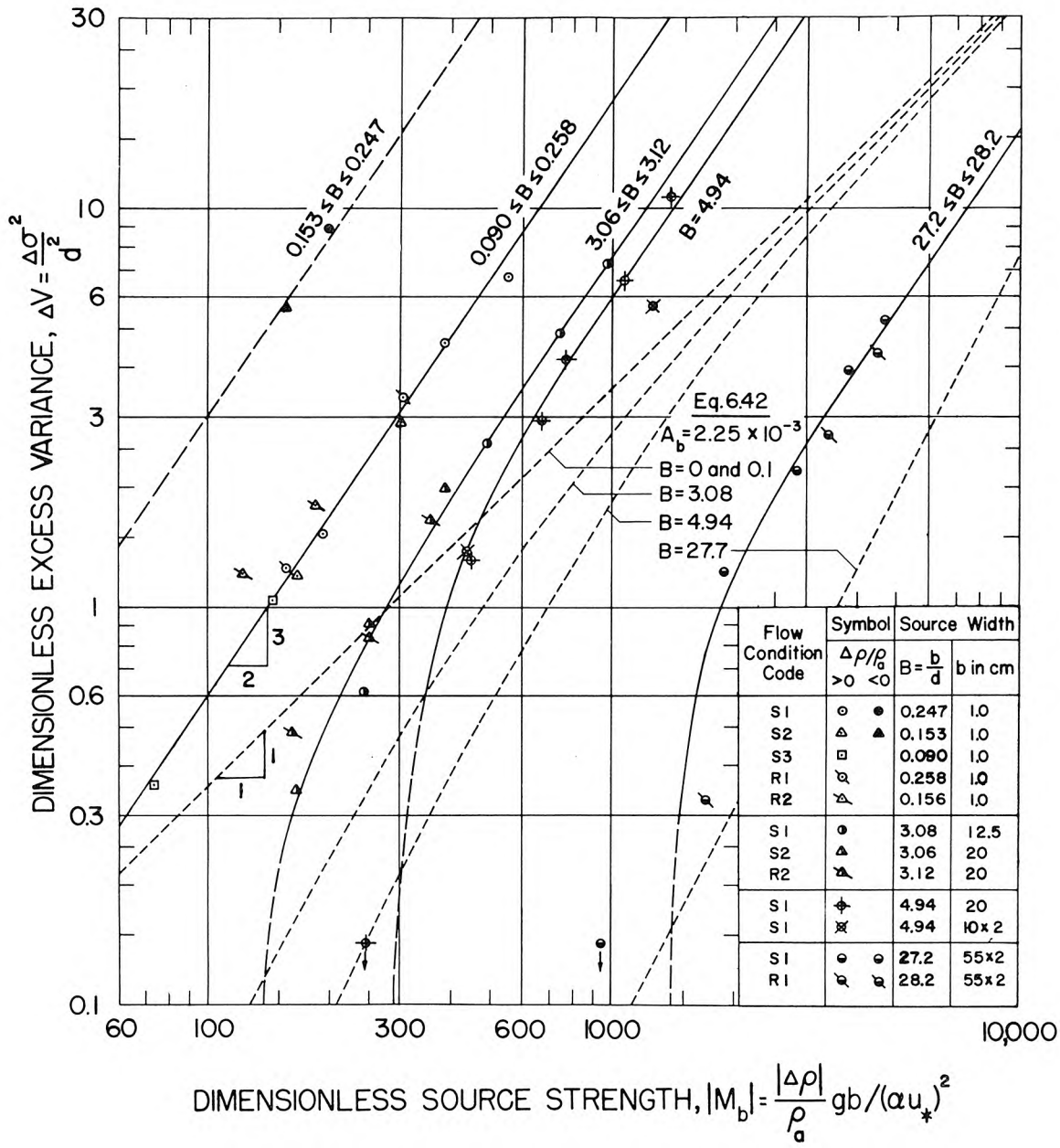

Figure 6.2 Comparison of ΔV given by Eq. 6.42 and by experiment.

which is the value obtained if one assumes that the lateral concentration distributions are Gaussian and that $(\partial\overline{\rho}/\partial z)_{ave}$ equals $(\overline{\rho}-\rho_a)_{max}/2\sigma$.

The agreement between the theory and the data is not good. In general, Eq. 6.42 yields smaller values of ΔV than were found by experiment. For $0.090 \leq B \leq 0.258$ or for the asymptotes for the larger values of B, the data yields $\Delta V \sim M_b^{3/2}$; however, for B = 0 or for the asymptotes for other B, Eq. 6.42 yields $\Delta V \sim M_b$.

The differences between theory and experiment are believed due to not considering the effects of vertical density gradients on λ_y and ϵ_y and due to deleting the inertial term $u\frac{\partial w}{\partial y}$ from the z-momentum equation, Eq. 6.4c. Richardson numbers that were calculated in Subsection 4.2.2 indicate that density gradients were large enough to reduce vertical mixing. Because one expects vertical mixing to decrease with increasing $\Delta\rho/\rho_a$ or M_b, and because vertical mixing suppresses density-induced circulation, one should expect ΔV to increase with M_b more rapidly than predicted by the theory which does not take into account the reduction of turbulent diffusion by vertical density gradients.

In Section 6.3 it was shown that deleting the term $u\frac{\partial w}{\partial x}$ from Eq. 6.4c is valid only if inequality 6.10 or 6.14 is satisfied. By using $\overline{\lambda_y \epsilon_y} = k u_* d$ and data from Tables 4.1 and 5.1 for flow S2, one obtains from inequality 6.14:

$$\frac{x}{d} >> 332 ,$$

or

$$X = \frac{x}{\bar{u}} \frac{\alpha u_*}{d} >> 2.28 \ . \tag{6.43}$$

Thus, deleting $u \frac{\partial w}{\partial x}$ from Eq. 6.4c is not valid in the important region $X < 2$ (see Fig. 5.5) and may cause large errors in Eq. 6.42. Very close to the source where $\frac{\partial |w|}{\partial x} > 0$, retaining $u \frac{\partial w}{\partial x}$ in Eq. 6.4c should yield smaller values of w and D_z than given by the present analysis, but for most values of X where $\frac{\partial |w|}{\partial x} < 0$, retaining $u \frac{\partial w}{\partial x}$ should yield higher values of w and D_z. The net effect of retaining $u \frac{\partial w}{\partial x}$ would probably be to yield higher values of ΔV than given by Eq. 6.42; however, this has not been proved.

6.5.2 Two Wide Parallel Streams. An analysis similar to that made above can also be made for the mixing of two infinitely wide parallel streams of different density. If one again assumes that $(D_z + \bar{\epsilon}_z)$ is not a function of z, one can take the derivative of Eq. 6.33 with respect to z and then take second moments in the z-direction to yield

$$D_z + \bar{\epsilon}_z = \frac{\bar{u}}{2} \frac{d\sigma_d^2}{dx} \tag{6.44}$$

where σ_d^2 is the variance of the lateral distribution of the gradient $\partial \bar{c}/\partial z$ or $\partial \bar{C}/\partial z$. Next, for calculating D_z it is assumed that

$$\frac{\partial \bar{\rho}}{\partial z} = \frac{\Delta \rho}{A_2 \sigma_d} \ , \tag{6.45}$$

where A_2 is a constant. Substituting Eq. 6.45 into Eq. 6.34 and using the resulting expression plus $\bar{\epsilon}_z = \alpha u_* d$ and Eq. 6.38 in Eq. 6.44 yields

$$\alpha u_* d + b_1 \frac{6d\overline{\lambda}_y}{k u_*} \left(\frac{g}{\rho_a} \frac{\Delta\rho}{A_2 \sigma_d} \frac{6d^2}{u_*} \right)^2 = \frac{\overline{u}}{2} \frac{d\sigma_d^2}{dx} \quad . \tag{6.46}$$

Dividing by $\alpha u_* d$ gives

$$1 + \frac{A_d^2 M_d^2}{V_d} = \frac{1}{2} \frac{dV_d}{dX} \quad , \tag{6.47}$$

where A_d is a group of dimensionless numbers,

$$A_d^2 = b_1 \left(\frac{6\alpha}{k} \right)^3 \frac{\overline{\lambda}_y}{A_2^2} \quad , \tag{6.48}$$

V_d is the normalized variance,

$$V_d = \sigma_d^2 / d^2 \quad ,$$

and M_d is the dimensionless source strength that uses the depth as a characteristic length and was defined in Eq. 5.8.

Integrating Eq. 6.47 and using the initial condition $V_d = 0$ at $X = 0$ yields

$$V_d(X, M_d) = 2X + A_d^2 M_d^2 \ell n \left(1 + \frac{V_d}{A_d^2 M_d^2} \right). \tag{6.49}$$

For $M_d = 0$, Eq. 6.49 reduces to

$$V_d(X, 0) = 2X \, . \tag{6.50}$$

Subtracting Eq. 6.50 from 6.49 and evaluating the difference, ΔV_d, for $X \to \infty$ yields

$$\Delta V_d = \lim_{X \to \infty} \left[A_d^2 M_d^2 \ell n \left(1 + \frac{V_d}{A_d^2 M_d^2} \right) \right] \to \infty \, . \tag{6.51}$$

Thus, the analysis shows that for two infinitely wide streams the effect of a density difference does not yield a finite excess variance as was found for a source of finite width. Consequently, this analysis suggests that the curves for increasing values of B on the ΔV-M_d graph in Fig. 5.3 do not collapse into one curve for large values of B. However, because ΔV_d goes to infinity logarithmically, the distance between successive curves continually decreases for increasing values of B.

6.6 APPLICATION OF THEORY TO MIT EXPERIMENTS

In this section Eq. 6.23 and 6.31 are used in an analysis of some experiments performed by Ippen, Harleman, and Lin (2) at MIT. The assumptions made in the derivation of the equations are more nearly satisfied in these experiments than in the experiments of this study; therefore, better agreement between theory and experiment is achieved.

6.6.1 Description of Experiments. The MIT study investigated the effects of longitudinal density gradients on longitudinal dispersion in estuaries. The experimental apparatus, which represented an idealized estuary and is shown schematically in Fig. 6.3, was a flume in which steady-state longitudinal density gradients could be established. The flume was 9.75 meteres long and 42 cm wide. The depth of water was 17.8 cm in all the experiments. Fresh water was pumped into the upstream end of the flume at a rate Q_f, and salt water, with a density greater than the fresh water, was

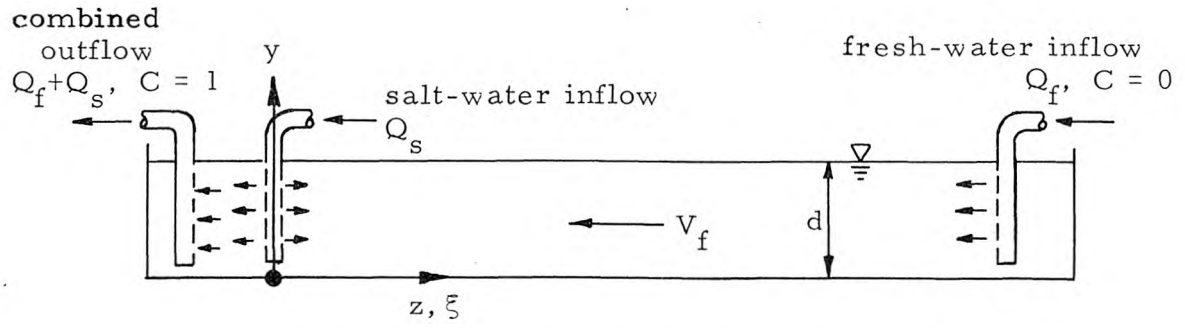

Fig. 6.3 Schematic diagram of the flume used in the MIT experiments (Ref. 2).

pumped into the flume through a manifold near the downstream end at a rate Q_s. Water was withdrawn from the extreme downstream end of the flume at a rate $Q_f + Q_s$. Pumping rates were slow such that throughflow velocities, V_f, were of the order of 0.05 cm/sec.

A homogeneous turbulent field was created by a nest of screens which was suspended in the fluid and was oscillated vertically in simple harmonic motion. The nest of screens was constructed from six pieces of flat expanded metal sheet, each of which lay in a horizontal plane and whose length and width were approximately equal to those of the flume. The sheets were spaced about 2.5 cm apart so that the depth of the nest was about 70 percent of the depth of the water in the flume; when the nest was oscillated with an amplitude of about 1 cm the entire depth was thoroughly mixed.

During each experiment the apparatus was operated until a steady-state distribution of salt concentration was reached. Water samples were then taken from the flume and analysed to determine the salt-concentration distribution in the flume. At steady state,

the downstream transport of salt by the throughflow velocity was balanced by the upstream transport of salt by turbulent diffusion and by longitudinal dispersion.

Values of the depth-averaged longitudinal turbulent diffusion coefficient, $\overline{\epsilon}_z$, were obtained from experiments in which dyed fresh water was used in place of the more dense salt water. A straight forward combination of formulae given on p. 21 of Ref. 2 yields

$$\overline{\epsilon}_z = 0.396\ af' , \tag{6.52}$$

where $\overline{\epsilon}_z$ is the diffusion coefficient in cm^2/sec, a is the oscillation amplitude in cm and f' is the frequency in cycles/sec. The coefficient 0.396 has the dimensions of cm because it includes a characteristic length of the mixing screens.

The vertical turbulent diffusion coefficient, ϵ_y, was obtained from a study by Harleman et al. (37). These measurements were not made in the flume but in a vertical cylinder about 180 cm high and 20 cm in diameter. Turbulence was produced in the cylinder by a nest of screens which was similar in construction to that used in the flume. The experimental data yielded

$$\overline{\epsilon}_y = 1.08\ a^2 f' . \tag{6.53}$$

Vertical density gradients larger than those observed in the experiments in the flume had no effect on the value of $\overline{\epsilon}_y$.

6.6.2 Theoretical Analysis of Experiment. For this problem, $\overline{u} = 0$ and $\overline{w} = -V_f$; therefore Eq. 6.23 is written as

$$-V_f \frac{\partial \overline{c}}{\partial z} = \frac{\partial}{\partial z}\left[(D_z + \overline{\epsilon}_z)\frac{\partial \overline{c}}{\partial z}\right] . \tag{6.54}$$

The expression for the dispersion coefficient is approximated by using only the first term of Eq. 6.31 to give

$$D_z = b_1 \frac{d^2}{\overline{\epsilon}_y}\left[\frac{g}{\rho_a}\frac{\partial \overline{\rho}}{\partial z}\frac{d^3}{\lambda_y \epsilon_y}\right]^2 . \tag{6.55}$$

This approximation is valid for these experiments because the first term of Eq. 6.31 was typically ten times the sum of the other two, and $\overline{\epsilon}_z$ was usually much larger than the last term which represents dispersion in the absence of a density gradient. Also, most of the approximations made in the derivation of Eq. 6.32 are valid. Because $u = 0$, inequality 6.14 is true. Calculations using Eq. 6.28 for w and experimental data typically yield values of 0.4 for the left-hand side of inequality 6.15; therefore, deleting $w\frac{\partial w}{\partial z}$ from the z-momentum equation is not totally unreasonable. Also the range of concentration with depth was typically less than 25 percent of the depth-averaged concentration.

In this analysis the density of the fresh water inflow is denoted by ρ_a and the difference in density between the combined outflow and ρ_a is denoted by $\Delta\rho$. The salt concentration of the fluid is normalized so that the relative concentration, C, at the combined outflow is unity, and the relative concentration of the fresh water inflow is

zero. Substituting Eq. 6.55 into 6.54, introducing C, and replacing the partial derivatives with total derivatives yields

$$-V_f \frac{d\bar{C}}{dz} = \frac{d}{dz}\left\{\left[\bar{\epsilon}_z + \frac{b_1 d^2}{\bar{\epsilon}_y}\left(g\frac{\Delta\rho}{\rho_a}\frac{d^3}{\overline{\lambda_y \epsilon_y}}\frac{d\bar{C}}{dz}\right)^2\right]\frac{d\bar{C}}{dz}\right\} . \tag{6.56}$$

Introducing the dimensionless z-coordinate

$$\xi = \frac{zV_f}{\bar{\epsilon}_z} \tag{6.57}$$

into Eq. 6.56, using Eq. 6.37, and multiplying by $\bar{\epsilon}_z/V_f^2$ yields

$$-\frac{d\bar{C}}{d\xi} = \frac{d}{d\xi}\left\{\left[1 + J\left(\frac{d\bar{C}}{d\xi}\right)^2\right]\frac{d\bar{C}}{d\xi}\right\} , \tag{6.58}$$

where

$$J = \frac{b_1 d^8 V_f^2}{\bar{\lambda}_y^2 (\bar{\epsilon}_z \bar{\epsilon}_y)^3}\left(g\frac{\Delta\rho}{\rho_a}\right)^2 \tag{6.59}$$

is dimensionless, and it is assumed that $\overline{\lambda_y \epsilon_y} = \bar{\lambda}_y \bar{\epsilon}_y$.

Eq. 6.58 is now solved with the boundary conditions

$$\bar{C} = 1 \text{ at } \xi = 0 \tag{6.60a}$$

and

$$\bar{C} = \frac{d\bar{C}}{d\xi} = 0 \text{ for } \xi \to \infty . \tag{6.60b}$$

Integrating Eq. 6.58 once and using the boundary conditions for $\xi \to \infty$ yields

$$-\bar{C} = \frac{d\bar{C}}{d\xi} + J\left(\frac{d\bar{C}}{d\xi}\right)^3 . \tag{6.61}$$

Eq. 6.61 with different values of J was integrated numerically for $\xi \geq 0$; the solutions are given graphically in Fig. 6.4. For $\xi < 0$, $\overline{C} = 1$.

6.6.3 Comparison of Theory with Experiment. In Fig. 6.5 longitudinal distributions of the observed depth-averaged concentration, $\overline{C}(\xi)$, are presented for four typical experiments with different values of the parameter J; theoretical curves are presented for comparison with the experimental data. In computing J, values of $\overline{\epsilon}_z$ were obtained from Eq. 6.52; $\overline{\lambda}_y$ was assumed equal to 1.0; $\overline{\epsilon}_y$ was obtained from Eq. 6.53; and $b_1 = 1.31 \times 10^{-5}$ was chosen, corresponding to the solution for $w(\eta)$ with boundary conditions $w = 0$ at $y = 0$ (no slip) and $\partial w/\partial y = 0$ at $y = d$ (no shear). Although the density difference, $\Delta\rho$, and the throughflow velocity, V_f, were the same in the four experiments presented in Fig. 6.5, the parameter J varied among these experiments because the frequency of the oscillating screens changed which varied $\overline{\epsilon}_z$ and $\overline{\epsilon}_y$.

The agreement between theory and experiment is reasonably good for Runs 21, 22 and 23, but only fair for Run 24. In general, the observed concentrations decrease with ξ slightly more rapidly than do the theoretical curves.

A more general comparison of theory with experiment is shown in Fig. 6.6. There the characteristic longitudinal distance ξ_*, defined in the insert of Fig. 6.6 as the difference between values of ξ where $\overline{C} = 1/4$ and $\overline{C} = 3/4$, is plotted on logarithmic coordinates

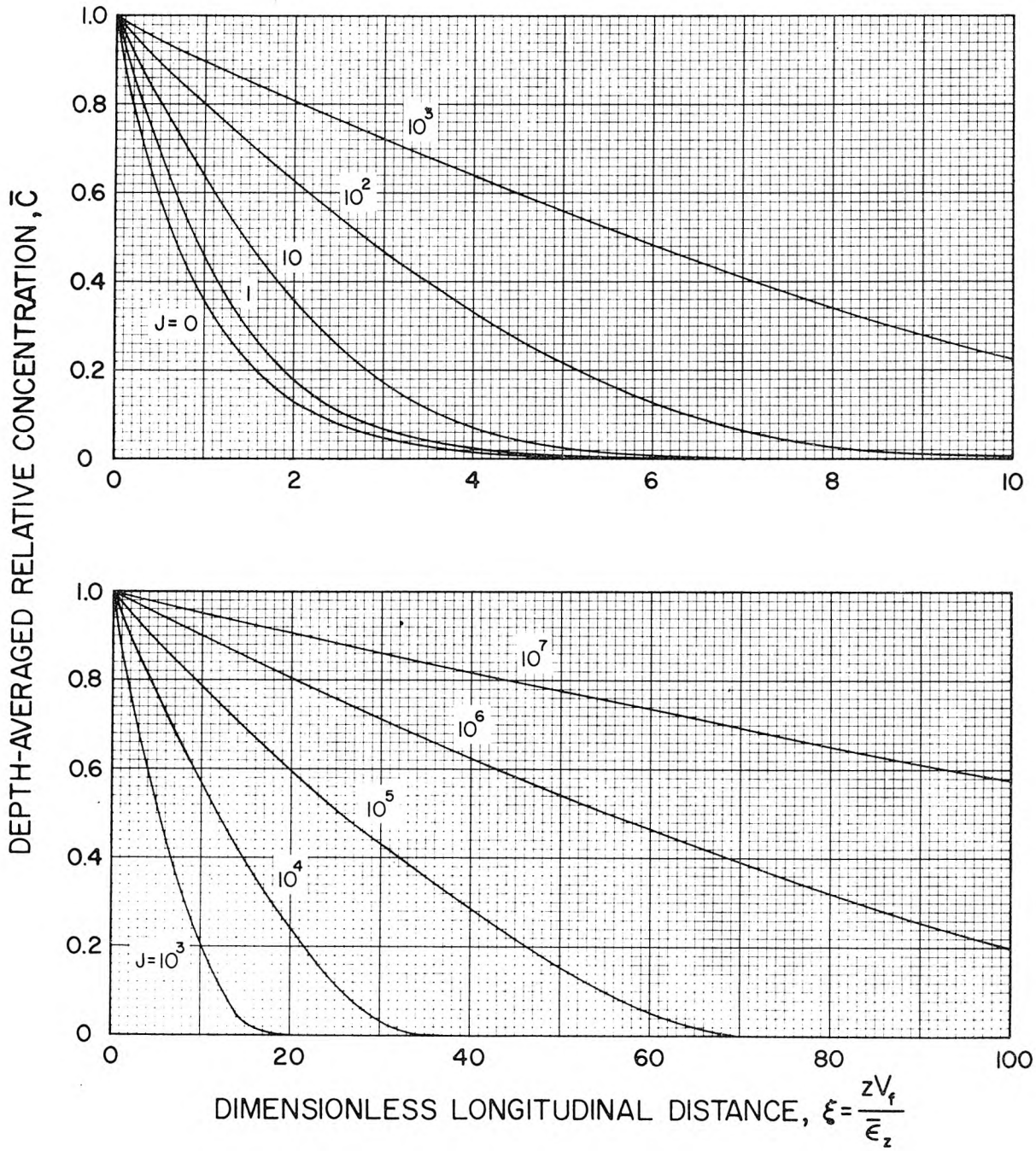

Figure 6.4 Solutions to Eq. 6.61, $-\bar{C} = \frac{d\bar{C}}{d\xi} + J\left(\frac{d\bar{C}}{d\xi}\right)^3$.

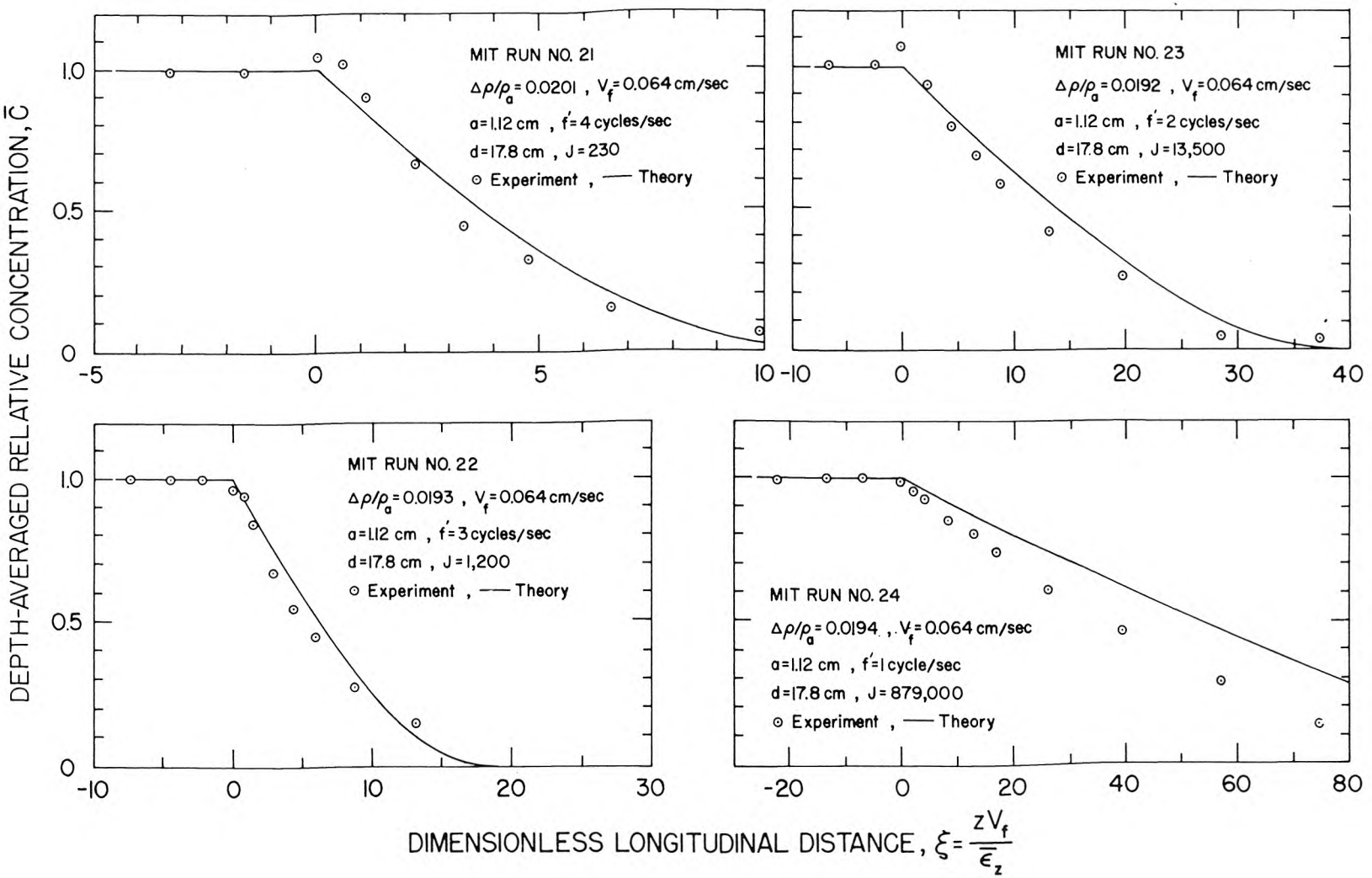

Figure 6.5 Depth-averaged relative concentration, $\bar{C}$, as a function of ξ, the dimensionless longitudinal coordinate, for MIT Runs 21 to 24. J computed using $b_1 = 1.31 \times 10^{-5}$. (Data from Ref. 3.)

as a function of J for all the experiments reported on in Ref. 2. Values of J for the experimental data were calculated using $b_1 = 1.31 \times 10^{-5}$.

The theoretical curve in Fig. 6.6, shown as a solid line, has a slope of 1/3 at large values of J and has the same shape as the distribution of the experimental data. However, the theoretical curve lies above or to the left of the data. The fact that the curve lies above the data implies that for a given density gradient the density-induced velocities and the dispersion coefficient, D_z, are less than that predicted by the theory. The lower velocities are believed due to resistance to flow offered by the screens and flume sidewalls which was not considered in the analysis.

Additional resistance to the flow can be introduced artificially into the analysis by using $b_1 = 2.76 \times 10^{-6}$, which corresponds to solutions with the boundary condition w = 0 at both y = d and y = 0. If this were done, the value of J for each data point would decrease by a factor $2.76 \times 10^{-6} / 1.31 \times 10^{-5} = 1/4.75$. Rather than multiplying the abscissas of all the experimental data points in Fig. 6.6 by 1/4.75 to compare the data with the modified analysis, the abscissa of the theoretical curve was multiplied by 4.75 and the new curve was drawn in Fig. 6.6 as a broken line. This new curve lies below or to the right of most of the data. The best fit is obtained with $b_1 \approx 5.7 \times 10^{-6}$.

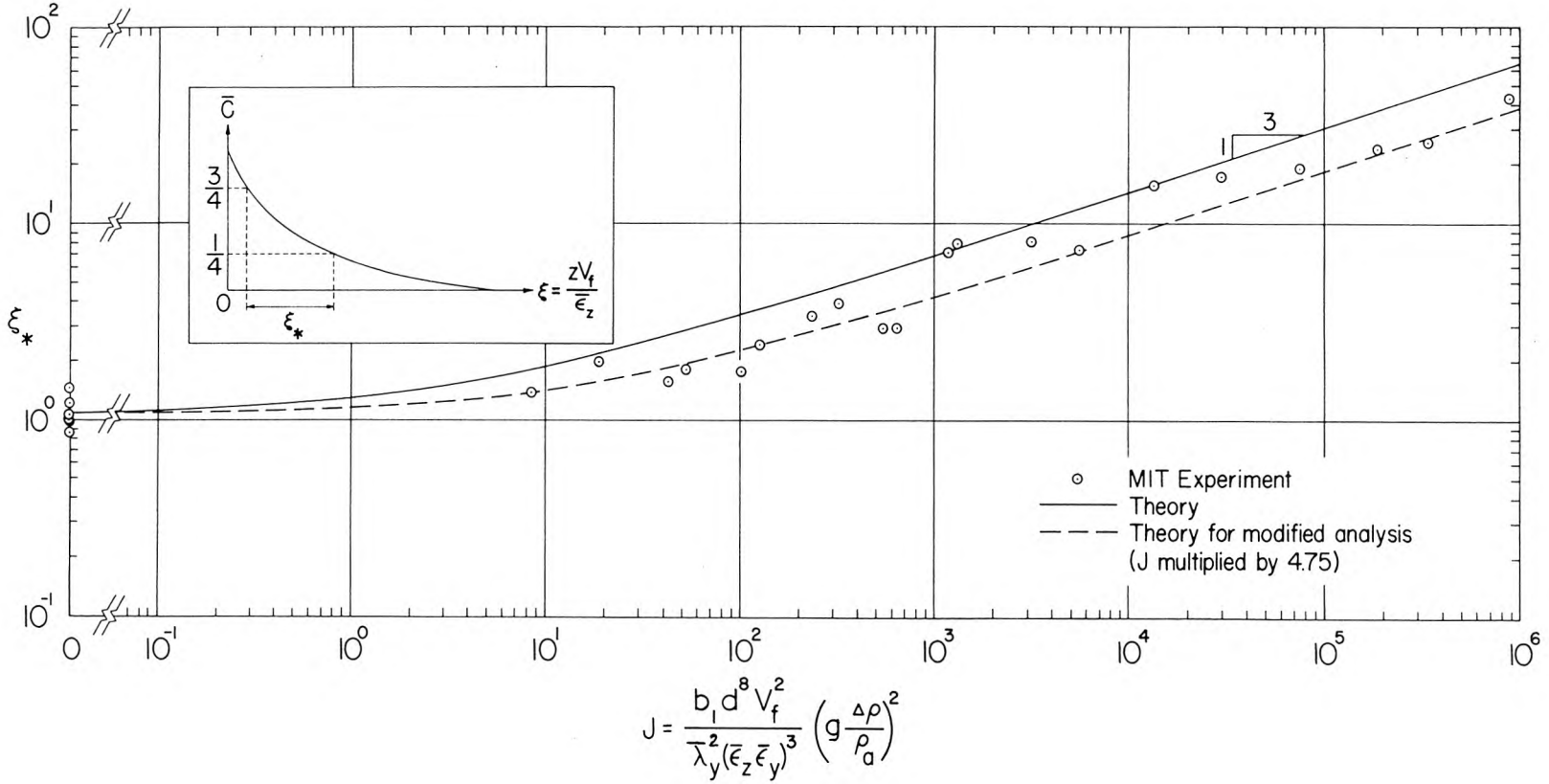

Figure 6.6 The dimensionless distance ξ_* as a function of the parameter J. (Data from Ref. 3.)

The results of the analysis of these experiments demonstrate that when the assumptions made in the derivations of Eq. 6.30 and 6.31 are valid, horizontal mixing by density induced circulation can be treated as a dispersion process, and the dispersion coefficient due to the density-induced velocities is given by Eq. 6.31. The important assumptions that must be satisfied are: (1) the horizontal length scales are much larger than the vertical length scales, (2) all accelerations are negligible, and (3) the fluid is well mixed over the vertical. When these assumptions are not satisfied, as was the case close to the source in the experiments of the present study, Eq. 6.31 should not be used.

CHAPTER 7

SUMMARY OF RESULTS

7.1 EXPERIMENTS

A summary of the results from experiments performed to observe lateral mixing of tracer fluids in turbulent open-channel flows is given below. In these experiments, tracer fluids were discharged at stream velocity from a source which occupied the entire depth, but only a fraction of the channel width.

7.1.1 Experiments without Density Differences. The results from experiments with neutrally buoyant tracer fluids agree with the results from previous investigations.

(1) Distributions of the depth-averaged concentration, $\bar{c}$, in wide open-channel flows are given by solutions to the equation,

$$\bar{u}\frac{\partial \bar{c}}{\partial x} = \bar{\epsilon}_z \frac{\partial^2 \bar{c}}{\partial z^2} \quad , \tag{2.11}$$

where x and z are the longitudinal and lateral coordinates, and $\bar{u}$ and $\bar{\epsilon}_z$ are depth-averaged values of the longitudinal velocity and the lateral turbulent diffusion coefficient for mass. Because Eq. 2.11 is valid, σ^2, the variance of the lateral distribution of $\bar{c}$ downstream from sources of finite width, and σ_d^2, the variance of the lateral distribution of $\partial\bar{c}/\partial z$ downstream from the confluence of two wide streams with different concentrations, grow linearly with x.

(2) The value of the dimensionless lateral turbulent diffusion coefficient, $\alpha = \epsilon_z / u_* d$, averaged over the experiments of this study is 0.135. (The quantity u_* is the shear velocity and d is the water depth.) This value is in the range of data from previous investigations (see Table 2.3).

(3) The average value of the dimensionless lateral turbulent diffusion coefficient for particles floating on the surface, $\alpha_s = \epsilon_{zs} / u_* d$, was found in this study to be 0.204. This value is also within the range of previously published data (see Table 2.2) and is consistent with the results of Sayre and Chang (5) in that $\alpha_s > \alpha$.

7.1.2 Experiments with Density Differences. Experiments in which there was a difference in density, $\Delta\rho$, between the tracer and the ambient fluids show that a density difference enhances the lateral mixing of these tracer fluids. More specific conclusions drawn from these experiments are as follows:

(1) When $\Delta\rho \neq 0$, the functions $\sigma^2(x)$ and $\sigma_d^2(x)$ are nonlinear for small x and grow more rapidly than when $\Delta\rho = 0$.

(2) Detailed concentration distributions in the flow cross-sections indicate that the more rapid growth of $\sigma^2(x)$ and $\sigma_d^2(x)$ is due to density-induced secondary flows (see Figs. 4.4 to 4.10).

(3) At large x, the curves of the functions $\sigma^2(x)$ and $\sigma_d^2(x)$ become linear and parallel to the curves from experiments with $\Delta\rho = 0$.

(4) A dimensional analysis of the problem and the data show that

$$V = V(X, B, M_b) \quad , \tag{5.5}$$

where $V = \frac{\sigma^2}{d^2}$ is the dimensionless variance,

$X = \frac{x}{u}\frac{\alpha u_*}{d}$ is the dimensionless longitudinal coordinate,

$B = \frac{b}{d}$ is the dimensionless source width, and

$M_b = \frac{\Delta\rho}{\rho_a} gb/(\alpha u_*)^2$ is a dimensionless source strength.

The quantity b is the width of the source, ρ_a is the density of the ambient fluid, and g is the acceleration due to gravity.

(5) The dimensionless excess variance, $\Delta V = \Delta\sigma^2/d^2$, where $\Delta\sigma^2$ is the difference at large x between the functions $\sigma^2(x)$ from experiments with $\Delta\rho \neq 0$ and $\Delta\rho = 0$, is a function of only M_b and B (ΔV is defined also in Fig. 5.1 and data are shown in Fig. 5.2). For B constant, ΔV increases with increasing M_b; for M_b constant, ΔV decreases with increasing B.

(6) For $B << 1$ and $|M_b|$ constant, ΔV for tracer fluids less dense than the ambient fluid is about five times as large as ΔV for tracer fluids more dense than the ambient fluid. However, for $B >> 1$, ΔV is the same for light and heavy tracer fluids.

(7) The dimensionless coordinate X required to attain any fraction, r, of the excess variance is independent of M_b and is only weakly dependent on B. Most of the excess variance is attained before $X \approx 2$. (The fraction r is defined in Fig. 5.1, and data are shown in Fig. 5.5.)

(8) By using the expression

$$V(X, B, M_b) = 2X + \frac{B^2}{12} + r\Delta V \qquad (5.12)$$

and the curves in Chapter 5 one can construct the function $\sigma^2(x)$.

(9) Because ΔV increases when B decreases with M_b constant, it is sometimes possible to obtain larger variances, and therefore, lower concentrations at large X by decreasing the width of a source of given strength.

7.2 THEORY

In Chapter 6, the equations of motion for a fluid with a horizontal density gradient were simplified by assuming that (a) horizontal length scales are much larger than vertical length scales, (b) all accelerations are negligible, and (c) the fluid is well mixed vertically. One then finds that:

(1) One can integrate the simplified equations of motion to obtain an expression for the distribution of the density-induced velocity as a linear function of the horizontal density gradient (Eq. 6.30).

(2) Using an expression given by Elder (4) for longitudinal dispersion, one can derive an expression for a lateral dispersion coefficient as a function of the density-induced velocity and the vertical diffusion coefficient (Eq. 6.31).

(3) Using Eq. 6.31 in an analysis to predict the dependence of ΔV on B and M_b gives results which do not agree well with the experimental data (see Fig. 6.2). The disagreement is due to using the simplified equations of motion, which are valid only at large x but not close to the source where the density differences are most important.

(4) Using Eq. 6.31 for predicting longitudinal salinity distributions in an idealized laboratory estuary (which is described in Section 6.6 and for which the simplified equations of motion are valid) yield results which agree well with experimental data of Ippen et al. (2).

LIST OF SYMBOLS

A	area under lateral distribution of depth-averaged relative concentration.
A_1	dimensionless coefficient defined by Eq. 6.35.
A_2	dimensionless coefficient defined by Eq. 6.45.
A_b	dimensionless coefficient defined by Eq. 6.40.
A_d	dimensionless coefficient defined by Eq. 6.48.
a	amplitude of mixing screen oscillation.
a_i	dimensionless coefficient in Eq. 6.30 for $w(\eta)$.
B	dimensionless source width, b/d.
b	source width.
b_i	dimensionless coefficient in Eq. 6.31 for D_z.
C	relative salt concentration.
$\overline{C}$	depth-averaged relative salt concentration.
C_v	coefficient of variation for the vertical distribution of C; defined by Eq. 4.14.
$\overline{C}_v$	concentration-weighted, laterally-averaged value of C_v, defined by Eq. 4.15.
c	salt concentration of fluid.
$\overline{c}$	depth-averaged salt concentration.
c'	$c-\overline{c}$.
c_a	salt concentration of ambient fluid.
c_t	salt concentration of tracer fluid in mixing tank.
c_{dt}	salt concentration of diluted tracer fluid.
c_d	salt concentration of diluting fluid.

LIST OF SYMBOLS (continued)

D	dilution ratio.
D_m	molecular diffusion coefficient.
D_x, D_z	dispersion coefficients in x- and z- directions.
d	water depth.
f	friction factor, $8(u_*/\overline{u})^2$.
f'	frequency of mixing screen oscillations.
f_1, f_2	functions.
g	acceleration due to gravity.
i, j	counting indicies in numerical integration.
J	dimensionless parameter defined by Eq. 6.59.
k	von Karman's constant.
ℓ_x, ℓ_y, ℓ_z	cosines of angles the x-, y-, and z- axes make with the vertical.
M_b	dimensionless source strength defined by Eq. 5.7d.
M_b^1	value of M_b on asymptote when $\Delta V = 1$; defined in Fig. 5.4.
M_d	dimensionless source strength defined by Eq. 5.8.
n	upper limit of index in summation.
n_i	number of particles caught in the i^{th} compartment.
$P(x, z)$	cumulative distribution of the lateral distribution of the depth-averaged concentration, or of floating particles.
p	pressure.
Q_f	fresh-water flow rate.
Q_s	salt-water flow rate.

LIST OF SYMBOLS (continued)

R_{T^o}	specific resistance at T^o C.
Ri	Richardson number defined by Eq. 2.18.
r	fraction of excess variance; defined in Fig. 5.1.
S	slope of energy grade line in the x-direction.
S'	slope of water surface in z-direction.
t	time.
u	velocity in x-direction.
$\overline{u}$	depth-averaged value of u.
u'	$u-\overline{u}$.
u_s	longitudinal velocity of floating particle.
u_*	shear velocity.
V	dimensionless variance, σ^2/d^2.
V_d	dimensionless variance, σ_d^2/d^2.
V_f	throughflow velocity.
v	velocity in y-direction.
w	velocity in z-direction.
$\overline{w}$	depth-averaged value of w.
w'	$w-\overline{w}$.
X	dimensionless longitudinal distance, defined by Eq. 5.7b.
x	longitudinal coordinate in experiments of this study; lateral coordinate in MIT experiments.
y	coordinate normal to channel bottom.
z	lateral coordinate in experiments of this study; longitudinal coordinate in MIT experiments.
$\bar{z}$	centroid of the lateral distribution of the depth-averaged concentration, or of floating particles.

LIST OF SYMBOLS (continued)

$\overline{z}_d$	centroid of the lateral distribution of the lateral gradient of the depth-averaged concentration.
z_1	lower limit of z in numerical integration.
$z_{15.9}$, z_{50}, $z_{84.1}$	values of z where P(x, y) = 15.9, 50, and 84.1 percent.
α, α_s	dimensionless lateral turbulent diffusion coefficients for mass, $\overline{\epsilon}_z/u_*d$ and ϵ_{zs}/u_*d.
β	dimensionless coefficient in Eq. 6.1.
$\Delta\rho$	difference in density between tracer fluid discharged from source and ambient fluid, $\Delta\rho > 0$ denotes heavy tracer fluid, $\Delta\rho < 0$ denotes light tracer fluid; also difference in density between ocean and river waters.
$\Delta\sigma^2$, $\Delta\sigma_d^2$	excess variance; see ΔV, ΔV_d and Fig. 5.1.
ΔV	dimensionless excess variance, $\Delta\sigma^2/d^2$.
ΔV_d	dimensionless excess variance, $\Delta\sigma_d^2/d^2$.
Δz	differential element of z in numerical integration.
$\delta(\ )$	Dirac delta function.
ϵ_x, ϵ_y, ϵ_z	turbulent diffusion coefficients for mass in x-, y- and z-directions.
ϵ_{xs}, ϵ_{zs}	ϵ_x and ϵ_z at free surface.
$(\epsilon_y)_o$	ϵ_y when $R_i=0$.
$\overline{\epsilon}_x$, $\overline{\epsilon}_z$	depth-averaged values of ϵ_x and ϵ_z.
ϵ'_x, ϵ'_z	$\epsilon_x - \overline{\epsilon}_x$ and $\epsilon_z - \overline{\epsilon}_z$.
ζ, ζ_1	dummy variables.
η, η', η''	dimensionless vertical coordinate, y/d.
λ_x, λ_y, λ_z	turbulent Schmidt numbers; ratios of $(\lambda_x\epsilon_x)/\epsilon_x$, etc.

LIST OF SYMBOLS (continued)

$\lambda_x\epsilon_x$, etc.	eddy viscosities.
$(\lambda_y\epsilon_y)_o$	$\lambda_y\epsilon_y$ when $R_i=0$.
ν	kinematic viscosity.
ξ	dimensionless longitudinal coordinate, $zV_f/\overline{\epsilon}_z$.
ξ_*	a characteristic dimensionless length defined in Fig. 6.6 .
π	3.1416 . . .
ρ	density of fluid.
$\overline{\rho}$	depth-averaged density.
ρ_a	density of ambient fluid.
ρ_1	density of fluid discharged from source.
σ^2	variance of the lateral distribution of the depth-averaged concentration.
σ_d^2	variance of the lateral distribution of the lateral gradient of the depth-averaged concentration.
σ_s^2	variance of the lateral distribution of floating particles.
τ_{xx}, τ_{xy}...	turbulent Reynold's stress in the x-direction on a plane normal to the y-direction, etc.
ϕ_1, ϕ_2	functions.
Ψ_1, Ψ_2	functions.

LIST OF REFERENCES

1. Prych, E. A., "Data Supplement to Report No. KH-R-21," W. M. Keck Lab. of Hyd. and Water Res. Tech. Memo.70-3, California Institute of Technology, Pasadena, California (May 1970).

2. Ippen, A. T., Harleman, D. R. F., and Lin, J. D., "Turbulent Diffusion and Gravitational Convection in an Idealized Estuary," Hydrodynamics Lab Tech. Rept. No. 38, MIT, Cambridge, Mass. (March 1960), 33 p.

3. Harleman, D. R. F., "Diffusion Processes in Stratified Flow," Chap. 12 in Estuary and Coastline Hydrodynamics, A. T. Ippen, Edit., McGraw-Hill, New York (1966), p. 575-597.

4. Elder, J. W., "The Dispersion of Marked Fluid in Turbulent Shear Flow," J. of Fluid Mech., 5, Part 4 (May 1959), p. 544-560.

5. Sayre, W. W. and Chang, F. M., "A Laboratory Investigation of Open-Channel Dispersion Processes for Dissolved, Suspended, and Floating Dispersants," U. S. Geol. Survey Prof. Paper 433-E, 71 p.

6. Engelund, Frank, "Dispersion of Floating Particles in Uniform Channel Flow," J. Hyd. Div., Proc. ASCE, 95, No. HY 4 (July 1969), p. 1149-1162.

7. Orlob, G. T., "Eddy Diffusion in Open Channel Flow," Contribution No. 19, Water Resources Center, Sanitary Eng. Research Lab., Univ. of Calif., Berkeley, Calif. (Nov. 1958), 151 p. See also "Eddy Diffusion in Homogeneous Turbulence," J. Hyd. Div., Proc. ASCE, 85, HY 9 (Sept. 1959), p. 75-101.

8. Sayre, W. W., and Chamberlain, A. R., "Exploratory Laboratory Study of Lateral Turbulent Diffusion at the Surface of an Alluvial Channel," U. S. Geol. Survey Circ. 484 (1964), 18 p.

9. Sullivan, P. J., "Dispersion in a Turbulent Shear Flow," Ph. D. Thesis, Churchill College, Univ. of Cambridge, Cambridge, England (Oct. 1968), 197 p.

10. Glover, R. E., "Dispersion of Dissolved or Suspended Materials in Flowing Streams," U. S. Geol. Survey Prof. Paper 433-B (1964), 32 p.

LIST OF REFERENCES (Continued)

11. Fischer, H. B., "Transverse Mixing in a Sand-Bed Channel," U. S. Geol. Survey Prof. Paper 575-D (1967), p. D267-D272.

12. Yatsukura, Nobuhiro, Fischer, H. B., and Sayre, W. W., "Measurement of Mixing Characteristics of the Missouri River between Sioux City, Iowa and Plattsmouth, Nebraska," unpublished manuscript, U. S. Geol. Survey Circ. in preparation.

13. Fischer, H. B., "The Effect of Bends on Dispersion in Streams," Water Resources Research, 5, No. 2 (April 1969), p. 496-506.

14. Okoye, J. K., Personal Communication (Ph. D. Thesis in preparation), W. M. Keck Lab. of Hyd. and Water Res., Calif. Inst. of Tech., Pasadena, Calif.

15. Vanoni, V. A., "Transportation of Suspended Sediment by Water," Trans. ASCE, 111 (1946), p. 67-133.

16. Jobson, J. E. and Sayre, W. W., "Vertical Transfer in Open Channel Flow," J. Hyd. Div., Proc. ASCE, 96, No. HY 3 (March 1970), p. 703-724.

17. Munk, W. H. and Anderson, E. R., "Notes on a Theory of the Thermocline," J. of Marine Res., 7 (1947), p. 276-295.

18. Ellison, T. H. and Turner, J. S., "Mixing of a Dense Fluid in a Turbulent Pipe Flow. Parts I and II," J. of Fluid Mech., 8, Part 4 (Aug. 1960), p. 514-544.

19. Taylor, G. I., "Observations and Speculations on the Nature of Turbulent Motion," Rept. and Memo. of Advis. Comm. for Aero., No. 345 (1917); reprinted in The Scientific Papers of G. I. Taylor, Vol. II edit. by G. K. Batchelor, Cambridge Univ. Press (1960), p. 69-78.

20. Okubo, Akira, "A Review of Theoretical Models for Turbulent Diffusion in the Sea," J. Ocean. Soc. Jap., 20th Anniv. Vol. (1962), p. 286-320.

21. Harleman, D. R. F., Jordaan, J. M., and Lin, J. D., "The Diffusion of Two Fluids of Different Density in a Homogeneous Turbulent Field," Hydrodynamics Lab. Tech. Rept. No. 31, MIT, Cambridge, Mass. (Feb. 1959), 107 p.

LIST OF REFERENCES (Continued)

22. Jen, Yuan, Wiegel, R. L., and Mobarek, Ismail, "Surface Discharge of Warm-Water Jet," J. Power Div., Proc. ASCE, 92, No. PO2 (April 1966), p. 1-30.

23. Hayashi, Taizo and Shuto, Nobuo, "Diffusion of Warm Water Jets Discharged Horizontally at the Water Surface," Proc. 12th Cong. of the IAHR, Ft. Collins, Colo., U.S.A., 4 (1967) p. 47-59.

24. Ippen, A. T., "Salinity Intrusion in Estuaries," Chap. 13 in Estuary and Coastline Hydrodynamics, A. T. Ippen, Edit., McGraw-Hill, New York (1966), p. 598-629.

25. Hansen, D. V. and Rattray, Jr., Maurice, "Gravitational Circulation in Straits and Estuaries," J. of Marine Res., 23, No. 2 (1965), p. 104-122.

26. Vanoni, V. A., Brooks, N. H., and Raichlen, Fredric, "A 40 Meter Precision Tilting Flume," W. M. Keck Lab. of Hyd. and Water Res. Tech. Memo. 67-3, Calif. Inst. of Tech., Pasadena, Calif. (Oct. 1967), 21 p.

27. International Critical Tables, McGraw-Hill, New York (1928).

28. Handbook of Chemistry and Physics, 39th ed., Chemical Rubber Publ. Co. (1957), p. 1909.

29. Mendenhall, William, Introduction to Probability and Statistics, 2nd ed., Wadsworth Publ. Co., Belmont, Calif. (1967) p. 205.

30. Ambramowitz, Milton and Stegun, I. A., ed., Handbook of Mathematical Functions, Nat. Bur. of Std., Appl. Math. Ser. 55 (1967), p. 941 and 984-985.

31. Einstein, H. A. and El Samni, E. A., "Hydrodynamic Forces on a Rough Wall," Rev. of Modern Phys., 21, No. 3 (July 1949), p. 520-524.

32. Taylor, Jr., H. R., "Exploratory Studies of Open-Channel Flow Over Boundaries of Laterally Varying Roughness," W. M. Keck Lab. of Hyd. and Water Res. Rept. No. KH-R-4, Calif. Inst. of Tech., Pasadena, Calif. (July 1961), 65 p.

33. Sharp, J. J., "Spread of Buoyant Jets at the Free Surface," J. Hyd. Div., Proc. ASCE, 95, No. HY3 (May 1969), p. 811-825.

LIST OF REFERENCES (Continued)

34. Sharp, J. J., "Spread of Buoyant Jets at the Free Surface - II," J. Hyd. Div., Proc. ASCE, 95, No. HY 5 (Sept 1969), p. 1771-1773.

35. Prandtl, Ludwig, "The Essentials of Fluid Dynamics," Blackie and Son, London (1952), p. 148-149.

36. List, E. J., "The Stability and Mixing of a Density-Stratified Horizontal Flow in a Saturated Porous Medium," W. M. Keck Lab. of Hyd. and Water Res. Rept. No. KH-R-11, Calif. Inst. of Tech., Pasadena, Calif. (Dec. 1965), 164 p.

37. Harleman, D. R. F., Hoopes, J. A., McDougall, D., Goulis, D. A., "Salinity Effects on Velocity Distributions in an Idealized Estuary," Hydrodynamics Lab. Tech. Rept. No. 50, MIT, Cambridge, Mass. (Jan 1962), 45 p.

APPENDIX

DATA TABLES

Table A1. Summary of data from experiments with the 1-cm, 12.5-cm and 20.0-cm-wide sources.

Experiment	Flow Condition Code	Source Width b in cm	Density Difference $\Delta\rho/\rho_a$	Dimensionless Source Strength M_b	Dimensionless Source Strength M_d	Excess Variance $\Delta\sigma^2$ in cm^2	Distance from Source x in cm	Centroid of $\bar{C}(z)$ $\bar{z}$ in cm	Area under $\bar{C}(z)$ in cm	Variance σ^2 in cm^2	Fraction of $\Delta\sigma^2$ r	Coefficient of Variation $\bar{C}_v$
113	S2	1.0	0.0160	157	1030	51.9	200	0.0	1.130	44.3	0.56	0.72
							500	0.0	1.029	90.1	0.96	0.27
							1000	-0.2	1.006	146.1	1.09	0.07
							1500	0.0	0.978	185.7	0.96	0.02
							2000	0.0	1.008	231.8	0.97	0.02
114	S2	1.0	0.0160	157	1030	51.9	200	0.0	1.067	41.2	0.50	0.70
							500	0.0	1.028	84.5	0.79	0.28
							1000	0.2	0.958	134.9	0.87	0.08
							1500	-0.3	1.010	188.6	1.02	0.03
							2000	0.3	1.022	241.3	1.16	0.01
115	S2	1.0	0	0	0	--	200	0.0	1.103	14.8	--	0.16
							500	0.3	1.146	47.8	--	0.11
							1000	0.0	1.040	92.2	--	0.05
							1500	0.0	1.045	137.0	--	0.04
							2000	-0.1	1.059	181.2	--	0.03
116	S2	1.0	0	0	0	--	200	0.0	1.098	16.2	--	0.16
							500	-0.1	1.082	43.6	--	0.09
							1000	0.8	1.038	93.9	--	0.06
							1500	0.4	0.999	129.8	--	0.03
							2000	-0.2	1.000	178.3	--	0.04
117	S2	1.0	0.0307	302	1980	124.0	150	-0.8	1.165	63.1	0.43	0.99
							400	-0.7	1.052	131.1	0.79	0.49
							700	-0.8	1.011	173.6	0.90	0.20
							1100	-1.2	1.001	217.2	0.95	0.08
							1500	-1.0	0.994	250.1	0.92	0.04
118	S2	1.0	0.0304	299	1960	124.0	150	0.0	1.158	64.8	0.44	1.03
							400	0.0	1.098	134.3	0.81	0.48
							700	-0.1	1.017	169.7	0.87	0.20
							1100	0.3	1.049	240.3	1.14	0.07
							1500	-0.1	1.026	271.6	1.10	0.04
							2000	0.0	0.991	298.5	0.95	0.02
120	S1	1.0	0	0	0	--	200	0.0	1.163	12.7	--	0.11
							500	0.4	1.160	33.6	--	0.06
							1000	0.2	1.128	64.5	--	0.02
							1500	0.5	1.098	94.1	--	0.01
							2000	-0.2	1.133	134.3	--	0.02
121	S1	1.0	0.0158	192	776	20.5	100	0.0	1.022	18.0	0.47	0.87
							200	0.0	1.068	32.6	0.82	0.54
							500	0.0	1.038	57.4	1.02	0.12
							1000	0.3	1.090	94.2	1.20	0.03
							1500	0.4	1.065	120.9	0.98	0.02
							2000	0.0	1.085	150.9	0.86	0.01
122	S1	1.0	0.0318	385	1560	75.0	150	-0.1	1.047	56.7	0.63	0.88
							300	0.1	1.090	85.8	0.90	0.41
							600	0.3	1.095	115.1	1.03	0.09
							1000	0.3	1.048	135.4	0.95	0.03
							1500	0.3	1.009	178.6	1.09	0.02
							2000	0.3	1.064	198.9	0.93	0.02
125	S3	1.0	0	0	0	--	200	0.0	1.034	16.9	--	0.11
							500	0.5	0.951	55.1	--	0.14
							1000	0.1	1.005	135.6	--	0.07
							1500	-0.3	0.971	222.8	--	0.04
							2000	-0.8	0.985	290.4	--	0.04
127	S3	1.0	0.0159	150	1670	128.1	150	0.0	1.183	44.6	0.28	1.21
							350	0.0	1.091	120.5	0.66	0.77
							600	-0.2	1.008	177.4	0.81	0.47
							900	-0.8	1.001	245.9	0.97	0.27
							1300	-0.7	0.968	312.4	1.01	0.14

Table A1. Continued

Experiment	Flow Condition Code	Source Width b in cm	Density Difference $\Delta\rho/\rho_a$	Dimensionless Source Strength M_b	Dimensionless Source Strength M_d	Excess Variance $\Delta\sigma^2$ in cm^2	Distance from Source x in cm	Centroid of $\bar{C}(z)$ $\bar{z}$ in cm	Area under $\bar{C}(z)$ in cm	Variance σ^2 in cm^2	Fraction of $\Delta\sigma^2$ r	Coefficient of Variation $\bar{C}_v$
128	S2	1.0	-0.0158	-155	-1010	232.8	200	0.9	0.959	75.3	0.25	1.05
							500	1.4	1.032	215.1	0.72	0.48
							750	0.2	0.953	246.4	0.76	0.18
							1000	0.3	1.025	309.8	0.93	0.07
							1500	0.7	1.017	382.7	1.03	0.04
							2000	-0.2	0.984	409.9	0.97	0.03
129	S3	1.0	0.0078	74	827	44.0	150	0.0	1.057	15.8	0.17	0.71
							300	0.0	1.035	46.9	0.43	0.66
							500	0.0	1.006	93.4	0.80	0.48
							800	-1.3	0.969	147.8	0.97	0.24
							1100	-0.7	0.986	204.2	1.19	0.14
							1500	-0.1	0.951	251.6	0.89	0.07
130	S1	1.0	0.0453	551	2230	110.1	150	0.0	1.119	74.0	0.59	0.98
							300	0.1	1.118	116.4	0.89	0.46
							600	1.2	1.091	152.7	1.04	0.10
							1000	1.1	1.074	181.6	1.07	0.04
							1500	1.2	1.042	207.9	1.01	0.02
							2000	0.8	1.039	235.5	0.96	0.02
136	S1	20.0	0	0	0	--	0	0.0	1.220	33.0	--	0.05
							200	0.0	1.207	45.9	--	0.03
							500	0.4	1.171	59.8	--	0.02
							1000	0.5	1.187	95.1	--	0.01
							1500	0.3	1.158	118.5	--	0.01
							2000	0.1	1.240	165.3	--	0.02
137	S1	20.0	0.00088	249	51	0.0	0	-0.2	1.109	31.9	--	0.04
							200	0.0	1.093	44.4	--	0.09
							500	0.2	1.046	62.9	--	0.07
							1000	0.0	1.082	96.8	--	0.02
							1500	0.3	1.032	122.4	--	0.01
							2000	-0.1	1.024	149.9	--	0.02
139	S1	20.0	0	0	0	--	0	0.3	1.051	32.0	--	0.01
							200	0.5	1.101	32.0	--	0.03
							500	1.4	0.877	60.0	--	0.03
							1000	0.9	1.018	90.5	--	0.02
							1500	0.4	1.009	119.4	--	0.01
							2000	0.5	0.987	150.5	--	0.01
140	S1	20.0	0.00158	449	91	21.5	0	0.1	1.018	33.8	0.08	0.03
							200	0.8	1.031	50.1	0.26	0.13
							500	0.7	1.084	79.8	0.81	0.10
							1000	0.6	1.026	112.2	0.89	0.03
							1500	0.6	1.014	144.7	1.04	0.02
							2000	0.0	0.995	172.9	0.97	0.02
141	S1	20.0	0.00238	673	136	47.9	0	0.0	0.983	33.5	0.03	0.01
							200	0.9	1.027	57.7	0.27	0.19
							500	1.4	1.059	100.7	0.80	0.20
							1000	1.2	1.009	136.0	0.90	0.05
							1500	1.1	1.060	171.9	1.04	0.02
							2000	0.6	1.074	205.3	1.12	0.03
142	S1	20.0	0.00487	1380	279	175.5	0	0.5	1.008	33.4	0.01	0.04
							200	1.1	1.089	85.7	0.24	0.40
							500	1.7	1.108	170.1	0.62	0.35
							1000	2.3	1.102	266.2	0.99	0.10
							1500	1.7	1.098	305.7	1.05	0.03
							2000	1.4	1.123	322.7	0.97	0.02
143	S1	20.0	0.00270	768	155	68.1	0	0.1	0.979	33.6	0.02	0.04
							200	0.7	1.011	60.6	0.24	0.24
							500	0.8	1.000	110.2	0.70	0.22
							1000	0.8	1.043	164.0	1.04	0.06
							1500	0.6	1.005	181.2	0.87	0.02
							2000	0.6	1.071	225.0	1.07	0.02
144	S1	20.0	0.00373	1060	214	108.0	0	-0.4	0.971	34.2	0.02	0.07
							200	-0.3	1.057	75.9	0.29	0.30
							500	0.0	1.046	141.0	0.73	0.27
							1000	0.0	1.040	199.4	0.99	0.08
							1500	-0.5	1.021	233.5	1.03	0.03
							2000	-0.4	1.022	259.2	0.99	0.02

Table A1. Continued

Experiment	Flow Condition Code	Source Width b in cm	Density Difference $\Delta\rho/\rho_a$	Dimensionless Source Strength M_b	Dimensionless Source Strength M_d	Excess Variance $\Delta\sigma^2$ in cm^2	Distance from Source x in cm	Centroid of $\bar{C}(z)$ $\bar{z}$ in cm	Area under $\bar{C}(z)$ in cm	Variance σ^2 in cm^2	Fraction of $\Delta\sigma^2$ r	Coefficient of Variation $\bar{C}_v$
147	S1	1.0	-0.0164	-199	-785	146.0	200	0.2	0.869	91.5	0.54	0.79
							400	-0.5	0.973	158.6	0.91	0.27
							800	-0.5	1.049	210.7	1.09	0.05
							1200	-0.1	1.061	226.4	1.02	0.03
							1600	-0.6	1.028	248.1	0.98	0.02
							2000	-0.4	1.035	257.7	0.88	0.02
150	S2	20.0	0	0	0	--	0	0.0	0.759	33.6	--	0.05
							200	0.1	0.768	48.2	--	0.08
							500	-0.1	0.781	77.5	--	0.06
							1000	0.1	0.734	108.0	--	0.02
							1500	0.2	0.746	158.4	--	0.02
							2000	0.2	0.764	217.6	--	0.02
151	S2	20.0	0.00079	165	54	15.0	0	0.1	0.769	31.9	0.03	0.05
							200	-0.2	0.766	49.2	0.04	0.04
							500	0.3	0.761	78.9	0.19	0.12
							1000	0.1	0.766	129.1	0.59	0.08
							1500	-0.2	0.761	181.3	1.08	0.04
							2000	-0.4	0.740	224.5	1.03	0.02
152	S2	20.0	0.00186	389	127	85.3	0	-0.3	0.790	33.4	0.02	0.04
							200	0.3	0.757	51.9	0.04	0.19
							500	-0.1	0.805	114.5	0.45	0.34
							1000	0.1	0.758	195.1	0.88	0.17
							1500	-0.3	0.749	251.5	1.01	0.06
							2000	0.2	0.732	298.7	1.05	0.04
153	S2	20.0	0	0	0	--	0	0.3	0.780	33.4	--	0.06
							200	0.0	0.773	48.1	--	0.06
							500	1.1	0.779	74.8	--	0.04
							1000	1.1	0.749	106.4	--	0.02
							1500	1.1	0.769	175.5	--	0.01
							2000	0.9	0.743	201.4	--	0.01
154	S2	20.0	0.00121	252	85	39.0	0	-0.2	0.778	32.2	0.01	0.02
							200	0.1	0.766	49.5	0.02	0.10
							500	0.4	0.773	92.0	0.41	0.23
							1000	1.0	0.760	153.6	0.86	0.13
							1500	1.0	0.748	212.3	1.22	0.05
							2000	0.7	0.737	245.6	0.94	0.03
156	S1	12.5	0	0	0	--	0	0.0	0.996	13.1	--	0.0
							200	0.3	1.048	25.8	--	0.03
							500	0.7	1.012	40.0	--	0.03
							1500	0.9	0.983	94.8	--	0.02
157	S1	12.5	0	0	0	--	0	0.0	1.076	13.1	--	0.0
							200	0.3	1.065	26.5	--	0.04
							500	1.0	1.009	40.1	--	0.02
							1000	1.2	0.996	69.3	--	0.02
							1500	1.1	1.029	108.0	--	0.01
							2000	0.8	1.019	128.6	--	0.01
158	S1	12.5	0.00132	248	81	10.0	0	-0.1	1.084	13.1	0.00	0.01
							200	0.5	1.127	29.8	0.12	0.14
							500	1.1	1.035	49.6	0.75	0.11
							1000	1.6	1.013	79.0	0.80	0.03
							1500	1.2	0.994	109.6	0.96	0.01
							2000	0.9	0.985	134.3	1.53	0.01
159	S1	12.5	0.00282	532	17	35.0	0	0.0	1.114	13.2	0.00	0.02
							200	0.5	1.097	36.5	0.23	0.23
							500	1.0	1.056	70.6	0.80	0.18
							1000	1.0	1.013	106.2	1.07	0.04
							1500	0.8	1.000	132.5	0.93	0.02
							2000	0.8	1.014	163.8	0.99	0.01
160	S1	12.5	0.00431	813	26	65.0	0	0.0	1.108	13.1	0.00	0.01
							200	0.3	1.104	41.4	0.20	0.30
							500	0.8	1.045	91.4	0.76	0.24
							1000	1.0	1.012	136.2	1.00	0.06
							1500	1.1	1.006	162.4	0.96	0.02
							2000	0.4	0.995	197.4	1.05	0.02

Table A1. Continued

Experiment	Flow Condition Code	Source Width b in cm	Density Difference $\Delta\rho/\rho_a$	Dimensionless Source Strength M_b	Dimensionless Source Strength M_d	Excess Variance $\Delta\sigma^2$ in cm^2	Distance from Source x in cm	Centroid of $\bar{C}(z)$ $\bar{z}$ in cm	Area under $\bar{C}(z)$ in cm	Variance σ^2 in cm^2	Fraction of $\Delta\sigma^2$ r	Coefficient of Variation $\bar{C}_v$
161	S1	12.5	0.00636	1260	39	119.0	0	0.1	1.141	13.0	0.00	0.0
							200	0.0	1.080	58.0	0.25	0.45
							500	0.7	1.068	128.7	0.73	0.30
							1000	0.8	1.018	189.0	0.99	0.07
							1500	0.8	1.039	223.7	1.04	0.02
							2000	0.9	1.029	241.8	0.95	0.02
162	S1	12.5	0	0	0	--	0	0.1	1.053	13.0	--	0.02
							200	-0.2	1.010	25.1	--	0.02
							500	0.4	1.001	40.5	--	0.03
							1000	0.3	1.005	71.1	--	0.02
							1500	0.2	1.002	109.3	--	0.02
							2000	-0.2	0.988	138.4	--	0.01
163	S1	12.5	0.00138	244	79	10.0	0	0.0	1.096	13.0	0.00	0.02
							200	0.0	1.054	27.6	0.46	0.17
							500	0.3	1.057	52.0	1.19	0.11
							1000	0.2	1.050	84.4	1.29	0.02
							1500	0.2	1.007	113.9	1.19	0.01
							2000	-0.1	1.015	140.8	0.78	0.01
164	S1	12.5	0.00275	488	158	42.0	0	0.0	1.065	13.7	0.00	0.01
							200	0.2	1.072	37.2	0.34	0.34
							500	0.2	1.105	78.8	0.92	0.21
							1000	0.1	1.017	111.6	0.95	0.04
							1500	0.1	1.017	143.2	0.98	0.02
							2000	0.0	1.038	176.0	1.02	0.02
165	S1	12.5	0.00414	735	238	79.0	0	0.1	1.096	13.1	0.00	0.02
							200	-0.1	1.115	49.6	0.34	0.44
							500	0.0	1.095	103.2	0.80	0.24
							1000	0.2	1.022	147.1	0.96	0.05
							1500	-0.1	0.993	180.7	1.00	0.02
							2000	-0.3	1.007	213.8	1.02	0.02
166	S1	12.5	0	0	0	--	1500	0.2	0.998	98.6	--	0.01
							2000	-0.3	1.014	126.1	--	0.01
167	S1	12.5	0.00543	965	312	118.9	0	0.0	1.090	13.4	0.00	0.02
							200	0.0	1.084	62.2	0.33	0.50
							500	0.2	1.104	139.6	0.83	0.26
							1000	0.0	1.022	191.3	1.01	0.06
							1500	0.1	1.017	221.2	1.00	0.02
							2000	-0.3	1.012	248.3	0.97	0.02
170	S1	2X10	0	0	0	--	0	0.0	0.486	34.6	--	0.01
							200	0.0	0.469	47.2	--	0.02
							500	0.0	0.454	61.7	--	0.01
							1000	0.0	0.425	94.6	--	0.01
							1500	0.0	0.443	126.2	--	0.01
							2000	0.0	0.437	151.3	--	0.01
171	S1	2X10	0.00145	438	89	22.5	0	0.0	0.489	33.6	0.00	0.02
							200	0.0	0.500	54.0	0.44	0.13
							500	0.0	0.496	84.3	0.97	0.07
							1000	0.0	0.469	116.5	1.03	0.03
							1500	0.0	0.446	146.9	1.02	0.02
							2000	0.0	0.452	176.9	1.07	0.01
172	S1	2X10	0.00414	1250	258	93.0	0	0.0	0.530	33.6	0.00	0.01
							200	0.0	0.492	75.0	0.33	0.31
							500	0.0	0.479	139.5	0.83	0.14
							1000	0.0	0.433	182.3	0.96	0.05
							1500	0.0	0.431	214.9	0.98	0.03
							2000	0.0	0.442	252.9	1.05	0.02
192	R2	1.0	0	0	0	--	200	-0.2	1.010	25.7	--	0.04
							400	-0.3	0.992	56.8	--	0.04
							800	-0.5	1.004	118.2	--	0.02
							1200	-0.4	1.004	175.9	--	0.01
							1600	-0.4	0.940	233.1	--	0.01
							2000	-0.1	0.950	289.9	--	0.01

Table A1. Continued

Experiment	Flow Condition Code	Source Width b in cm	Density Difference $\Delta\rho/\rho_a$	Dimensionless Source Strength M_b	Dimensionless Source Strength M_d	Excess Variance $\Delta\sigma^2$ in cm^2	Distance from Source x in cm	Centroid of $\bar{C}(z)$ $\bar{z}$ in cm	Area under $\bar{C}(z)$ in cm	Variance σ^2 in cm^2	Fraction of $\Delta\sigma^2$ r	Coefficient of Variation $\bar{C}_v$
193	R2	1.0	0	0	0	--	200	-0.3	0.961	23.6	--	0.04
							400	-0.2	0.978	57.2	--	0.04
							800	-0.4	0.999	124.0	--	0.02
							1200	-0.5	1.006	188.3	--	0.01
							1600	0.3	0.963	234.1	--	0.01
							2000	-0.2	0.944	289.8	--	0.01
194	R2	1.0	0.0545	185	1180	73.7	150	0.0	1.160	65.9	0.65	0.57
							300	-0.1	1.029	96.7	0.76	0.23
							600	0.4	0.984	153.4	0.91	0.06
							900	0.0	0.988	204.4	0.95	0.03
							1200	-0.4	0.971	256.1	1.08	0.02
							1500	0.2	0.959	293.1	0.98	0.02
195	R2	1.0	0.0360	122	784	50.0	150	-0.2	1.144	46.8	0.57	0.53
							300	-0.3	1.028	75.7	0.69	0.20
							600	0.0	1.008	124.7	0.77	0.05
							1000	0.0	1.003	192.2	0.92	0.02
							1400	0.1	1.004	259.6	1.07	0.01
							1800	0.1	1.002	324.4	1.17	0.01
196	R1	1.0	0	0	0	--	200	-0.7	1.030	19.4	--	0.07
							400	-0.3	1.035	41.6	--	0.02
							800	0.1	1.014	83.1	--	0.03
							1200	0.3	1.054	125.8	--	0.01
							1600	0.6	1.002	162.4	--	0.01
							2000	-0.4	1.021	207.0	--	0.01
197	R1	1.0	0.0388	157	610	19.0	200	0.1	1.094	48.9	1.52	0.15
							400	0.1	1.008	59.4	1.02	0.04
							800	0.4	1.025	103.3	1.07	0.02
							1200	0.0	1.032	147.6	1.29	0.01
							1600	0.7	1.001	181.4	0.89	0.01
							2000	0.1	1.010	225.8	1.04	0.01
198	R1	1.0	0.0756	305	1187	51.1	200	-0.4	1.065	60.3	0.79	0.18
							400	-0.4	1.037	86.7	0.91	0.05
							800	0.1	1.001	126.5	0.87	0.02
							1200	-0.4	1.026	173.4	0.98	0.01
							1600	0.8	1.027	215.0	0.99	0.01
							2000	-0.2	1.021	257.5	1.01	0.01
199	R2	20.0	0	0	0	--	0	0.2	0.941	32.5	-	0.01
							200	0.4	0.965	59.0	--	0.03
							500	0.9	0.978	106.7	--	0.02
							900	1.0	0.968	171.4	--	0.01
							1300	0.4	1.001	241.2	--	0.01
							1700	1.1	0.985	297.0	--	0.01
200	R2	20.0	0.00263	162	52	20.0	0	0.5	0.705	32.4	0.00	0.06
							150	0.8	0.768	61.9	0.39	0.11
							300	0.6	0.764	86.9	0.48	0.14
							700	0.9	0.740	159.1	0.91	0.05
							1100	0.6	0.745	223.5	0.97	0.02
							1500	1.0	0.755	288.3	1.06	0.01
201	R2	20.0	0.00406	253	81	34.5	0	0.2	0.725	32.2	-.01	0.03
							150	0.4	0.775	63.5	0.27	0.21
							300	0.5	0.786	102.1	0.72	0.23
							600	0.7	0.747	152.5	0.80	0.10
							900	0.9	0.752	208.3	1.05	0.04
							1300	1.0	0.750	270.5	1.03	0.02
202	R2	20.0	0.00571	354	113	64.7	0	0.4	0.736	33.1	0.01	0.02
							150	0.5	0.784	71.7	0.26	0.23
							350	0.6	0.779	131.0	0.67	0.25
							600	1.0	0.748	191.3	0.98	0.12
							900	1.2	0.731	245.5	1.09	0.05
							1300	1.2	0.745	299.7	0.96	0.03

Table A2. Summary of data from experiments with the wide source.

Experiment	Flow Condition Code	Density Difference $\Delta\rho/\rho_a$	Dimensionless Source Strength M_b	Dimensionless Source Strength M_d	Excess Variance $\Delta\sigma_d^2$ in cm^2	Distance from Confluence x in cm	Centroid of $\partial\bar{C}/\partial z$ $\bar{z}_d$ in cm	Area under $\bar{C}(z)$ in cm	Variance σ_d^2 in cm^2	Fraction of $\Delta\sigma_d^2$ r	Coefficient of Variation $\bar{C}_v$
175	S1	0	0	0	--	0	0.0	55.000	0.0	--	0.0
						200	0.1	55.110	8.4	--	0.01
						500	0.6	55.550	23.8	--	0.02
						1000	0.4	55.330	52.1	--	0.01
						1500	0.3	55.275	79.2	--	0.0
177	S1	0	0	0	--	0	0.0	55.000	0.0	--	0.0
						200	0.0	54.505	9.6	--	0.01
						500	0.5	55.495	24.7	--	0.02
						1000	-0.2	54.835	52.7	--	0.01
						1500	0.3	55.275	81.9	--	0.01
						2000	0.3	55.275	121.4	--	0.01
178	S1	0.00057	936	34	0.0	0	0.0	55.000	0.0	--	0.0
						200	0.1	55.110	10.2	--	0.04
						500	0.3	55.275	30.1	--	0.03
						1000	0.5	55.440	49.8	--	0.01
						1500	0.6	55.550	86.4	--	0.01
						2000	0.3	55.275	111.0	--	0.01
179	S1	0.00114	1870	69	20.0	0	0.0	55.000	0.0	0.00	0.0
						200	-0.2	54.835	15.8	0.38	0.09
						500	-0.3	54.725	44.1	1.04	0.05
						1000	-0.6	54.340	80.0	1.24	0.02
						1500	-0.2	54.835	103.1	0.92	0.01
						2000	-0.1	54.890	138.0	1.19	0.01
180	S1	0.00173	2820	104	35.9	0	0.0	55.000	0.0	0.00	0.0
						200	-0.4	54.615	25.8	0.49	0.11
						500	0.1	55.055	58.6	0.98	0.06
						1000	-0.4	54.615	91.2	1.00	0.02
						1500	-0.5	54.505	118.2	0.93	0.01
						2000	-0.4	54.560	155.3	1.14	0.01
181	S1	0.00232	3780	140	64.0	0	0.0	55.000	0.0	0.00	0.0
						200	-0.6	54.395	30.5	0.35	0.13
						500	-0.6	54.340	80.9	0.90	0.07
						1000	-0.7	54.230	117.1	0.97	0.02
						1500	-0.7	54.285	163.2	1.22	0.02
						2000	-0.5	54.450	181.4	1.05	0.01
183	S1	0.00286	4660	172	85.8	0	0.0	55.000	0.0	0.00	0.0
						200	0.3	55.275	28.9	0.24	0.17
						500	0.8	55.770	88.5	0.76	0.09
						1000	0.7	55.715	118.1	0.73	0.03
						2000	-0.8	54.175	211.1	1.13	0.01
203	R1	0	0	0	--	0	0.0	55.000	0.0	--	0.0
						200	-1.0	53.955	20.6	--	0.0
						500	-2.3	52.690	56.7	--	0.02
						1000	-1.2	53.735	104.2	--	0.0
						1500	-1.7	53.350	160.8	--	0.02
						2000	0.1	55.110	205.2	--	0.01
204	R1	0	0	0	--	0	0.0	53.955	0.0	--	0.0
						200	-1.5	52.690	19.5	--	0.02
						500	-1.7	52.690	48.7	--	0.01
						1000	-2.1	53.240	102.8	--	0.0
						1500	-2.6	52.910	165.2	--	0.01
						2000	-2.4	52.580	223.7	--	0.01
205	R1	0.00432	1700	60	4.6	0	0.0	55.000	0.0	0.00	0.0
						200	-0.7	54.285	25.1	1.36	0.08
						500	-1.5	53.515	57.3	1.32	0.03
						1000	-1.5	53.460	108.3	0.56	0.01
						1500	-1.9	53.075	166.6	1.32	0.01
						2000	-1.7	53.295	216.1	0.22	0.0
206	R1	0.00861	3360	120	38.0	0	0.0	55.000	0.0	0.00	0.0
						200	-0.7	53.460	45.0	0.65	0.14
						500	-1.5	52.415	94.5	1.07	0.04
						1000	-1.5	52.745	150.9	1.11	0.02
						1500	-1.9	52.415	197.3	0.91	0.01
						2000	-1.7	52.855	255.9	1.00	0.01
207	R1	0.0114	4450	178	61.2	0	0.0	55.000	0.0	0.00	0.0
						200	-0.2	54.780	55.3	0.56	0.18
						500	-1.5	53.460	112.5	0.94	0.06
						1000	-0.5	54.450	157.4	0.79	0.02
						1500	-1.5	53.460	236.6	1.16	0.01
						2000	-0.5	54.505	283.4	1.04	0.01

Table A3. Summary of data from experiments with floating particles.

Experiment Number	Flow Condition Code	Source Width b (cm)	Particle Velocity u_s (cm/sec)	Distance Down-stream x (cm)	Number of Particles	Variance σ_s^2 (cm^2)	Coordinate of Centroid $\bar{z}$ (cm)
101	S3	None	54.5	100	186	7	0.5
				200	393	15	0.2
				350	398	50	0.5
				600	416	96	1.1
				1000	400	169	1.8
				1500	402	256	2.1
				2000	403	342	4.5
102	S1	None	43.3	200	404	12	0.2
				500	409	40	-0.1
				1000	402	74	-0.6
				1500	400	108	-1.0
				2000	660	142	0.3
103	S2	None	54.3	200	409	14	0.6
				500	404	49	0.8
				1000	539	121	1.9
				1500	471	174	1.4
				2000	512	228	1.8
104	S2	2.0	53.7	200	801	16	1.0
				500	1199	44	-0.6
				1000	807	90	0.0
				1500	1221	141	1.2
				2000	1242	210	1.4
105	S3	2.0	53.5	200	408	27	-1.2
				500	407	72	-0.8
				1000	410	144	-0.5
				1500	400	234	-0.6
				2000	402	272	0.2
106	S1	2.0	43.0	200	398	20	0.2
				500	406	29	0.8
				1000	398	66	0.0
				1500	402	117	1.2
				2000	405	135	1.3
108	S2	1.0	53.2	200	407	16	0.9
				500	404	41	0.9
				1000	401	104	1.4
				1500	403	174	3.0
				2000	390	210	1.5
123	S1	1.0	42.4	200	413	13	0.3
				500	412	37	0.7
				1000	400	76	2.1
				1500	392	117	2.0
				2000	383	151	1.7
145	S1	2.0	42.6	200	413	11	-0.4
				500	402	40	-0.8
				1000	411	84	-0.2
				1500	431	136	-1.0
				2000	386	190	0.9
168	S1	12.5	42.5	200	400	12	1.4
				500	418	42	0.9
				1000	393	89	0.9
				1500	407	120	1.2
				2000	407	161	-1.1
184	S1	55.0	42.0	200	410	20	1.0
				500	398	45	1.6
				1000	405	63	2.1
				1500	409	95	2.4
				2000	401	127	2.3
186 + 191	R1	None	49.5	200	402	25	0.1
				500	420	52	0.1
				1000	832	105	0.7
				1500	840	172	1.2
				2000	819	241	1.6
188	R2	None	59.5	200	399	33	0.6
				500	407	104	-0.3
				1000	403	173	1.2
				1500	404	277	1.2
				2000	407	408	1.0